HIGH STRENGTH-HIGH TEMPERATURE LAMINATED SANDWICH BEAMS

by

MOHAMED DA I. ARAFA

A Dissertation submitted to the

Graduate School-New Brunswick

Rutgers, The State University of New Jersey

in partial fulfillment of the requirements

for the degree of

Doctor of Philosophy

Graduate Program in Civil And Environmental Engineering

Written under the direction of

Professor P.N. Balaguru

and approved by

_____

_____

_____

_____

New Brunswick, New Jersey

[October, 2007]

ABSTRACT OF THE DISSERTATION

HIGH STRENGTH-HIGH TEMPERATURE LAMINATED SANDWICH BEAMS

By MOHAMED DA I. ARAFA

Dissertation Director:

Professor P.N. Balaguru

Structural sandwich panels are commonly used in marine and aerospace applications. They are composed of a core and skins bonded together using polymer matrices. Polyvinyl chloride (PVC)/carbon sandwich beams having organic resins as adhesives are known for their high strength to weight ratio. One of the major concerns is their vulnerability to fire. The organic matrices not only deteriorate at temperatures above 300°C but also emit toxins.

The research presented in this dissertation deals with the development of PVC/carbon sandwich panels using an inorganic matrix. The matrix can sustain temperature up to 1000°C and emits no toxins.

The primary objective of the research presented in this dissertation was to evaluate the feasibility of the matrix for manufacturing sandwich panels. The evaluation was carried out by fabricating sandwich beams and testing them in flexure and high temperature fire exposure.

The variables investigated were: foam density, type and volume fraction of carbon fibers used for skins and extra insulation for fire protection. Strength, stiffness and high temperature resistance properties were measured.

For temperature resistance evaluation, Ohio State University test, the NBS test, and heated element exposure test were used. The results obtained show that inorganic polymer can be effectively used to fabricate fire resistant sandwich beams. The strength and stiffness properties of beams fabricated with inorganic polymer are about -3% and +14% of values obtained for organic polymer skins. The samples with inorganic polymer skin and 1 mm coating easily passed the Federal Aviation Administration (FAA) requirements for fire tests. When exposed to heating element, the beams can sustain 300°C for indefinite duration and 700°C for 5 minutes. Preliminary studies are also presented for an all inorganic sandwich beams that can sustain 1050°C. Analytical procedures are presented to estimate the moment capacities of the beams.

Acknowledgements

To begin with, I would like to thank God the Gracious Almighty for giving me the strength during my years of study. I would like to extend my gratitude to Prof. P.N. Balaguru for his support and guidance, not only on the academic level, but on the personal level as well. I would like to thank Prof. H. Najm for having his door open for me whenever I needed an advice. I would like to thank Prof. A. Maher and Dr. A.. Pelegri for taking time to be my dissertation committee.

I am also grateful to Dr. Richard Lyon, and the Federal Aviation Administration for providing the financial support that was needed to conduct my research. In addition, Mr. Chris Kilbourn from DIAB group should be acknowledged for providing all the PVC that was used in this study.

I would like to deeply thank my mother for all the support and encouragement. I would like to thank my sister for standing by me. I would like to thank my lovely wife for being the best companion in the journey of life. I would like to thank my father and grandparents, may God bless their souls and shower them with mercy. I would like also to extend my gratitude to my in-laws (Father, mother, brothers and grandfather) and Dr. A. Azzam. Without you all I would not have been able to achieve anything. Thank you for supporting me, believing in me, being patient and for the love that was and will always be my encouragement for achievements.

I would like to thank Mr. Ed Depaolo and Mr. Brian Falconer from Severud Associates for granting me enough time to finish.

I would like to especially thank Christian DeFazio and Dr. Mohamed Nazier. I would also like to acknowledge Connie Dellamura, Azam Kalantari, Patrick Szary, Linda Szary, and

Edward Wass. I would like also to thank Aly Fahmy, Philip Feltz, Salaheldin Hamed, Radwa Omar, Ahmed Shaker, Yahia Tokal, and Ahmed Turk, for their help.

TABLE OF CONTENTS

LIST OF TABLES

LIST OF FIGURES

Chapter 1

Introduction

1.1 Statement of the Problem

Sandwich panel construction has been extensively studied since the fifties. A Polyvinyl Chloride (PVC) foam core reinforced with carbon laminates, one of many configurations available, has been widely used in the marine and aerospace industry. The most commonly used adhesives to join the skin and the core are organic resins. This system has great mechanical and impact resistance properties; however it has very poor fire characteristics. In fact, it was reported that 40 percent of the passengers that survive the impact of an aircraft accident die in a post-crash fire and that 20 percent of accident fatalities are caused by fire (Lyon at al., 1997). It is for this reason that Cost Guards began to prohibit the use of composites in the ships' primary structure except for small size ones (Grenier, 1998).

For fireproof characteristics, the carbon skin is known for its high strength, even at relatively high temperatures (up to 450^{o}C in an oxidizing environment and up to 3000^{o}C in non-oxidizing conditions), and the fact that it does not emit toxins or smokes that are dangerous to inhale. On the other hand, PVC cores have a maximum operating temperature of 70^{o}C and 85^{o}C when used with external skin, and they reach the softening point after 3 to 7 minutes for a 10 mm thick core when exposed to a temperature of 90^{o}C (DIAB, 2007). The enhanced fireproof organic resins soften and lose most of their strength at 200^{o}C, and ignite and emit smokes and toxins at 400-600^{o}C, which are dangerous to inhale (Lyon at al., 1997).

Thus, there is a major need for sandwich panels that have improved fire properties in terms of smoke emission, ignition, and structural integrity to allow the escape of passengers and/or for fire fighters to extinguish fires without the loss of lives.

1.2 Scope and Purpose of the Investigation

This dissertation is part of the ongoing research on inorganic polysialate resin, known as Geopolymer, which is being conducted at Rutgers, The State University of New Jersey. Geopolymer is an inorganic matrix that is known for low curing temperature, low cost, and fireproof characteristics.

Studies have been sponsored by the Federal Aviation Administration (FAA) to evaluate the mechanical properties of Geopolymer and composites made with Geopolymer matrix, and to study their potential use for aircraft components.

In previous research studies were conducted on compatibility of the Geopolymer matrix with different materials like carbon, glass, aramid, steel, balsa, and inorganic materials such as inorganic syntactic foam, clay bricks, and concrete (Hammell, 2000; Papakonstantinou, 2003; Giancaspro, 2004; and Nazier, 2004). Therefore, this study focuses on the evaluation of Geopolymer matrix to fabricate sandwich panels using PVC core. Mechanical properties and the fire characteristics of sandwich panels made with PVC core and inorganic skins were studied.

1.3 Organization of Contents

Chapter 2 provides a basic introduction to the main constituents of sandwich construction materials and configurations. Review of the past work and analytical approaches of sandwich beams are also presented in this chapter.

Chapter 3 presents the mechanical properties evaluation of sandwich beams made out of PVC core and skins fabricated using inorganic matrix. A comparison is made with organic resins to evaluate whether the inorganic system has competitive mechanical properties.

Chapter 4 focuses on the analytical aspects of failure mechanisms in the sandwich beams reinforced with inorganic skin. A mathematical model and a lower bound solution to predict the failure loads are also presented. A comparison is made between the experimental results and the analytical results to evaluate the validation of the mathematical model.

Chapter 5 gives a guide to design sandwich beams using an optimum weight design approach for a given stiffness. Design aids and charts are given to help the designer through the process. A design example is shown to demonstrate the different design alternatives.

Chapter 6 deals with the fire properties of PVC sandwich panels. Panels tested in National Bureau of Standards (NBS) smoke test and the Ohio State University (OSU) heat release at the Federal Aviation Administration (FAA) technology center. Evaluation of the fire properties according to the FAA fire standards is made to investigate its compliance with the FAA standards.

Chapter 7 presents test results of sandwich panels in flexure under elevated temperature. The effect of the core density and number of layers of reinforcement was studied and evaluated at different exposure temperatures.

Chapter 8 provides a preliminary study on the formulation of inorganic core using cenospheres and Geopolymer. Sandwich beams made out of the inorganic core and high alumina fibers are tested in flexure. The mechanical properties are once again evaluated after exposing the beams to 1050^{o}C.

Conclusions and suggestions for future research are presented in chapter 9.

Chapter 2

State of the Art

2.1 Introduction

Sandwich structures are composed of three main components: thin stiff facings, which provide the necessary stiffness and strength, a lightweight core that provides the lever arm for the forces developed into skins through shear transfer, and adhesives that bond the core and the skins. The adhesives also transfer the forces between the core and skins, allowing the various elements to act as one unit. The concept of sandwich beams performance in bending can be seen in figure 2.1, the schematic illustration of typical sandwich beam layers is shown in figure 2.2, and the effect of thickness on the bending strength is displayed in figure 2.3.

Fairbarn described the principles of sandwich structures for the first time in 1849, and its regular application was started during World War II with the "Mosquito" aircraft (Abot, 2000). Today, they are used extensively in aircraft, spaceships, naval ships, automotive, construction, and sports equipments. Even the human skull is made up of two layers of almost fully dense compact bones that are separated by a "core" of lower density foam-like bone. Likewise, the iris leaf is made up of two stiff fiber composite-like outer skins, separated by a core of lower density cells (Triantafillou, 1987). In 2000, every commercial and military aircraft depended on the integrity and reliability offered by lightweight structural cores (Kindinger, 2003).

One main concern with sandwich structures is its vulnerability to fire. It has been estimated that 40 percent of passengers who survive the impact of an aircraft accident, die in a post-

crash fire. Moreover, fires are the cause of twenty percent of all airplane fatalities (Lyon et al., 1997).

Therefore, research was initiated at Rutgers University, funded by the Federal Aviation Administration (FAA), to develop lightweight high temperature resistant composite structural elements. This dissertation is part of that particular research program. The main objective of the research reported in this dissertation to develop lightweight structural panels that will reduce the risk of lives lost in the case of fires either due to toxic smokes, fire progression, or structural failure.

This chapter covers background information on structural sandwich structure materials. The core, skin, and adhesives are presented in detail. Also covered in this chapter is previous work done with various systems, and analytical models and failure assessments.

2.2 Core Materials

The most common lightweight structural cores used are: honeycomb, wood, and foam.

2.2.1 Honeycomb

Honeycomb cores are available for sandwich structures produced form different materials. These materials are:

- Kraft paper: relatively low strength, good insulating properties, available in large quantities, lowest cost
- Thermoplastics (Polyurethane and Polypropylene): Good insulating properties, good energy absorption and/or redirection, smooth cell walls, moisture and chemical resistance, environmentally compatible, aesthetically pleasing, relatively low cost

- Aluminum: Best strength-to-weight ratio and energy absorption, good heat transfer properties, electromagnetic shielding properties, thinnest cell walls, machinable, relatively low cost
- Steel (Carbon steel and stainless steel): Strong, good heat transfer properties, electromagnetic shielding properties, heat resistance
- Specialty metals (Titanium, nickel-base alloys and cobalt base alloys): Relatively high strength-to-weight ratio, good heat transfer properties, chemical resistance, heat resistance to very high temperature
- Aramid fiber: flammability resistance, fire retardance, good insulating properties, low dielectric properties, good formability
- Fiberglass: Tailorable shear properties by lay-up, low dielectric properties, good insulating properties, good formability
- Carbon: Good dimensional stability and retention, high-temperature property retention, high stiffness, very low coefficient of thermal expansion, tailorable thermal conductivity, relatively high shear modulus, very expensive
- Ceramic: Heat resistance to very high temperatures, good insulating properties, available in very small cell sizes, very expensive (Kindinger, 2003)

Honeycombs have various cell configurations; the most common is hexagonal because it is considered one of the most efficient shapes. A reinforcement layer can be fitted in the cellular structure along the nodes in the ribbon direction to form the reinforced hexagonal configuration, having the advantage of increasing the mechanical properties. If the core needs to be curved or formed around one axis, a hexagonal honeycomb, which is over-expanded in the width direction and termed an OX cell configuration, can be used. The OX cell increases shear properties in the width direction and decreases length, or longitudinal

shear properties compared with a hexagonal honeycomb. By narrowing the node relative to the length, a free cell wall results in a square cell configuration, which provides nearly equal shear strength and modulus in the length and width directions. A Flex-Core or double-Flex-Core cell configuration is preferred when compound curvatures are required. A Tube-Core spirally wrapped cylinder or a cross-core cell configuration is used in applications requiring energy absorption or impact resistance. Some of the typical cell configurations are shown in figure 2.4 (Kindinger, 2003).

Given very small bonding area between the core and the skin, honeycomb cores are almost solely used with high performance resin systems so that the required adhesion to the skin can be attained (Giancaspro, 2004).

2.2.2 Wood

Wood can be described as 'nature's honeycomb' as it has a structure that on a microscopic scale, is similar to the cellular hexagonal structure of a synthetic honeycomb. When used in a sandwich structure with the grain running perpendicular to the plane of the skins, the resulting component shows properties similar to those made with man-made honeycombs. However, despite various chemical treatments available, all wood cores are susceptible to moisture attack and will rot if not well surrounded by laminate or resin (SP Systems, 2001).

2.2.2.1 Balsa

Balsa wood density ranges (0.096- 0.288 g/cm^3) which is less than one-half of the density of conventional wood products (0.48- 0.72 g/cm^3). However, it is known by its high specific strength and stiffness when it is compared to other wood. This comparison is shown in table 2.1. The most known type is the end-grain balsa, which gives high compressive strength through the thickness of the sandwich panel. Appearing in the 1940's in flying boat hulls,

balsa wood cores reinforced with aluminum skin were capable of sustaining repeated impact of landing on water. This performance brought the attention of the marine industry to the capabilities of balsa as a core material in the FRP construction. In addition to its high compressive strength, Balsa is a highly efficient insulator against cold and it will not deform when heated. It also acts as an insulating and protective layer in a fire, with the core charring slowly, allowing the non-exposed (inner) skin to remain structurally sound. Moreover, it exhibits high buoyancy and is easily worked and handled with simple tools and inexpensive equipment. One disadvantage of balsa wood is its high minimum density. This problem is intensified by the fact that balsa can absorb very large quantities of resin during lamination. Therefore, balsa wood is normally restricted to projects where optimum weight saving is not required or where locally high-stressed areas are present. The principal uses of balsa wood are for life-saving equipment, floats, rafts, insulation, cushioning, sound modifiers, and models (Miller, 1999; SP Systems, 2001; Giancaspro, 2004).

2.2.2.2 Cedar

Another type of wood sometimes used as a core material is cedar. In marine construction it is often the material used as the 'core' in strip-plank construction, with a composite skin on each side and the grain of the cedar running parallel to the laminate faces. The cedar fibers run along the length of the boat giving fore and aft stiffness, while the fibers in the FRP skins are laid at ±45 giving torsional rigidity, and protecting the wood (SP Systems, 2001).

2.2.3 Foam

Foams are one of the most common forms of core material. They can be manufactured from a variety of synthetic polymers including polystyrene (PS), polyurethane (PU), polymethyl methacrylamide (acrylic), polyetherimide (PEI), styreneacrylonitrile (SAN) and

polyvinyl chloride (PVC). They can be supplied in densities ranging from less than 0.03 g/cm^3 to more than 0.3 g/cm^3, although the most used densities for composite structures range from 0.04 to 0.2 g/cm^3. They are also available in a variety of thicknesses, typically from 5 mm to 50 mm.

2.2.3.1 Polystyrene

Polystyrene foams are used widely in sail and surfboard fabrication, where their lightweight, low cost, and easy to rub down characteristics are of great importance. They are rarely used in high performance component construction because of their low mechanical properties. In addition, they cannot be used in combination with polyester resin systems because the styrene present in the resin dissolves them (SP Systems, 2001).

2.2.3.2 Polyurethane

Polyurethane foams have moderate mechanical properties. One of their major drawbacks is their surface tendency to deteriorate with age at the resin/core interface, causing skin delamination failure. Therefore, their applications are usually restricted to the production of formers to create frames or stringers for stiffening components. However, polyurethane foams can be used in lightly loaded sandwich panels or for thermal insulation. The foam also has relatively high service temperature properties (150°C), and decent acoustic absorption. The foam can be cut and it is machinable to required shapes or profiles (SP Systems, 2001).

2.2.3.3 Polymethyl methacrylamide

Polymethyl methacrylamide (acrylic) foams exhibit some of the highest specific strengths and stiffness of foam cores. They have high dimensional stability, which makes them suitable in using with conventional elevated temperature curing prepregs. Their use is almost limited

to aerospace industry because of their high cost. They are mainly used in the manufacturing of aerospace composite parts such as helicopter rotor blades, and aircraft flaps (SP Systems, 2001).

2.2.3.4 Polyetherimide

As new techniques develop for the blowing of foams from thermoplastics, the range of expanded materials of this type continues to increase. Typical is PEI foam, an expanded polyetherimide/polyether sulphone, which combines outstanding fire performance with high service temperature. Although it is expensive, this foam can be used in structural, thermal, and fire protection applications in the service temperature range –194°C to +180°C. It is highly suitable for aircraft and train interiors, as it can meet some of the most stringent fire resistant specifications (SP Systems, 2001).

2.2.3.5 Styrene acrylonitrile

Styrene acrylonitrile is a common thermoplastic used to make light, rigid, molded products such as piping, golf club heads (used for its good shock absorbance), automotive body parts, wheel covers, enclosures, protective head gear, and toys including LEGO® bricks. It is a copolymer made by polymerizing Styrene and acrylonitrile in the presence of polybutadiene. SAN foams behave in a similar way to toughened cross-linked PVC foams. They have most of the static properties of cross-linked PVC cores, but have higher strain capacity and toughness. They are therefore able to absorb impact levels that PVC foams cannot withstand. SAN foams' toughness properties are inherent in the polymer itself, and therefore do not change with age. SAN foams have a higher temperature performance and better static properties than the PVC foams. Heat-stabilized grades of SAN foams can also be more simply used with low-temperature curing prepregs (SP Systems, 2001; Kindinger, 2003).

2.2.3.6 Polyvinyl chloride

Henry Victor Regnault discovered polyvinyl chloride accidentally in 1835 and in another occasion by Eugen Baumann in 1872. In both incidents, the polymer developed as a white solid inside flakes of vinyl chloride that had been left exposed to sunlight. In 1926, Waldo Semon developed a method to plasticize PVC by mixing some additives, which resulted in a flexible and easily processed material that could be used in commercial applications.

Closed-cell polyvinyl chloride (PVC) foams are one of the most commonly used core materials for the construction of high performance sandwich structures. PVC foams offer a balanced combination of static and dynamic properties as well as good resistance to water absorption. They also have a large operating temperature range of typically -240°C to +80°C, and are resistant to many chemicals. Although PVC foams are generally flammable, there are fire-retardant grades that can be used in many fire-critical applications, such as train components. When used as a core for sandwich construction with FRP skins, its reasonable resistance to styrene means that it can be used safely with polyester resins and is therefore popular in many industries. It is normally supplied in sheet form, either plain, or grid-scored to allow easy forming to shape. There are two main types of PVC foam: cross-linked and uncross-linked, with the uncross-linked foams sometimes being referred to as 'linear'. The uncross-linked foams are stronger, more flexible foams, and are easier to heat around curves. However, these foams have some lower mechanical properties than an equivalent density of cross-linked PVC, and a lower resistance to elevated temperatures and styrene. Their cross-linked counterparts are harder but more brittle and will produce a stiffer panel, which in turn is less susceptible to softening or creeping in hot climates. A new generation of toughened PVC foams is becoming available now, which trades some of the basic mechanical properties of the cross-linked PVC foams for some of the improved toughness of the linear

foams. Owing to the nature of the PVC/polyurethane chemistry in cross-linked PVC foams, these materials need to be thoroughly sealed with a resin coating before they can be safely used with low-temperature curing prepregs. Although special heat stabilization treatments are available for these foams, these treatments are primarily designed to improve the dimensional stability of the foam and to reduce the amount of gassing that is given off during elevated temperature processing (SP Systems, 2001).

2.2.3.7 Comparison of Core Materials

The shear and compressive strengths of core depends on the core density. The relation between the core mechanical properties and the density is shown in figure 2.5. The different materials show an increase in both shear and compressive strength as the core becomes more dense. It should be noted that this comparison is for only the core material. When skins are added, it should be looked at as a sandwich structure. For example, low-density polymeric foam materials, while contributing only slightly to the weight of a sandwich laminate, often have a very open surface cell structure, which can allow a large mass of resin to be absorbed. Thus, the total weight of the sandwich structure will increase dramatically. Generally, as the density of the foam decreases, the void ratio increases, and this problem becomes more severe. Honeycombs, however, do not face this problem since a well-formulated adhesive will form a small bonding fillet only around the honeycomb cell walls. Other aspects should be considered when comparing the different core materials such as: Moisture resistance, chemical resistance, flammability resistance, energy absorption, fatigue strength, abrasion resistance, acoustic attenuation, and cost. Depending on the application and its requirement, the suitable core material can be chosen. A comparison between

honeycomb, balsa, and foam is shown in table 2.2, and a demonstrative relation between the performance and cost of the various core materials is shown in figure 2.6.

2.2.3.8 Syntactic foam

The term syntactic is taken from the Greek word "syntaktikos" which means to put together. Syntactic foams consist of a polymer matrix called the binder and gas-filled aggregates (filler). The filler is in the form of hollow spherical particles, called microspheres, microcapsules or microballons, dispersed within the matrix (Shutov, 1982).

The microspheres are composed from a thin shell filled with gas, which allows the cellular structure to be much lighter than one containing compact filler from the same material.

The filler microspheres may be glass, polymeric, carbon, ceramic, or metallic. The main requirements for the microspheres are to be spherical, non-cohesive, strong, intact, moisture and chemically resistant, and hydrolytically stable. Some additional specification may be needed depending on the application, for example if high-temperature resistance is required.

The foam cellular structure depends on the size, content, and distributive uniformity of the filler. The final material is granted to have a completely enclosed cells, and it is for this reason that they are called "absolute closed-cell foams". Additionally, all the microspheres have the same size and are uniformly dispersed in the matrix. Thus, syntactic foamed materials have better specific strength than conventional chemically or blown foamed plastics (Shutov, 1983).

Some of the commercially available microspheres are: 3M™ Bubbles like Scotchlite™ and Zeeospheres™; Fillite™, also known as Cenospheres™; Perlite; and Macrolite®. These commercially available microspheres have been widely used as aggregates in the production of lightweight concrete.

Perlite is not a trade name but a generic term for naturally occurring siliceous rock. The distinguishing feature between Perlite and other volcanic glasses is that when heated to a certain point in its softening range, it expands from four to twenty times its original volume. This expansion is due to the presence of two to six percent combined water in the crude Perlite rock. When quickly heated to above 871°C, the crude rock pops in a manner similar to popcorn as the combined water vaporizes and creates countless tiny bubbles which account for the amazing lightweight and other extraordinary physical properties of expanded Perlite. The different types of Perlite can be see in figure 2.7 (Perlite & Redco II, 2003) .

Macrolite, a processed mineral oxide manufactured by Kinetico, is used as an efficient filter media for the removal of oxidized iron and suspended matter. It is chemically inert and is not affected by acids and bases. Tests have shown that its attrition rate is nearly zero (Kinetico, 2007).

The Fillite™ is extracted from crushed fuel ash, derived from coal-fired power stations. Fillite™ or Cenospheres™ are aluminosilicate based and are used as lightweight fillers with applications in a variety of industrial and commercial products. Fillite Cenospheres are fillers typically used to replace minerals and resins where the benefits may be as diverse as weight reduction, improved thermal insulation, reduced shrinkage, and improved fire resistance. A scanning electron photomicrograph (SEM) for the Fillite™ spheres can be seen in figure 2.8 (Trelleborg, 2007).

3M™ glass bubbles are manufactured through a multi-step process in which glass is formed at high temperature from soda-lime-borosilicate milled to fine particle size, and then run through a high-temperature heat transfer process. During this process the viscosity of the glass drops to a level at which surface tension causes the particle to form a perfect sphere. High temperature then causes a latent blowing agent in the glass to decompose to a gas, and

the pressure of this gas causes the particle to expand from a small, solid sphere to a larger, hollow sphere. This trapped gas is at approximately one-third atmosphere, greatly contributing to the low density of 3M™ Glass Bubbles (3M™, 2007).

A comparison between some of the different commercially available microspheres is shown in table 2.3.

2.3 Reinforcing Skin

The main function of the reinforcement skins in sandwich structure is to generate tensile and compressive force to form a couple and generate moment resistance. The fiber reinforcement is the principal constituent in a fiber-reinforced composite skin and occupies the largest volume fraction in a composite laminate comparing to the matrix. The commercially available fibers have varying properties and consequently, affect the properties of the resulting composite (Mallick, 1993). The typical fiber reinforcements used in the composite industry are glass, carbon, aramid, and ceramic fibers. The properties and characteristics of these fibers are explained in more details in the following sections.

2.3.1 Glass fibers

Glass fibers are the most common of all reinforcing fibers used in fiber composite polymers (FRP) and are conventionally called GFRP or glass fiber composite polymers. The key advantages of GFRP include low cost, high tensile strength, excellent chemical resistance, and fine insulating properties. The main drawbacks of glass fibers include low tensile modulus, sensitivity to abrasion with handling, relatively low fatigue resistance, and high hardness (Giancaspro, 2004).

The two most common types of glass fibers used in the fiber-reinforced plastics industry are Electrical glass (also known as E-glass) and Structural glass (commonly referred to as S-

glass). Other less common types include Chemical glass (or C-glass) and Alkali-Resistant glass (or AR-glass) (Giancaspro, 2004).

2.3.2 Carbon fibers

Carbon fibers have the highest modulus of all commercially available reinforcing fibers. The main advantages of carbon fibers are their high tensile strength-to-weight ratios as well as high tensile modulus-to-weight ratios. Composites made from carbon fiber are five times stronger than grade 1020 steel for structural parts, yet are still five times lighter. In comparison to 6061 aluminum, carbon fiber composites are seven times stronger and two times stiffer, nonetheless 1.5 times lighter (Walsh, 2003). Carbon fibers have high fatigue strengths as well, and a very low coefficient of linear thermal expansion and, in some cases, negative thermal expansion. This feature provides dimensional stability, which allows the composite to achieve near zero expansion to temperatures as high as 300°C in critical structures such as spacecraft antennae (Giancaspro, 2004). As an inorganic material, carbon fibers are not affected by moisture, atmosphere, solvents, bases, and weak acids at room temperature (Judd, 1971). However, oxidation becomes a problem at elevated temperatures for low-modulus, PAN-based fibers and high-modulus, PAN- or pitch-based fibers. The threshold for oxidation for extended operating times is 350 °C or 450 °C, respectively. Impurities tend to catalyze oxidation at these low temperatures and somewhat improved oxidation resistance can be expected with higher-purity fibers (McKee, 1981).

Precursor sources used in the carbon fibers processing operation are PAN (polyacrylonitrile), pitch, and rayon. Although the specific processing details for each precursor are different, the basic sequence is almost the same, involving spinning,

stabilization, carbonization, and the application of a finish or sizing to facilitate handling, as shown in figure 2.9. Discontinuous carbon fiber whiskers are also now produced in a batch process from hydrocarbon gases using a vapor-liquid-solid growth mechanism (Walsh, 2003). The basic mechanical properties of PAN-based and pitch-based carbon fiber are presented in table 2.4 and table 2.5.

2.3.3 Aramid

Aramid fiber is a synthetic organic polymer fiber (an aromatic polyamide) produced by spinning a solid fiber from a liquid chemical blend. Aramid fiber is bright golden yellow in color, and is most commonly known as "Kevlar®," its DuPont trade name. The key properties for these fibers are their low specific gravity, high tensile strength, excellent impact resistance, good abrasion resistance, good chemical resistance, and good resistance to thermal degradation. They are 43% lighter than glass and approximately 20% lighter than most carbon fibers. However, the predominant drawbacks of Kevlar® fibers include a low compressive strength, degradation when exposed to ultraviolet light for some grades, and considerable difficulty in machining and cutting due to its high shear strength. At the same time this drawback is considered an advantage because it allows its application as ballistic protective material such as bullet proof vests (Giancaspro, 2004).

2.3.4 Ceramic fibers

Ceramic fibers, in this case, deal with the continuous-length fibers that are used to reinforce ceramic-matrix composites (CMC). They are usually produced by spinning and heat treating chemically derived precursors. There are two types of ceramic fibers: Oxide fibers and non-oxide fibers. Oxide fibers are based on the alumina-silica (Al_2O_3-SiO_2) system and on α-alumina (α -Al_2O_3), while non-oxide fibers are based primarily on β -phase silicon carbide

(SiC). These fibers are typically produced with small diameters (<20 μm) and in polycrystalline form with small grain sizes (<1 μm). The polycrystalline fibers are easier to handle and have lower fabrication costs, but less temperature and creep resistance. However, the performance of CMC's reinforced with ceramic fibers can compete with metallic alloys at low and elevated temperature (Wilson, 2003).

The oxide-based fibers can be used in temperature up to 1100 °C. Their key advantages are low cost compared to non-oxide-based fibers, chemical stability, and corrosion resistance. They can be used in many applications, such as sleeves for pipes and electrical cables, high-temperature shields, and gasket seals. Typical properties for commercially available oxide-based fibers are shown in table 2.6 (Wilson, 2003).

The non-oxide-based fibers can be used in temperature greater than 1100 °C. They have better creep resistance and strength retention under combined conditions of temperature and stress. They also have higher thermal and electrical conductivity. Nevertheless, under oxidizing conditions, the exposed surface of silicon-based fibers will disintegrate slowly due to the silicon reacting with oxygen forming silica. Hence, when such conditions exist, SiC-based fibers are preferable for their good oxidation resistance. Extensive efforts are being made to use SiC/SiC CMC in gas turbine engines for components that require service for long hours under combustion gas environments. Typical properties for commercially available non-oxide-based fibers are shown in table 2.7 (Wilson, 2003).

2.4 Matrix

The main functions of the matrix in a composite are:

- Holding the fibers together in a structural unit
- Protecting the fibers from external damage

- Transferring the loads to the fibers
- Contributing in needed properties like ductility, toughness, electrical insulation or high-temperature resistance

The matrix and fibers must be chemically compatible to prevent any undesired chemical reaction on the fibers' surfaces, which may affect the bond strength between the two or may even cause the disintegration of the fibers. This problem seems to be more severe in a high-temperature composite (Gibson, 1994).

Generally, matrices are divided into two main classes based on the chemical composition. They are divided into organic matrices and inorganic matrices, each of these will be discussed in more detail.

2.4.1 Organic resins

Organic resins or polymers are the most widely used matrix material in the world of composites. Polymers can be classified under two types: thermoplastic and thermoset, according to the type of the cross-links formed between the molecules which greatly impact the effect of heat on their properties (Gibson, 1994).

Thermoset resins form three-dimensional molecular cross-links during the curing process. Consequently, once cured, the molecules cannot be melted or reshaped. The higher the density of the cross-linking, the more rigid and thermally stable the resin will be. The resin may soften at high-temperatures, which may be used to create a bend or a curve. The most common used thermoset resins are epoxy, polyester, vinylester, phenolics, cyanate esters, bismaleimides, and polymides (Gibson, 1994; Mazumdar, 2002). The continuous-use temperatures for these resins are shown in figure 2.10 and some of their basic mechanical proprieties are shown in table 2.8.

Thermoplastics do not form cross-linked chains during the curing process which in turn gives them the ability of melting by heating then solidifying again by cooling. They are more flexible and tougher than the thermoset resins. Thermoplastcis can be either amorphous or semi-crystalline. They have very low creep resistance especially in elevated temperature. Typical thermoplastics include nylon, polypropylene (PP), polycarbonate, polyether-ether ketone (PEEK), and polyphenylene sulfide (PPS) (Mazumdar, 2002). The continuous-use temperature ranges are shown in figure 2.11 and some of the properties are shown in table 2.9.

2.4.2 Inorganic resin

The main advantage of using inorganic resins is their ultra high temperature resistance. It was reported that none of the organic resins are heat resistant and that nature states that only minerals can provide heat and fire resistance. In the aftermath of several catastrophic incidents in France between 1970 and 1973 involving plastic materials, Joseph Davidovits worked on developing a new inorganic polymer. This polymer was based on geophysics and geochemistry so it was patent as Geopolymer and it is also known as polysialate. (Davidovits, 2002).

Since the characteristics of such a polymer are crucial for the aircraft industry, The Federal Aviation Administration (FAA) has been sponsoring research programs to evaluate the mechanical properties of Geopolymer matrix composites as part of an initiative to research fireproof material for aircraft interiors. The best indicator for its fire resistance was the flashover time obtained from the ISO 9705 room corner test. Flashover occurs in a closed compartment when flammable gasses from incomplete material combustion are heated to the ignition point. This puts an end to the lives of survivors in a plane in aircraft post-crash

scenarios. The performance of Geopolymer was compared to the different resins available and its importance is proven in figure 2.12 (Lyon, 1997). Research was conducted in Rutgers University and elsewhere to evaluate the properties of the new polymer and its potential use.

The research at Rutgers University started with tests to evaluate the properties of an unreinforced Geopolymer matrix in tension, flexure, compression, strain capacities and surface energy. The mechanical properties of the matrix reinforced with several fabrics like SiC and carbon were evaluated for samples exposed to temperatures from 200 to 1000°C. An example of the remaining flexural strength of samples using different resins is shown in figure 2.13. The optimum curing process to minimize the void content and to maximize the volume of fibers and subsequently, the flexural strength, was reported to be 80°C under 3 MPa pressure. It was found that the polysialate composites were brittle and that the Geopolymer matrix was compatible with carbon and SiC fibers. It was also determined that the stiffness of beams made of polysialate composites did not decrease under cyclic loading (Foden, 1999).

The influence of reinforcement type in inorganic laminate composites was evaluated. It was shown that carbon laminates using Geopolymer resin can achieve a flexural strength as high as 510 MPa. Because of the high alkali nature of the matrix, glass fibers degraded and the fibers fused with the matrix giving only 100 MPa. Steel wire meshes gave 140 MPa of flexural strength but they exhibited a much more ductile behavior than carbon and glass laminates. It was shown that the wet-dry resistance depended on the silica/alumina ratio as well as the curing temperature. The reduction in silica/alumina ratio will result in a more durable matrix. The composite maintained 53% of its flexural strength and 30% from the flexural modulus after one hour exposure to 600°C. It was reported that the optimum temperature for strength and durability is 150°C and strength decreased when cured to

200°C. It was also reported that the shrinkage of the matrix was one of the Geopolymer drawbacks and is the cause of some mechanical strength loss (Hammell, 2000).

The application of a Geopolymer matrix widened to include its usage as a protective coating for concrete structures. The durability studies of the coating included wetting and drying, freezing and thawing, and scaling. The results for the wet-dry and scaling tests are shown in figures 2.14 and 2.15. After testing concrete beams strengthened with Geopolymer/carbon systems, it was concluded that it was feasible to strengthen concrete structures with the inorganic system. The Geopolymer is very compatible with concrete structures as the constituent materials of the coating chemically react with the concrete. The Portland cement used in concrete is a calcium aluminosilicate system where as the cement in the coating is potassium aluminosilicate. Any free hydroxide in concrete will react with silica in the coating and vice versa. Because of its compatibility with concrete, delamination failure could be eliminated with the proper design, while it is a major problem with organic systems. In addition to its dominance in terms of adhesion, it does not involve any toxic substances and leftovers can be treated as ordinary waste, which is a very important aspect in construction. Steel beams were also reinforced with inorganic systems. These tests showed that Geopolymer could be effectively used as a protective coating for steel but to strengthen steel, large carbon areas were needed (Garon, 2000).

Syntactic foam was produced by mixing ceramic spheres (Macrolite™) with a Geopolymer matrix. Different mixing ratios and sphere sizes were used. The syntactic foam was tested in tension and compression, and had the values of 3.7 and 39 MPa, respectively. The samples retained their compressive strength after exposure to 800°C for 15 minutes. Other samples were made by mixing polystyrene spheres with the polysialate resin giving compressive strength of 0.1 MPa for density of 0.088 g/cc. Fire properties of the two types of syntactic

foam were evaluated by testing them in "Ohio State University (OSU)" and the "NBS Smoke Burner" smoke tests, which are the main FAA fire cabin safety tests. Despite the exhibition of flaming combustion for the polystyrene samples, all samples passed the FAA criteria. Sandwich panels were made with the syntactic foam core and reinforced with glass, Ar-glass, carbon, Nicalon fabrics, and tows. The sandwich panels' degradation was negligible up to 400^{o}C. At higher temperatures, the skin degraded faster than the core (Papakonstantinou, 2003).

More hybrid laminates were prepared and tested. It was concluded that during the preparation that the 12K high modulus carbon was easier to handle and that more than 1% sizing was damaging the composite strength. The optimum pressure for E-glass/Geopolymer composites was 1 MPa and for carbon/Geopolymer composites this pressure was found to be 3 MPa. Flexural strength of E-glass composites could reach 122 MPa. The results obtained from the witness panels showed that carbon and aramid composites retained some load after the initial fracture, while E-glass composites showed no post-peak strength. This confirmed the conclusion reached by Hammell earlier, that glass fibers become fused because of the alkali nature of the resin. The 12K high modulus carbon composites had a modulus of elasticity of 576 GPa. In addition to the hybrid laminates, sandwich beams were fabricated using balsa wood as a core material and different inorganic composite skins as reinforcement. In addition, comparisons were made with similar organic sandwich beams. After running some flexural tests, it was concluded that it was feasible to fabricate sandwich beams using balsa and Geopolymer based composites. High modulus carbon provided the best strength increase and that the increase in fiber area caused a consistent increase in flexural stiffness. By comparing the beams reinforced with organic composites, it was concluded that the bond between balsa wood and organic reinforcements

was poor as some delamination failures occurred, which did not happen with reciprocal inorganic beams. The beams reinforced with organic skin had 70% more moment capacity and almost the same flexural stiffness. Bare balsa wood and reinforced panels were tested in the OSU and NBS smoke tests. The results, demonstrated in tables 2.10 and 2.11, show that the bare panels and panels reinforced with organic skins failed the FAA passing criteria and only the samples reinforced with Geopolymer-based skins passed (Giancaspro, 2004).

Inorganic composites were used to strengthen concrete and clay brick walls in shear. The gained strength was about the same as the strength provided by organic composites. The same conclusions were found for masonry bricks reinforced for out-of-plane loadings. Extensive research was done on applying the Geopolymer based resin as a protective coating for concrete structures. Because of the growing graffiti problem, the Geopolymer mix could be modified to be graffiti-proof and color pigments could be added to the mix to give the concrete a protective and decorative coating. A demonstrative example on the graffiti-proof nature of a Geopolymer coating is shown in figure 2.16. Only dry cloth was used to remove the graffiti and no special procedures were needed (Nazier, 2004).

2.5 Common configuration of sandwich panels

Since sandwich panels applications are used for wide variety of applications, different types of cores, facings and adhesive, where combined create thousands of configurations. The most common configurations, their applications, their advantages, and their disadvantages are presented in this section.

2.5.1 Metal facings/plywood core (or particle board)

Steel or Aluminum can be used as facings with plywood or particle board core. The facings act as a protective layer for the core while also as they increasing the strength and stiffness. It

is for this reason that they are typically used in building construction and industrial applications. The main advantages of this type of system are that it is highly resistant to puncture, readily available, and is much more rigid than raw plywood. The disadvantages are the sandwich panel can be heavy, is not fire-resistant, and it is moisture absorbent; consequently allowing the metal facings to corrode if they are not treated (M.C. Gill, 1997).

2.5.2 Metal facings/foam core

The main characteristics of this type of system are that they have relatively low weight and are low cost. It has very good resistance for point load and impact load. On top of all previously mentioned, it has excellent thermal insulation properties, which qualified it to be used in non-structural applications, such as refrigerated carts. The main significant weaknesses of this type of system include corrosion to the metal facings, delamination, low service temperatures, poor fatigue resistance, and high smoke evolution (M.C. Gill, 1997).

2.5.3 Fiberglass reinforced plastic (FRP) facings/foam core

Foam core panels reinforced with FRP facings are broadly used in commercial refrigeration construction. This configuration has some advantages including a low purchase cost for commodity type foams, very low panel weights, superior thermal insulation, low moisture absorption, and very good corrosion resistance, since no metallic parts are involved. However, these types of panels have little resistance to repetitive flexure, can delaminate easily, and have high smoke evolution in a fire (M.C. Gill, 1997). Nevertheless, this system when used with structural grade foams and facings can be applied in several structural applications, such as marine and aerospace applications; and most of the disadvantages can be trounced.

2.5.4 Aluminum Facings / Aluminum Honeycomb Core

This system is a very common sandwich construction first used in the aerospace industry. It possesses a high specific strength (strength-to-weight ratio), excellent rigidity, and a reasonably low cost. Many different combinations of different core configurations, facing thicknesses, and alloys can be constructed. This system has non-burning and non-smoking properties, but very poor burn-through and high-heat conduction. Also, Corrosion is a major problem with this system especially that it is predominantly aluminum metal. The aluminum is also subject to denting and permanent distortion, point load failure. If the facing is punctured, the aluminum honeycomb cells may fill with liquid (M.C. Gill, 1997).

2.5.5 Aluminum facings/Balsa wood core

This system has been used in aircrafts for more than 40 years. It has very good stiffness and core shear resistance, good thermal insulation properties, and very good point load resistance. The main disadvantages include corrosion problems for aluminum facings, as mentioned earlier, relatively heavy weight; since only two core weights are available (0.1 and 0.15 g/cc), aluminum facings are less dent resistant than FRP, the edges between the core and facings are not sealed properly with the correct adhesive, the panel can absorb water (M.C. Gill, 1997).

2.5.6 Fiberglass reinforced plastic (FRP) facings/Balsa wood core

This system has a woven fiberglass cloth fused to the balsa core so very little adhesive is used. Moreover, this system has excellent dent and point load resistance. It is completely non-metallic and hence, corrosion resistant, radar transparent, and has a relatively low cost. The main drawbacks to this system are that water absorption can occur if the edges are not properly sealed and it is relatively heavy (M.C. Gill, 1997).

2.5.7 Fiberglass reinforced plastic (FRP) facings / Nomex® honeycomb core

Nomex® honeycomb is made of aramid fiber papers and is a very resilient core material. Reinforced with either woven or unidirectional fiberglass, this type of panel is commonly used for aircraft flooring as well as other interior panels. It is advantageous in that it is highly fatigue resistant, lightweight, radar transparent, and can be formed into simple curves. The main disadvantages are its edge delamination tendency; high smoke emission level, if using an epoxy adhesive and facing resin, a high initial cost, and the honeycomb cells may fill with a liquid if the facing is punctured (M.C. Gill, 1997).

2.5.8 Carbon – phenolic / Nomex® honeycomb core

This system is relatively new and it is made from unidirectional or woven carbon facings reinforcing a Nomex® honeycomb core. It is considered one of the most expensive systems, which limits its use to the aircraft and aerospace industry. Obviously, it is much more firm than other panels of the same weight, and when used with different facings, its thickness allows good flexibility in design. This system has excellent fatigue resistance and can sustain repetitive high-pressure loading, such as in caster wheels and stiletto heels. When exposed to fire, the phenolic facing resin prevents high smoke emission levels. The most significant disadvantages include a high initial cost, required edge treatments, and the honeycomb cells may fill with liquid if punctured. In addition, galvanic corrosion can take place between the carbon facings and adjacent metallic materials unless protected with fiberglass overlays and / or stainless steel, or expensive titanium (Giancaspro, 2004 and M.C. Gill, 1997).

2.6 Methods of analysis

The analyses of sandwich beams have been studied extensively. A review of the different analysis methods is presented in this section. The review of analytical work presented here could be divided into three main categories:

- Static bending theories for laminated composites
- Failure analysis for sandwich construction
- Methods of optimization

2.6.1 Static bending theories for laminated composites

First, it should be mentioned that all theories do not account for delamination, and they deal with reinforcing skins of uniform thickness. The beam span divided by beam depth is defined as the aspect ratio, which is used to classify the beams from thin to thick. The beam is considered thick, if the aspect ratio is smaller than 4, moderately thick for ratios between 4 and 10, and thin for ratios greater than 10 (Abot, 2000). The mathematical theories that dealt with composite laminated plates have been based on one of the following approaches:

1. Equivalent single-layer theories (2-D)
    - Classical laminated plate theory
    - Shear deformation laminated plate theory
2. Three-dimensional elasticity theory (3-D)
    - Traditional 3-D elasticity formulations
    - Layer-wise theories
3. Multiple model methods (2-D and 3-D)

The equivalent single layer theories are derived from 3-D elasticity theory. Byy making the necessary simplifications and assumptions dealing with the kinematics of deformation or the

state of stress through the thickness, this allows the reduction to a 2-D problem. A comparison between the various theories, finite element modeling, and experimental results is shown in figure 2.17. The three-dimensional elasticity theories consider each layer as a 3-D solid (Reddy, 2004).

2.6.1.1 Classical Laminated Plate Theory

The classical laminated plate theory or CLPT for short is based on the classical plate theory by Kirchoff. From Kirchoff's hypotheses, it is assumed that straight lines perpendicular to the midsurface remain straight, the transverse normals do not experience elongation, and the transverse normals rotate such that they remain perpendicular to the midsurface after deformation. Additionally for the laminated plate theory, it is assumed that the layers are perfectly bonded, the material of each layer is linearly elastic and orthotropic, each layer has a uniform thickness, the displacements are small, and the transverse shear stresses on the top and bottom surface of the laminate are zero (Abot, 2000 and Reddy, 2004).

These assumptions and approximations are acceptable for thin, homogeneous beams. Shear deformation can not be neglected in thick beams (Abot, 2004).

2.6.1.2 Shear deformation laminated plate theory

The shear deformation theory is a refinement applied to add more shear deformation. It could be reached by modifying one of the Kirchoff hypotheses; that transverse normals do not remain perpendicular to the midsurface after deformation. The first order shear deformation laminate plate theory assumes a first order displacement field. And another assumption is made that the shear strains are constant through the thickness. Shear correction factors could be used to account for the parabolic nature of the shear strains

(Reddy, 2004). By considering shear deformation, the solution is acceptable for thin and moderate thin beams but not for thick laminates (Abot, 2004).

By assuming higher order displacement fields, the kinematics of thick laminates could be described better and the shear correction factor may not be needed. The major drawbacks of the Higher-order theories are that they require more computational effort and are difficult to interpret physically (Reddy, 2004).

2.6.1.3 Layer-wise theories

In the layer-wise models, the plate is divided in a number of layers. Piecewise approximations are then made for the variables in the thickness and direction in each layer. Each layer can have linear, quadratic or higher-order polynomials or even trigonometric functions to describe the displacement field. The layer-wise theories are very powerful to model moderate thick and thick beams. The number of independent variables is directly proportional to the number of layers. As the number of layers or pieces increases, the accuracy of the solution and the computational effort increases (Abot, 2004).

2.6.2 Failure Analysis

2.6.2.1 Previous work summary and review

Sandwich panels can fail in several ways and in a complex manner. The failure can be caused by skin material failure or core failure. The faces and cores can yield plastically or fracture depending on the nature of materials from which they are prepared. Delamination can cause the failure by loosing the bond between the core and the skin. Compression failures in the skin are more likely, especially due to local buckling of the compression skin, or as "wrinkling" failure (Triantafillou, 1987).

For a given loading configuration, failure mode maps were constructed for sandwich beams with rigid polyurethane foam aluminum faces. The face thickness to span length ratio and the core relative density determine the failure mode to be face yield, face wrinkling, and core shear (Triantafillou, 1987).

Aluminum honeycomb and PVC foam cores reinforced with carbon/epoxy systems were tested and different failure modes were detected. Failure modes were found to be highly dependent on the material properties, geometric dimensions, and type of loading. High density core was found to follow the Tsai-Wu failure criteria for a two-dimensional state of stress. Three-point and four-bending tests were preformed on simply supported and cantilever beams. A map between the span length and the failure critical load was drawn for the given loading conditions and cross sections. As a result, the failure mode between core failure and face wrinkling could be determined (Daniel, 2002; Daniel, 2003). A special attention was made for the wrinkling failure by testing columns and beams made from the aforementioned sandwich system. It was found that no wrinkling failures occur with honeycomb cores which was credited to the honeycomb's high stiffness in the through-the-thickness direction. It was found that wrinkling failure loads depended on the elastic tensile and shear moduli. It was also concluded that wrinkling may occur while the core is still in the linear elastic range, which is more likely to happen with thin long beams. If the core degraded, the critical wrinkling stress was reduced dramatically (Gdoutos, 2002).

Polyurethane foam cores reinforced with carbon/epoxy facings were tested. The predicted failure loads were calculated based on the classical and first shear deformation theory, which failed in accurately predicting the failure loads when compared to experimental results. The elasticity solution along with failure criteria gave better predicted values for the failure load (Swanson, 2003).

In another study, Polystyrene and PVC foams were used together as core and the skin was used as carbon, glass, and Kevlar®. Bending and compression tests were preformed on the constituent materials as well as the sandwich structures. It was found that the failure of the top skin was initiated by local wrinkling on the compression side and that the fracture stress was higher for carbon than glass and Kevlar®. The deformation to failure was the lowest in systems reinforced with Kevlar®, but the wrinkling failure was not sudden like the other systems. Finite element analysis was carried out to simulate the response of the structure during different tests. The analysis predicted the behavior in the elastic zone correctly, but it could not show a good compatibility in the post-elastic zone. An example of the experimental load-deflection curve and its correspondent FEM is shown in figure 2.18 (Borsellino, 2004).

Using vacuum-assisted resin transfer molding, PVC foam and balsa wood cores reinforced with E-glass/epoxy system were tested in flexural, in three-point and four-point bending. Failure in thick beams was found to be initiated by the core because of the high shear stress. Balsa cores failed along the grains (the thickness direction), which led to face delamination. However, the PVC core yielded without cracks, while thin beams failed in the tension skin. When it is compared to balsa core, PVC core preformed better with thick beams than thin beams (Dai, 2003). One can notice that no compression skin failure was detected in this study.

Composite Sandwich beams were fabricated using PVC foam cores and glass/vinylester face sheets. These beams were tested in three-point bending with simply supported and clamped configurations to investigate the failure modes. It was found that face wrinkling, core shear, and indentation, were the initial collapse mechanisms. Based on the experimental results, wrinkling failure was dominant in simply supported configurations; while tension yield was

the dominant mode of failure with the clamped boundary conditions. An analytical and an FE model were introduced. The FE model was adjusted to account for the predicted mode of failure based on the experimental results. For simply supported conditions, this could be achieved by modeling the face sheets as elastic-perfectly plastic material, with compressive yield strength equal to the wrinkling stress. Conversely for the clamped conditions, the face sheets were modeled as linear elastic material (Tagarielli, 2004). By modifying the model, the FE method could predict the behavior even for the post-peak region. The comparison between experimental, analytical, and FE model is shown in figure 2.19.

2.6.2.2 Summary of previous work

By examining the previous work, it can be concluded that the main failure modes are tension yield in the face, core shear, wrinkling, indentation, and delamination. The failure mode is highly dependent on the sandwich beam geometric dimensions, supporting conditions, and materials used. Therefore, an experimental program is needed whenever new configurations are intended for use. The different analytical models available can be either calibrated or modified to better predict the failure loads for the different configuration.

2.6.3 Minimum weight optimization

The minimum weight design is considered the main goal for any engineering design aspect, especially when it comes to sandwich structures. The main objective behind using the sandwich structure concept is to minimize the weight and maximize the strength and/or stiffness. In other words, the main purpose is to maximize the strength-to-weight and/or stiffness-to-weight ratios.

For sandwich beams with aluminum skins and polyurethane foam cores, analysis was made based on deflection of the beam to be the sum of bending and shear deflection, and on the

observation that the shear modulus of polyurethane foam cores is proportional to the square of its density. An experimental study was preformed to support the analysis method to minimize the weight for a given stiffness for the aforementioned system (Gibson, 1984).

A model was developed to minimize the weight of circular sandwich plates with aluminum skins and polyurethane foam cores for a given bending stiffness. The model was used to identify the core density as well as the face thickness (Demsetz, 1986).

Beams with PVC foam core and E-glass/vinylester faces were tested in three-point and four-point bending. Using optimization techniques, the system could be minimized for weight, and stiffness; while skin and core thicknesses could be found (Lingard, 1993).

Beams with PVC foam cores and woven glass/epoxy skin were optimized for strength in three-point bending and simply supported conditions. The optimization method introduced in the form of failure mechanism maps and contours by which the minimum weight could be determined in terms of the core depth-to-span ratio and the facing thickness to core thickness ratio (Steeves, 2004-a). An experimental investigation was carried out to support the analytical results. It was again concluded that simple beam theory was not appropriate for thick beams, but it gave good quality results for thin beams (Steeves, 2004-b).

Table 2.1 Mechanical Properties of balsa compared to other wood (Giancaspro, 2004)

Species	Weight (lbs/ft^3)	Stiffness	Flexural Strength	Compressive Strength	Specific Stiffness	Specific Flexural Strength	Specific Compressive Strength
Balsa	8	72	70	75	9	9	9
Balsa	**10**	**100**	**100**	**100**	**10**	**10**	**10**
Balsa	14	156	161	149	11	12	11
Spruce	28	230	260	289	8	9	10
Yellow Pine	28	222	277	288	8	10	10
Douglas Fir	30	241	291	341	8	10	11
Hickory	50	379	638	514	8	13	10
Oak	48	295	430	366	6	9	8
Basswood	26	261	288	288	10	11	11
Black Walnut	37	301	506	512	8	14	14

Table 2.2 Comparison of selected properties for different core types (Kindinger, 2003)

Property	**Honeycomb**	**Balsa**	**Foam**
Density (g/cm^3)	Expanded: 0.032-0.19 Corrugated: 0.16-0.88	0.096-0.29	0.032-0.3
Moisture Resistance	Excellent	Fair	Excellent
Chemical Resistance	Fair to Excellent	Fair to very good	Fair to very good
Flammability Resistance	Excellent	Poor	Fair to Excellent
High-Temperature Resistance	Adhesive bonded: to 177°C Braze welded: 370°C to 815°C depending on material	to 95°C	to 80°C; varies by type Mechanical properties decrease significantly at higher temperatures
Strength and Stiffness	Excellent	Excellent	Fair
Energy absorption and crush strength	Fair to Excellent	Very good	Fair to poor
Fatigue strength	Good to Excellent	Very good	Fair to poor
Abrasion Resistance	Good integrity	Fair	Friable
Acoustic attenuation	Yes	Yes	Yes
Formability	Various cell configurations for different shapes	Must cut, or use joined strips	Requires molds or scoring
Cost	Inexpensive (kraft paper) to very expensive (carbon)	Moderate	Very inexpensive (polystyrene) to expensive (polymethacrylimide)

Table 2.3 Comparison between some of the commercially available microspheres

	Color	Diameter (microns)	Density (g/cc)	Particle Crushing Strength (MPa)	Melting Temperature ^{o}C
Macrolite™	Gray	500-2800	0.40-0.49	NA	1100
Perlite	White	75-4000	0.04-0.4	NA	1250
Fillite™	Gray	5-500	0.35-0.45	10.3-20.6	1200-1350
Scotchlite™	White	11-120	0.125-0.6	1.7-124	600
Zeeospheres™	White or Gray[1]	1-200	2.1-2.5	414	1020

[1] depends on the grade

Table 2.4 Properties of PAN-based carbon fibers (Walsh, 2003)

Property	Commercial, standard modulus	Aerospace		
		Standard Modulus	Intermediate Modulus	High Modulus
Tensile Modulus, GPa	228	220-241	290-297	345-448
Tensile Strength, Mpa	380	3450-4830	3450-6200	3450-5520
Elongation at break, %	1.6	1.5-2.2	1.3-2	0.7-1
Density, g/cc	1.8	1.8	1.8	1.9
Filament diameter, μm	6-8	6-8	5-6	5-8

Table 2.5 Properties of Pitch-based carbon fibers (Walsh, 2003)

Property	Low Modulus	High Modulus	Ultra-High Modulus
Tensile Modulus, GPa	170-241	380-620	690-965
Tensile Strength, Mpa	1380-3100	1900-2750	2410
Elongation at break, %	0.9	0.5	0.4-0.27
Density, g/cc	1.9	2	2.2
Filament diameter, μm	11	11	10-11

Table 2.6 Properties of commercial oxide-based ceramic fibers (Wilson, 2003)

Tradename	Manufacturer	Composition, wt%	Density, g/cc	Average diameter, μm	Filaments per tow	2003 cost, $/Kg	Avg. RT tensile strength, MPa	Avg. RT tensile moulus, GPa
Alumina-Silica based								
Altex	Sumitomo	85 A+ 15 S	3.3	15	500-1000	330-550	2000	210
Alcen	Nitivy	70 A+ 30 S, (80+20, 60+40)	3.1	7-10	1000	NA	2000	170
Nextel 312	3M	62 A+ 24 S+ 14 B_2O_3	2.7	10-12	420-780	190-230	1700	150
Nextel 440	3M	70 A+ 28 S+ 2 B_2O_3	3.05	10-12	420-780	380-490	2000	190
Nextel 550	3M	73 A+27 S	3.03	10-12	420-780	475-730	2000	193
α-alumina based								
Almax	Mitsui Mining	99.5 A	3.6	10	1000	815	1800	330
Nextel 610	3M	>99 A	3.9	12	420-780-2600	330-660	3100	373
Nextel 650	3M	89 A+ 10 ZrO_2 + 1 Y_2O_3	4.1	11	780	400-660	2500	358
Nextel 720	3M	85 A+ 15 S	3.4	12	420-780	440-1010	2100	260
Saphikon	Saphikon	100 A	3.98	125	1	50,000	3500	460

A, Alumina; S, Silica

Table 2.7 Properties of commercial non-oxide-based ceramic fibers (Wilson, 2003)

Tradename	Manufacturer	Composition, wt%	Density, g/cc	Average diameter, μm	Filaments per tow	2003 cost, $/Kg	Avg. RT tensile strength, MPa	Avg. RT tensile moulus, GPa
Silicon-carbide based								
Nicalon, NL200	Nippon Carbon	56 Si+ 32 C+12 O	2.55	14	500	~2000	3000	220
Hi-Nicalon	Nippon Carbon	62 Si+ 37 C+0.5 O	2.74	14	500	8000	2800	270
Hi-Nicalon type S	Nippon Carbon	69 Si+ 31 C+0.2 O	3.05	12	500	13000	~2500	400-420
Tyranno lox M	Ube Industries	55 Si+ 32 C+10 O+ 2 Ti	2.48	11	400-800	1000-1500	3300	187
Tyranno ZMI	Ube Industries	57 Si+ 35 C+7.6 O+ 1 Zr	2.48	11	400-800	1000-1600	3300	200
Tyranno SA 1-3	Ube Industries	68 Si+ 32 C+0.6 Al	3.02	7.5-10	800-1600	~5000	2800	375
Sylramic	Dow Corning	67 Si+ 29 C+0.8 O+2.3 B+0.4 N+2.1 Ti	3.05	10	800	10,000	3200	~400
Sylramic-iBN	Dow Corning, NASA	Sylramic + in situ BN surface	3.05	10	800	>10,000	3200	~400
SCS-6-9	Textron Speciallity Materials	70 Si+30 C	~3	70-140	1	~9,000	~3500	350-390
Ultra SCS	Textron Speciallity Materials	70 Si+30 C	~3	140	1	~9,000	~6000	390
Carbon-based								
T300	Amoco	92 C+8 N	1.76	7	1000 to 12,000	100-250	3700	231
IM7	Hercules (Hexcel)	>99 C, trace N	1.77	5	6000-12000	50-70	5300	275
UHM	Hercules (Hexcel)	>99 C, trace N	1.87	4.5	3000-12000	100-350	3500	440
P120	Amoco	>99 C	2.17	10	2000	1900	2400	830
K321	Mitsubishi Kasei	>99 C, trace N	1.90	10	1000 to 12,000	NA	2000	176

Table 2.8 Typical thermosetting resin (Mazumdar, 2002)

Resin Material	Density, g/cc	Tensile Modulus, GPa	Tensile Strength, MPa
Epoxy	1.2-1.4	2.5-5.0	50-110
Phenolics	1.2-1.4	2.5-4.1	35-60
Polyester	1.1-1.4	1.6-4.1	35-95

Table 2.9 Typical thermoplastic resin (Mazumdar, 2002)

Resin Material	Density, g/cc	Tensile Modulus, GPa	Tensile Strength, MPa
Nylon	1.1	1.3-3.5	55-90
PEEK	1.3-1.35	3.5-4.4	100
PPS	1.3-1.4	3.4	80
Polyester	1.3-1.4	2.1-2.8	55-60
Polycarbonate	1.2	2.1-3.5	55-70
Acetal	1.4	3.5	70
Polyethylene	0.9-1.0	0.7-1.4	20-35
Teflon	2.1-2.3	-	10-35

Table 2.10 Heat release test results for OSU (Giancaspro, 2004)

Specimen identification	Peak HRR (kW/m^2)	t_{PHRR} (s)	Heat release ($kW \cdot min/m^2$) 2 min	Heat release ($kW \cdot min/m^2$) 5 min	FAA test result (65·65) (pass/fail)	Specimen behavior/appearance
OSU Balsa 1[a]	165	176	166	438	Fail	Ignited almost immediately
OSU Balsa 2[a]	163	9	169	290	Fail	Ignited almost immediately
OSU Balsa 3[a]	184	11	177	272	Fail	Ignited almost immediately
Average	171	65	171	333	All failed	All samples charred severely and/or were destroyed
Standard deviation	11.22	95.85	5.64	91.43		
OSU Reinf[b]	104	214	70	275	Fail	Started to flame up after about 30 s
OSU 2	53	106	21	130	Pass	Some charring; cracking of fireproofing
OSU 4	28	292	4	36	Pass	Charring and substantial cracking of fireproofing
OSU 5	11	518	−8	−7	Pass	Blisters, cracking; some charring
OSU 7	4	94	−10	−16	Pass	Blisters; slight charring near flame application point
OSU 11	3	605	−14	−23	Pass	Substantial charring (10.5 min of exposure)
Balsa (core only)[c]	125	125	—	40	Fail	—
GRP (no core)[c]	132	105	—	77	Fail	—
GRP/Balsa Core[c]	157	220	—	103	Fail	—

[a]Control sample: no reinforcement, no fireproofing.
[b]Reinforcement only, no fireproofing.
[c]Reference: U.S. Coast Guard (Grenier 1996).

Table 2.11 NBS smoke test results (Giancaspro, 2004)

Specimen identification	Reinforcement	Thickness of fireproofing (mm)	FAA test result		Specimen behavior/appearance
			^4D_m	$^4D_m < 200$ (pass/fail)	
NBS Balsa 1[a]	—	—	26	Pass	Ignited almost immediately
NBS Balsa 2[a]	—	—	31	Pass	Ignited almost immediately
NBS Balsa 3[a]	—	—	25	Pass	Ignited almost immediately
Average for balsa (control) samples			27	All pass	All samples charred severely
Standard deviation for balsa (control) samples			2.84		
NBS Reinf 3k Uni[b]	3k Uni C	0	8	Pass	Slight charring on edges; swelling of facings
NBS Reinf 3k Woven[b]	3k Woven C&G	0	41	Pass	Surface turned white; slight charring on edges
NBS 3	3k Woven C&G	3	51	Pass	Moderate surface cracking
NBS 6	3k Woven C&G	6	34	Pass	Moderate surface cracking
NBS 9	3k Woven C&G	9	27	Pass	Moderate surface cracking

[a]Control sample: no reinforcement, no fireproofing.
[b]Reinforcement only, no fireproofing.

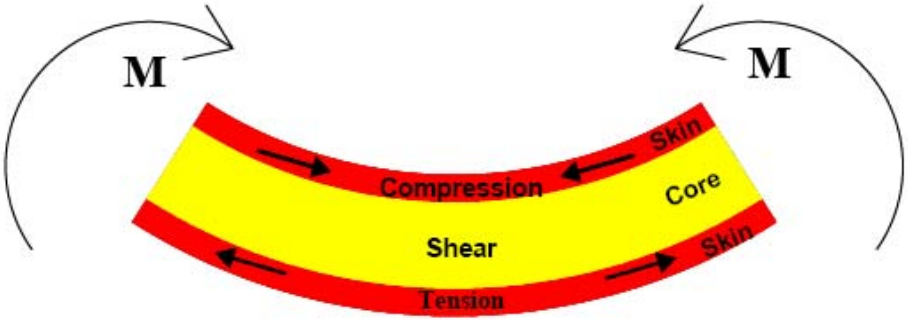

Figure 2.1 Sandwich beam behavior under bending

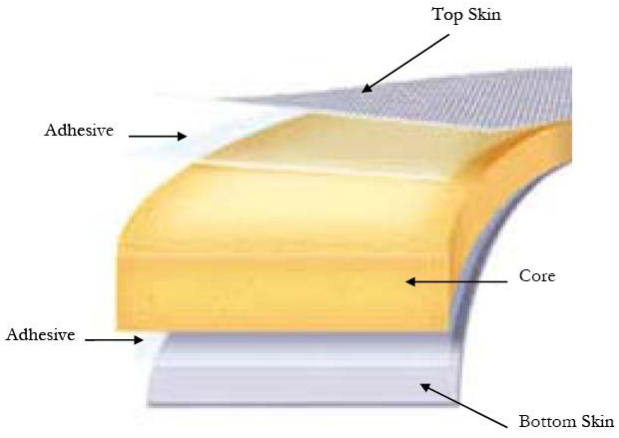

Figure 2.2 Typical layers of a sandwich structure

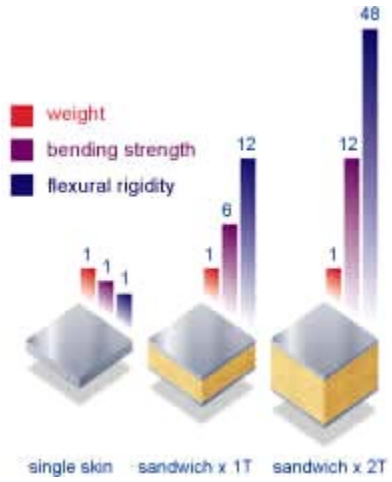

Figure 2.3 Effect of thickness on sandwich structure (DIAB Group, 2007)

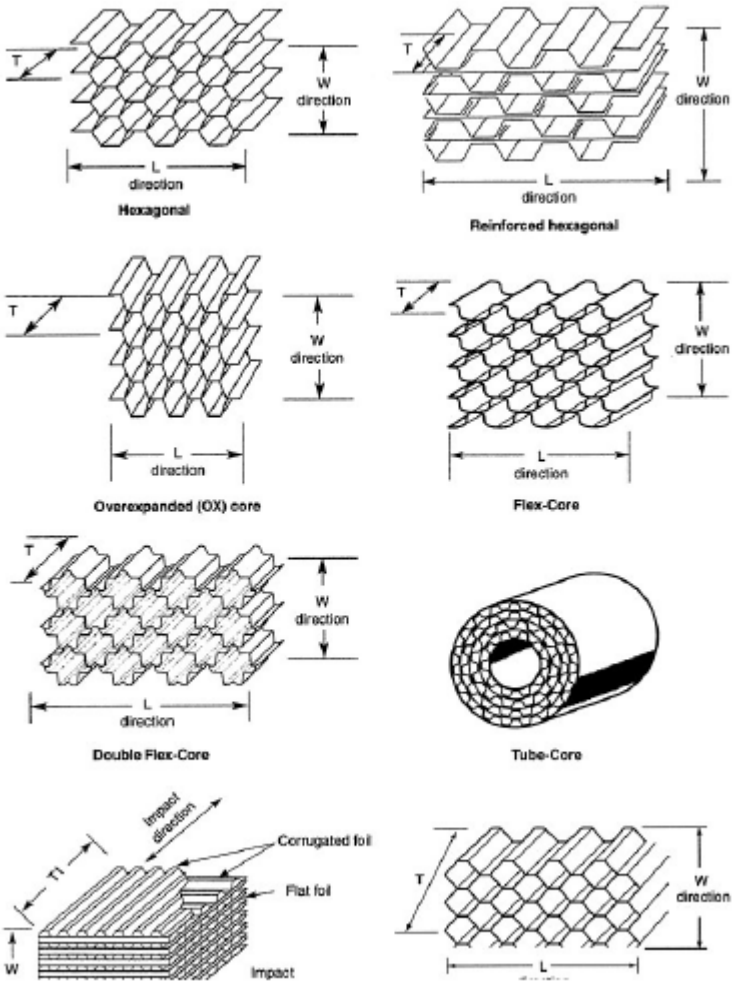

Figure 2.4 Honeycomb Cell Configuration (Kindinger, 2003)

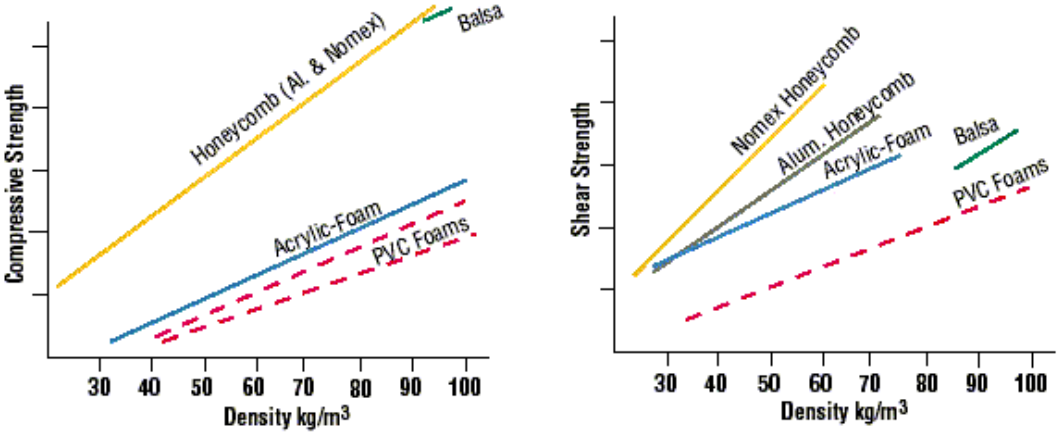

(a) Compressive Strength vs. Core Density

(b) Shear Strength vs. Core Density

Figure 2.5 Comparison of the core mechanical properties (SP Systems, 2001)

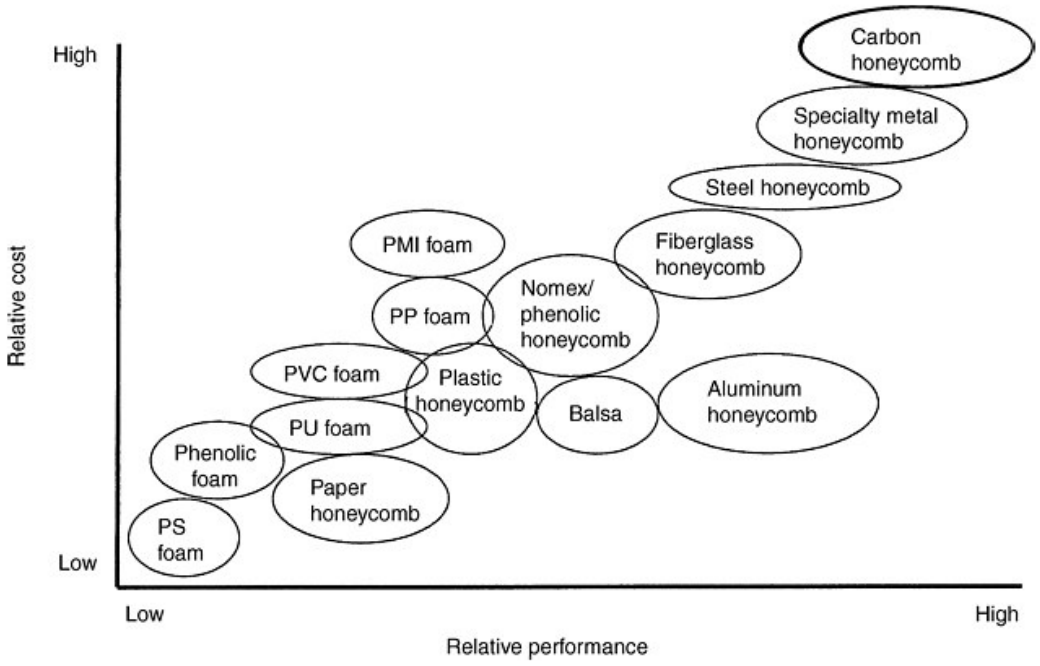

Figure 2.6 Cost versus performance of various lightweight cores (Kindinger, 2003)

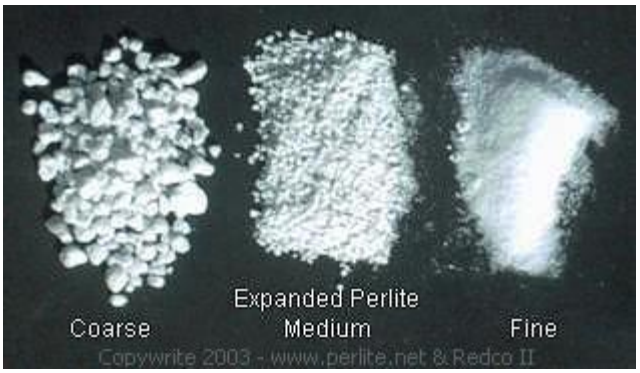

Figure 2.7 Different types of perlite (Perlite & RedcoII, 2003)

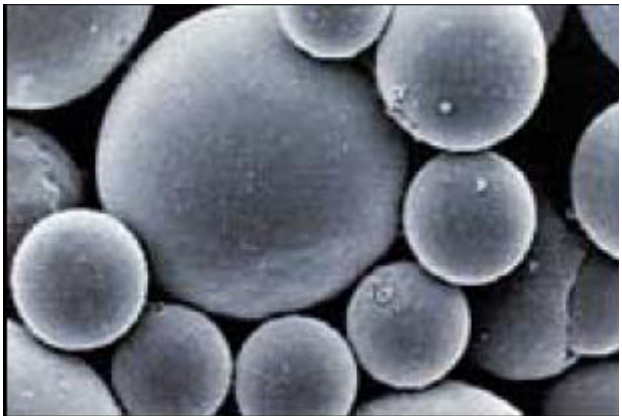

Figure 2.8 Scanning electron photomicrograph (SEM) of Fillite™ particles (Trelleborg, 2007)

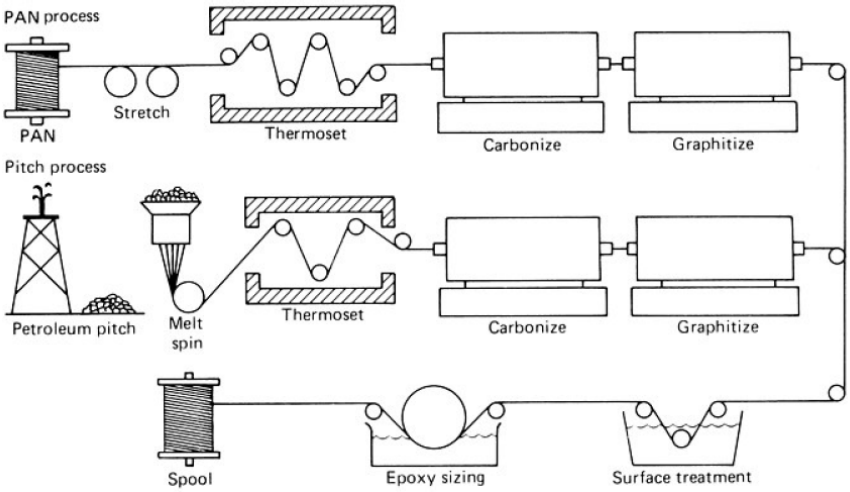

Figure 2.9 The processing sequence of PAN-based and Pitch-based carbon fibers precursor (Walsh, 2003)

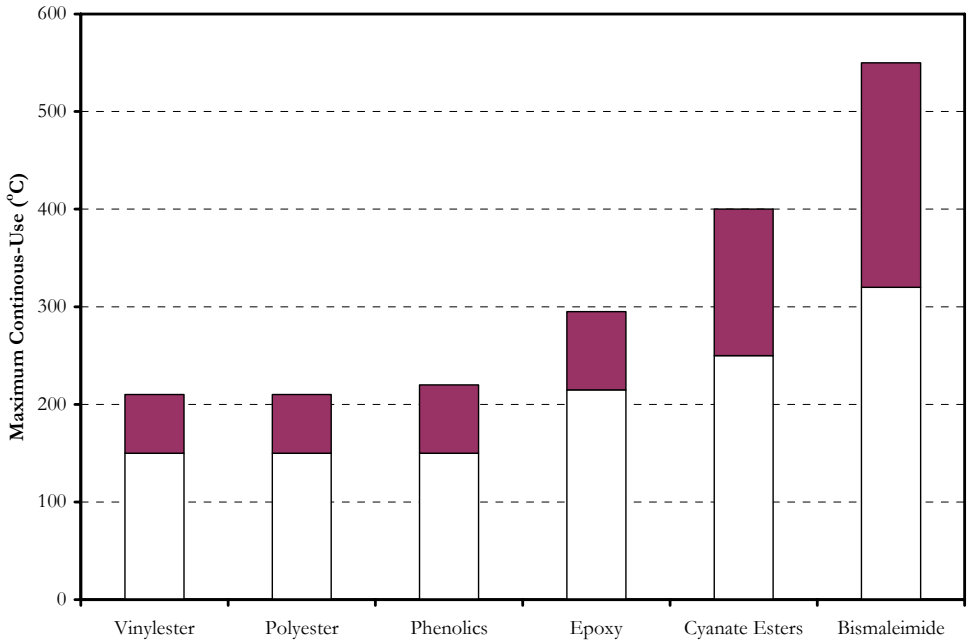

Figure 2.10 Maximum continuous-use of thermoset resins (Mazumdar, 2002)

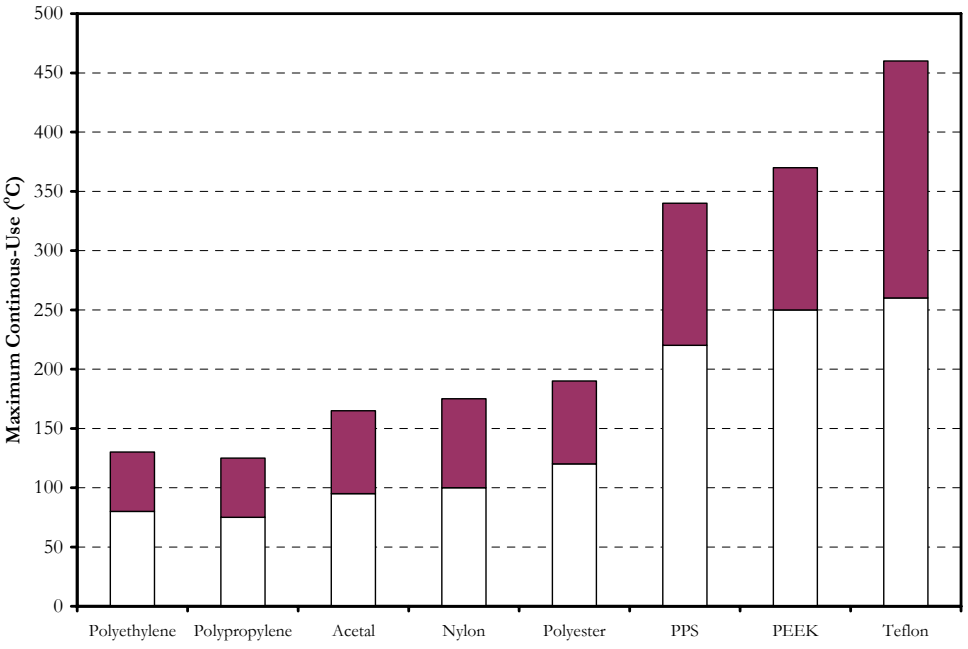

Figure 2.11 Maximum continuous-use of thermoplastic resins (Mazumdar, 2002)

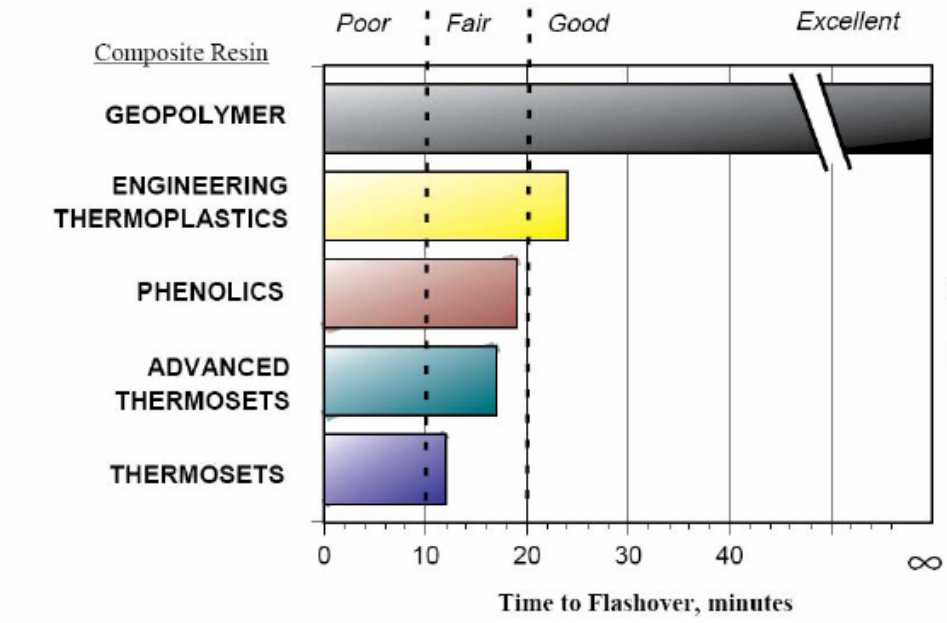

Figure 2.12 Time to flashover for different resin systems (Lyon, 1997)

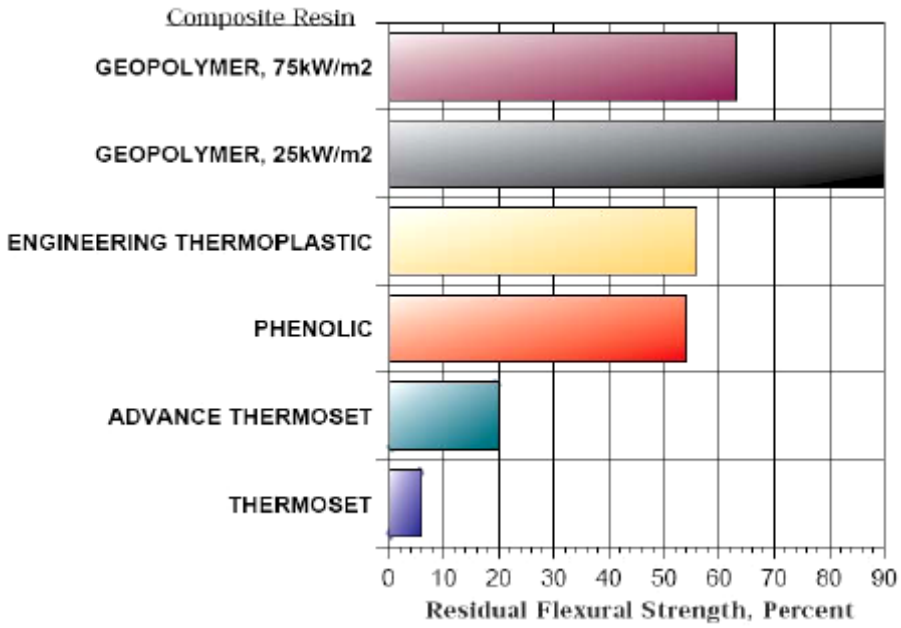

Figure 2.13 Residual warp direction flexural strength of crossply laminates after thermal exposure (Lyon, 1997)

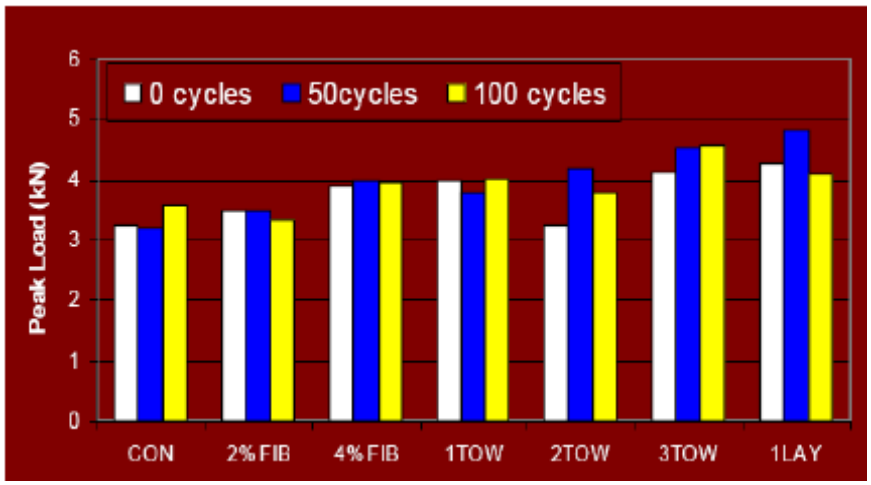

Figure 2.14 Peak Loads after wet-dry exposure (Garon, 2000)

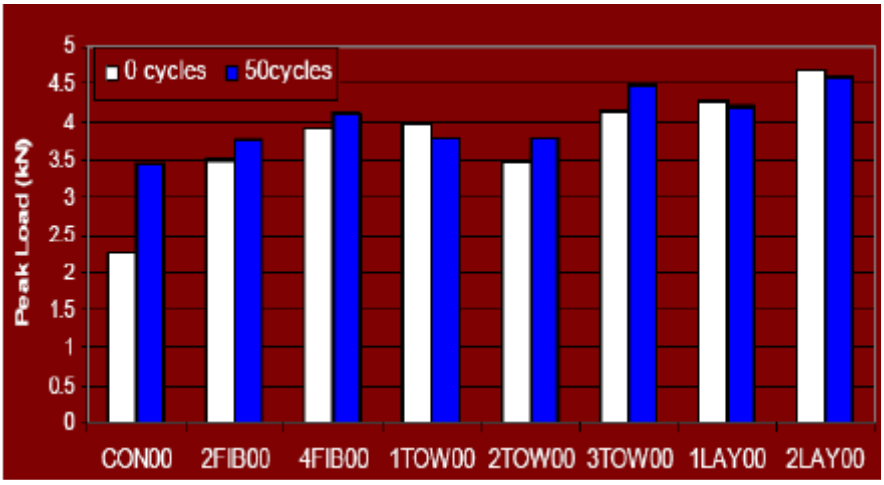

Figure 2.15 Peak Loads after Scaling Exposure (Garon, 2000)

Figure 2.16 Polysialate as graffiti proof coating (Nazier, 2004)

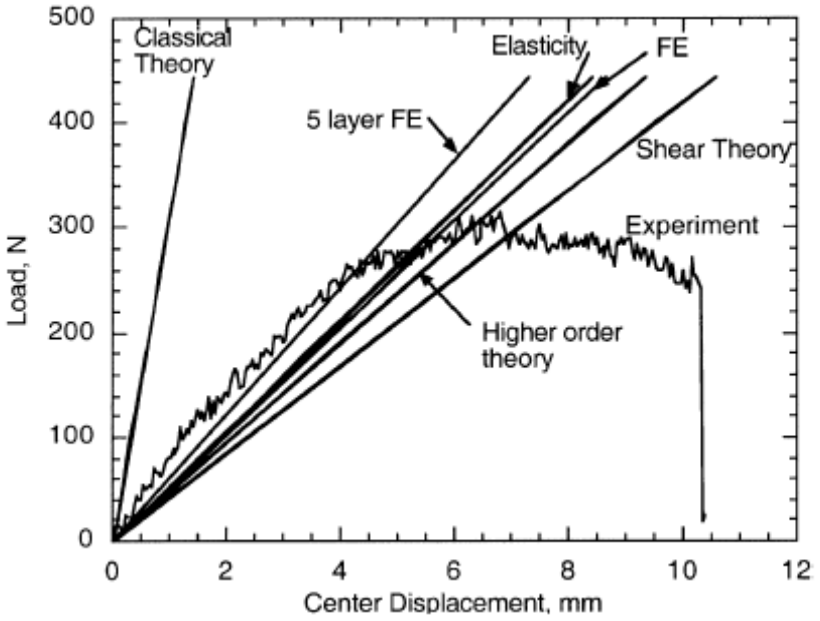

Figure 2.17 Load-deflection response for three-point bending test of sandwich beams and analytical prediction from various theories (Kim, 2001)

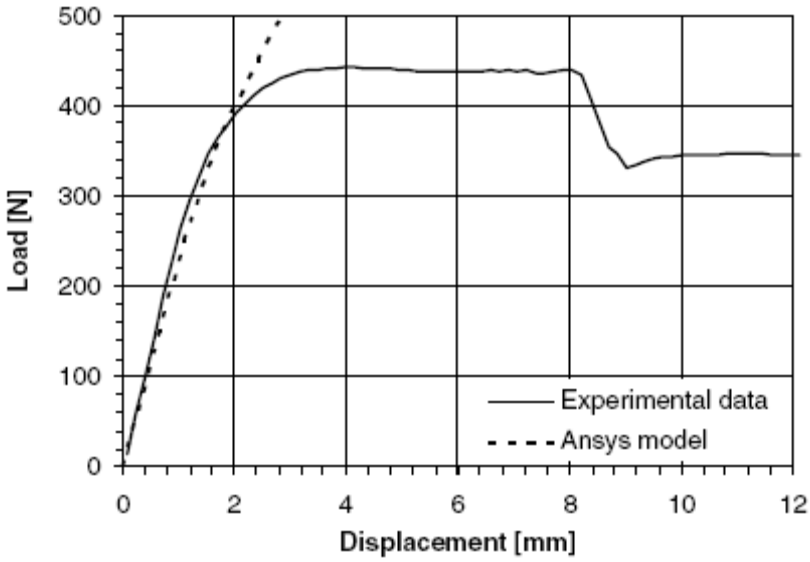

Figure 2.18 Load-deflection response for three-point bending test versus the finite element analysis prediction (Borsellino, 2004)

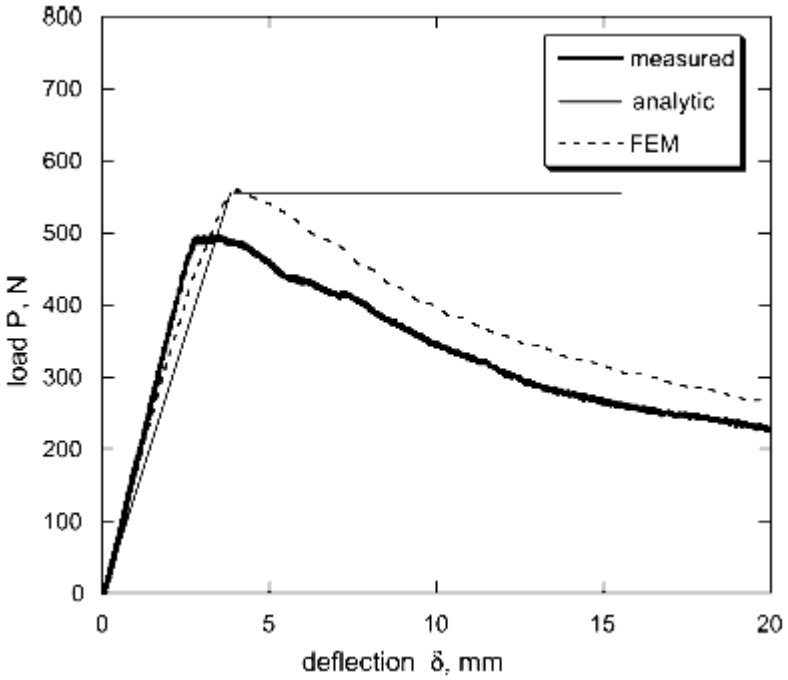

Figure 2.19 Load-deflection response for simply supported beam in three-point bending versus the analytical and the finite element solution (Tagarielli, 2004)

Chapter 3

Sandwich Beams: Experimental Study

3.1 Introduction

Fairbarn described the principles of sandwich structures for the first time in 1849 (Allen, 1969). They are widely used in applications that require high strength, stiffness, and lightweight.

The system typically consists of two thin-stiff facings or skins and a thicker soft lightweight core. The facing materials are usually made of laminate composites (carbon or glass) or metals. The core is typically made of foam, honeycombs or wood. This system is widely used in aerospace, marine, and sometimes in conventional construction applications.

The main role of the core is to provide the system with the necessary thickness to ensure sufficient flexural stiffness. Note that, the stiffness of a beam is proportional to the cube of its thickness. The core must have enough strength to transfer the forces between the skins in the form of shear forces. Simply, the facings resist the normal forces and the core resists the shear forces. Sandwich structures made using organic carbon/epoxy facings have been evaluated extensively. One of the major drawbacks of this type of system is the lack of fire resistance, which may cause loss of structural integrity and loss of lives due to smoke and flame progression. The results presented in this chapter deal with sandwich beams that are more fire-resistant. Using Geopolymer matrix, Polyvinyl chloride (PVC) foam cores were reinforced by carbon fibers to obtain rigid and high-temperature, high-strength sandwich panels.

A comparison is made between the behaviors of the PVC sandwich beams reinforced with inorganic composite and those reinforced with organic composite. The influence of density and grade of core on strength, stiffness, toughness, and specific strength was evaluated for a number of reinforcement (skin) ratios.

3.2 Research Program

Commercially available Divinycell™ closed-cell PVC foam was used for the entire program. The mechanical properties of the five types of foams used for the current study are presented in Table 3.1. The test variables, beam designations, and details are presented in Tables 3.3, 3.4 and 3.5. For each designation, three identical beams were prepared and tested, resulting in a total of 195 beams.

The primary variables are described in the following sections:

3.2.1 Core grade and density

The core of a sandwich beam has several important functions. It provides the necessary moment arm to resist the bending moment in the form of a couple. Also it has to be rigid enough in shear to transmit the forces to the facings and to prevent the facings from sliding. If the core is weak in shear, the facings will not be able to generate full load capacity and the sandwich beam will loose stiffness.

Different grades are produced and these grades are classified based on the application. The commercially available grades are:

- Divinycell™ H : All purpose grade
- Divinycell™ HT: Aerospace prepreg grade
- Divinycell™ HP: Elevated temperature grade
- Divinycell™ HD: Shock loading grade

- Divinycell™ HCP: Buoyancy grade

The Divinycell™ grades H and HT were chosen in this study. The HT grade is formulated for use in applications requiring improved mechanical properties and epoxy prepreg compatibility.

The mechanical properties of the core vary with the density. These mechanical proprieties include tensile strength and modulus, compressive strength and modulus, and shear strength and modulus. These properties tend to vary almost linearly with the density (Abot, 2000).

Five groups of different grades and densities were used. Three groups were from the H-grade and two groups of the HT-grade. For the HT-grade, densities of 50 and 110 kg/m^3 were used, while the densities were 130, 200 and 250 kg/m^3 for the H-grade.

3.2.2 Type of Adhesive

Organic resins have been widely used in the preparation of the laminate and sandwich beam composites. However, these resins lose their strength and emit smoke and toxins when exposed to fire. In this study, a high temperature inorganic resin was used to develop a fire resistant sandwich composite. A comparison between these two resins was studied by preparing several samples using epoxy resin.

3.2.3 Type of Reinforcement

The skins of sandwich composites are used to provide the strength and the stiffness; therefore, high stiffness-high strength laminates are used. The most common commercially available laminate composites are carbon/epoxy, glass/epoxy and aluminum/epoxy systems. These laminates are composed of different types of fabrics and various laminate orientation and lay-up. Carbon is known for its high specific strength and stiffness. As previously

mentioned, glass and Geopolymer are not compatible as the glass gets affected by the Geopolymer alkalinity. Therefore, carbon fibers were chosen as the skin for the PVC sandwich beams in this study.

Three different commercially available carbon fibers were used:

- The K63712, which is a 12K high modulus coal tar pitch-based carbon tow. It has a tensile modulus of 640 GPa and area of 1.14 mm^2 and it is given a designation of "H-12K HMC" throughout the dissertation.
- The K63312, which is a 12K moderate high modulus coal tar pitch-based carbon tow. It has a tensile modulus of 440 GPa area of 1.14 mm^2 and it is given a designation of "N-12K MMC" throughout the dissertation.
- The Unidirectional carbon tape, which is a 3K unidirectional carbon tape. It has a tensile modulus of 230 GPa and area of 0.11 mm^2 /end. There are about 43.4 ends for a width of 50 mm. The total area of one tape is about 4.77 mm^2. It is given a designation of "T-3K Uni C Tape".

A summary of the different used fibers and their properties are presented in table 3.2.

3.2.4 Amount of Reinforcement

For the samples reinforced with carbon tows, one, two and three tows were used. For the samples reinforced with carbon tape, one and two layers of carbon tape were used.

3.2.5 Symmetry of reinforcement

After some preliminary tests, it was noticed that the tension side reinforcements were more efficient because of the absence of buckling, wrinkling, and the concentration of stresses caused by the load rollers contacting the compression side. Therefore, nonsymmetrical

reinforcements were chosen for further evaluation. Two and three tows were used for the compression side balancing one tow on the tension side.

3.3 Sample Designation

Samples were grouped into three main groups based on the type of reinforcement and the first letter was chosen to represent reinforcement designation (H for H-12K HMC, N for N-12K MMC and T for T-3K Uni C Tape). Within each group, the samples were categorized based on the core density, and the density value was added to the designation following the reinforcement letter. Based on the reinforcement symmetry and amount of reinforcement, a number followed by a letter was given. The number illustrates the amount of tows or layers if carbon tape was used. The letters were "C" for compression reinforcement and "T" for tension reinforcement. For beams reinforced using organic adhesive, the letter "E" was added at the end of the designation. All control beams were given a "C" as a starting letter followed by the core density.

For example, a control beam with a core density of 50 kg/m^3 has the designation of "C50". A beam reinforced with H-12K HMC and a core of a density of 130 kg/m^3, with three tows on the compression side and one tow on the tension side using inorganic adhesive, has a designation of "H130-3C-1T". However, a beam made of core of density of 50 kg/m^3 and N-12K MMC tows with symmetrical reinforcement of three tows using organic adhesive, has the designation of "N-50-3C-3T-E". A beam reinforced using T-3K Uni C Tape and a core of 250 kg/m^3 with symmetric reinforcement on each side of 2 layers of tape, will have the designation of "T250-2C-2T" as long as the inorganic adhesive is used.

3.4 Specimen Preparation

The PVC beams were cut from commercially available 1500 x 1500 x 13 mm sheets. The beams were cut out of the sheets using a table saw for the cores having a density more than 110 kg/m^3, while a blade was used for lighter cores. The beams were 13 mm thick, 51 mm wide and 356 mm long. The actual dimensions were taken using a digital caliber of the accuracy of 0.01 mm and the cores were weighed. There was no special treatment or preparation of surface, unless dust or impurities were visually spotted.

For the beams reinforced with carbon tows, the surface was first wetted by a small amount of resin then the tows were placed on the core. Subsequently, the tows were hand-impregnated with the resin and were spread to ensure the impregnation of most of the filaments with resin. The prepared beams remained at ambient conditions in the laboratory environment for approximately twenty-four hours until the resin had been cured sufficiently to facilitate handling. The same procedures were followed to reinforce the other side of the beam.

For the beams reinforced with the carbon tape, the core surface was wetted by the resin after wetting the tape on a flat surface. Glue rollers were used to ensure complete fiber wetting. If two layers were used, the layers were first prepared and laid on top of each other then placed on the core.

When the organic resin was used, some precautions were taken to avoid the development of the resin thin plate. This is one of the main reasons of the delamination failure and the miscalculations of moment capacity, giving additional thickness and extra stiffness. This was done to guarantee a fair comparison between the behavior of the organic and inorganic resins. The samples were allowed to cure in open air at room temperature (approximately 22°C) for three weeks.

3.5 Test Setup

After leaving the samples for three weeks to cure, the beam weights and dimensions were taken; then a quarter span four-points bending test was conducted over a simply supported span in accordance with ASTM C393 (ASTM, 1999). A schematic diagram of the four-point flexure test setup is shown in figure 3.1. Beams were tested using a span of 305 mm. This yielded a span-to-depth ratio of 23:1, which satisfies the standard requirements of a span-to-depth ratio greater than 20. Aluminum flashings, as it is recommended by the ASTM, were used under the load points to avoid the mix between the deflection and the bearing failure readings. An MTS Sintech 10/GL was used to test the beams under deflection control at a deflection rate of 2 mm/min. Load and deflection under the load point readings were taken and the failure mode was recorded using photographs.

3.6 Test Results

Tables 3.6 to 3.8 present the test results that include the maximum moment capacity, the stiffness, the toughness, the increase percentage of the moment capacity and the stiffness increase over control beams. The apparent stresses, the specific apparent stresses, the tensile stress in the fibers at maximum load and the failure mode are presented in tables 3.9 to 3.11. The ultimate moment is calculated using the simple structure analysis equation: $M_u = P_u a / 2$ where P_u is the ultimate load and a is the shear span which is the distance from the left (or right) point load to the left (or right) support. The flexural stiffness was calculated using the equation:

$$EI = \frac{\Delta P}{\Delta \delta} \frac{a^2 (3L - 4a)}{12} \tag{3.1}$$

Where EI is the equivalent flexural stiffness, ΔP is the load increment, and $\Delta\delta$ is the corresponding deflection increment under the load. The span length is denoted L while a is the shear span.

The energy or toughness, U, is equal to the area under the load-deflection curve. As a standard for comparison, the area under the curve was computed up to a deflection of $L/50$ (6 mm) using a simple trapezoidal approximation. If the beam failed at a deflection less than 6 mm, then the toughness was calculated up to the failure deflection.

3.6.1 Failure modes

Four main patterns of failure have been recognized for sandwich beams in three- and four-point bending: face yield, wrinkling of the compressive face sheet, core shear, and indentation underneath the loading rollers (Steeves et al., 2004). These modes of failure are shown in figure 3.2. Further discussion on the failure modes and critical loads are presented in the next chapter accompanied with mathematical formulations.

3.6.1.1 Core Shear

Based on the shear distribution shown in figure 3.3, the shear distribution across the thickness can be assumed constant; and the entire shear can be assumed to be taken by the core. The core shear failure occurs when the shear stress in the core exceeds the ultimate shear capacity of the core material.

3.6.1.2 Indentation

The indentation failure is considered as bearing failure. It occurs at the loading rollers when the facing and the core start to yield under the load.

3.6.1.3 Face wrinkling

Face wrinkling is basically a face compression failure in the form of localized short-wavelength buckling. The wrinkling strength of the sandwich beam depends on the facings' tensile modulus and the core tensile and shear modulus. It was reported that failure by face wrinkling is prevalent in the case of low through-the-thickness stiffness and long beam spans (Gdoutos et Al., 2003).

3.6.1.4 Face delamination

Delamination between the core and outer facings is the last failure mode. This failure mode is characterized by a distinct separation between the facings and core material. The bond between the facing and the core breaks down, allowing the materials to separate.

3.6.1.5 Failure Mechanism for tested beams

When loading the beam up to failure, the load deflection curve starts with a linear portion, and then, it gradually starts loosing linearity up to a certain point. After this point some beams exhibit sudden failure and others fail in a ductile manner. The change from linearity corresponds to the yield of the core and the failure point is the point where the core reaches its ultimate capacity. Usually, an audible splintering was heard before reaching the ultimate capacity.

All the failure modes mentioned in section 3.6.1 were observed during this study except for delamination, thus confirming an excellent bond between the PVC core and the inorganic Geopolymer resin.

The initiation of a certain failure mode might trigger and interact with another failure mode (Daniel et al., 2002). Therefore, one must distinguish between the observed failure mode and the initiating failure mode. All the failure modes mentioned in Tables 3.9 to 3.11 are the

observed failure modes after the beam reaches its maximum capacity. That does not necessarily mean that it is the initiating failure mode. It is strongly believed that the final failure of the beam (at ultimate load) occurs when the strains in the different layers are not compatible because of the high strain capacity and plasticity of the core when it is compared to the low strain capacity of the skin.

Compression failure was most likely with beams with low density cores (50 Kg/m^3) and beams that are reinforced using the organic adhesive. However, bearing failure occurred with beams with low density cores and high reinforcement area, and beams with organic resin. Beams that are reinforced using organic adhesive exhibit bearing and bearing mixed with wrinkling as well. This failure can be seen in figure 3.27. Some of the beams exhibit a constant increase in load capacity after exceeding the non linear part. These beams are: N110-1C-1T-E, N130-1C-1T-E, N250-1C-1T-E, H110-2C-1T, H110-3C-1T, H110-1C-1T-E, H130-1C-1T, H130-1C-1T-E, H250-1C-1T-E, H250-3C-3T, H200-2C-1T, H200-3C-1T. This behavior is a result of wrinkling failure in the beam. As thin stiff reinforcements are used, this wrinkling has the form of a narrow crack on the compression side. Usually, beams failed by wrinkling will show a buckling wave, but with the very stiff reinforcements the fibers tend to break in a shorter wave length, like the one shown in figure 3.28. As the load is increasing on the beam, it deflects more closing up the crack. As a result, the cracked reinforcements bear against each other, which allow the beam to carry additional load. This crack was seen and photographed in most of the cases. Wrinkling failure is not mentioned in table 3.10 for beams H110-2C-1T and H110-3C-1T because these two beams had split which did not allow a proper investigation as it might have been the same location of the compression crack. This kind of behavior is more likely with beams reinforced with one tow

on each side and beams having organic adhesive. A picture is shown in figure 3.29. This failure is more probable with stiff reinforcement like the H-12K HMC.

Most of the beams that failed in tension, failed in one of two ways. The first one is by just cracks in the tension reinforcement which is called "Tension Failure". The second way is by complete splitting of the beam. This is noted in the tables as "split location".

3.6.2 Maximum Moment Capacity

3.6.2.1 Beams Reinforced with Inorganic Composite

The control beams were tested with up to 10 mm deflection then the test was stopped as the beams exhibited very large curvature. Also, the beams' overhangs began to slide inwards increasing the length of the beam over the span length and causing inaccurate readings with no signs of approaching failure. The control beams' maximum moment was calculated up to this point and recorded as shown in Tables 3.6 to 3.8. These beams provided maximum moments of 0.5, 1.2, 1.5, and 3.3 N-m for cores of 50, 110, 130, and 250 Kg/m^3, respectively. The variation in moments is consistent with the core density. The addition of one N-12K MMC tow on the tension and compression sides resulted in significant increases of maximum moment, providing moments of 15.1, 15.6, 15.2, and 18.5 N-m, respectively. The addition of one H-12K HMC on both tension and compression faces resulted in less significant increases, providing moments of 7.6, 13.5, 20, and 18.1 N-m, respectively and 19.6 N-m for the core of 200 $kg/m^{3.}$ This core had a maximum moment for the control beam of 2.3 N-m. Generally, the increase in moment capacity provided by the N-12K MMC is higher despite the fact that this carbon tow has lower strength than the H-12K HMC. This is the result of the higher strain capacity that the N-12K MMC has, and is true for all the aforementioned beams except for H130-1C-1T. This beam failed because of wrinkling with a

constant increase in the load after the non-linear part. The addition of one carbon tape of the T-3K Uni C Tape provided maximum moments of 27.5, 43.9, 42.4, and 36.6 N-m, respectively.

The maximum moments did not triple, by tripling the area of reinforcement for the N-12K MMC. The maximum moments were 26.6, 34.4, 36.7, and 31.5 N-m, respectively. Tripling the area of the H-12K HMC resulted in maximum moments of 20.9, 29.1, 29.9, and 38.3 N-m, respectively and 40.0 N-m for the core of 200 kg/m^3. Doubling the area of T-3K Uni C Tape provided maximum moments of 30.2, 71.3, 62.7, and 67.0 N-m, respectively. The ratios of the maximum moment in the case of double the reinforcement area to the correspondent values of one tape are 1.1, 1.6, 1.49 and 1.85, respectively. Theses ratios come closer to two with the increase of density except for the 130 Kg/m^3. The test responses between 110 and 130 Kg/m^3 are mixed and do not follow the same pattern because the density difference between the two is not significant. Also, it is compensated by the difference in grade, as the 110 Kg/m^3 is HT-grade (Aerospace grade) while the 130 Kg/m^3 is H-grade.

3.6.2.2 Comparison with Beams Reinforced with Unsymmetrical Composite

In a trial for compensation of the lack of strength on the compression side, unsymmetrical reinforcements were used by doubling and tripling the reinforcement area on the compression side.

Applying two tows of N-12K MMC on the compression side and one in tension, lead to maximum moment values of 15.4, 14.6, 16.1, and 17.8 N-m, respectively. These values are of the same order as the correspondent values for symmetrical reinforcements using one tow. The maximum moment values for beams reinforced with two tows of H-12K HMC in

compression and one in tension are 9.9, 13.9, 14.0, and 21.7 N-m, respectively and 23.8 N-m for the core with density of 200 Kg/m^3. These values are not necessarily higher than the correspondent values for symmetrical reinforcements using one tow. This leads to the conclusion that doubling the reinforcement area on the compression side does not provide additional moment capacity.

By tripling the area of fibers on the compression side over the tension side for the N-12K MMC, the maximum moment values were 18.6, 17.3, 13.6, and 19.0 N-m, respectively. These values are relatively higher than the correspondent values for symmetrical reinforcements using one tow, and unsymmetrical reinforcements with double the reinforcement area on the compression side, except for the N130-3C-1T beam. For the H-12K HMC, the maximum moment values were 9.6, 15.2, 14.9, and 19.7, respectively and 26.3 N-m for the core with density of 200 Kg/m^3. These values were mostly higher than the correspondent symmetrical reinforcements using one tow, except for H130-3C-1T, which is not appropriate to compare with H130-1C-1T, as the latter had wrinkling failure with false increasing in load capacity. These values are not necessarily higher than the correspondent unsymmetrical reinforced beams with double the reinforcement area on the compression side. This confirms the conclusion made earlier; it is not effective to add reinforcement on the compression side to increase the moment capacity of the beam.

3.6.2.3 Comparison with Beams Reinforced with Organic Composite

The load deflection behavior of the beams reinforced with organic adhesive was more ductile than the beams reinforced with inorganic resin. The maximum moments did not follow a trend to be either higher or lower than their correspondent beams reinforced with inorganic resin. Out of the sixteen beams reinforced with organic adhesive represented in

this study, ten beams provided higher maximum moments, two beams had almost the same maximum moments as the inorganic one (N130-1C-1T-E and H250-3C-3T-E), and four beams had lower values of maximum moments (N50-1C-1T-E, N130-3C-3T-E, H130-1C-1T-E and H130-3C-3T-E). However, some of the beams having higher or equal values as the inorganic beams had taken advantage of the false increase in moment capacity associated with the wrinkling failure (N110-1C-1T-E, N130-1C-1T-E, N250-1C-1T-E, H110-1C-1T-E, H250-1C-1T-E and H250-3C-3T-E). The beams reinforced with organic skin had an average of 3% higher moments at failure. The beams reinforced with inorganic systems are viable for use in terms of ultimate moment requirements, but the organic system is more ductile.

3.6.3 Stiffness

3.6.3.1 Beams Reinforced with Inorganic Composite

The stiffness was calculated from the slope of the initial linear portion of the load-deflection curves. As expected, the increase in the stiffness over the control samples was considerable; the increases ranged from 980% to 13855% for the N-12K MMC (440 GPa modulus fibers), 1374% to 15552% for the H-12K HMC (640 GPa modulus fibers) and 3534% to 20036% for the T-3K Uni C Tape. As expected, the use of higher modulus carbon caused higher stiffness. The average ratio increase was about 1.2, which is slightly lower than the ratio of the carbon modulus (1.45). This ratio increase is consistent with the increase of the core density. For cores with lower densities, the increases were higher. Tripling the amount of reinforcement did not increase the stiffness three times. The increase was two fold. The author believes that the decrease in efficiency of fibers is due to processing. The more tows added to the core, the more rolling was needed to ensure full impregnation of the resin. This

process damages some fibers and also creates change in orientation of fibers, thus reducing the efficiency of the fibers.

3.6.3.2 Comparison with Beams Reinforced with Unsymmetrical Composite

By investigating tables 3.6 and 3.7, it is evident that extra reinforcement added to the compression side did not increase the stiffness significantly. In some cases, there was no increase at all (H110 and H200 group).

3.6.3.3 Comparison with Beams Reinforced with Organic Composite

For cores with low density, the stiffness of the inorganic and organic systems were the same. For higher densities, the stiffness of the inorganic system mostly showed higher values than the counterpart organic systems. Beams reinforced with inorganic skin had an average of 14% higher stiffness.

3.6.4 Toughness and Ductility

3.6.4.1 Beams Reinforced with Inorganic Composite

As mentioned earlier, the toughness was calculated as the area under the load-deflection curve up to a deflection of 6 mm. The toughness increased up to 100 folds over the control samples.

For the N-12K MMC group, the toughness increased with the fiber areas. The toughness almost doubled with tripling the fiber areas. It increased with the core density, except for the N110 group as this group exhibited very brittle behavior for the inorganic group.

For the H-12K HMC group, the toughness increased with the fibers area and the core density as for the N-12K MMC group, but it was more consistent with core density.

For the T-3K Uni C Tape, the increase with the fibers area and core density was observed as well. By doubling the fibers area, the toughness became 1.2, 1.8, 2.0 and 1.7 times its value for the beams reinforced with one tape for the 50, 110, 130 and 200 Kg/m^3 cores respectively.

3.6.4.2 Comparison with Beams Reinforced with Unsymmetrical Composite

Adding more reinforcement to the compression side provided slightly higher toughness. In some cases, the toughness did not increase at all, like for the N110, H110 and H200 groups. By examining the load deflection curves for these groups, the unsymmetrical reinforced samples for the H110 and H200 exhibited a deflection way larger than the 6 mm limit so the actual toughness values are higher.

3.6.4.3 Comparison with Beams Reinforced with Organic Composite

The toughness for the beams reinforced with organic composite and beams reinforced with inorganic ones did not follow any particular trend. Sometimes, the inorganic beams had higher toughness and sometimes this was not the case.

Generally, the beams reinforced with organic composites had more ductile behavior than the inorganic ones.

3.6.5 Apparent Stress

Apparent stress was calculated, assuming that the cross section was homogenous using the equation:

$$\sigma = \frac{6M}{bc^2} \tag{3.2}$$

3.6.5.1 Beams Reinforced with Inorganic Composite

The apparent stress for the beams reinforced with inorganic composites was affected by the fiber types and the core density.

For the N-12K MMC group, the apparent stress was 10, 10, 11 and 13 MPa for 50, 110, 130 and 250 Kg/m^3 cores respectively, for beams reinforced with one tow. The variation was about 30% from the lightest core to the densest one. Beams reinforced with three tows had apparent stress of 18, 22, 26 and 21 for the different core densities. When the specific apparent stress was calculated by dividing the apparent stress by the beam total weight in grams, a mean value of 0.2 MPa/gm was found.

For the H-12K HMC group, the same trend was observed. The apparent stress within this group had a lower average than the N-12K MMC group (10.25 MPa versus 11 MPa). This was caused by the lower strain capacity for the H-12K HMC (640 GPa modulus fibers). The mean value of specific apparent stress was also 0.2 MPa/gm.

The T-3K Uni C Tape group had significantly higher apparent stress (an average of 33.75 MPa). This was achieved because of the higher axial stiffness gained from the higher reinforcement area ratio rather than the modulus. The mean value of specific apparent strength was 0.5 MPa/gm.

3.6.5.2 Comparison with Beams Reinforced with Unsymmetrical Composite

More reinforcement added to the compression side had, if any, a slight effect on the apparent stress (maximum increase was 10%). Three tows on the compression side did not add any significant apparent strength. This is better shown by looking at the specific apparent strength as the weight gained due to additional reinforcement on the compression side was accompanied with insignificant gained strength.

3.6.5.3 Comparison with Beams Reinforced with Organic Composite

The beams reinforced with organic composite exhibited higher apparent strength. The difference was about 25%. They all have higher specific strength as the organic resin has lower density (1.2 g/cc) than the inorganic one (1.4 g/cc) (Davidovits, 1989), tables 3.9 and 3.10.

3.6.6 Fibers Stress at Maximum Load

Maximum fiber stress in tension $\sigma_{t,f}$ was calculated using the equation:

$$\sigma_{t,f} = \frac{M}{A_{tf} c} \tag{3.3}$$

M is the moment, or in this case, the ultimate moment . A_{tf} is the area of reinforcement on the tension side, and c is the core depth.

3.6.6.1 Beams Reinforced with Inorganic Composite

The stress in the fibers increased with the core density. For the N-12K MMC, it ranged form 323 MPa for symmetrical single tow with core 50 Kg/m^3, to 841 MPa for the corresponding beam with 250 Kg/m^3. For H-12K HMC, the stress increased from 359 MPa to 911 MPa for singly symmetrically reinforced beams with core density of 50 and 250 Kg/m^3, respectively. This behavior is caused by the higher shear modulus for denser cores which allows better transfer of forces to the reinforcement skins.

3.6.6.2 Comparison with Beams Reinforced with Unsymmetrical Composite

For the unsymmetrical reinforcement, the neutral axis will be shifted towards the compression reinforcement. From equilibrium, the tension and compression force should be equal. As the compression reinforcement is double or triple the tension, the stress in the

tension reinforcement will be doubled or tripled as well. The stress values shown in tables 3.9 to 3.11 are the tension reinforcement stress.

3.6.6.3 Comparison with Beams Reinforced with Organic Composite

Same pattern as the one discussed in the maximum moment section was noticed. Some of these beams had higher fiber stress; some had almost the same, while others had lower fiber stress. But generally, the organic skin had a higher average of fibers stress of 3%. One may conclude that the type of resin is not a factor that affects the efficiency of the skin system and that organic and inorganic resins are equivalent.

3.6.7 Strain at elastic limit

The strain in the skin at elastic limit was calculated using the equation:

$$\varepsilon = \frac{M}{EI} \times \frac{c}{2} \tag{3.4}$$

3.6.7.1 Beams Reinforced with Inorganic Composite

The calculated strain values for the different skin types are presented in tables 3.12, 3.14 and 3.16. The average strain was found to be 0.17%, 0.13% and 0.19% for the N-12K MMC (440 GPa modulus fibers), the H-12K HMC (640 GPa modulus fibers) and the T-3K Uni Carbon tape (230 GPa modulus fibers), respectively. These values are about 30% of the ultimate strain at failure for the carbon tows (440 and 640 GPa modulus fibers) and 13% of the ultimate strain at failure for the carbon tape.

3.6.7.2 Beams Reinforced with Organic Composite

The beams reinforced with organic skin exhibited higher strains than their inorganic counterparts. The average strain values were 0.2% and 0.16% for the N-12K MMC (440

GPa modulus fibers) and the H-12K HMC (640 GPa modulus fibers), respectively. These values represent 33% and 40% of the ultimate strain at failure for the fibers.

3.6.8 Principal stresses calculation

The maximum stress in the skin was only 53% of the fibers tensile strength and the maximum strain was found to be only 40% of the fibers ultimate strain at failure, thus the failure mechanism was still unidentified and more investigations were needed to explain the failure mechanism. Therefore, calculations for the principal stresses in the core were provided.

The tension and compression stresses in the PVC core in the vicinity of the skin can be calculated, once the stresses in the skin have been found.

$$\sigma_c = \sigma_f \times \frac{E_c}{E_f} \tag{3.5}$$

The shear stress in the core is assumed to be constant through the thickness, and can be found using this equation(3.6).

$$\tau = \frac{P}{2bc} \tag{3.6}$$

Once, the stresses are calculated in the vicinity of the skin, the principal stresses can be calculated to investigate if the failure was initiated by the core.

$$\sigma_{1,2} = \frac{\sigma_c}{2} \pm \sqrt{\left(\frac{\sigma_c}{2}\right)^2 + \tau^2} \tag{3.7}$$

$$\tau_{\max} = \sqrt{\left(\frac{\sigma_c}{2}\right)^2 + \tau^2} \tag{3.8}$$

The principal stresses calculations at the elastic limit are presented in tables 3.12, 3.14 and 3.16, and are compared to the corresponding core yield stresses (Shear, tension, and

compression). The principal stresses calculations at the ultimate moment are also presented in tables 3.13, 3.15 and 3.17, and are compared to the corresponding core ultimate stresses (Shear, tension, and compression).

For the elastic limit, it was noticed that the ratio between the applied stresses and the yield stresses for shear and compression were generally higher than the tension one. Consequently, it can be concluded that the failure is generally initiated by shear and/or compression in the core. The stress ratio values decreased with the increase in the core density, it dropped from 175% for the 50 Kg/m^3 core to 33% for the corresponding beam with 250 Kg/m^3 core. The author believes that because of the excess resin absorbed by the lower density cores, providing the cells with additional bracing against deformation, there was a further decrease in the stress ratios for the higher density cores. Only the stresses in the core that has a density of 50 Kg/m^3 exceeded the yield stress regardless of the skin used.

For principal stresses calculated at ultimate moment, same observations could be detected. The principal stresses to ultimate core stresses ratios decreased with the increase of the core density. Only, beams made of the 50 Kg/m^3 core had stresses that approached and/or exceeded the ultimate stresses of the core, tables 3.13, 3.15 and 3.17.

Therefore, it can be concluded that the principal stresses calculation based on basic solid mechanics is not sufficient to describe the failure mechanism in these sandwich beams. Further calculations and discussion are presented in the following chapter.

3.6.9 Comparison with sandwich beams with balsa cores

Sandwich beams made of long grain balsa were fabricated and tested in a previous study by Giancaspro (Giancaspro, 2004). In order to compare between the performance of beams having balsa cores and beams having PVC cores, beams with same dimensions (13 mm thick

and 50 mm wide) and same reinforcement (one and three tows of H-12K HMC, 640 GPa modulus fibers) are presented in table 3.18. The density, maximum moment and flexural stiffness are also shown in table 3.18.

For the control samples, the balsa beams had 20 times the moment capacity and 28 times the stiffness of the PVC beam. By increasing the reinforcement ratio to 0.18%, the moment capacity of sandwich beam having balsa core was double the capacity for the PVC sandwich beam. The flexural stiffness for balsa sandwich beam was 2.4 times the stiffness for the PVC sandwich beam. By tripling the reinforcement ratio, the balsa sandwich beam had only 40% higher moment capacity but the stiffness was 2.2 times the corresponding PVC sandwich beam.

3.7 Observations

Based on the experimental results represented this chapter, several observations can be made regarding the beams reinforced with inorganic composites:

- It is feasible to fabricate sandwich panels using PVC core and carbon/Geopolymer composites. Excellent bond could be achieved between the inorganic resin and the PVC core, and the bond is strong enough to eliminate skin delamination.
- The light cores tend to absorb more resin than the denser ones, which may affect its specific strength, and could be critical in applications where the weight is a major issue.
- Increase of carbon provides increase in moment capacity but the processing needs improvement to obtain proportional increase.
- The increase in density provides consistent increase in moment capacity.

- The flexural stiffness increased with the increase in carbon fiber areas in a way similar to the increase in the moment capacity.
- The denser the core is, the higher the stiffness that could be attained.
- Compression failure tends to happen with the beams fabricated with low density cores.
- N-12K MMC (440 GPa modulus fibers) fibers provide higher moment capacity than H-12K HMC (640 GPa modulus fibers), even though it has a lower modulus.
- Providing unsymmetrical reinforcement does not improve the flexural capacity or the stiffness but the ductility increases considerably.
- The toughness increases as the reinforcement area increases. Beams reinforced with N-12K MMC (440 GPa modulus fibers) provide higher toughness than the ones reinforced with H-12K HMC (640 GPa modulus fibers). On the whole, beams reinforced with carbon tape (230 GPa modulus fibers) exhibited the largest toughness.

By comparing similar beams reinforced using the epoxy/carbon skin; the following observations can be made.

- Beams reinforced with organic composites are lighter than the corresponding beams reinforced with inorganic resin. The difference in density between the organic resin and the inorganic one is 14%.
- The organic resin provides only 3% higher moment capacity than those reinforced with inorganic resin
- For the stiffness, the inorganic resin exhibited 14% higher stiffness over the organic resin.

- Organic composites are recommended when ductility is a design parameter.

Based on the principal stresses calculation, the following observations can be found.

- The failure in the skin occurs at a fraction of the ultimate strength of the fibers. In other words, the skin is not fully stressed at failure.
- The principal stresses in the core are high in shear and compression, and the basic solid mechanics calculations can not describe the failure mechanism.

By comparing balsa sandwich beams and PVC sandwich beams reinforced with inorganic/carbon skin (Table 3.18); the following observations can be made:

- Without skin and 36% more dense, balsa beams have 2000% more moment capacity and 2750% more stiffness than PVC beam.
- For reinforced beams, the balsa beams have an average of 170% more moment capacity and 230% more stiffness. The difference decreases with the increase of the reinforcement ratio.
- The long grain balsa sandwich beams have higher mechanical properties but their use is only limited to one dimensional elements (beams). However, the Polyvinyl (PVC) sandwich beams can be used in fabricating two dimensional elements (plates and shells).

Table 3. 1 PVC core properties

Property	HT50	HT110	H130	H200	H250
Thickness, h mm	13	13	13	13	13
Density, ρ_c Kg/m^3	50	110	130	200	250
Out of Plane Compressive strength, F_{3c} Mpa*	0.7	2.1	2.5	4.4	5.8**
Out of Plane Compressive Modulus, E_{3c} MPa	75	150	175	310	400
In Plane Tensile Strength, F_{1t} MPa	1.5	3.3	4.2	6.4	8.8
In Plane Tensile Modulus, E_{1t} MPa	95	175	140	230	300
Yield Transverse Shear Strength, F_{13y} MPa	0.6	1.6	1.8	NA	NA
Ultimate Transverse Shear Strength, F_{13u} MPa	NA	NA	2.0	3.3	4.5
Transverse Shear Modulus, G_{13} MPa	19	40	52	85	108

NA= Not Available

*Values vary based on the direction

** Ranges between 4.2 and 5.8 MPa (Abot, 2000)

Table 3. 2 Carbon skin properties

	H-12k HMC	N-12k MMC	T-3k Uni C Tape
Description	Carbon tow	Carbon tow	Unidirectional carbon tape
Filaments per end	12,000	12,000	3,000
Tensile Strength, Mpa	2,620	2,620	3,500
Tensile Modulus, Gpa	640	440	230
Ultimate Elongation, %	0.4	0.6	1.5
Density, g/cm^3	2.12	2.06	1.81
Filament diameter, μm	11	11	7

Table 3. 3 Sample details for samples reinforced with N-12K MMC

Sample ID	Core		Reinforcement Width		Weight		Additional weight per tow
	Depth	Width	Compression	Tension	Core	Beam	
	mm	mm	mm	mm	gm	gm	gm/tow
N50-1C-1T	13.27	50.46	11	8	12.6	42.1	15
N50-3C-3T	13.15	50.20	36	35	12.6	72.2	10
N50-2C-1T	13.22	50.35	25	11	12.5	52.1	13
N50-3C-1T	13.05	49.88	36	11	12.9	55.2	11
N50-1C-1T-E	13.03	50.83	11	10	13.1	35.4	11
N50-3C-3T-E	13.01	50.73	29	26	13.1	48.4	6
N110-1C-1T	13.57	50.73	11	14	25.3	55.4	15
N110-3C-3T	13.66	50.69	39	39	25.3	77.2	9
N110-2C-1T	13.55	50.83	23	15	25.5	59.2	11
N110-3C-1T	13.55	50.66	32	11	25.3	66.7	10
N110-1C-1T-E	13.03	50.72	15	9	25.5	44.5	10
N110-3C-3T-E	12.99	50.66	29	28	25.3	60.1	6
N130-1C-1T	12.90	50.68	12	12	26.1	46.4	10
N130-3C-3T	12.96	50.62	34	36	26.2	61.3	6
N130-2C-1T	12.87	50.65	27	14	25.3	49.6	8
N130-3C-1T	12.95	50.88	38	14	25.2	53.7	7
N130-1C-1T-E	12.98	50.60	13	9	25.6	39.4	7
N130-3C-3T-E	13.00	50.81	35	28	25.1	49.7	4
N250-1C-1T	12.95	51.43	10	13	53.9	73.2	10
N250-3C-3T	12.97	53.67	30	29	56.5	87.0	5
N250-2C-1T	12.93	51.57	22	13	52.7	77.1	8
N250-3C-1T	12.85	49.67	36	12	51.0	76.3	6
N250-1C-1T-E	12.78	51.60	13	10	54.7	67.6	6
N250-3C-3T-E	12.84	51.12	27	35	53.7	73.9	3

Table 3. 4 Sample details for samples reinforced with H-12K HMC

Sample ID	Core		Reinforcement Width		Weight		Additional weight per tow
	Depth	Width	Compression	Tension	Core	Beam	
	mm	mm	mm	mm	gm	gm	gm/tow
H50-1C-1T	12.95	51.45	14	14	14.0	37.6	12
H50-3C-3T	13.03	51.85	45	45	14.0	60.3	8
H50-2C-1T	12.97	50.48	30	16	13.0	44.9	11
H50-3C-1T	12.90	51.09	45	13	13.1	47.9	9
H50-1C-1T-E	13.17	50.15	9	14	12.4	32.5	10
H50-3C-3T-E	13.23	50.23	29	25	12.8	42.8	5
H110-1C-1T	13.57	50.73	17	15	28.8	52.7	12
H110-3C-3T	13.66	50.69	45	45	29.2	75.9	8
H110-2C-1T	13.55	50.83	32	16	29.1	57.9	10
H110-3C-1T	13.55	50.66	45	16	30.2	68.2	10
H110-1C-1T-E	13.03	50.72	14	11	25.5	42.5	9
H110-3C-3T-E	12.99	50.66	35	28	25.4	55.5	5
H130-1C-1T	12.85	51.69	21	17	32.5	56.0	12
H130-3C-3T	13.04	52.05	51	51	32.2	72.5	7
H130-2C-1T	13.03	52.07	34	18	32.1	55.6	8
H130-3C-1T	12.99	51.99	51	20	32.2	57.6	6
H130-1C-1T-E	12.97	50.78	12	12	25.1	39.0	7
H130-3C-3T-E	12.99	50.51	29	31	25.7	46.2	3
H250-1C-1T	12.92	50.67	14	12	53.9	74.4	10
H250-3C-3T	12.97	51.24	40	38	55.4	90.5	6
H250-2C-1T	12.81	51.67	27	10	56.7	80.9	8
H250-3C-1T	12.78	51.57	37	11	56.7	82.3	6
H250-1C-1T-E	12.89	50.83	12	9	53.3	64.0	5
H250-3C-3T-E	12.89	49.92	29	34	52.3	70.5	3
H200-1C-1T	12.72	51.64	20	20	47.1	74.7	14
H200-3C-3T	12.77	51.95	51	51	48.1	91.2	7
H200-2C-1T	12.73	51.77	34	26	47.2	76.6	10
H200-3C-1T	12.73	51.97	51	21	47.7	79.4	8

Table 3. 5 Sample details for samples reinforced with T-3K Uni C Tape

Sample ID	Core		Reinforcement Width		Weight		Additional weight per tape
	Depth	Width	Compression	Tension	Core	Beam	
	mm	mm	mm	mm	gm	gm	gm/tape
C50	13.07	52.03	0	0	14.4	14.4	0
T50-1C-1T	13.32	50.30	50	50	12.8	59.7	23
T50-2C-2T	13.15	49.77	49	49	12.4	73.9	15
C110	13.50	50.60	0	0	28.5	28.5	0
T110-1C-1T	12.96	50.81	50	50	25.6	65.6	20
T110-2C-2T	12.99	50.75	50	50	25.6	81.9	14
C130	13.04	47.64	0	0	29.5	29.5	0
T130-1C-1T	12.96	50.69	50	50	25.3	55.1	15
T130-2C-2T	12.85	49.00	49	49	24.9	72.2	12
C250	12.93	50.78	14	12	54.2	54.2	0
T250-1C-1T	12.92	50.67	50	50	53.9	76.2	11
T250-2C-2T	12.97	51.24	50	50	55.4	89.8	9

Table 3. 6 Test results for samples reinforced with N-12K MMC

Sample ID	Max Moment	Stiffness	Toughness	Increase		
	M_u	EI	U	Weight, W	M_u	EI
	N.m	$N.m^2$	N.mm	%	%	%
C50	0.5	0.4	21	-	-	-
N50-1C-1T	15.1	21	1130	234	2920	5660
N50-3C-3T	26.6	49	2560	473	5211	13287
N50-2C-1T	15.4	25	1327	317	2989	6796
N50-3C-1T	18.6	29	1429	328	3628	7851
N50-1C-1T-E	12.6	24	1220	170	2414	6472
N50-3C-3T-E	28.3	51	2634	269	5560	13855
C110	1.2	1.0	57	-	-	-
N110-1C-1T	15.6	31	960	119	1199	3111
N110-3C-3T	34.4	73	1836	205	2765	7537
N110-2C-1T	14.6	37	656	132	1113	3796
N110-3C-1T	17.3	44	779	164	1339	4513
N110-1C-1T-E	20.6	24	1361	75	1619	2394
N110-3C-3T-E	35.9	63	3486	138	2896	6508
C130	1.5	1.3	75	-	-	-
N130-1C-1T	15.2	30	1286	78	914	2293
N130-3C-3T	36.7	70	2338	134	2345	5515
N130-2C-1T	16.1	38	1390	96	975	2956
N130-3C-1T	13.6	35	1165	113	807	2695
N130-1C-1T-E	15.4	22	1141	54	929	1653
N130-3C-3T-E	28.3	64	2158	98	1785	4993
C250	3.3	2.6	153	-	-	-
N250-1C-1T	18.5	33	1439	36	460	1201
N250-3C-3T	31.5	90	3293	54	855	3442
N250-2C-1T	17.8	45	1764	46	438	1665
N250-3C-1T	19.0	55	1905	50	475	2060
N250-1C-1T-E	20.7	28	1408	24	527	980
N250-3C-3T-E	35.4	70	3414	38	972	2641

Table 3.7 Test results for samples reinforced with H-12K HMC

Sample ID	Max Moment	Stiffness	Toughness	Increase		
	M_u	EI	U	Weight, W	M_u	EI
	N.m	$N.m^2$	N.mm	%	%	%
C50	0.5	0.4	21	-	-	-
H50-1C-1T	7.6	22	607	169	1509	6246
H50-3C-3T	20.9	55	1718	331	4338	15553
H50-2C-1T	9.9	26	1114	245	2005	7346
H50-3C-1T	9.6	24	1014	266	1948	6669
H50-1C-1T-E	11.4	25	1199	162	2330	7176
H50-3C-3T-E	24.0	55	2485	234	4996	15553
C110	1.2	1.0	57	-	-	-
H110-1C-1T	13.5	37	1527	83	1018	3828
H110-3C-3T	29.1	87	3201	160	2309	9064
H110-2C-1T	13.9	32	1212	99	1052	3298
H110-3C-1T	15.2	30	1095	126	1160	3017
H110-1C-1T-E	19.3	26	1270	67	1491	2674
H110-3C-3T-E	34.3	106	3821	119	2735	11059
C130	1.5	1.3	75	-	-	-
H130-1C-1T	20.0	37	1383	72	1271	2861
H130-3C-3T	29.9	98	3528	125	1946	7718
H130-2C-1T	14.0	44	1615	73	858	3454
H130-3C-1T	14.9	52	1774	79	920	4046
H130-1C-1T-E	16.5	29	1293	55	1030	2245
H130-3C-3T-E	20.2	73	2476	80	1284	5728
C250	3.3	2.6	153	-	-	-
H250-1C-1T	18.1	38	1651	38	456	1375
H250-3C-3T	38.3	123	3222	63	1079	4719
H250-2C-1T	21.7	59	1775	43	568	2211
H250-3C-1T	19.7	66	1990	45	506	2478
H250-1C-1T-E	22.5	38	1553	20	593	1398
H250-3C-3T-E	38.0	94	3377	35	1068	3581
C200	2.3	1.4	93	-	-	-
H200-1C-1T	19.6	41	1749	59	754	2861
H200-3C-3T	40.0	107	4485	90	1637	7557
H200-2C-1T	23.8	38	1379	62	933	2629
H200-3C-1T	26.3	36	1070	66	1044	2438

Table 3.8 Test results for samples reinforced with T-3K Uni C Tape

Sample ID	Max Moment	Stiffness	Toughness	Increase		
	M_u	EI	U	Weight, W	M_u	EI
	N.m	$N.m^2$	N.mm	%	%	%
C50	0.5	0.4	21	-	-	-
T50-1C-1T	27.5	52	2736	366	5752	14876
T50-2C-2T	30.2	70	3188	496	6321	20037
C110	1.2	1.0	57	-	-	-
T110-1C-1T	43.9	86	3029	156	3531	8940
T110-2C-2T	71.3	126	5541	220	5794	13179
C130	1.5	1.3	75	-	-	-
T130-1C-1T	42.4	82	2692	118	2807	6486
T130-2C-2T	62.7	120	5555	190	4196	9518
C250	3.3	2.6	153	-	-	-
T250-1C-1T	36.3	93	1854	38	1018	3535
T250-2C-2T	67.0	166	3109	63	1963	6426

Table 3.9 Stress calculations and failure mode for samples reinforced with N-12K MMC

Sample ID	Apparent Stress	A. Stress/weight	Fibers Stress	Observed Failure Mode
	σ	σ^*	$\sigma_{t,f}$	
	MPa	MPa/gm	MPa	
C50	0.3	0.0	-	-
N50-1C-1T	10	0.2	323	Tension Failure (Split at midspan)
N50-3C-3T	18	0.3	272	Bearing
N50-2C-1T	11	0.2	732	Tension Failure (Split at midspan)
N50-3C-1T	13	0.2	1092	Tension Failure (Split at midspan)
N50-1C-1T-E	9	0.2	469	Split under the right load and bearing
N50-3C-3T-E	20	0.4	408	Bearing, Test stopped
C110	0.8	0.0	-	-
N110-1C-1T	10	0.2	685	Tension Failure (Split at midspan)
N110-3C-3T	22	0.3	659	Tension Failure
N110-2C-1T	9	0.2	828	Tension Failure
N110-3C-1T	11	0.2	884	Tension Failure
N110-1C-1T-E	14	0.3	643	Initiated by wrinkling and bearing then tension failure
N110-3C-3T-E	25	0.4	591	Wrinkling and bearing
C130	1.1	0.0	-	-
N130-1C-1T	11	0.2	692	Tension Failure (Split under right load)
N130-3C-3T	26	0.4	597	Tension and shear under left load
N130-2C-1T	12	0.2	683	Tension Failure (Split under left load)
N130-3C-1T	10	0.2	679	Tension Failure (Split at midspan)
N130-1C-1T-E	11	0.3	710	Initiated by wrinkling and bearing then tension failure
N130-3C-3T-E	20	0.4	554	Initiated by wrinkling and bearing then tension failure
C250	2.3	0.0	-	-
N250-1C-1T	13	0.2	841	Iintiated by tension followed by spliting under the loads
N250-3C-3T	21	0.2	635	Tension Failure (Split at midspan)
N250-2C-1T	12	0.2	1098	Tension Failure (Split at midspan)
N250-3C-1T	14	0.2	909	Tension Failure (Split at midspan)
N250-1C-1T-E	15	0.2	731	Initiated by wrinkling and bearing then tension failure
N250-3C-3T-E	25	0.3	684	Initiated by wrinkling and bearing then tension failure

Table 3.10 Stress calculations and failure mode for samples reinforced with H-12K HMC

Sample ID	Apparent Stress	A. Stress/weight	Fibers Stress	Observed Failure Mode
	σ	σ^*	$\sigma_{t,f}$	
	MPa	MPa/gm	MPa	
C50	0.3	0.0	-	-
H50-1C-1T	5	0.1	359	Wrinkling Failure
H50-3C-3T	14	0.2	330	Bearing Failure
H50-2C-1T	7	0.2	355	Tension Failure
H50-3C-1T	7	0.1	594	Tension Failure (Split at midspan)
H50-1C-1T-E	8	0.2	614	Wrinkling and bearing, test stopped
H50-3C-3T-E	16	0.4	292	Bearing Failure, test stopped
C110	0.8	0.0	-	-
H110-1C-1T	9	0.2	512	Tension Failure (Split at midspan)
H110-3C-3T	18	0.2	248	Tension Failure (Split at midspan)
H110-2C-1T	9	0.2	464	Tension Failure (Split at midspan)
H110-3C-1T	10	0.1	457	Tension Failure (Split at midspan)
H110-1C-1T-E	13	0.3	710	Wrinkling and bearing followed by spliting at midspan
H110-3C-3T-E	24	0.4	514	Wrinkling and bearing followed by spliting at midspan
C130	1.0	0.0	-	-
H130-1C-1T	14	0.3	750	Wrinkling and Tension failure
H130-3C-3T	20	0.3	434	Tension Failure (Split at midspan)
H130-2C-1T	9	0.2	498	Tension Failure (Split at midspan)
H130-3C-1T	10	0.2	555	Wrinkling and Tension failure
H130-1C-1T-E	12	0.3	730	Wrinkling and bearing followed by spliting under right load
H130-3C-3T-E	14	0.3	386	Wrinkling and bearing followed by spliting at midspan
C250	2.3	0.0	-	-
H250-1C-1T	13	0.2	911	Iintiated by tension followed by spliting under the loads
H250-3C-3T	27	0.3	689	Tension Failure
H250-2C-1T	15	0.2	1046	Iintiated by tension followed by spliting under the loads
H250-3C-1T	14	0.2	1442	Tension Failure (Split under right load)
H250-1C-1T-E	16	0.3	715	Wrinkling followed by spliting at midspan
H250-3C-3T-E	27	0.4	615	Wrinkling followed by spliting at midspan
C200	1.7	0.0	-	-
H200-1C-1T	14	0.2	649	Wrinkling and Tension failure
H200-3C-3T	28	0.3	582	Tension Failure
H200-2C-1T	17	0.2	605	Wrinkling and Tension failure
H200-3C-1T	19	0.2	283	Wrinkling and Tension failure

Table 3.11 Stress calculations and failure mode for samples reinforced with T-3K Uni C Tape

Sample ID	Apparent Stress	A. Stress/weight	Fibers Stress	Observed Failure Mode
	σ	σ^*	$\sigma_{t,f}$	
	MPa	MPa/gm	MPa	
C50	0.3	0.0	-	-
T50-1C-1T	18	0.3	359	Wrinkling Failure
T50-2C-2T	21	0.3	330	Bearing Failure and Shear
C110	0.8	0.0	-	-
T110-1C-1T	31	0.5	512	Tension Failure (Split at midspan)
T110-2C-2T	50	0.6	248	Tension Failure (Split at midspan)
C130	1.1	0.0	-	-
T130-1C-1T	30	0.5	750	Wrinkling and Tension failure
T130-2C-2T	47	0.6	434	Tension Failure (Split at midspan)
C250	2.3	0.0	-	-
T250-1C-1T	26	0.3	911	Iintiated by tension followed by spliting under the loads
T250-2C-2T	47	0.5	689	Tension Failure

Table 3.12 Principal stresses calculation for samples reinforced with N-12K MMC at elastic limit

Sample ID	Face Comp. St.	Core Shear	Face Tens. St.	Core Normal Stresses		Core Principal Stresses			Strain	Core Principal Stresses Ratio		
	$\sigma_{c,f}$	$\tau_{,c}$	$\sigma_{t,f}$	$\sigma_{c,c}$	$\sigma_{t,c}$	τ_{max}	σ_1	σ_2	ε	$\tau_{max}/\tau_{yeild,c}$	$\sigma_1/\sigma_{tyiedl,c}$	$\sigma_2/\sigma_{cyeild,c}$
	MPa	MPa	MPa	MPa	MPa	MPa	MPa	MPa	%	%	%	%
N50-1C-1T	323	0.48	323	-0.07	0.09	0.48	0.45	-0.52	0.12	80	60	148
N50-3C-3T	272	0.28	272	-0.06	0.07	0.28	0.25	-0.31	0.13	47	33	88
N50-2C-1T	366	0.79	732	-0.08	0.20	0.80	0.76	-0.83	-	133	101	238
N50-3C-1T	364	1.18	1092	-0.08	0.29	1.19	1.15	-1.22	-	198	153	350
N50-1C-1T-E	469	0.56	469	-0.10	0.13	0.56	0.51	-0.61	0.15	94	68	175
N50-3C-3T-E	408	0.56	408	-0.09	0.11	0.56	0.52	-0.61	0.19	94	69	173
N110-1C-1T	685	0.58	685	-0.15	0.18	0.59	0.52	-0.66	0.19	37	31	63
N110-3C-3T	659	0.61	659	-0.14	0.18	0.61	0.54	-0.68	0.23	38	33	65
N110-2C-1T	414	0.66	828	-0.09	0.22	0.66	0.62	-0.70	-	41	37	67
N110-3C-1T	295	0.96	884	-0.06	0.24	0.96	0.93	-0.99	-	60	56	94
N110-1C-1T-E	643	0.85	643	-0.14	0.17	0.86	0.79	-0.92	0.21	53	48	88
N110-3C-3T-E	591	0.74	591	-0.13	0.16	0.75	0.68	-0.81	0.22	47	41	77
N130-1C-1T	692	0.69	692	-0.15	0.19	0.69	0.62	-0.77	0.17	38	29	61
N130-3C-3T	597	0.59	597	-0.13	0.16	0.60	0.53	-0.66	0.20	33	25	53
N130-2C-1T	342	0.58	683	-0.07	0.18	0.58	0.55	-0.62	-	32	26	50
N130-3C-1T	226	0.58	679	-0.05	0.18	0.58	0.56	-0.60	-	32	26	48
N130-1C-1T-E	710	0.94	710	-0.15	0.19	0.94	0.87	-1.02	0.25	52	41	82
N130-3C-3T-E	554	0.71	554	-0.12	0.15	0.71	0.65	-0.77	0.20	40	31	62
N250-1C-1T	841	0.77	841	-0.18	0.23	0.78	0.69	-0.87	0.19	19	16	30
N250-3C-3T	635	0.78	635	-0.14	0.17	0.79	0.72	-0.85	0.16	19	16	29
N250-2C-1T	549	1.01	1098	-0.12	0.30	1.01	0.95	-1.07	-	25	22	37
N250-3C-1T	303	0.90	909	-0.06	0.25	0.91	0.87	-0.94	-	22	20	32
N250-1C-1T-E	731	0.87	731	-0.16	0.20	0.88	0.80	-0.95	0.19	22	18	33
N250-3C-3T-E	684	0.70	684	-0.15	0.18	0.70	0.63	-0.78	0.22	17	14	27

Table 3.13 Principal stresses calculation for samples reinforced with N-12K MMC at ultimate moment

Sample ID	Face Comp. St.	Core Shear	Face Tens. St.	Core Normal Stresses		Core Principal Stresses			Core Principal Stresses Ratio		
	$\sigma_{c,f}$	$\tau_{,c}$	$\sigma_{t,f}$	$\sigma_{c,c}$	$\sigma_{t,c}$	τ_{max}	σ_1	σ_2	$\tau_{max}/\tau_{ult,c}$	$\sigma_1/\sigma_{t\text{-}ultl,c}$	$\sigma_2/\sigma_{c\text{-}ult,c}$
	MPa	MPa	MPa	MPa	MPa	MPa	MPa	MPa	%	%	%
N50-1C-1T	1248	1.86	1248	-0.18	0.23	1.86	1.77	-1.96	345	118	279
N50-3C-3T	738	0.76	738	-0.11	0.14	0.76	0.70	-0.81	140	47	116
N50-2C-1T	640	1.39	1281	-0.09	0.24	1.39	1.34	-1.44	258	90	205
N50-3C-1T	522	1.70	1566	-0.08	0.29	1.70	1.66	-1.74	315	111	248
N50-1C-1T-E	948	1.13	948	-0.14	0.18	1.13	1.06	-1.20	210	71	172
N50-3C-3T-E	795	1.10	795	-0.12	0.15	1.10	1.04	-1.15	203	69	165
N110-1C-1T	1260	1.07	1260	-0.37	0.43	1.09	0.91	-1.27	76	27	61
N110-3C-3T	920	0.84	920	-0.27	0.31	0.86	0.72	-0.99	59	22	47
N110-2C-1T	589	0.94	1178	-0.17	0.40	0.94	0.85	-1.03	65	26	49
N110-3C-1T	466	1.52	1397	-0.14	0.48	1.52	1.45	-1.59	105	44	76
N110-1C-1T-E	1369	1.82	1369	-0.40	0.47	1.83	1.63	-2.03	127	49	97
N110-3C-3T-E	1011	1.27	1011	-0.30	0.35	1.28	1.13	-1.43	89	34	68
N130-1C-1T	1292	1.29	1292	-0.44	0.35	1.30	1.08	-1.53	65	26	61
N130-3C-3T	1034	1.03	1034	-0.35	0.28	1.04	0.87	-1.22	52	21	49
N130-2C-1T	687	1.17	1373	-0.23	0.38	1.18	1.06	-1.29	59	25	52
N130-3C-1T	384	0.98	1151	-0.13	0.31	0.98	0.92	-1.05	49	22	42
N130-1C-1T-E	975	1.29	975	-0.33	0.27	1.30	1.14	-1.47	65	27	59
N130-3C-3T-E	771	0.99	771	-0.26	0.21	1.00	0.86	-1.13	50	21	45
N250-1C-1T	1190	1.09	1190	-0.93	0.70	1.19	0.72	-1.65	26	8	37
N250-3C-3T	888	1.10	888	-0.69	0.52	1.15	0.80	-1.50	26	9	33
N250-2C-1T	745	1.37	1490	-0.58	0.87	1.40	1.11	-1.69	31	13	38
N250-3C-1T	472	1.41	1415	-0.37	0.83	1.42	1.24	-1.60	32	14	36
N250-1C-1T-E	1209	1.44	1209	-0.94	0.71	1.52	1.05	-1.99	34	12	44
N250-3C-3T-E	874	0.89	874	-0.68	0.51	0.96	0.62	-1.30	21	7	29

Table 3.14 Principal stresses calculation for samples reinforced with H-12K HMC at elastic limit

Sample ID	Face Comp. St.	Core Shear	Face Tens. St.	Core Normal Stresses		Core Principal Stresses			Strain	Core Principal Stresses Ratio		
	$\sigma_{c,f}$	$\tau_{,c}$	$\sigma_{t,f}$	$\sigma_{c,c}$	$\sigma_{t,c}$	τ_{max}	σ_1	σ_2	ε	$\tau_{max}/\tau_{yeild,c}$	$\sigma_1/\sigma_{tyiedl,c}$	$\sigma_2/\sigma_{cyeild,c}$
	MPa	MPa	MPa	MPa	MPa	MPa	MPa	MPa	%	%	%	%
H50-1C-1T	359	0.31	359	-0.05	0.07	0.31	0.28	-0.33	0.12	51	37	95
H50-3C-3T	330	0.26	330	-0.05	0.06	0.26	0.24	-0.29	0.14	44	32	82
H50-2C-1T	178	0.27	355	-0.03	0.07	0.27	0.25	-0.28	-	44	34	80
H50-3C-1T	198	0.55	594	-0.03	0.11	0.55	0.53	-0.56	-	91	71	160
H50-1C-1T-E	614	0.51	614	-0.09	0.11	0.51	0.46	-0.55	0.19	85	62	158
H50-3C-3T-E	292	0.41	292	-0.04	0.05	0.41	0.39	-0.44	0.13	69	52	124
H110-1C-1T	512	0.41	512	-0.15	0.18	0.41	0.34	-0.49	0.12	26	21	47
H110-3C-3T	248	0.20	248	-0.07	0.08	0.20	0.16	-0.24	0.07	13	10	23
H110-2C-1T	232	0.35	464	-0.07	0.16	0.35	0.31	-0.38	-	22	19	36
H110-3C-1T	152	0.34	457	-0.04	0.16	0.34	0.32	-0.36	-	21	19	35
H110-1C-1T-E	710	0.78	710	-0.21	0.24	0.79	0.69	-0.90	0.21	49	42	85
H110-3C-3T-E	514	0.65	514	-0.15	0.18	0.65	0.58	-0.73	0.11	41	35	69
H130-1C-1T	750	0.53	750	-0.26	0.20	0.54	0.41	-0.67	0.15	30	20	54
H130-3C-3T	434	0.30	434	-0.15	0.12	0.31	0.24	-0.39	0.10	17	11	31
H130-2C-1T	249	0.33	498	-0.09	0.14	0.33	0.29	-0.38	-	19	14	30
H130-3C-1T	185	0.33	555	-0.06	0.15	0.33	0.30	-0.36	-	18	14	29
H130-1C-1T-E	730	0.73	730	-0.25	0.20	0.74	0.61	-0.86	0.19	41	29	69
H130-3C-3T-E	386	0.45	386	-0.13	0.11	0.45	0.38	-0.52	0.12	25	18	41
H250-1C-1T	911	0.91	911	-0.71	0.53	0.97	0.62	-1.33	0.18	24	14	46
H250-3C-3T	689	0.65	689	-0.54	0.40	0.70	0.43	-0.97	0.13	17	10	34
H250-2C-1T	523	1.25	1046	-0.41	0.61	1.27	1.06	-1.47	-	31	24	51
H250-3C-1T	481	1.56	1442	-0.38	0.84	1.58	1.39	-1.76	-	39	32	61
H250-1C-1T-E	715	0.95	715	-0.56	0.42	0.99	0.71	-1.27	0.14	24	16	44
H250-3C-3T-E	615	0.65	615	-0.48	0.36	0.69	0.45	-0.93	0.15	17	10	32
H200-1C-1T	649	0.39	649	-0.39	0.29	0.43	0.24	-0.63	0.12	15	7	29
H200-3C-3T	582	0.41	582	-0.35	0.26	0.44	0.27	-0.62	0.12	15	8	28
H200-2C-1T	303	0.28	605	-0.18	0.27	0.29	0.20	-0.38	-	10	6	17
H200-3C-1T	94	0.16	283	-0.06	0.13	0.16	0.13	-0.19	-	6	4	9

Table 3.15 Principal stresses calculation for samples reinforced with H-12K HMC at ultimate moment

Sample ID	Face Comp. St.	Core Shear	Face Tens. St.	Core Normal Stresses		Core Principal Stresses			Core Principal Stresses Ratio		
	$\sigma_{c,f}$	$\tau_{,c}$	$\sigma_{t,f}$	$\sigma_{c,c}$	$\sigma_{t,c}$	τ_{max}	σ_1	σ_2	$\tau_{max}/\tau_{ult,c}$	$\sigma_1/\sigma_{t\text{-}ultl,c}$	$\sigma_2/\sigma_{c\text{-}ult,c}$
	MPa	MPa	MPa	MPa	MPa	MPa	MPa	MPa	%	%	%
H50-1C-1T	640	0.55	640	-0.09	0.12	0.55	0.50	-0.59	101	33	85
H50-3C-3T	585	0.47	585	-0.09	0.11	0.47	0.42	-0.51	87	28	73
H50-2C-1T	368	0.55	736	-0.05	0.14	0.55	0.52	-0.58	102	35	82
H50-3C-1T	247	0.68	740	-0.04	0.14	0.68	0.66	-0.70	126	44	100
H50-1C-1T-E	875	0.72	875	-0.13	0.16	0.73	0.66	-0.79	134	44	113
H50-3C-3T-E	662	0.94	662	-0.10	0.12	0.94	0.89	-0.99	173	59	141
H110-1C-1T	1006	0.80	1006	-0.29	0.34	0.81	0.67	-0.96	57	20	46
H110-3C-3T	734	0.58	734	-0.22	0.25	0.59	0.49	-0.70	41	15	33
H110-2C-1T	368	0.55	736	-0.11	0.25	0.55	0.50	-0.61	38	15	29
H110-3C-1T	294	0.66	881	-0.09	0.30	0.66	0.62	-0.70	46	19	33
H110-1C-1T-E	1077	1.19	1077	-0.32	0.37	1.20	1.04	-1.36	83	32	65
H110-3C-3T-E	879	1.11	879	-0.26	0.30	1.11	0.98	-1.24	77	30	59
H130-1C-1T	981	0.69	981	-0.34	0.27	0.71	0.54	-0.88	35	13	35
H130-3C-3T	752	0.53	752	-0.26	0.21	0.54	0.41	-0.67	27	10	27
H130-2C-1T	506	0.67	1013	-0.17	0.28	0.68	0.59	-0.76	34	14	31
H130-3C-1T	384	0.69	1151	-0.13	0.31	0.69	0.62	-0.76	35	15	30
H130-1C-1T-E	914	0.91	914	-0.31	0.25	0.92	0.77	-1.08	46	18	43
H130-3C-3T-E	512	0.59	512	-0.17	0.14	0.60	0.51	-0.68	30	12	27
H250-1C-1T	1326	1.32	1326	-1.04	0.78	1.42	0.90	-1.94	31	10	43
H250-3C-3T	1080	1.02	1080	-0.84	0.63	1.10	0.68	-1.52	24	8	34
H250-2C-1T	677	1.62	1354	-0.53	0.79	1.64	1.37	-1.90	36	16	42
H250-3C-1T	564	1.84	1691	-0.44	0.99	1.85	1.63	-2.07	41	19	46
H250-1C-1T-E	894	1.19	894	-0.70	0.52	1.24	0.89	-1.58	27	10	35
H250-3C-3T-E	797	0.84	797	-0.62	0.47	0.90	0.58	-1.21	20	7	27
H200-1C-1T	1386	0.83	1386	-0.84	0.62	0.93	0.51	-1.35	28	8	31
H200-3C-3T	1063	0.75	1063	-0.64	0.48	0.81	0.49	-1.13	25	8	26
H200-2C-1T	413	0.38	826	-0.25	0.37	0.40	0.27	-0.52	12	4	12
H200-3C-1T	215	0.37	645	-0.13	0.29	0.37	0.31	-0.44	11	5	10

Table 3.16 Principal stresses calculation for samples reinforced with T-3K Uni C Tape at elastic limit

Sample ID	Face Comp. St.	Core Shear	Face Tens. St.	Core Normal Stresses		Core Principal Stresses			Strain	Core Principal Stresses Ratio		
	$\sigma_{c,f}$	$\tau_{,c}$	$\sigma_{t,f}$	$\sigma_{c,c}$	$\sigma_{t,c}$	τ_{max}	σ_1	σ_2	ε	$\tau_{max}/\tau_{yeild,c}$	$\sigma_1/\sigma_{tyiedl,c}$	$\sigma_2/\sigma_{cyeild,c}$
	MPa	MPa	MPa	MPa	MPa	MPa	MPa	MPa	%	%	%	%
T50-1C-1T	304	0.31	304	-0.12	0.16	0.31	0.25	-0.37	0.19	52	33	107
T50-2C-2T	125	0.25	125	-0.05	0.06	0.25	0.23	-0.28	0.12	42	30	79
T110-1C-1T	506	0.51	506	-0.41	0.48	0.55	0.34	-0.76	0.21	34	21	72
T110-2C-2T	319	0.64	319	-0.26	0.30	0.66	0.53	-0.79	0.19	41	32	75
T130-1C-1T	506	0.51	506	-0.48	0.38	0.56	0.32	-0.80	0.20	31	15	64
T130-2C-2T	326	0.66	326	-0.31	0.25	0.67	0.52	-0.83	0.18	37	25	66
T250-1C-1T	605	0.61	605	-1.32	0.99	0.90	0.24	-1.55	0.21	22	5	54
T250-2C-2T	473	0.95	473	-1.03	0.77	1.08	0.57	-1.60	0.19	27	13	55

Table 3.17 Principal stresses calculation for samples reinforced with T-3K Uni C Tape at ultimate moment

Sample ID	Face Comp. St.	Core Shear	Face Tens. St.	Core Normal Stresses		Core Principal Stresses			Core Principal Stresses Ratio		
	$\sigma_{c,f}$	$\tau_{,c}$	$\sigma_{t,f}$	$\sigma_{c,c}$	$\sigma_{t,c}$	τ_{max}	σ_1	σ_2	$\tau_{max}/\tau_{ult,c}$	$\sigma_1/\sigma_{t\text{-}ultl,c}$	$\sigma_2/\sigma_{c\text{-}ult,c}$
	MPa	MPa	MPa	MPa	MPa	MPa	MPa	MPa	%	%	%
T50-1C-1T	542	0.55	542	-0.22	0.28	0.56	0.45	-0.67	103	30	95
T50-2C-2T	295	0.59	295	-0.12	0.15	0.60	0.54	-0.66	111	36	94
T110-1C-1T	826	0.83	826	-0.67	0.79	0.90	0.56	-1.23	62	17	59
T110-2C-2T	666	1.34	666	-0.54	0.63	1.37	1.10	-1.64	95	33	78
T130-1C-1T	843	0.85	843	-0.80	0.64	0.94	0.54	-1.34	47	13	54
T130-2C-2T	614	1.23	614	-0.58	0.47	1.27	0.98	-1.56	63	23	62
T250-1C-1T	717	0.72	717	-1.56	1.17	1.06	0.28	-1.84	24	3	32
T250-2C-2T	659	1.33	659	-1.43	1.07	1.51	0.79	-2.22	34	9	38

Table 3.18 Comparison between sandwich beams having balsa cores and sandwich beams having PVC cores

Reinforcement		PVC			Balsa*			Ratio	
Type	Ratio	Core density	M_u	EI	Core density	M_u	EI	$M_{u,Balsa}/M_{u,PVC}$	EI_{Balsa}/EI_{PVC}
-	%	Kg/m^3	N.m	$N.m^2$	Kg/m^3	N.m	$N.m^2$		
Control	0.00	50	0.5	0.4	68	10	11	20.0	27.5
1 Tow H-12K HMC	0.18	50	7.6	22	66	15	53	2.0	2.4
3 Tows H-12K HMC	0.53	50	20.9	55	65	30	121	1.4	2.2

* (Giancaspro, 2004)

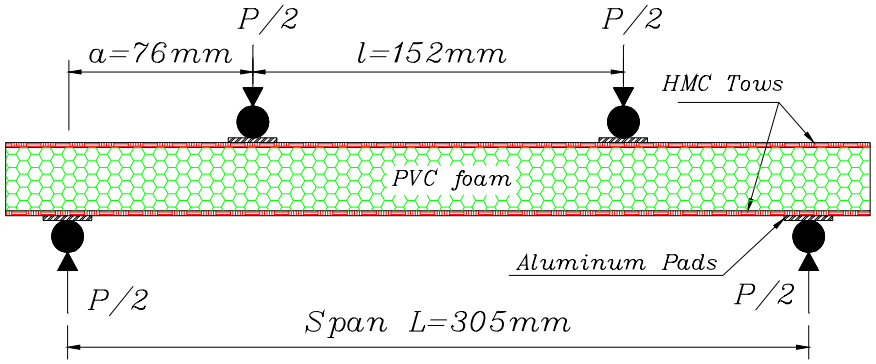

Figure 3.1 Four-points bending test setup

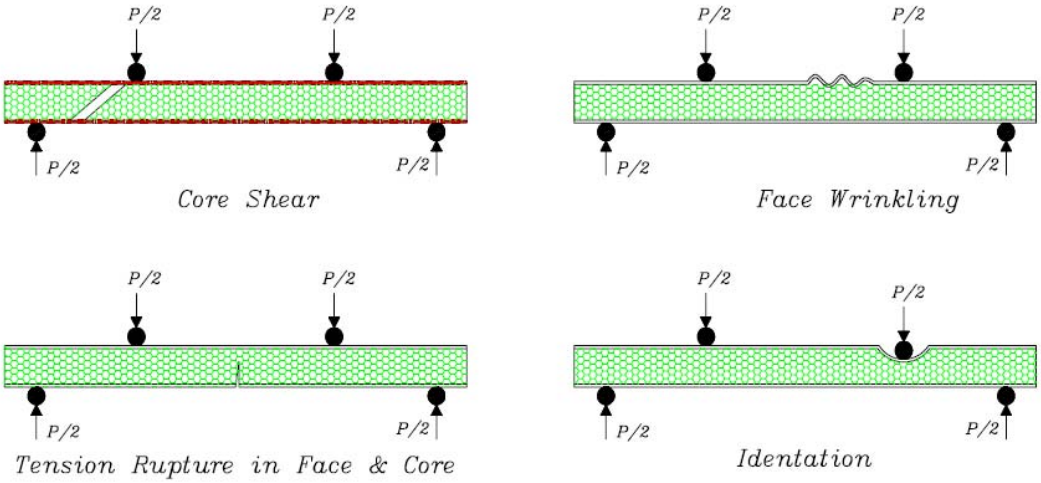

Figure 3.2 Sandwich beams common failure modes

Figure 3. 3 Shear stress distribution in a sandwich beam cross section

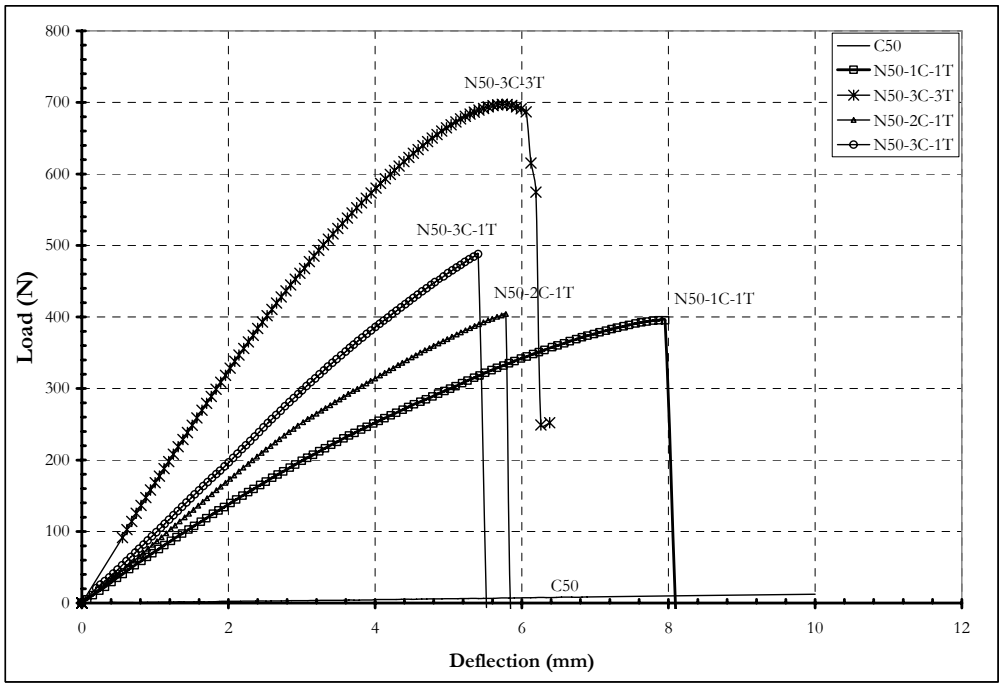

Figure 3.4 Load-deflection for PVC core of 50 Kg/m^3 and N-12K MMC with inorganic resin

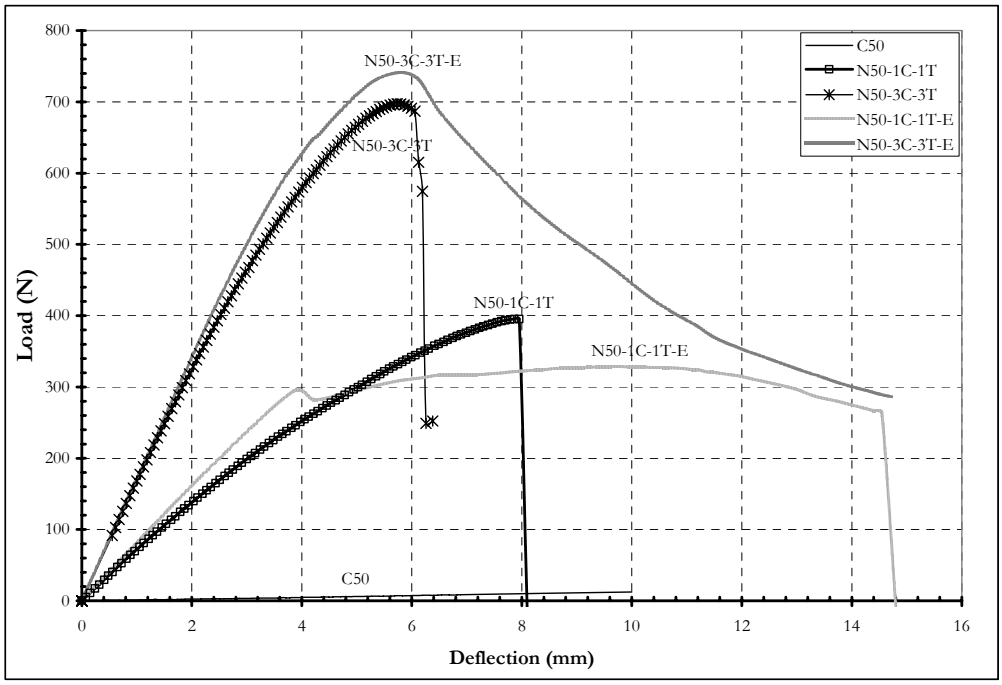

Figure 3.5 Load-deflection for PVC core of 50 Kg/m^3 and N-12K MMC with organic resin

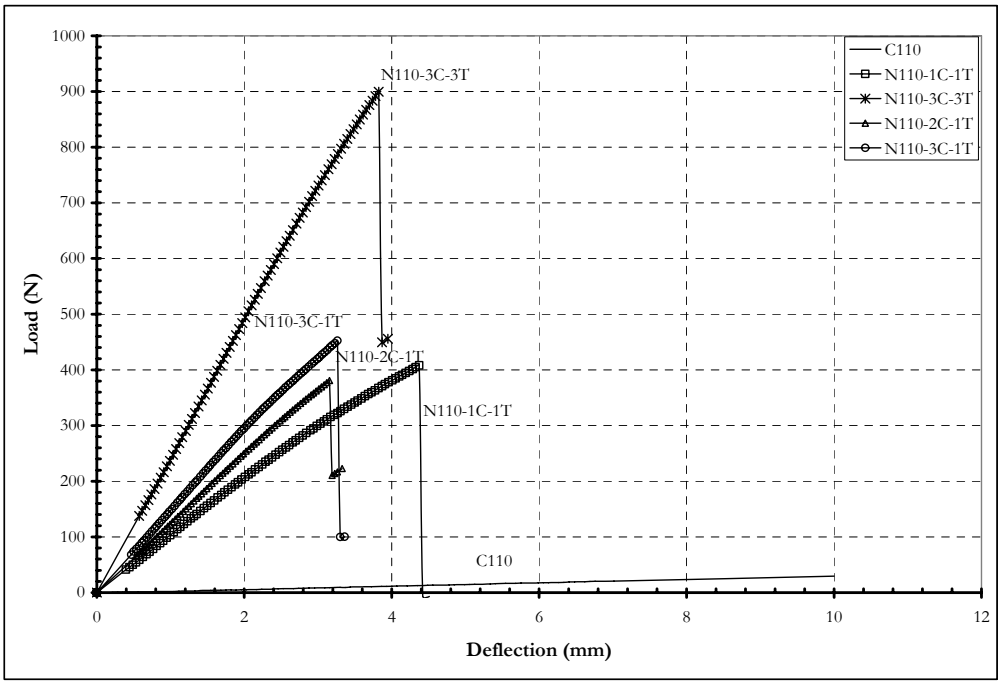

Figure 3.6 Load-deflection for PVC core of 110 Kg/m^3 and N-12K MMC with inorganic resin

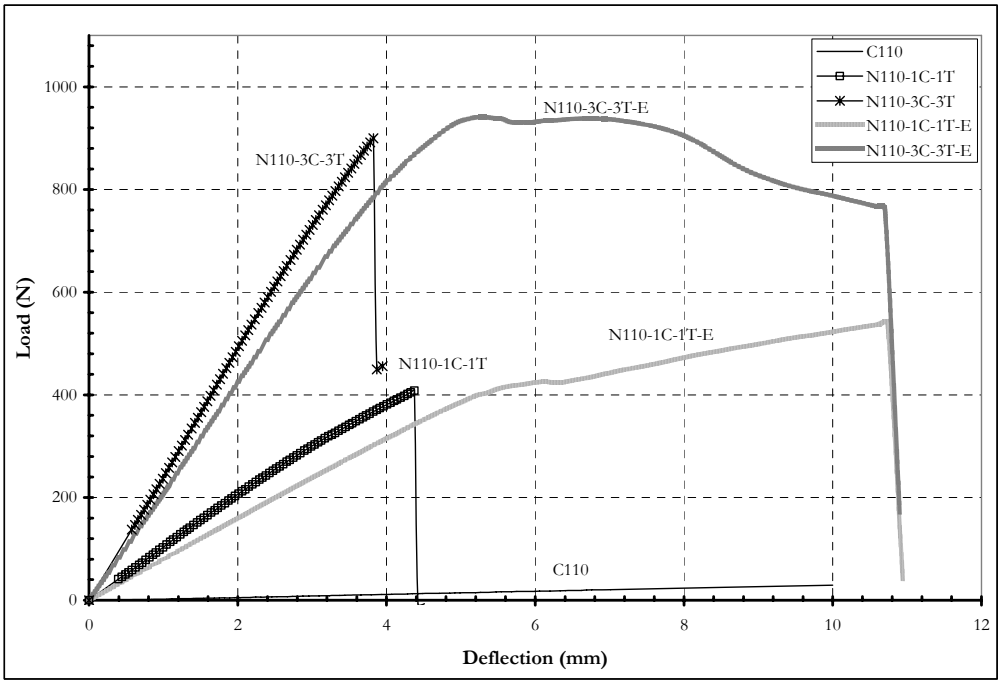

Figure 3.7 Load-deflection for PVC core of 110 Kg/m^3 and N-12K MMC with organic resin

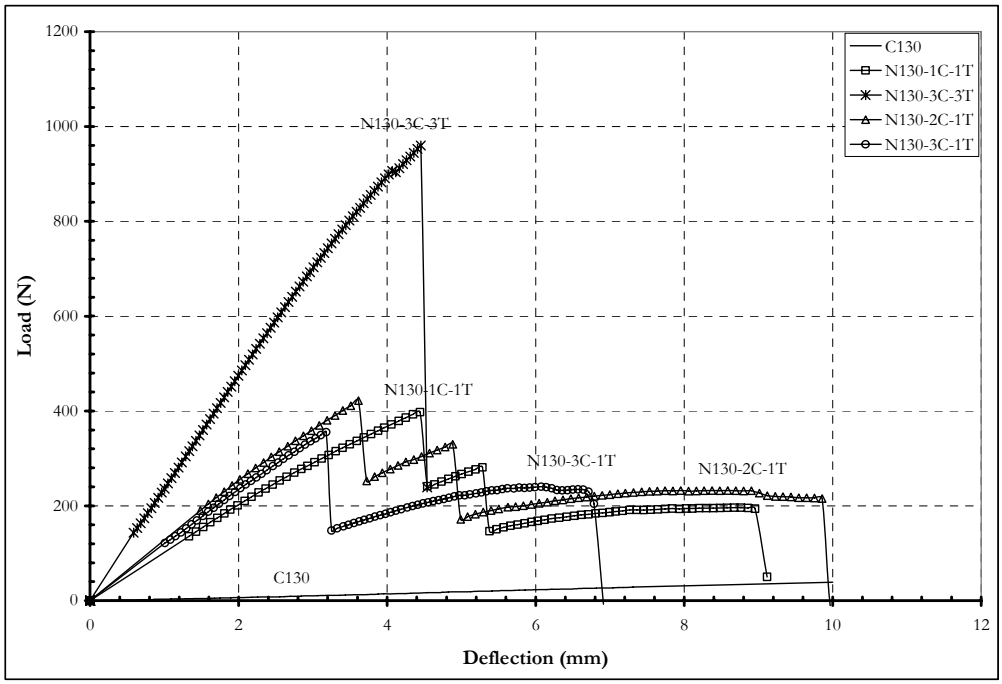

Figure 3.8 Load-deflection for PVC core of 130 Kg/m^3 and N-12K MMC with inorganic resin

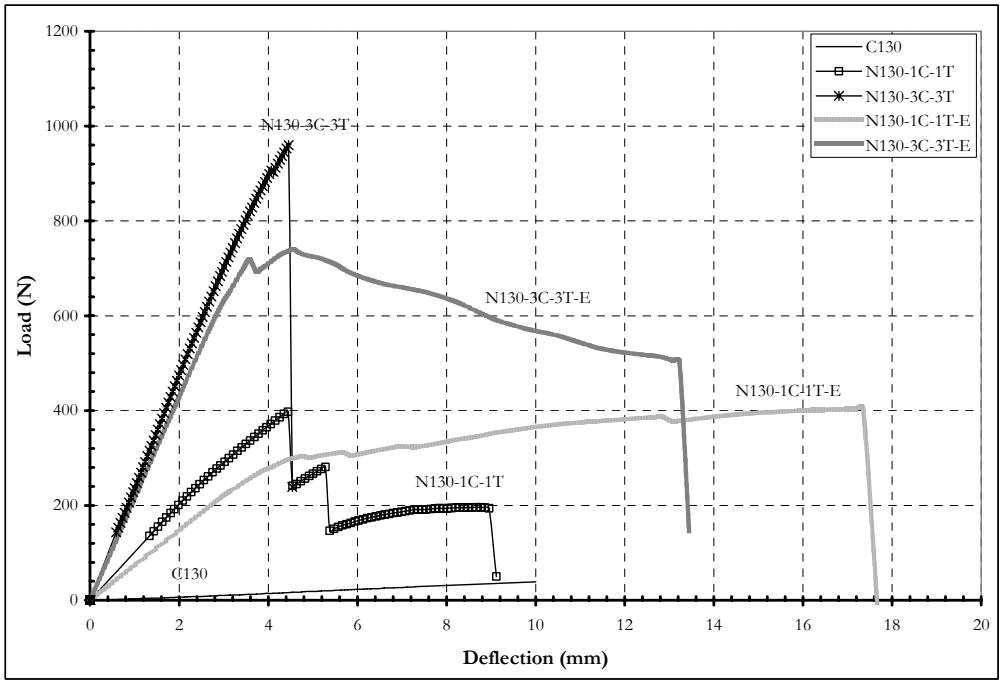

Figure 3.9 Load-deflection for PVC core of 130 Kg/m^3 and N-12K MMC with organic resin

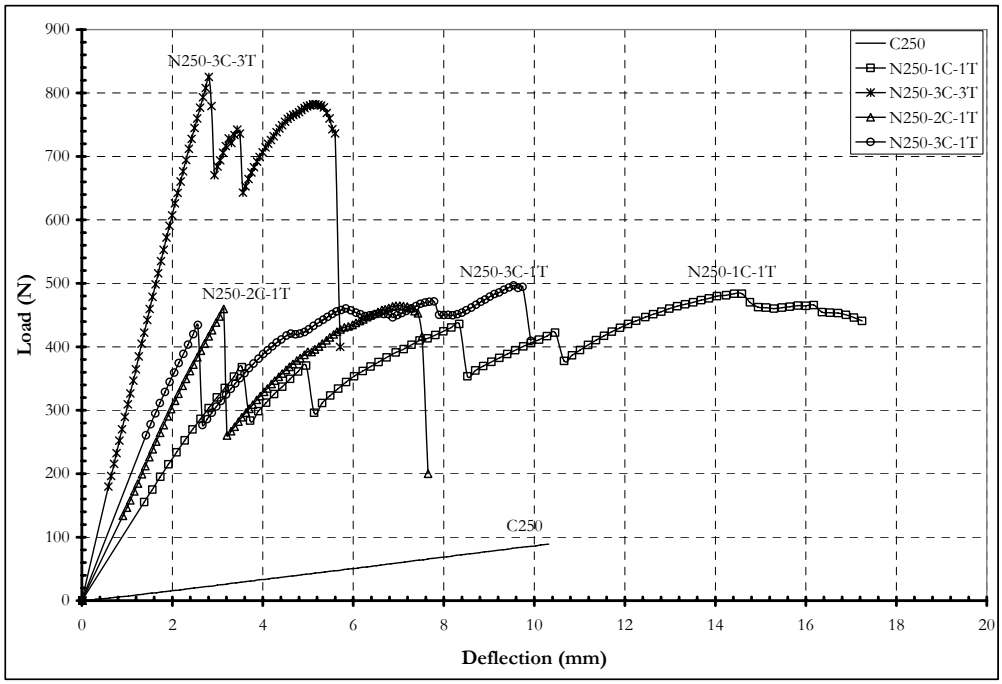

Figure 3.10 Load-deflection for PVC core of 250 Kg/m^3 and N-12K MMC with inorganic resin

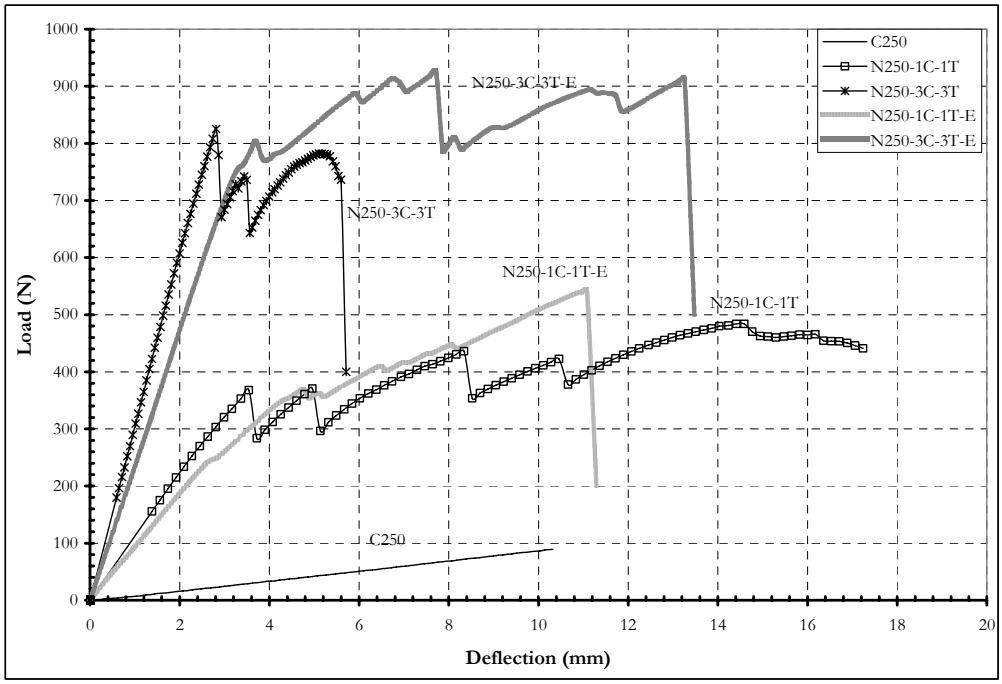

Figure 3.11 Load-deflection for PVC core of 250 Kg/m^3 and N-12K MMC with organic resin

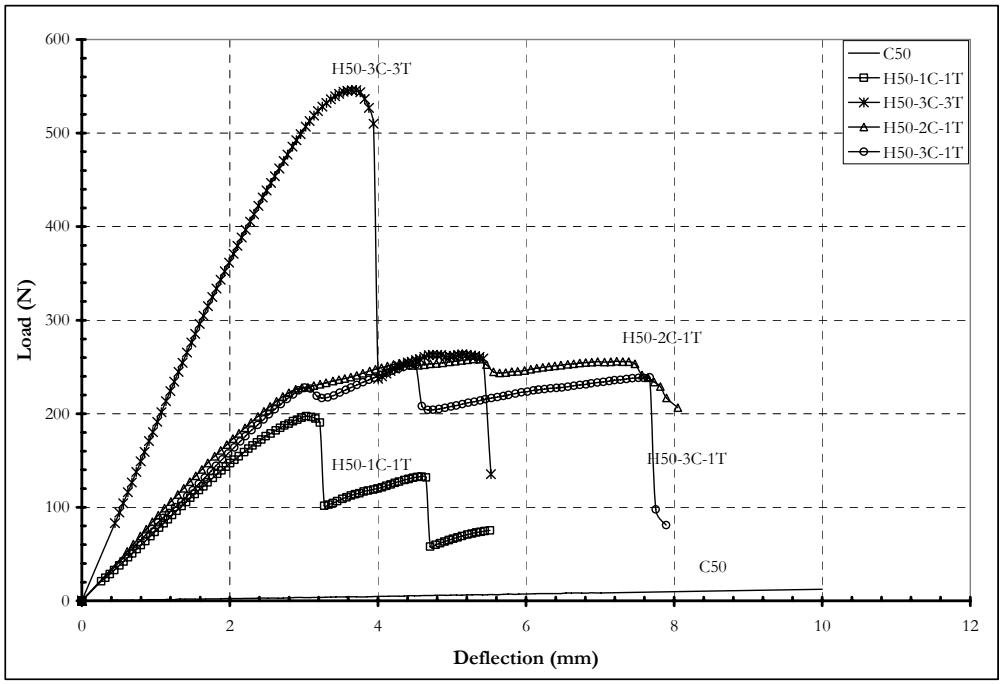

Figure 3.12 Load-deflection for PVC core of 50 Kg/m^3 and H-12K HMC with inorganic resin

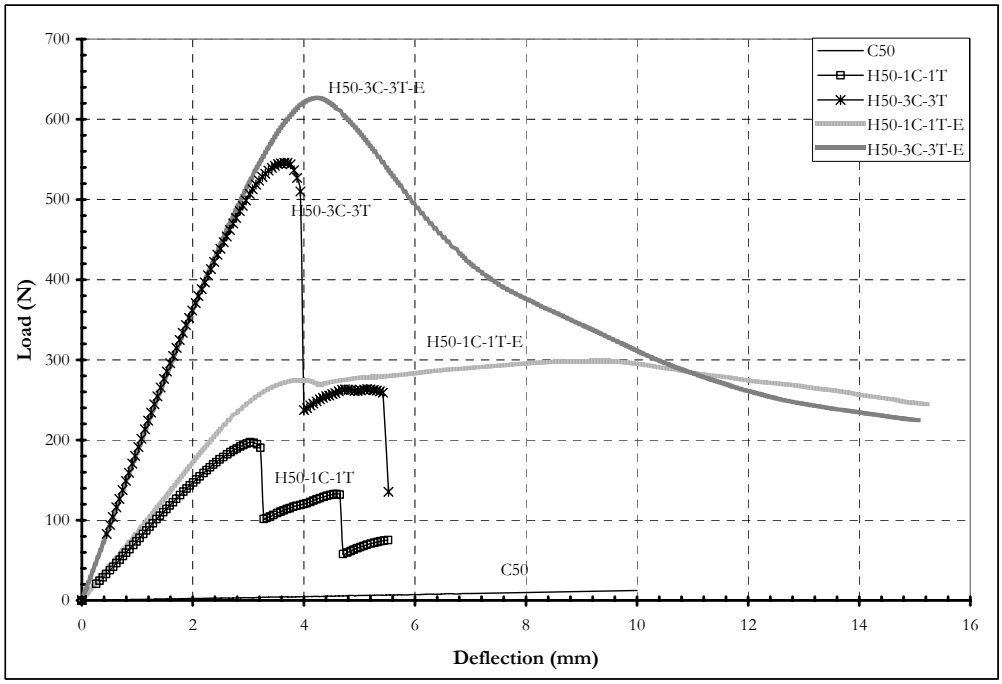

Figure 3.13 Load-deflection for PVC core of 50 Kg/m^3 and H-12K HMC with organic resin

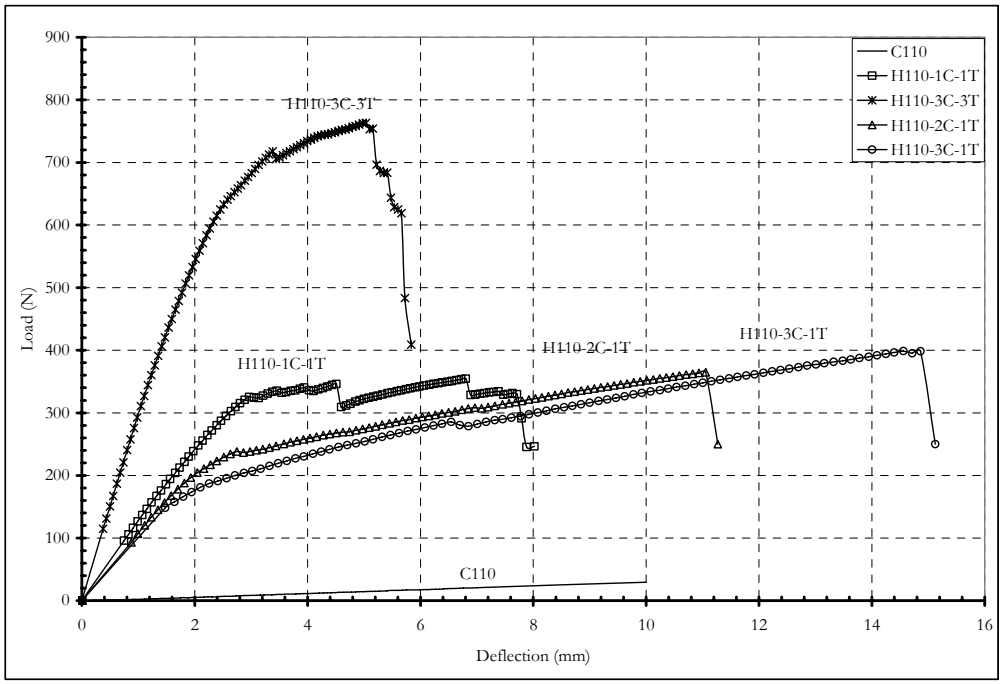

Figure 3.14 Load-deflection for PVC core of 110 Kg/m^3 and H-12K HMC with inorganic resin

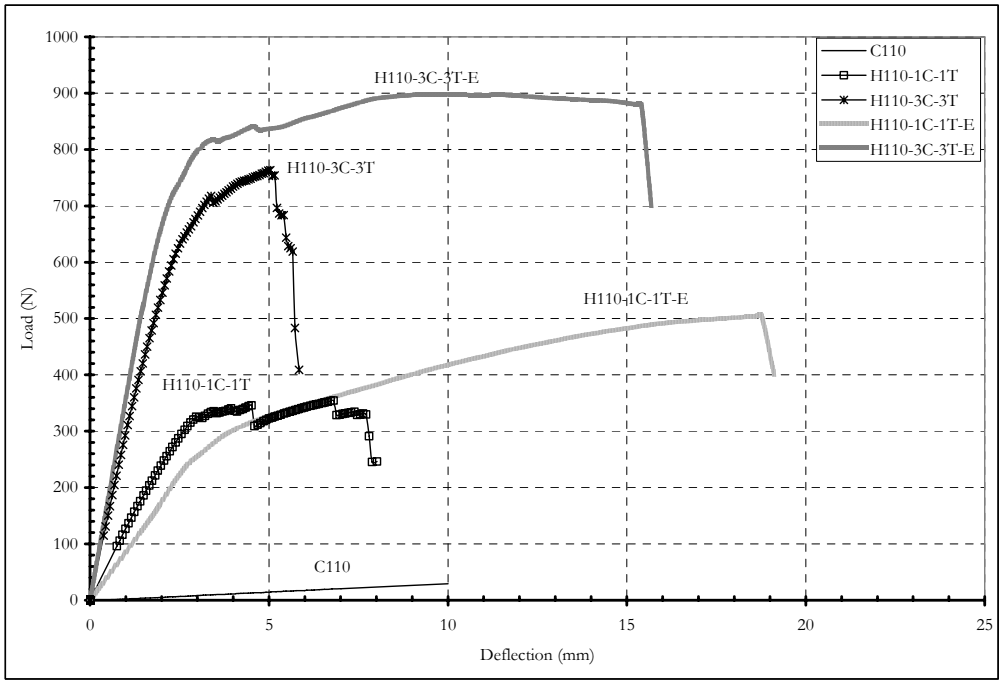

Figure 3.15 Load-deflection for PVC core of 110 Kg/m^3 and H-12K HMC with organic resin

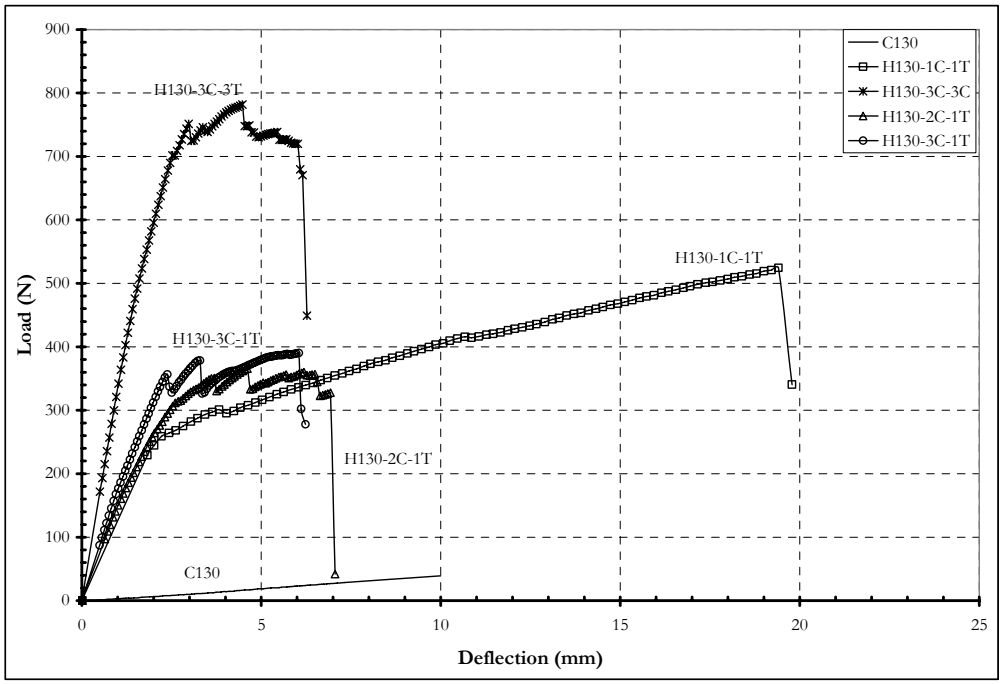

Figure 3.16 Load-deflection for PVC core of 130 Kg/m^3 and H-12K HMC with inorganic resin

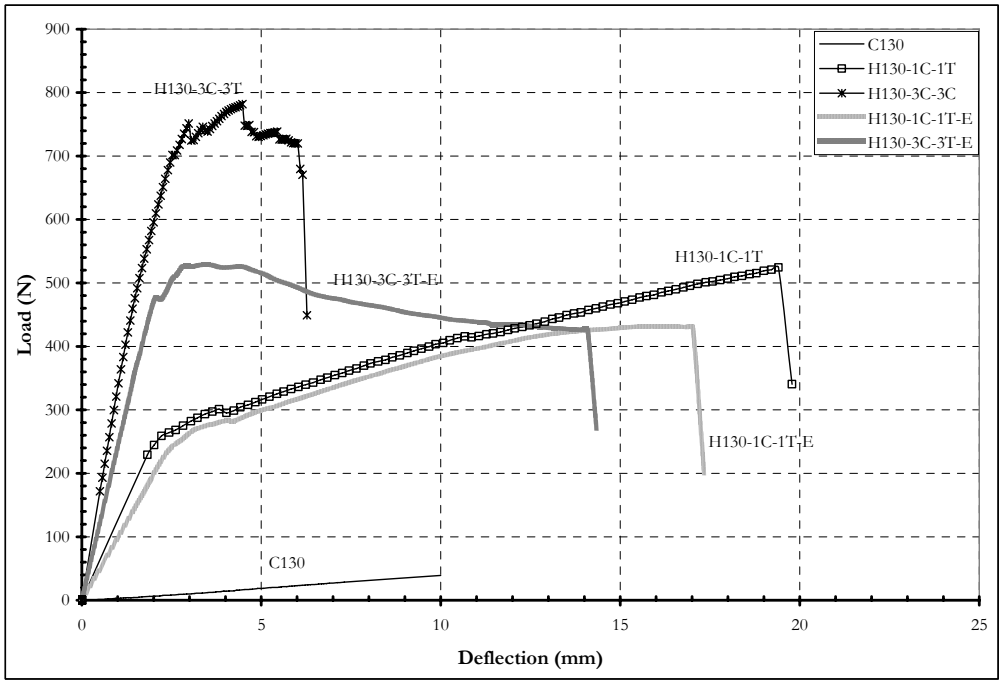

Figure 3.17 Load-deflection for PVC core of 130 Kg/m^3 and H-12K HMC with organic resin

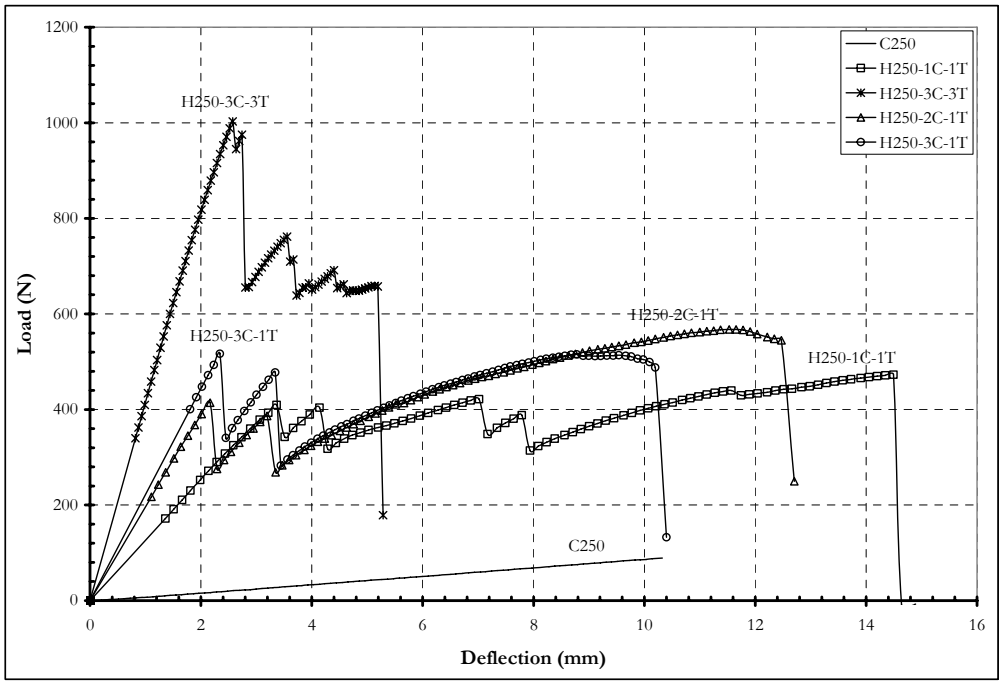

Figure 3.18 Load-deflection for PVC core of 250 Kg/m^3 and H-12K HMC with inorganic resin

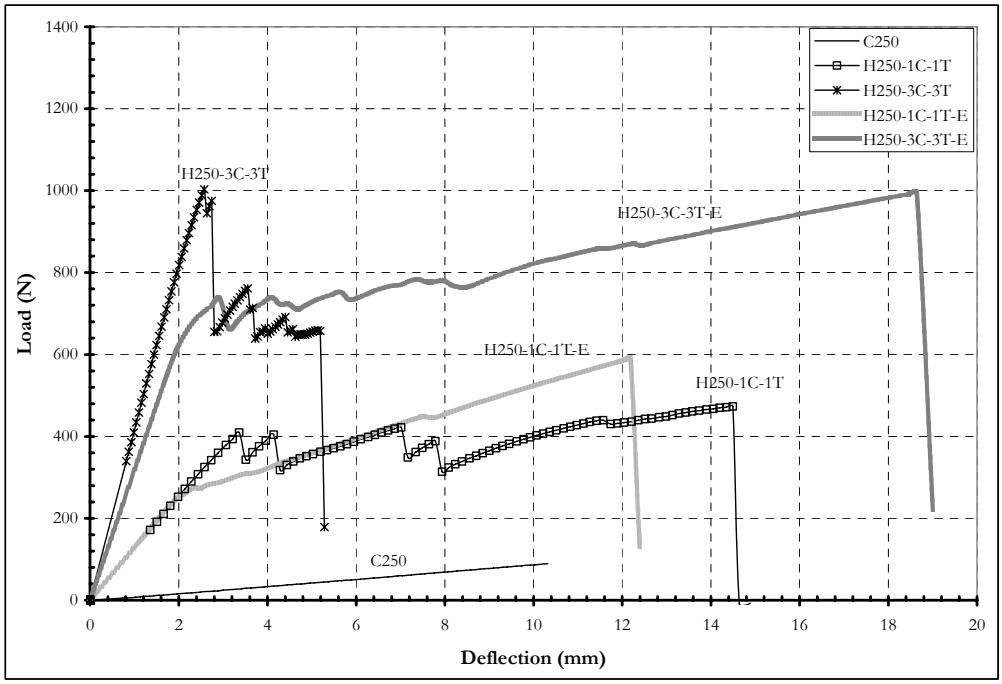

Figure 3.19 Load-deflection for PVC core of 250 Kg/m^3 and H-12K HMC with organic resin

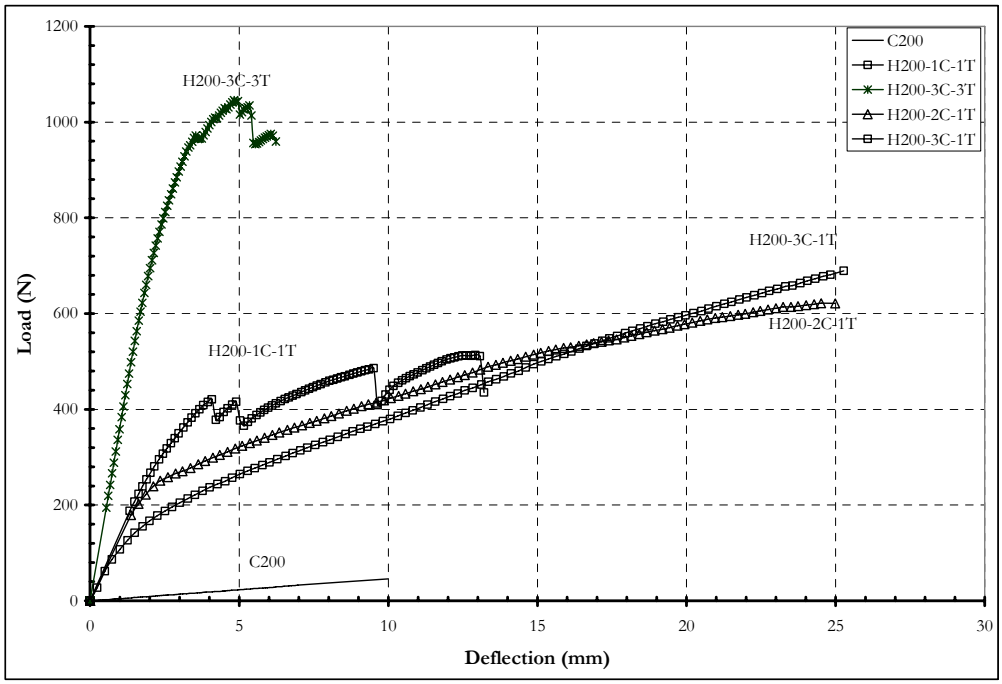

Figure 3.20 Load-deflection for PVC core of 200 Kg/m^3 and H-12K HMC with inorganic resin

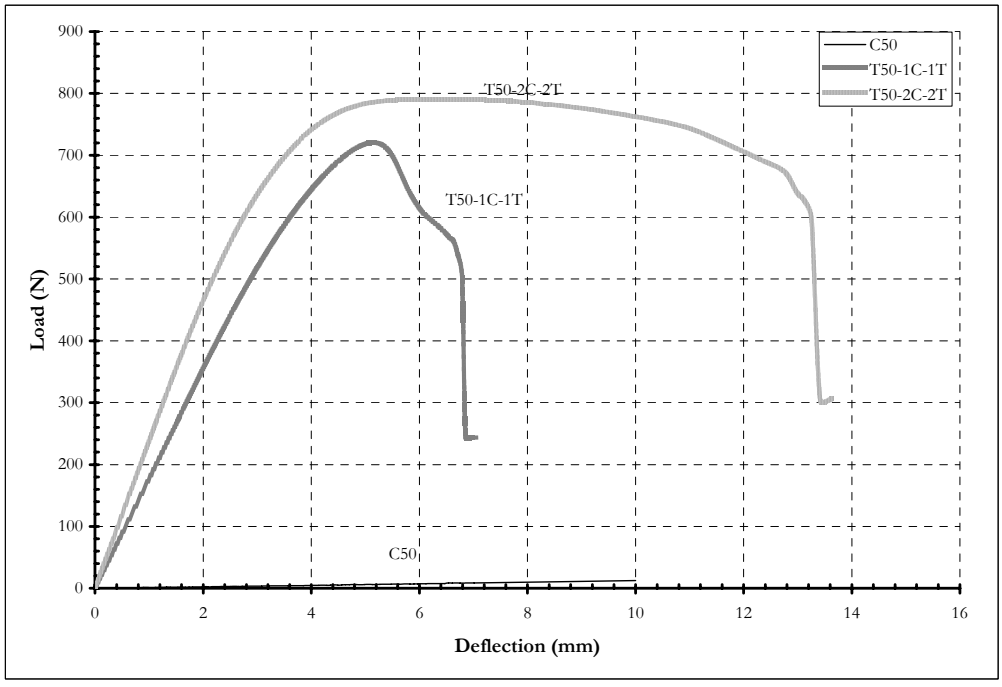

Figure 3.21 Load-deflection for PVC core of 50 Kg/m^3 and T-3K Uni C Tape with inorganic resin

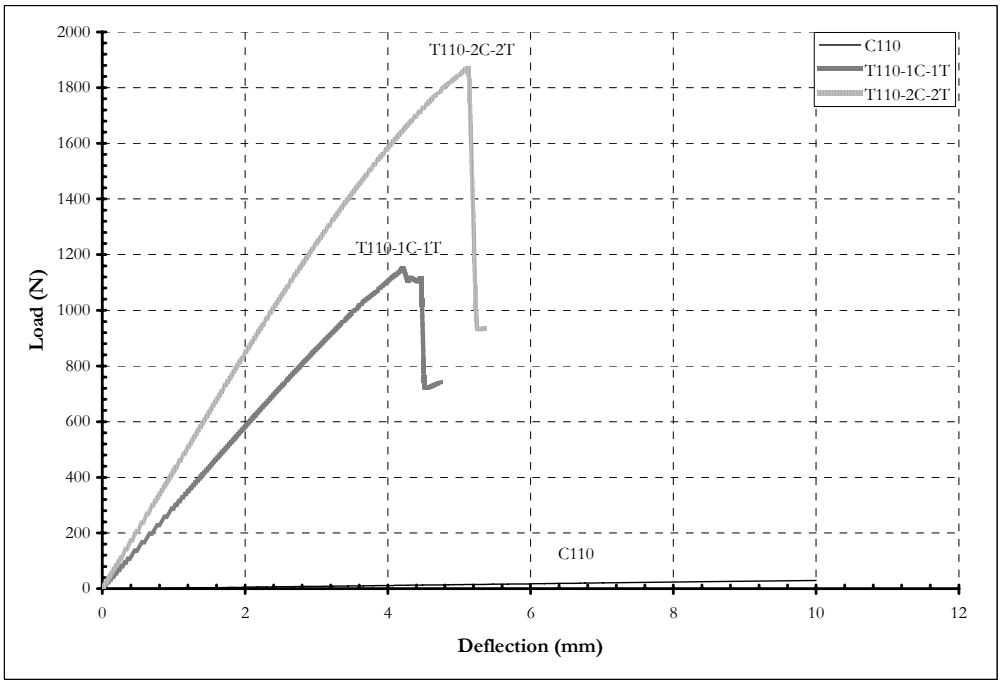

Figure 3.22 Load-deflection for PVC core of 110 Kg/m^3 and T-3K Uni C Tape with inorganic resin

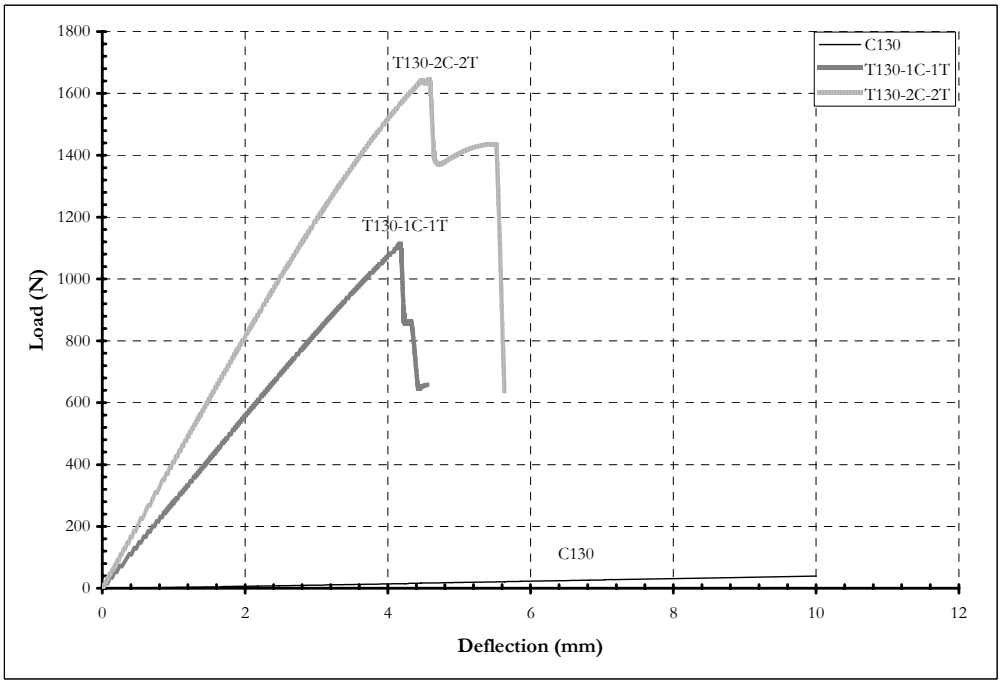

Figure 3.23 Load-deflection for PVC core of 130 Kg/m^3 and T-3K Uni C Tape with inorganic resin

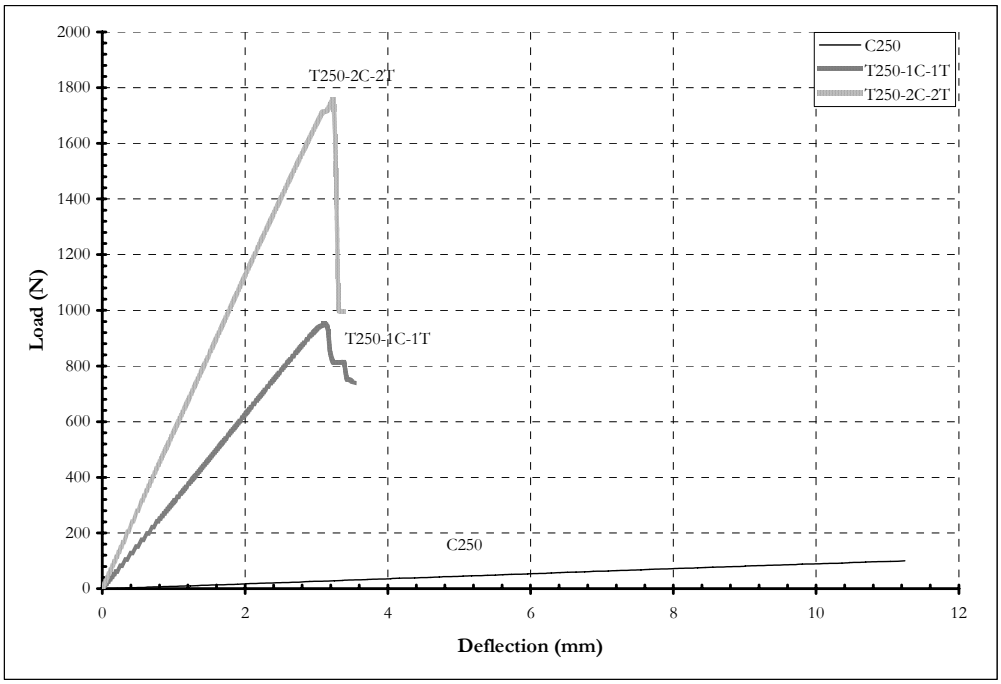

Figure 3.24 Load-deflection for PVC core of 250 Kg/m^3 and T-3K Uni C Tape with inorganic resin

Figure 3.25 Tension split at midspan

Figure 3. 26 Shear failure (near right support) and bearing failure (under left load roller)

Figure 3. 27 Close-up for bearing failure under left load roller

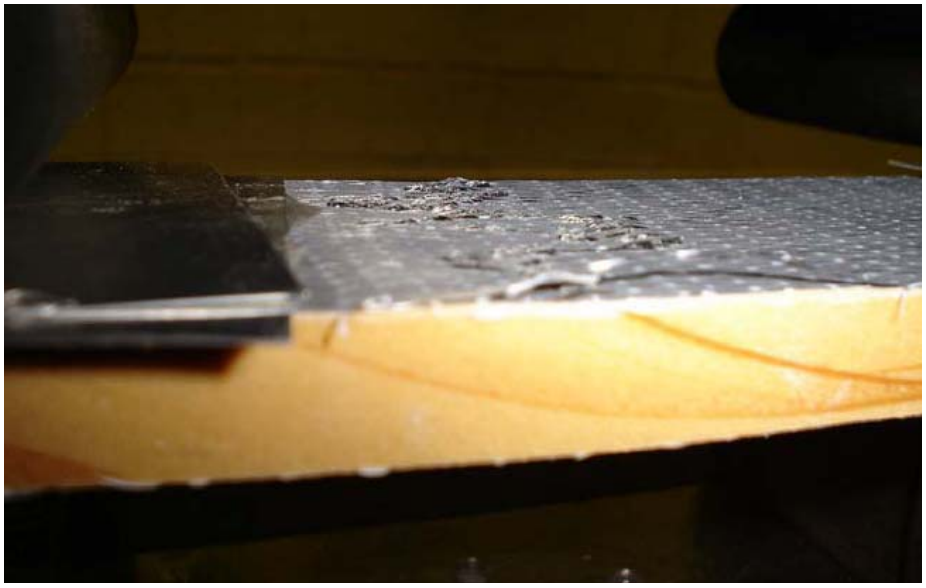

Figure 3. 28 Wrinkling failure for inorganic composite

Figure 3. 29 Wrinkling and tension splitting failure for organic composites

Chapter 4

Analytical Model and Failure Analysis

4.1 Introduction

Several analytical models and failure criteria are available for sandwich structures subjected to flexure. These models were intended to deal with the commercially used Carbon/Epoxy facings with PVC and honeycomb cores. Only a few models dealt with inorganic sandwich structures. The model by Papakonstantinou (Papakonstantinou, 2003) provides analytical procedures for the inorganic systems reinforcing rigid syntactic cores. Since the inorganic core is rigid and brittle, its behavior differs totally from the flexible PVC cores. With loading, rigid cores exhibit elastic behavior up to cracking, then, post cracking with an effective cross section, which is inelastic up to failure. Experimental results for PVC sandwich beams showed an elastic behavior up to core yield followed by inelastic behavior up to failure. The analyses presented in this chapter investigate the behavior of the beams up to failure. A lower bound solution is introduced to predict the failure load for beams loaded in quarter span four-point bending that will be used to develop design guides and recommendations.

The behavior of sandwich structures is affected by: the mechanical properties of the facings, the adhesive, and the core. The cellular nature of the core is not conducive for the use of classical bending and mechanics theories to accurately predict the failure loads (Swanson et al, 2003).

The organic matrices have a low modulus of elasticity and a large strain capacity as compared to the reinforcing fibers. Therefore, they transfer the load effectively in the longitudinal direction of the fibers. The inorganic matrix has very low tensile strain capacity and it cracks

at early stages of loading. Misalignment of fibers has a more significant effect on composites made with inorganic matrices (Hammell, 2000).

4.2 Analytical model assumptions

The analytical model proposed in this chapter is based on the following assumptions.

- The shear deflection is to be taken into consideration.
- For symmetrically reinforced beams, the neutral axis is assumed to be in the middle and the difference between the tension and compression elastic modulus of the core is neglected.
- The width of the reinforcement is used is the effective width of the beams regardless of the width of the core.
- The thickness of the skin is negligible compared to the thickness of the core and hence neglected in the computations.
- The strain distribution is linear within the cross section.
- Perfect bond is assumed between the skin and the core.

4.3 Failure modes

4.3.1 Core Shear

The core has the role of transmitting the forces between the facings by shear; therefore, the core has to have enough shear capacity. If the core lacks in shear capacity the beam will fail due to shear in the core. This is more likely in beams with high span to depth ratio. From basic mechanics of materials, the shear stress in the core can be calculated using the following equation

$$\tau = \frac{V}{D}\frac{\Sigma(SE)}{b} \tag{4.1}$$

V is the shear force. D is the flexural rigidity. b is the width. $\Sigma(SE)$ represents the sum of the first moment of area above the neutral axis. It includes the first moment of area of reinforcement and half of the core. The neutral axis is assumed in the middle for all symmetrically reinforced beams.

$$\Sigma(SE) = E_f A_f \frac{c}{2} + E_c b_c \frac{c^2}{8} \tag{4.2}$$

E_f is the tensile modulus of the skin, A_f is the skin area, E_c is the core modulus, and c is the core thickness.

The flexural rigidity can be expressed in terms of

$$D = 2E_f A_f \left(\frac{d}{2}\right)^2 + E_c \frac{b_c c^3}{12} \tag{4.3}$$

d is the distance between the skins.

The second term in equations (4.2) and (4.3) is based on the contribution of the core. The tensile modulus of the fibers is much larger than the corresponding modulus of the core. The second term can be neglected for the rigidity and stiffness calculation without significant loss of accuracy.

After neglecting the second term, equation (4.3) becomes

$$D = E_f A_f \frac{d^2}{2} \tag{4.4}$$

By substituting equations (4.2) and (4.4) in equation (4.1), the shear stress in the core becomes

$$\tau = \frac{V}{bd} \tag{4.5}$$

Or the shear stress is distributed uniformly across the thickness. The load that can lead to failure initiated by core shear can be expressed after substituting the shear force with $P/2$ as

$$P = 2\tau_{\max} bd \tag{4.6}$$

4.3.2 Tension failure in skin

The tension failure in the skin occurs when the tensile stress in the skin reaches its ultimate value.

The maximum fiber stress at failure is given

$$\sigma_t = \beta_1 E_f \varepsilon_{fu} \tag{4.7}$$

β_1 is a factor to account for misalignment of the fibers and ε_{fu} is the maximum fibers strain at failure (provided by the manufacturer or the literature, 0.4 % for H-12K HMC) and E_f is the fibers tensile modulus.

Then the moment that causes a failure due to tension is

$$M = \beta_2 A_f \sigma_t d \tag{4.8}$$

β_2 is the effective fiber area factor that counts for the damaged fibers during the preparation process. This factor varies based on the type of the fibers used.

For the quarter span four point flexural,

$$M = \frac{PL}{8} \tag{4.9}$$

From equations (4.7) to (4.9), the maximum load that can cause a failure due to tension in the skin is

$$P = 8\beta_1 \beta_2 A_f E_f \varepsilon_{fu} d/L \tag{4.10}$$

4.3.3 Wrinkling Failure

For organic composites, the term wrinkling refers to modes having wavelengths up to the thickness of the core. An example of this failure mode is shown in figure 4.2. Buckling is used in a more generic way, referring to instabilities regardless of the mode's wavelength. Sandwich structures may exhibit very little or no post-wrinkling load carrying capability, hence the failure is usually catastrophic (Ley et al., 1999).

Because of the brittleness of the inorganic composites, its tendency to buckle or to exhibit a wrinkling failure will be accompanied by a fracture in the compression skin. This breakage has creates small, but yet, visible cracks; an example of this failure mode is shown in figure 4.1.

The critical wrinkling stress was determined by Hoff and Mautner, 1945.

$$\sigma_w = \gamma \sqrt[3]{E_f E_c G_c} \tag{4.11}$$

Where γ is a knockdown factor. This factor was studied extensively and determined analytically and experimentally. The range for the knockdown factor is still debatable based on the assumptions made in the analysis or the correlation of the experimental results, but it is generally a function of the skin and core thickness and Young's moduli (Ley et al., 1999). It can be taken from 0.5 to 0.65 (Konsta-Gdoutos et al., 2005) or it can be determined experimentally (Lingard, 1993).

The critical load that can cause face wrinkling for the given loading and boundary conditions can be expressed as

$$P = 8A_f \sigma_w d / L \tag{4.12}$$

4.3.4 Indentation

Due to low bending stiffness of thin skin and low strength of lightweight core materials, sandwich structures are prone to damage when subject to concentrated loadings (Zenkert et al., 2004). For organic composites, this failure can be observed as local core yielding accompanied by local deformation of the core and the skin into the core. This causes a multiaxial state of stress in the indenter environs. For such system, the beam on elastic foundations model gives satisfying results (Daniel et al, 2002). A model for elastic face sheets and a rigid-ideally plastic core, under three points bending, was also introduced by (Steeves et al., 2004).

By extending the Hertz theory, the solution of the contact problem was presented by approximating the surfaces of the punch and elastic body in the vicinity of the contact by paraboloids of revolution. The solution considered an absolutely rigid body and elastic surface (Argatov, 2006). This solution considered a local effect of a point load over a three dimensional media and it may be a suitable methodology for solving the contact and indentation problem in case of plates subjected to concentrated point loads. On the other hand, the solution presented in this section consider the problem of a line load parallel to the supports for a plate with two supported edges and free along the sides or for beams. In addition, the plate is considered to behave plastically as the stiff layer of reinforcement will provide enough rigidity for the contact area to promptly exceed the elastic limit of the foam core.

For inorganic composites, the behavior is different as the brittleness of the facings will instigate the skin to crush under the indenting roller. During this research, pads were used to avoid such failure. The crush of skin could be mitigated but not the multiaxial state of the

stress in the vicinity of the load rollers. The previously described behavior strengthened the use of rigid-plastic model.

4.3.4.1 Mathematical modeling for indentation in inorganic skin as rigid-plastic beam

It is assumed that the load rollers are far apart enough so no interference of stress fields exist. The load $P/2$ at quarter span causes a bending moment of $M = PL/8$ on the cross section under the load. The upper skin is subjected to a compressive force $F = M/d$ and the bottom skin is subjected to tension force of the same magnitude. The core beneath the roller locally deforms and is subjected to vertical uniform compressive stress q, distributed over the length of the indentation. The length of this indentation zone is taken as 2λ. The length 2λ is very small compared to the beam and the shear span. The assumption that the full shear force is still acting over the indentation length is valid. The described model is shown in figure 4.3.

By using the simple beam theory,

$$q = \frac{dV}{dx} \tag{4.13}$$

$$\frac{dM}{dx} = F\frac{du}{dx} + V \tag{4.14}$$

The bending moment in the facings can be expressed as

$$M = -E_f I_f \frac{d^2u}{dx^2} \tag{4.15}$$

From equilibrium the beam-column equation can be written as

$$\frac{d^4u}{dx^4} + \frac{F}{E_f I_f}\frac{d^2u}{dx^2} = \frac{-q}{E_f I_f} \tag{4.16}$$

The general solution for this equation can be expressed as

$$u = A_1 \cos(\xi x) + A_2 \sin(\xi x) + A_3 x + A_4 - \frac{qx^2}{2F} \tag{4.17}$$

A_1, A_2, A_3 and A_4 are constants to be determined by using the boundary conditions and ξ is the wave number and $q = \sigma_c b$.

$$\xi = \sqrt{\frac{F}{E_f I_f}} \tag{4.18}$$

The boundary conditions are

$$u'(x = 0) = 0 \tag{4.19}$$

The shear force on the cross section equals $P/2$

$$u'''(x = 0) = \frac{P}{2E_f I_f} \tag{4.20}$$

At the end of the indentation zone, the vertical deformation of the core vanishes.

$$u(x = \lambda) = 0 \tag{4.21}$$

At the end of the indentation zone at the top skin, the local bending of the skin caused by the loading roller disappears because of the plasticity of the core, and so the fourth boundary condition can be expressed as.

$$u''(x = \lambda) = 0 \tag{4.22}$$

By applying equations (4.19) to (4.22) into equation (4.17), the constants can be found as

$$A_1 = \frac{2d}{L\xi}\left(\frac{1 - \cos(\xi\lambda) - \xi\lambda \sin(\xi\lambda)}{\sin(\xi\lambda) - \xi\lambda \cos(\xi\lambda)}\right) \tag{4.23}$$

$$A_2 = -\frac{2d}{L\xi} \tag{4.24}$$

$$A_3 = \frac{2d}{L} \tag{4.25}$$

$$A_4 = \frac{2d}{L\xi}\left(\frac{1-\cos(\xi\lambda)-\xi\lambda\sin(\xi\lambda)}{\sin(\xi\lambda)-\xi\lambda\cos(\xi\lambda)}\right)+\frac{d(\xi\lambda)^2}{L\xi}\left(\frac{1+\cos(\xi\lambda)}{\sin(\xi\lambda)-\xi\lambda\cos(\xi\lambda)}\right) \quad (4.26)$$

By substituting $I_f = bt^3/12$ and knowing that the slope of the face vanishes after the indentation zone, the load can be shown as

$$P = 2A_f\left[\frac{4dE_f\sigma_c^2}{3L}\left(\frac{\sin(\xi\lambda)-\xi\lambda\cos(\xi\lambda)}{1-\cos(\xi\lambda)}\right)^2\right]^{1/3} \quad (4.27)$$

4.3.4.2 Lower bound solution for the indentation problem

By investigating equation(4.27), the total load applied that can cause indentation in the facing is a function of the fibers area and modulus, the core thickness and compression strength, and the span and the length of the indentation zone.

The maximum of the previous equation can be found by setting $\xi\lambda = n\pi$, $n=1$ should be a reasonable assumption as the inorganic skin is too brittle to exhibit any higher modes

$$P_{\max} = 2A_f\left(\frac{\pi^2 dE_f\sigma_c^2}{3L}\right)^{1/3} \quad (4.28)$$

The bending moment on the sandwich cross section is $M = PL/8$, the fiber stress is $\sigma_f = M/dA_f$. By applying and arranging the terms, the core compression stress due to the local effect of the applied load is

$$\sigma_c = \frac{P}{\pi A_f}\sqrt{\frac{3\sigma_f}{E_f}} \quad (4.29)$$

This can be introduced as a lower bound solution of the problem that can help the designers to identify a design load for the beams loaded in quarter span four point bending.

The indentation is not only a failure mode, but it is additional stress that acts on the sandwich beams and it is not accounted. This additional stress is in the form of vertical crushing compressive stress that acts in the vicinity of the loading points.

$$\sigma_f = \left(\frac{E_f}{192}\right)^{1/3}\left(\frac{\pi L \sigma_c}{c}\right)^{2/3} \le \sigma_w \le E_f \varepsilon_{fu} \tag{4.30}$$

This equation shows that the maximum attainable stress in the fibers is affected by fibers modulus and the core compressive strength. The effect of the core compressive strength is of second order when it is compared to the fibers modulus contribution. The maximum attainable stress can not exceed the critical wrinkling stress or the fiber maximum tensile strength.

Introducing this equation as a lower bound solution can be a great help for the design procedures. The use of this equation is limited to the loading conditions and the boundary conditions described in the problem statement. Following the same procedure, similar formulations can be obtained for different loadings and boundary conditions.

The previous equation shows the effect of the various parameters on the effectiveness of the fiber usage. A dramatic reduction occurs to the maximum stress that the fibers can reach because of the use of flexible core and the indentation effect.

4.3.4.3 Stress reduction

By using equation (4.30), the maximum attainable fibers stress and the critical wrinkling stress were plotted versus a practical range of the depth to span ratio. Figure 4.4 to 4.18, show the change of stresses of the different types of skins in combination with the different core densities. The wrinkling stress is not a function of the span. It is a function of the core modulus, compressive strength, and the facings modulus.

4.4 Model Verification

The experimental results presented in chapter 3 were used for evaluation of the analytical model. The load-deflection curves presented in chapter 3 were used to obtain the midspan deflection. The objective is to construct the load-deflection curves analytically and predict the failure load.

4.4.1 Hypothesis and philosophy

The main objectives are to explain the failure mechanism and to introduce a simple method for the designer to use. The failure hypothesis introduced here suggests that the initial linear portion of the load-deflection starts to deviate from its linear portion when at least one or more of the tension, compression, or shear stress in the core reaches its upper limit. The beam will completely fail when one of those stresses reaches its ultimate limit and the mechanism of transferring the forces from the core to the skin is interrupted.

The cross section of the beam under the load is subjected to a moment and a shear from basic structure analysis. Two elements in the core are investigated: One right below the top skin and the other right above the bottom in the vicinity of the skin. The normal stresses in the core can be given by equation (4.31).

The one at the lower half bottom of the core is subjected to tension stresses that acts horizontally on the element. The shear stress distribution within the cross section can be assumed to be constant, and the shear stress at this element can be fairly assumed to be equal to the max shear stress in the cross section.

The second element is at the upper half of the core, this element is subjected to shear and a horizontal compression that comes from the skin, and can be calculated using equation (4.31). In addition to the aforementioned stresses, the imposed vertical crushing

compression stress that is caused by the indentation process, is to be considered and can be calculated using equation (4.29).

$$\sigma_C^{t,c} = \sigma_f^{t,c} \times \frac{E_c}{E_f} \tag{4.31}$$

The combination of normal and shear stresses acting on these elements will cause a state of principal stresses. The principal normal stresses can be calculated using equation (4.32) and the maximum shear stress can be calculated using equation(4.33).

$$\sigma_{1,2} = \frac{\sigma_x + \sigma_y}{2} \pm \sqrt{\left(\frac{\sigma_x - \sigma_y}{2}\right)^2 + \tau_{xy}^2} \tag{4.32}$$

$$\tau_{\max} = \sqrt{\left(\frac{\sigma_x - \sigma_y}{2}\right)^2 + \tau_{xy}^2} \tag{4.33}$$

For the lower element, σ_x is the tension stress transferred from the skin and σ_y is zero.

For the upper element, σ_x is the compression stress transferred from the skin and σ_y is the imposed indentation stress.

4.4.2 Program description

The analytical load deflection curves for the various beams were generated using a simple MATLAB program; a flowchart to describe the program is presented in figure 4.19.

The first set of input variables were: the fibers modulus, failure strain, area, and effective area factor. Then, the core shear modulus, compression modulus, compression, and shear capacity are entered along with all the span and geometric data. The initial linear part is then calculated using the stiffness equation. The maximum load due to fibers tension failure, core shear failure, and the wrinkling failure are calculated and the smallest value is set to be the maximum load for the analytical load-deflection curve.

4.4.3 Modification factors

The different introduced modification factors are shown in table 4.1. These factors were chosen based on the observations made during the fabrication process and the experimental results.

The misalignment factor, β_1, was chosen based on the examination of the behavior of the different fibers during the fabrication process. The H-12K HMC fibers were very hard to handle and tended to twist while bonding them to the core. N-12K MMC fibers were much easier to handle, and did not tend to curl. Therefore, the misalignment factor was chosen 0.8 and 0.9, for the H-12K HMC and N-12K MMC, respectively. The fibers in the carbon tape, T-3K Uni C Tape, were maintained straight with cross glass tows, the factor was taken 0.95. Theses factors were verified experimentally.

The effective fiber area factor, β_2, counts for the damaged fibers during the preparation process. This factor should decrease with the increase of the fibers area, as more tows are added; the more rolling is required, which damages the fibers more. The H-12K HMC fibers are more likely to break with rolling due to the fibers' high stiffness.

4.4.4 Model evaluation

4.4.4.1 Analytical load-deflection curves

As expected, the model predicts the linear behavior well, figures 4.26 to 4.49. The failure loads are underestimated for the low density cores and were in good agreement within the intermediate densities and were overestimated for the dense cores.

The lower density core has larger voids between the cells and the matrix flows between the cells during the fabrication process. When it hardens, it fills these voids in the vicinity of the skins, restraining the cells from deformation. This provides lateral support for the cell walls

against buckling near the compression skin. This observation is supported by larger weight gain for low density cores as compared to high density cores. The post linear behavior is very hard to predict and needs non linear modeling.

4.4.4.2 Failure criteria

Tables 4.2 to 4.10 show the stress calculation results based on the aforementioned hypotheses. The linear limit calculations show that all the beams pass the limit of the core to yield, and the ultimate stress calculations show that all the beams pass the limit of the core ultimate strength. The calculations show that the core can fail in compression, shear, and tension, or in a combination. The most likely failure mode in the core is compression. The imposed indentation stress can not be neglected as by comparing the results shown in these tables with the stress calculation results shown in the experimental investigation in chapter 3. Although, the failure hypotheses are satisfied but the ratios between the cores limit stresses and the calculated ones exceed unity. It can be proven by looking at the calculated values that this ratio decreases with the denser cores. Again, this behavior was exhibited because of the matrix filling of the voids, which gives additional strength to the core in the vicinity of the skin.

The lower bound solution provided a lower envelope for the failure load. Only one beam T250-2C-2T failed at a smaller load. The difference between the lower bound load and the failure load did not exceed 1% for that beam. It should be recommended for the design that higher factors of safety should be used with denser cores.

Table 4.1 Modification factors

Skin	β_1	β_2			γ
		1 Tow or Tape	2 Tapes	3 Tows	
H-12K HMC	0.8	0.8	-	0.64	0.6
N-12K MMC	0.9	0.9	-	0.81	0.7
T-3k Uni C Tape	0.95	0.9	0.9	-	0.5

Table 4.2 Stress calculation and principal stress to yield stress ratios for beams reinforced with H-12K HMC

Sample ID	Face Comp. St.	Core Shear	Face Tens. St.	Core Normal Stresses		Ind. Stress	Core Principal Stresses			Core Principal Stresses Ratio		
	$\sigma_{c,f}$	$\tau_{,c}$	$\sigma_{t,f}$	$\sigma_{c,c}$	$\sigma_{t,c}$	$\sigma_{y,c}$	τ_{max}	σ_1	σ_2	$\tau_{max}/\tau_{yeild,c}$	$\sigma_1/\sigma_{tyiedl,c}$	$\sigma_2/\sigma_{cyeild,c}$
	MPa	MPa	MPa	MPa	MPa	MPa	MPa	MPa	MPa	%	%	%
H50-1C-1T	359	0.31	359	-0.05	0.07	-1.78	0.91	1.78	-1.83	152	237	523
H50-3C-3T	330	0.26	330	-0.05	0.06	-1.97	1.00	1.96	-2.00	166	261	573
H110-1C-1T	512	0.41	512	-0.15	0.18	-3.17	1.57	3.08	-3.23	98	186	307
H110-3C-3T	248	0.20	248	-0.07	0.08	-1.35	0.67	1.30	-1.38	46	79	131
H130-1C-1T	750	0.53	750	-0.26	0.20	-5.32	2.59	5.12	-5.37	144	244	430
H130-3C-3T	434	0.30	434	-0.15	0.12	-2.97	1.44	2.85	-3.00	80	136	240
H250-1C-1T	911	0.91	911	-0.71	0.53	-7.16	3.35	6.58	-7.29	83	149	251
H250-3C-3T	689	0.65	689	-0.54	0.40	-5.91	2.76	5.45	-5.99	68	124	206

Table 4.3 Stress calculation and principal stress to ultimate stress ratios for beams reinforced with H-12K HMC

Sample ID	Face Comp. St.	Core Shear	Face Tens. St.	Core Normal Stresses		Ind. Stress	Core Principal Stresses			Core Principal Stresses Ratio		
	$\sigma_{c,f}$	$\tau_{,c}$	$\sigma_{t,f}$	$\sigma_{c,c}$	$\sigma_{t,c}$	$\sigma_{y,c}$	τ_{max}	σ_1	σ_2	$\tau_{max}/\tau_{yeild,c}$	$\sigma_1/\sigma_{tyiedl,c}$	$\sigma_2/\sigma_{cyeild,c}$
	MPa	MPa	MPa	MPa	MPa	MPa	MPa	MPa	MPa	%	%	%
H50-1C-1T	640	0.55	640	-0.09	0.12	-4.23	2.14	4.21	-4.30	396	281	615
H50-3C-3T	585	0.47	585	-0.09	0.11	-4.65	2.33	4.61	-4.69	431	307	671
H110-1C-1T	1006	0.80	1006	-0.29	0.34	-8.73	4.29	8.51	-8.81	298	258	419
H110-3C-3T	734	0.58	734	-0.22	0.25	-6.84	3.37	6.68	-6.90	234	202	328
H130-1C-1T	981	0.69	981	-0.34	0.27	-7.96	3.88	7.69	-8.02	194	183	321
H130-3C-3T	752	0.53	752	-0.26	0.21	-6.77	3.30	6.56	-6.81	165	156	273
H250-1C-1T	1326	1.32	1326	-1.04	0.78	-12.58	5.92	11.69	-12.73	132	133	283
H250-3C-3T	1080	1.02	1080	-0.84	0.63	-11.60	5.47	10.85	-11.69	122	123	260

Table 4.4 Stress calculation and principal stress to yield stress ratios for beams reinforced with N-12K MMC

Sample ID	Face Comp. St.	Core Shear	Face Tens. St.	Core Normal Stresses		Ind. Stress	Core Principal Stresses			Core Principal Stresses Ratio		
	$\sigma_{c,f}$	$\tau_{,c}$	$\sigma_{t,f}$	$\sigma_{c,c}$	$\sigma_{t,c}$	$\sigma_{y,c}$	τ_{max}	σ_1	σ_2	$\tau_{max}/\tau_{yeild,c}$	$\sigma_1/\sigma_{tyiedl,c}$	$\sigma_2/\sigma_{cyeild,c}$
	MPa	MPa	MPa	MPa	MPa	MPa	MPa	MPa	MPa	%	%	%
N50-1C-1T	323	0.48	323	-0.07	0.09	-1.57	0.89	1.64	-1.71	148	219	488
N50-3C-3T	272	0.28	272	-0.06	0.07	-1.34	0.70	1.34	-1.39	116	178	398
N110-1C-1T	685	0.58	685	-0.15	0.18	-4.96	2.48	4.88	-5.03	155	296	479
N110-3C-3T	659	0.61	659	-0.14	0.18	-5.24	2.62	5.17	-5.31	164	313	505
N130-1C-1T	692	0.69	692	-0.15	0.19	-4.78	2.42	4.73	-4.88	134	225	391
N130-3C-3T	597	0.59	597	-0.13	0.16	-4.28	2.16	4.23	-4.36	120	202	349
N250-1C-1T	841	0.77	841	-0.18	0.23	-6.44	3.22	6.35	-6.53	80	144	225
N250-3C-3T	635	0.78	635	-0.14	0.17	-4.70	2.41	4.70	-4.83	60	107	167

Table 4.5 stress calculation and principal stress to ultimate stress ratios for beams reinforced with N-12K MMC

Sample ID	Face Comp. St.	Core Shear	Face Tens. St.	Core Normal Stresses		Ind. Stress	Core Principal Stresses			Core Principal Stresses Ratio		
	$\sigma_{c,f}$	$\tau_{,c}$	$\sigma_{t,f}$	$\sigma_{c,c}$	$\sigma_{t,c}$	$\sigma_{y,c}$	τ_{max}	σ_1	σ_2	$\tau_{max}/\tau_{yeild,c}$	$\sigma_1/\sigma_{tyiedl,c}$	$\sigma_2/\sigma_{cyeild,c}$
	MPa	MPa	MPa	MPa	MPa	MPa	MPa	MPa	MPa	%	%	%
N50-1C-1T	1248	1.86	1248	-0.18	0.23	-11.92	6.16	12.02	-12.21	1140	802	1744
N50-3C-3T	738	0.76	738	-0.11	0.14	-5.97	3.03	5.96	-6.07	841	397	867
N110-1C-1T	1260	1.07	1260	-0.37	0.43	-12.36	6.09	12.09	-12.46	423	366	593
N110-3C-3T	920	0.84	920	-0.27	0.31	-8.63	4.26	8.44	-8.71	296	256	415
N130-1C-1T	1292	1.29	1292	-0.44	0.35	-12.21	6.02	11.91	-12.35	301	284	494
N130-3C-3T	1034	1.03	1034	-0.35	0.28	-9.76	4.81	9.52	-9.87	241	227	395
N250-1C-1T	1190	1.09	1190	-0.93	0.70	-10.84	5.07	10.03	-10.96	113	114	243
N250-3C-3T	888	1.10	888	-0.69	0.52	-7.77	3.71	7.24	-7.94	82	82	176

Table 4.6 stress calculation and principal stress to yield stress ratios for beams reinforced with T-3K Uni C Tape

Sample ID	Face Comp. St.	Core Shear	Face Tens. St.	Core Normal Stresses		Ind. Stress	Core Principal Stresses			Core Principal Stresses Ratio		
	$\sigma_{c,f}$	$\tau_{,c}$	$\sigma_{t,f}$	$\sigma_{c,c}$	$\sigma_{t,c}$	$\sigma_{y,c}$	τ_{max}	σ_1	σ_2	$\tau_{max}/\tau_{yeild,c}$	$\sigma_1/\sigma_{tyiedl,c}$	$\sigma_2/\sigma_{cyeild,c}$
	MPa	MPa	MPa	MPa	MPa	MPa	MPa	MPa	MPa	%	%	%
T50-1C-1T	304	0.31	304	-0.12	0.16	-1.99	0.98	1.91	-2.04	163	255	582
T50-2C-2T	125	0.25	125	-0.05	0.06	-0.58	0.37	0.63	-0.68	61	84	195
T110-1C-1T	506	0.51	506	-0.41	0.48	-4.48	2.09	4.13	-4.54	131	250	432
T110-2C-2T	319	0.64	319	-0.26	0.30	-2.51	1.29	2.42	-2.68	81	146	255
T130-1C-1T	506	0.51	506	-0.48	0.38	-4.23	1.94	3.82	-4.30	108	182	344
T130-2C-2T	326	0.66	326	-0.31	0.25	-2.47	1.26	2.35	-2.66	70	112	212
T250-1C-1T	605	0.61	605	-1.32	0.99	-5.57	2.21	4.34	-5.65	55	99	195
T250-2C-2T	473	0.95	473	-1.03	0.77	-4.30	1.89	3.53	-4.55	47	80	157

Table 4.7 Stress calculation and principal stress to ultimate stress ratios for beams reinforced with T-3K Uni C Tape

Sample ID	Face Comp. St.	Core Shear	Face Tens. St.	Core Normal Stresses		Ind. Stress	Core Principal Stresses			Core Principal Stresses Ratio		
	$\sigma_{c,f}$	$\tau_{,c}$	$\sigma_{t,f}$	$\sigma_{c,c}$	$\sigma_{t,c}$	$\sigma_{y,c}$	τ_{max}	σ_1	σ_2	$\tau_{max}/\tau_{yeild,c}$	$\sigma_1/\sigma_{tyiedl,c}$	$\sigma_2/\sigma_{cyeild,c}$
	MPa	MPa	MPa	MPa	MPa	MPa	MPa	MPa	MPa	%	%	%
T50-1C-1T	542	0.55	542	-0.22	0.28	-4.73	2.32	4.57	-4.79	429	305	685
T50-2C-2T	295	0.59	295	-0.12	0.15	-2.13	1.17	2.17	-2.29	216	145	327
T110-1C-1T	826	0.83	826	-0.67	0.79	-9.32	4.40	8.73	-9.40	306	265	448
T110-2C-2T	666	1.34	666	-0.54	0.63	-7.55	3.75	7.26	-7.80	261	220	371
T130-1C-1T	843	0.85	843	-0.80	0.64	-9.10	4.23	8.38	-9.18	212	399	367
T130-2C-2T	614	1.23	614	-0.58	0.47	-6.38	3.15	6.04	-6.63	157	288	265
T250-1C-1T	717	0.72	717	-1.56	1.17	-7.19	2.90	5.72	-7.28	65	65	125
T250-2C-2T	659	1.33	659	-1.43	1.07	-7.06	3.11	5.93	-7.36	69	67	127

Table 4.8 Analytical and experimental results for beams reinforced with H-12K HMC

Sample ID	Analytical Failure Load				Experimental		Mode of failure	
	Tension (N)	Shear (N)	Wrinkling (N)	Lower Bound (N)	Ultimate (N)	Elastic Limit (N)	Analytical	Observed
H50-1C-1T	682	260	180	82	198	111	Wrinkling	Wrinkling
H50-3C-3T	1651	842	435	248	546	308	Wrinkling	Bearing
H110-1C-1T	705	768	300	173	345	166	Wrinkling	Tension
H110-3C-3T	1752	2246	746	526	763	243	Wrinkling	Tension
H130-1C-1T	684	1005	335	193	524	230	Wrinkling	Tension& Wrinkling
H130-3C-3T	1674	2848	819	580	782	405	Wrinkling	Tension
H250-1C-1T	633	1744	520	298	473	281	Wrinkling	Tension
H250-3C-3T	1752	6035	1441	937	1003	640	Wrinkling	Tension

Table 4.9 Analytical and experimental results for beams reinforced with N-12K MMC

Sample ID	Analytical Failure Load				Experimental		Mode of failure	
	Tension (N)	Shear (N)	Wrinkling (N)	Lower Bound (N)	Ultimate (N)	Elastic Limit (N)	Analytical	Observed
N50-1C-1T	940	216	229	74	395	102	Shear	Tension
N50-3C-3T	2555	691	622	224	695	256	Wrinkling	Bearing
N110-1C-1T	868	531	341	150	408	222	Wrinkling	Tension
N110-3C-3T	2358	1894	927	451	900	645	Wrinkling	Tension
N130-1C-1T	825	619	373	166	398	213	Wrinkling	Tension & Shear
N130-3C-3T	2237	1814	1011	497	960	554	Wrinkling	Tension
N250-1C-1T	828	1166	629	263	484	260	Wrinkling	Tension
N250-3C-3T	2555	4662	1457	790	825	590	Wrinkling	Tension

Table 4.10 Analytical and experimental results for beams reinforced with T-3K Uni C Tape

Sample ID	Analytical Failure Load				Experimental		Mode of failure	
	Tension (N)	Shear (N)	Wrinkling (N)	Lower Bound (N)	Ultimate (N)	Elastic Limit (N)	Analytical	Observed
T50-1C-1T	4872	880	444	241	720	404	Wrinkling	Bearing
T50-2C-2T	9832	888	1017	483	790	333	Shear	Shear & Bearing
T110-1C-1T	4783	2304	799	497	1150	705	Wrinkling	Bearing
T110-2C-2T	9588	2309	1601	996	1867	895	Wrinkling	Bearing
T130-1C-1T	4783	2592	918	559	1111	667	Wrinkling	Bearing
T130-2C-2T	9566	2592	1820	1114	1642	873	Wrinkling	Bearing
T250-1C-1T	4768	5814	1537	886	951	802	Wrinkling	Wrinkling
T250-2C-2T	9536	5814	3075	1772	1755	1260	Wrinkling	Wrinkling

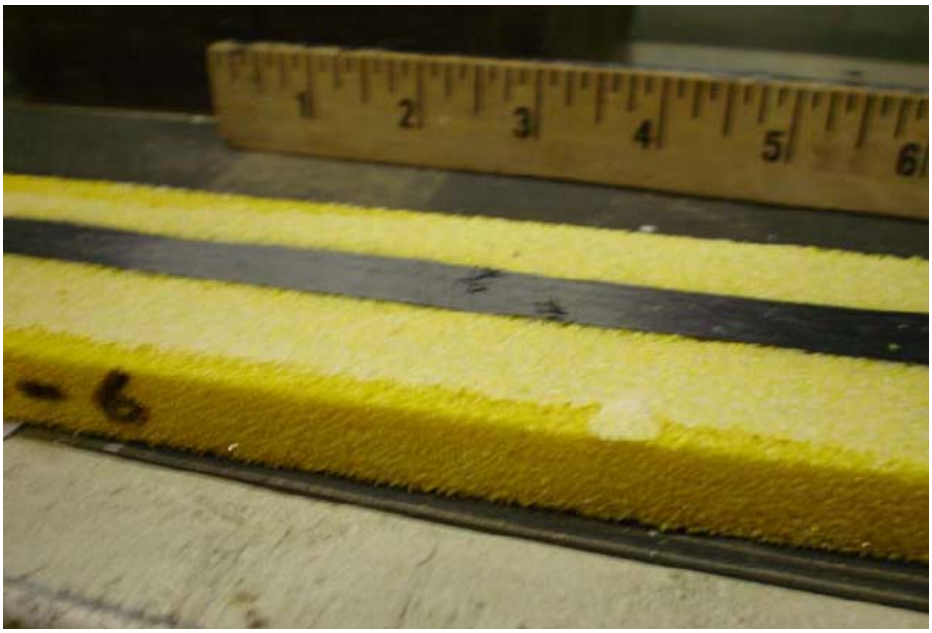

Figure 4.1 Wrinkling failure for inorganic composites

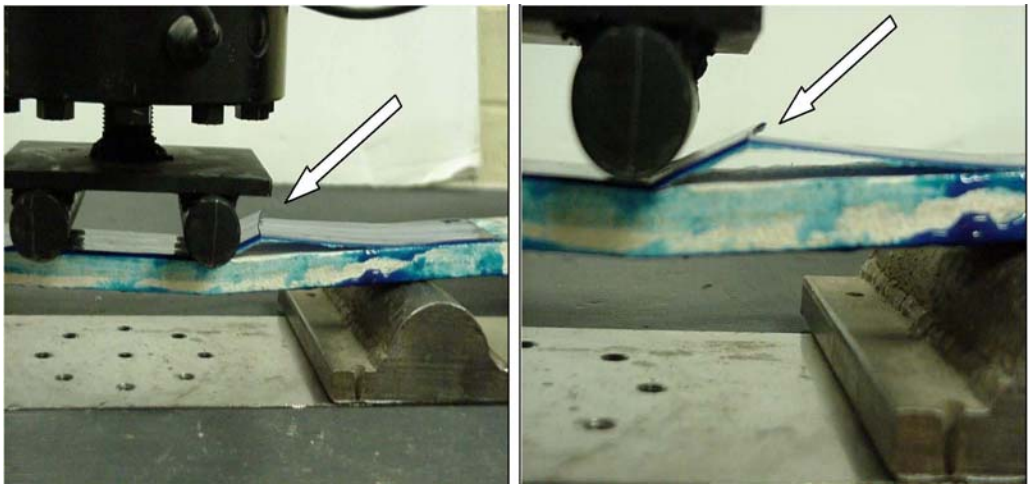

Figure 4.2 Wrinkling failure for organic composite (Giancaspro, 2004)

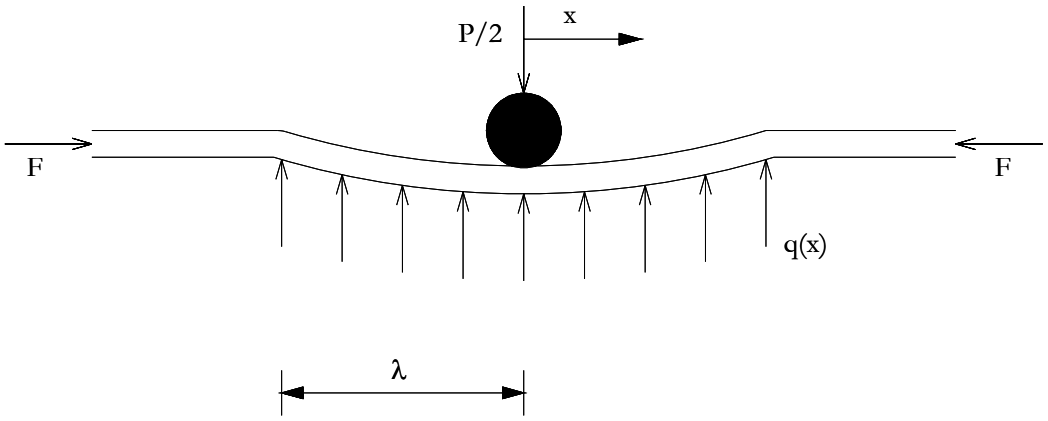

Figure 4.3 Indentation zone underneath loading rollers

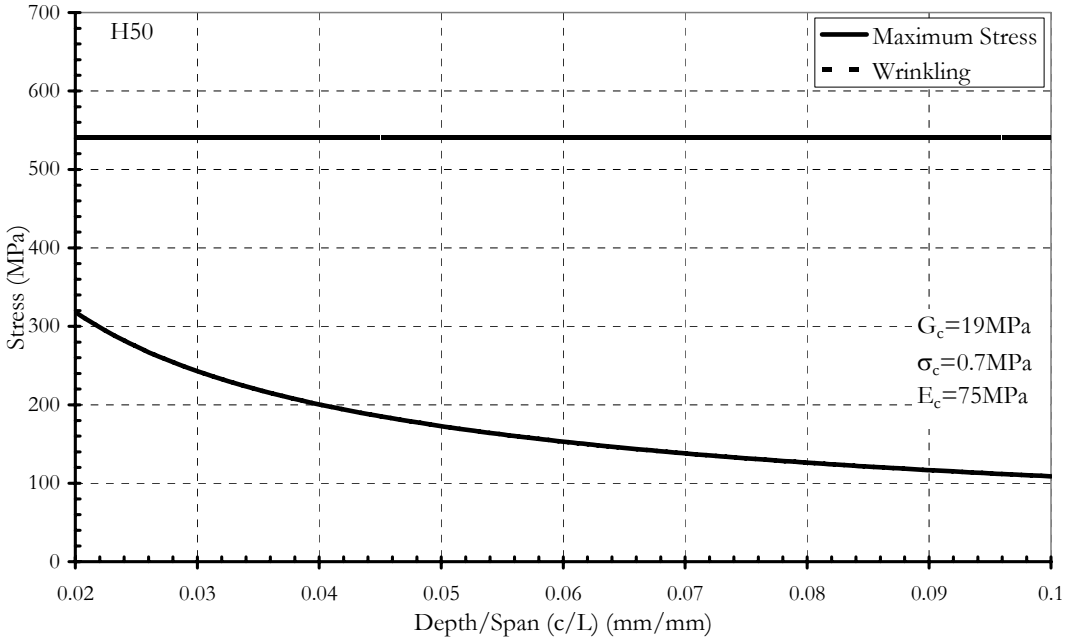

Figure 4.4 Maximum fiber stress for H-12K HMC and 50 Kg/m^3 core for various depth/span ratios

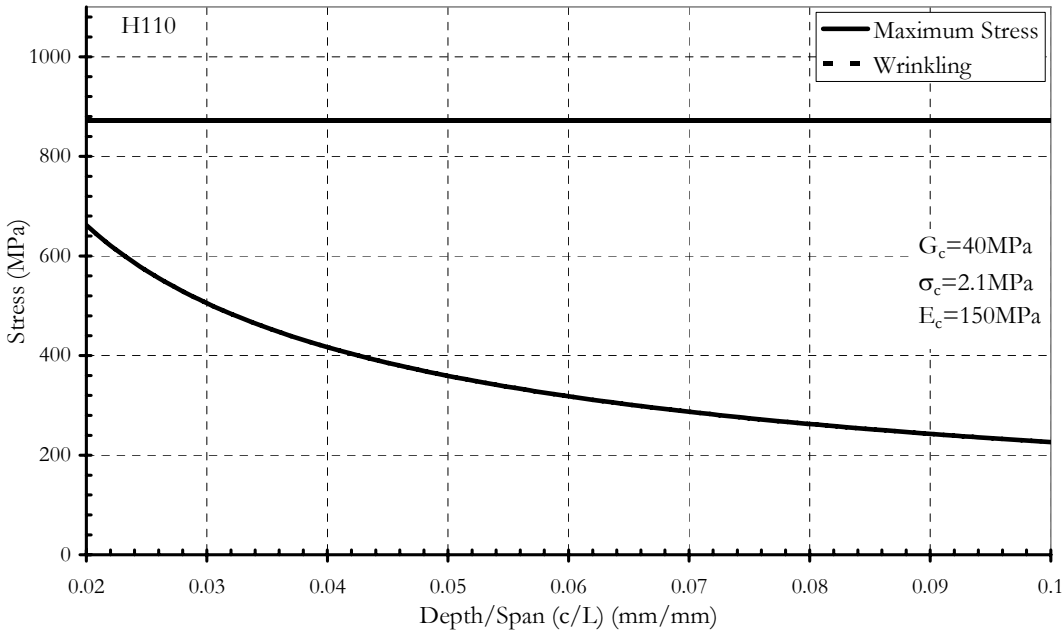

Figure 4.5 Maximum fiber stress for H-12K HMC and 110 Kg/m^3 core for various depth/span Ratios

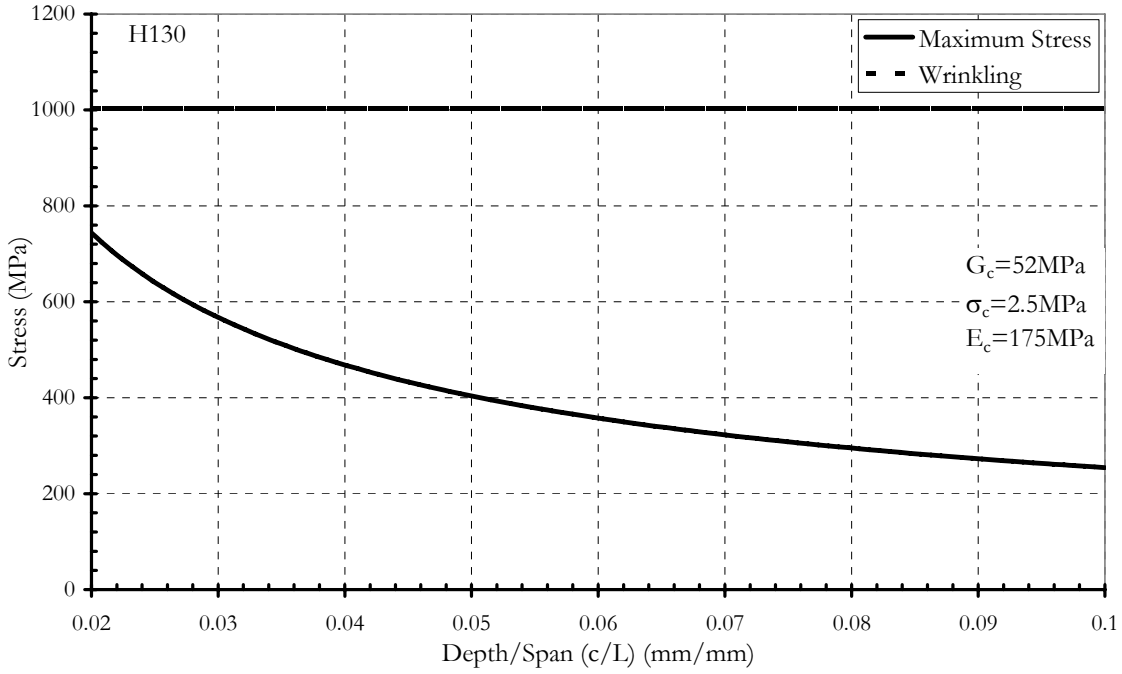

Figure 4.6 Maximum fiber stress for H-12K HMC and 130 Kg/m^3 core for various depth/span ratios

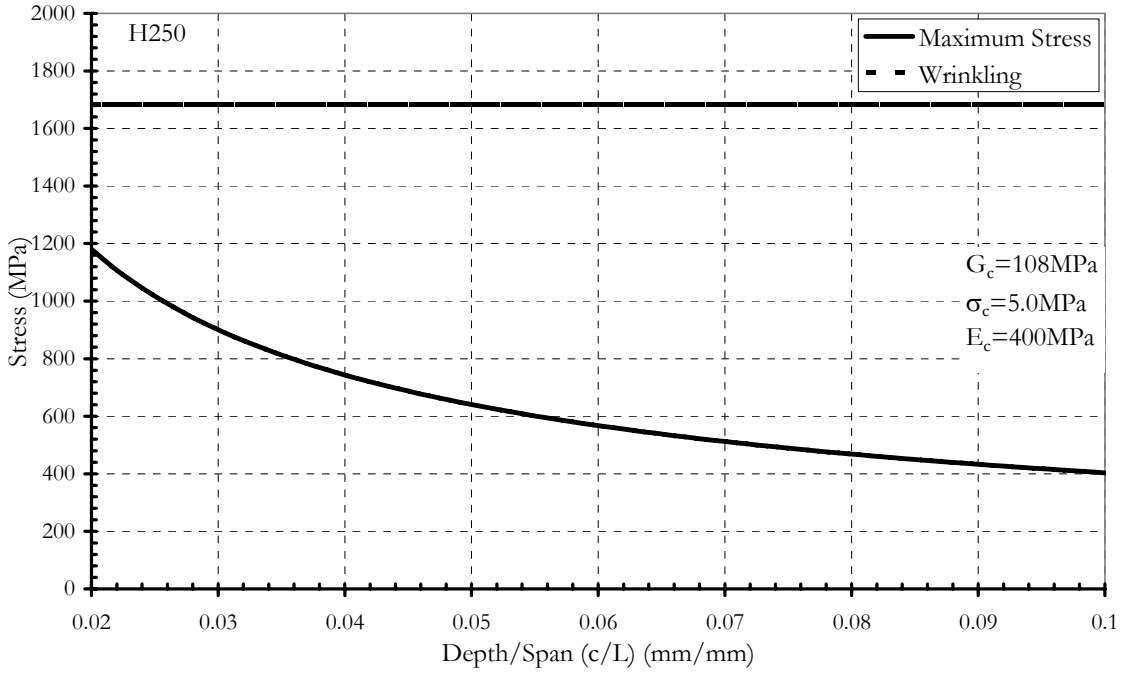

Figure 4.7 Maximum fiber stress for H-12K HMC and 250 Kg/m^3 core for various depth/span ratios

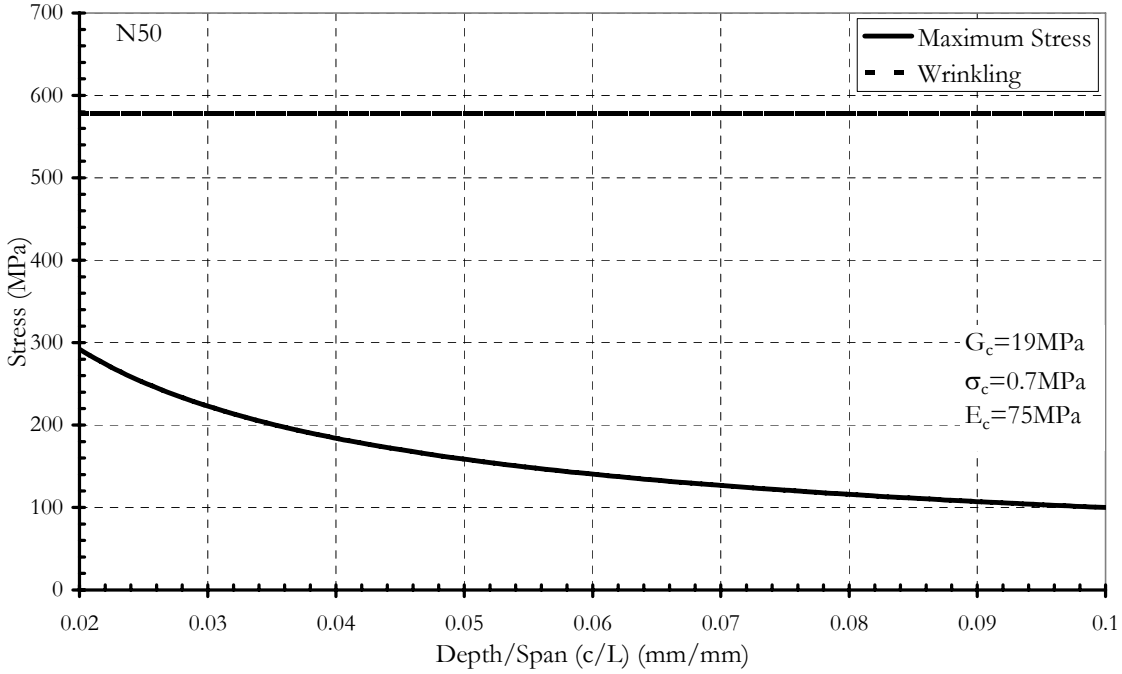

Figure 4. 8 Maximum fiber stress for N-12K MMC and 50 Kg/m^3 Core for various depth/span ratios

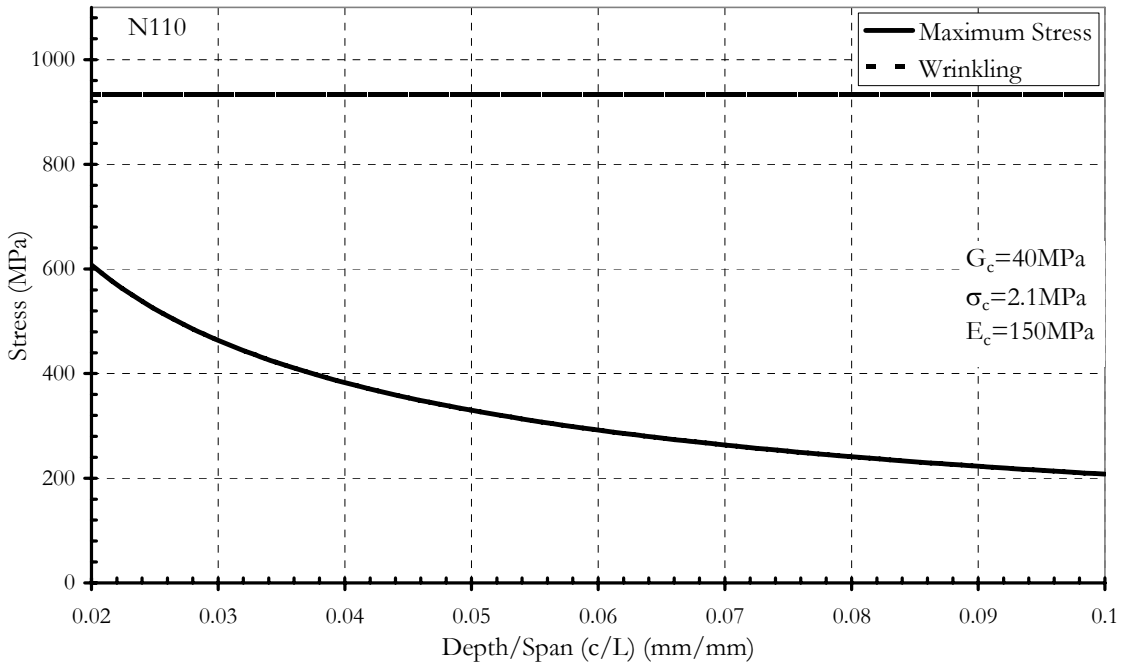

Figure 4.9 Maximum fiber stress for N-12K MMC and 110 Kg/m^3 core for various depth/span ratios

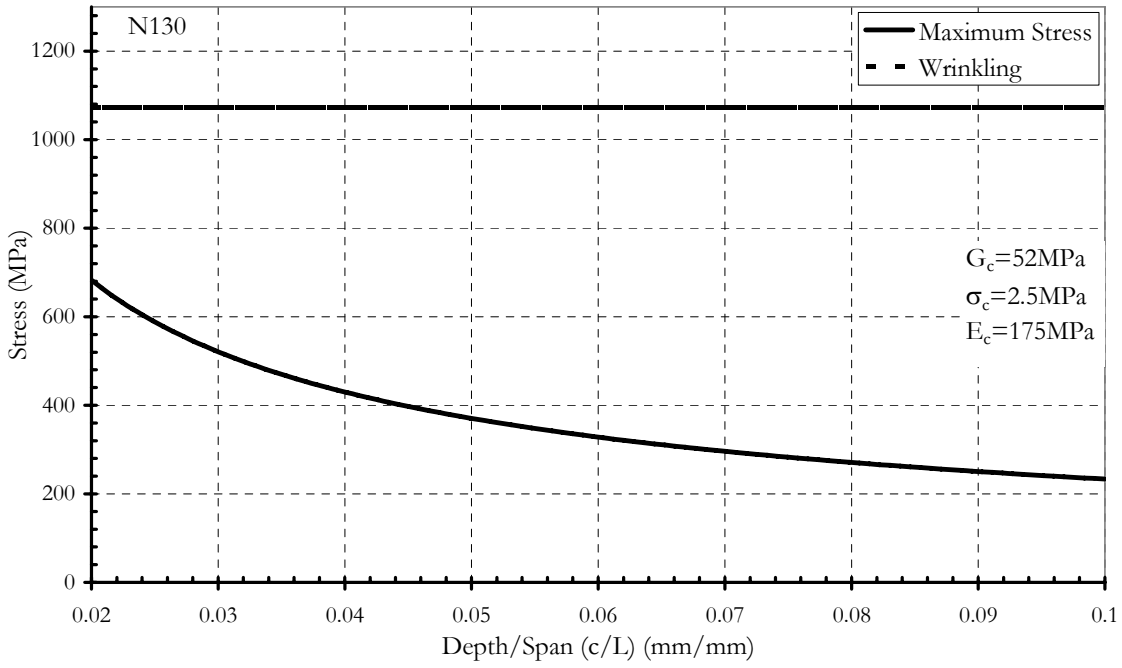

Figure 4.10 Maximum fiber stress for N-12K MMC and 130 Kg/m^3 core for various depth/span ratios

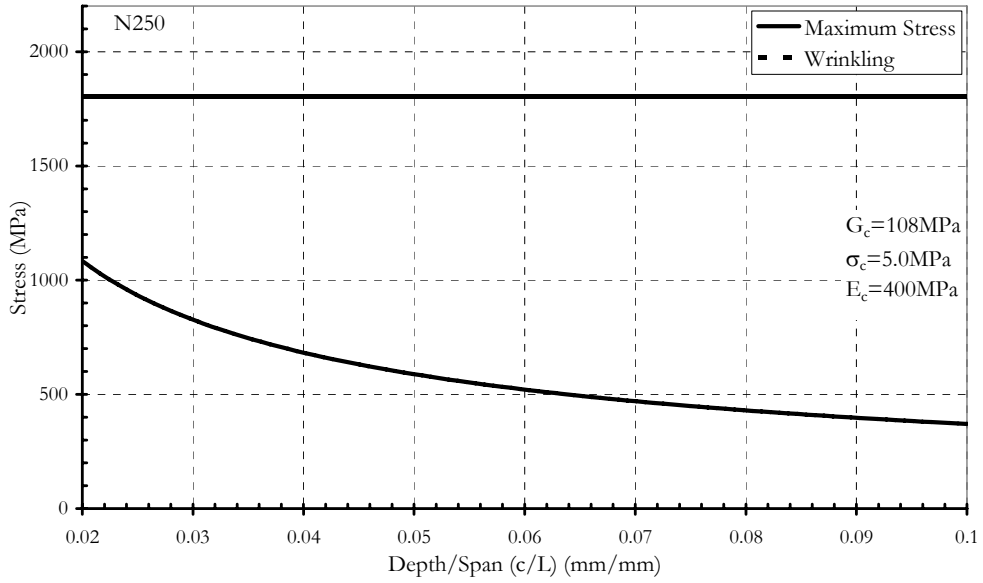

Figure 4.11 Maximum fiber stress for N-12K MMC and 250 Kg/m^3 core for various depth/span ratios

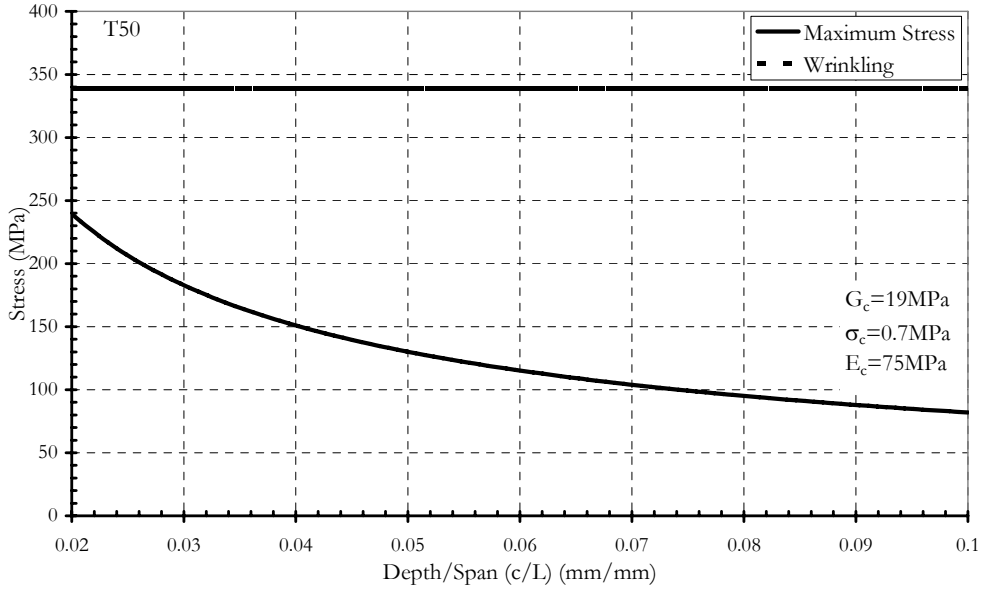

Figure 4.12 Maximum fiber stress for T-3K Uni C Tape and 50 Kg/m^3 core for various depth/span ratios

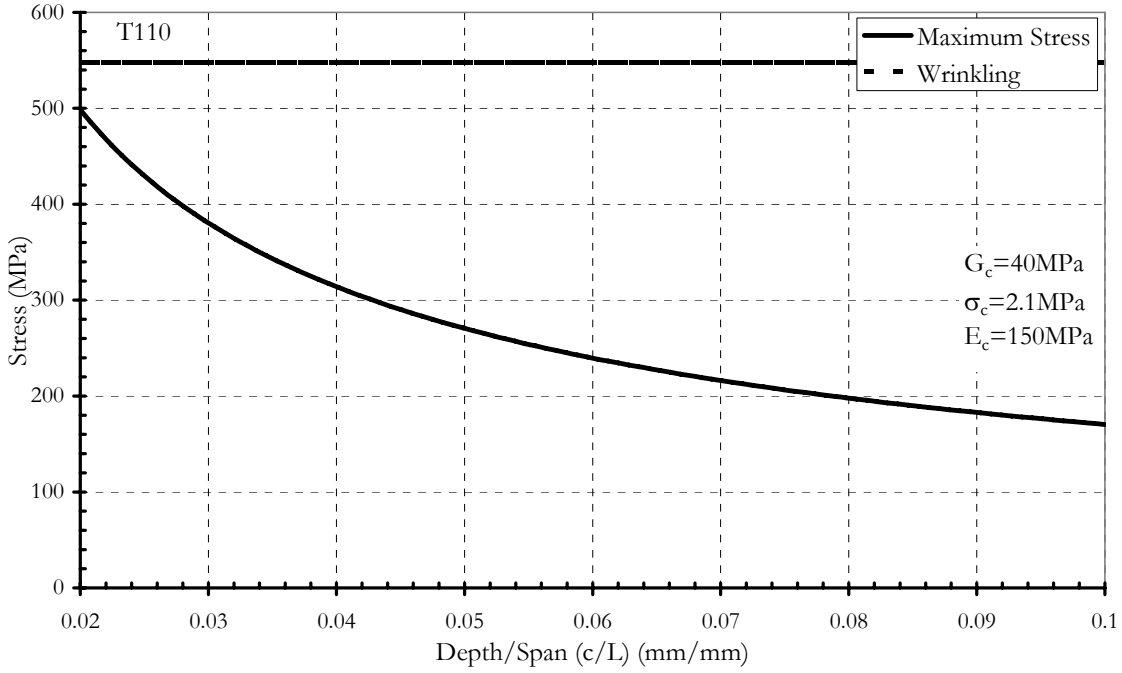

Figure 4.13 Maximum fiber stress for T-3K Uni C Tape and 110 Kg/m^3 core for various depth/span ratios

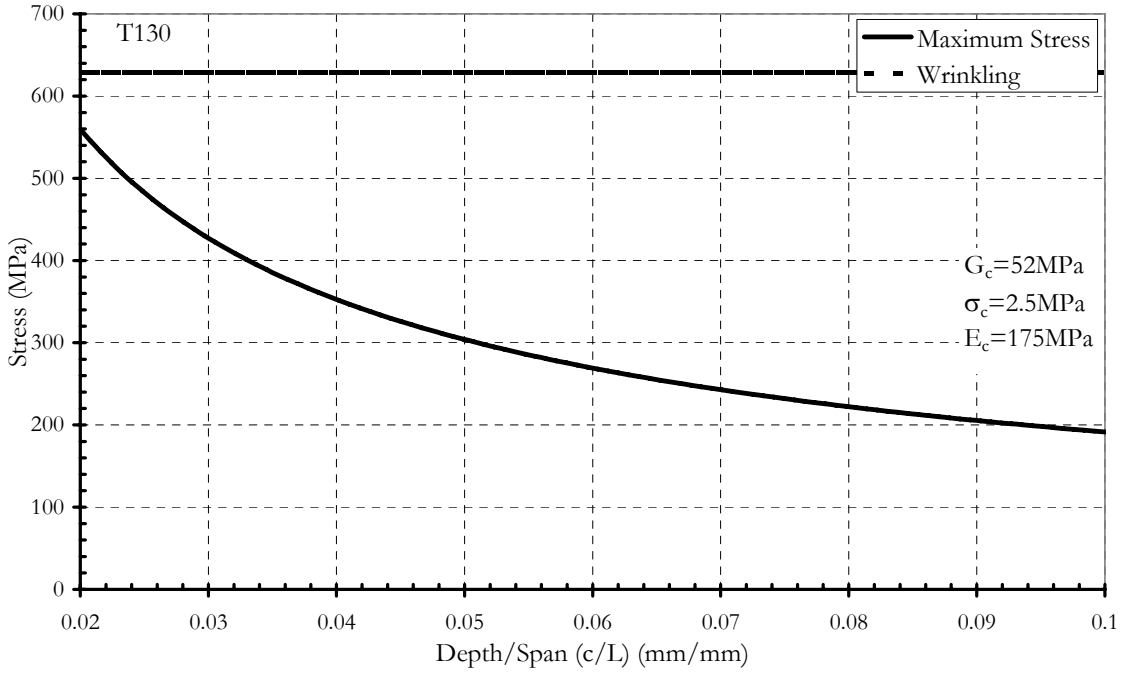

Figure 4.14 Maximum fiber stress for T-3K Uni C Tape and 130 Kg/m^3 core for various depth/span ratios

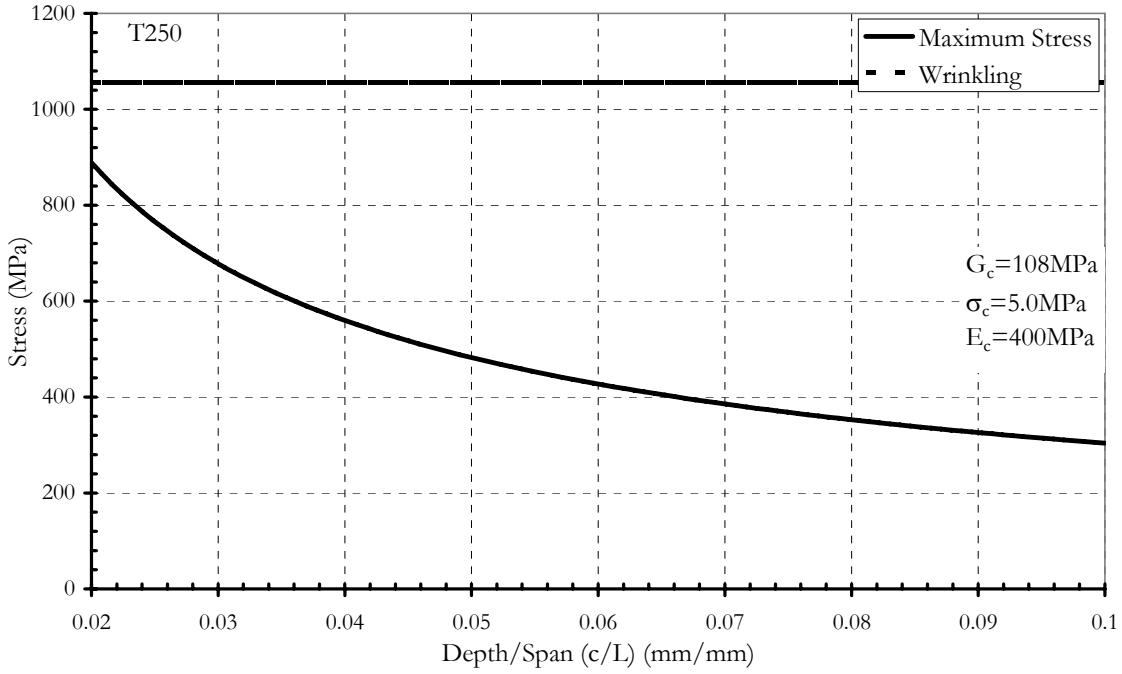

Figure 4.15 Maximum fiber stress for T-3K Uni C Tape and 250 Kg/m^3 core for various depth/span ratios

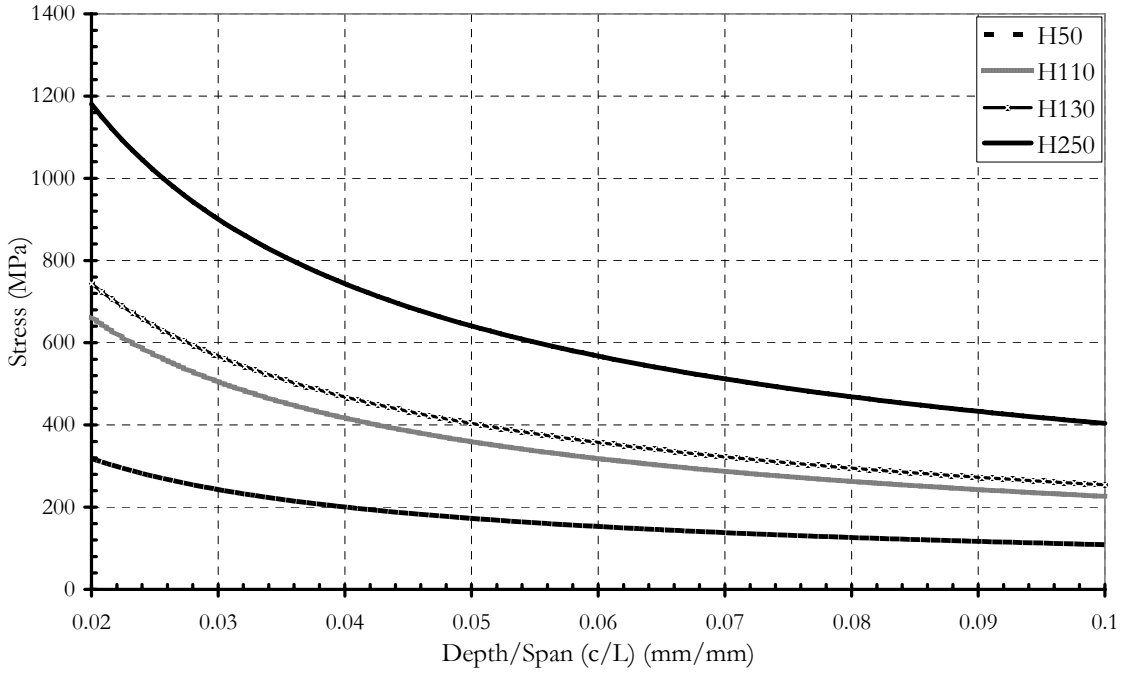

Figure 4.16 Effect of PVC core density on the maximum attainable fiber stress for H-12K HMC

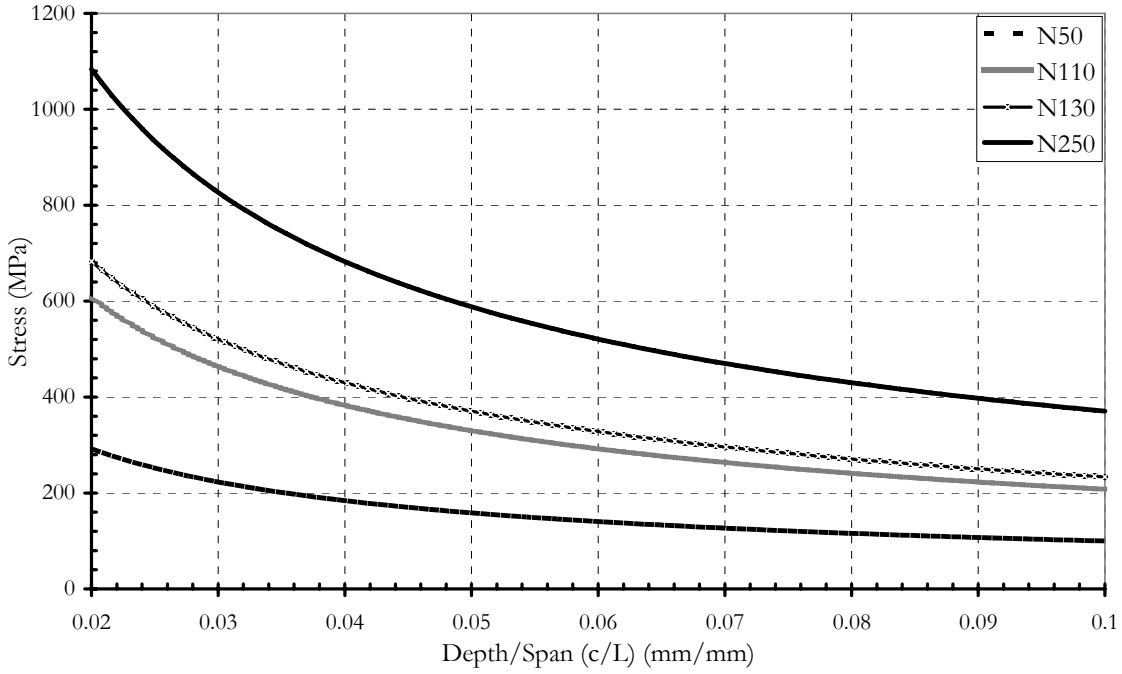

Figure 4.17 Effect of PVC core density on the maximum attainable fiber stress for N-12K MMC

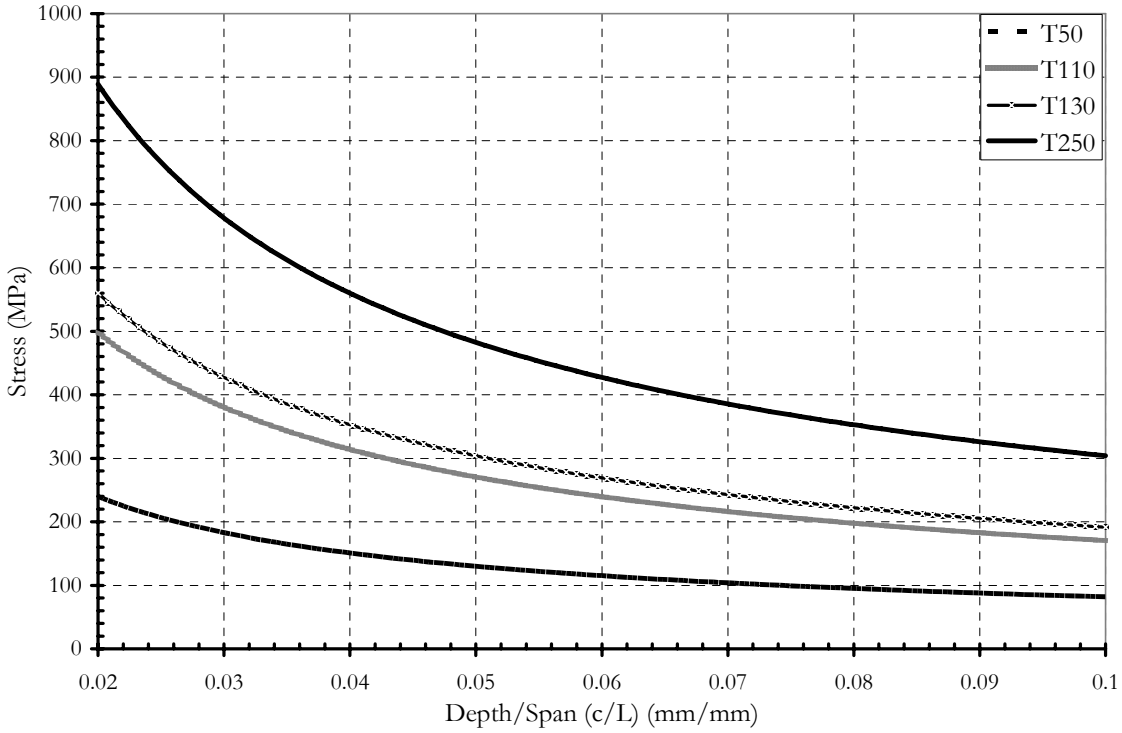

Figure 4.18 Effect of PVC core density on the maximum attainable fiber stress for T-3K Uni C Tape

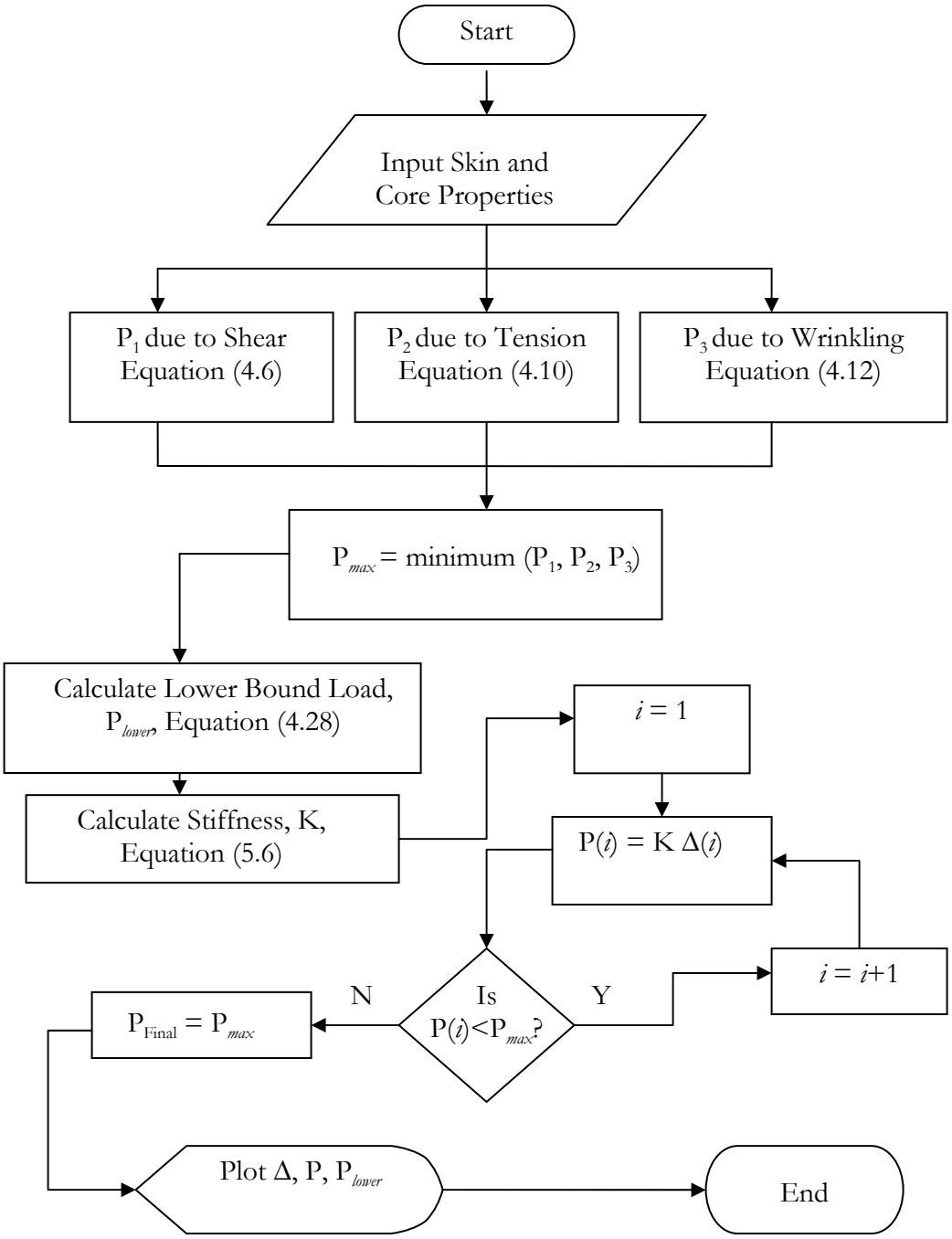

Figure 4.19 Analytical load-deflection curve flowchart

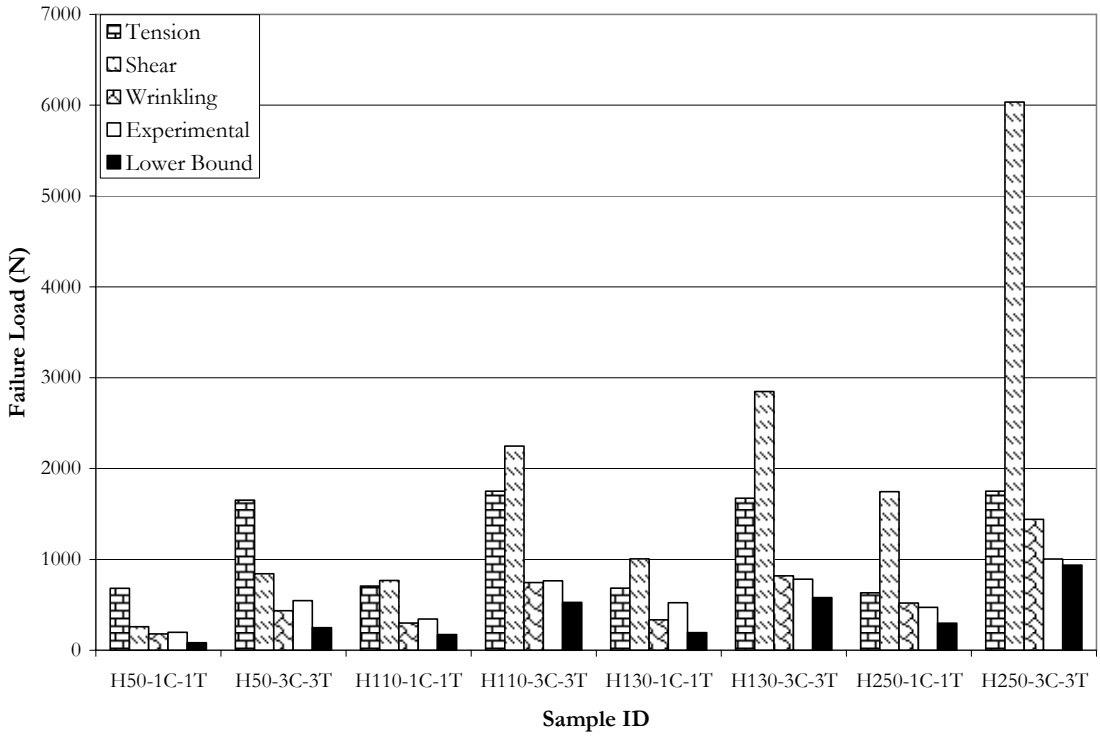

Figure 4.20 Failure modes and maximum loads for H-12K HMC

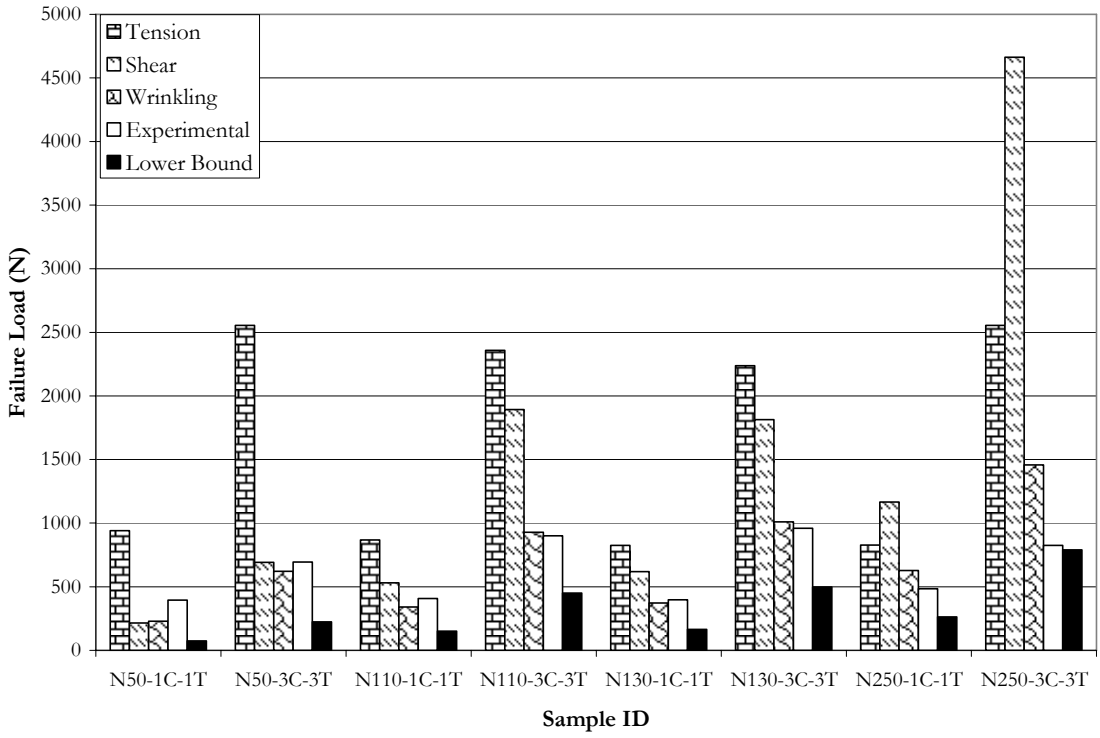

Figure 4.21 Failure modes and maximum loads for N-12K MMC

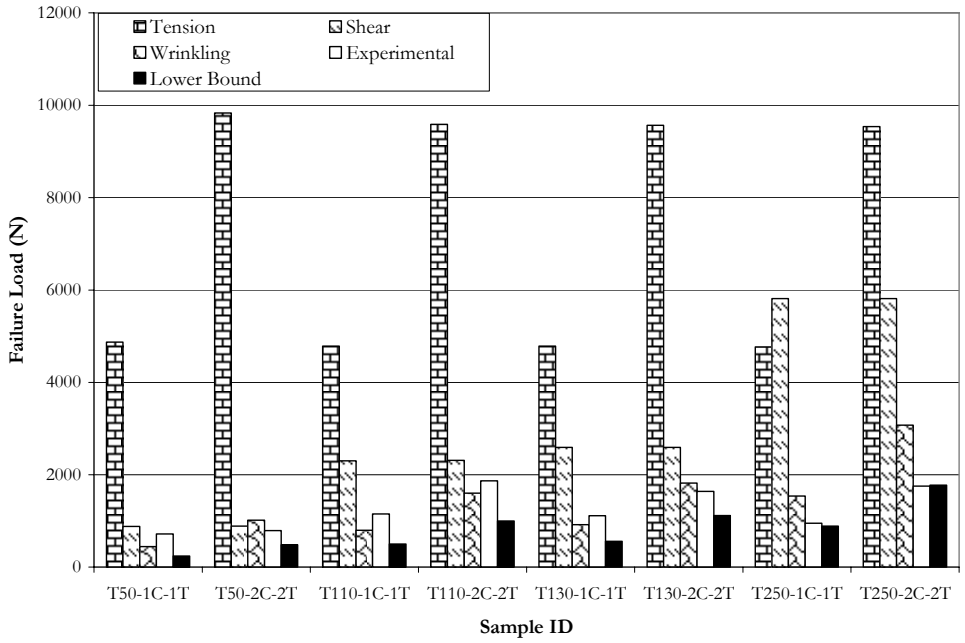

Figure 4.22 Failure modes and maximum loads for T-3K Uni C Tape

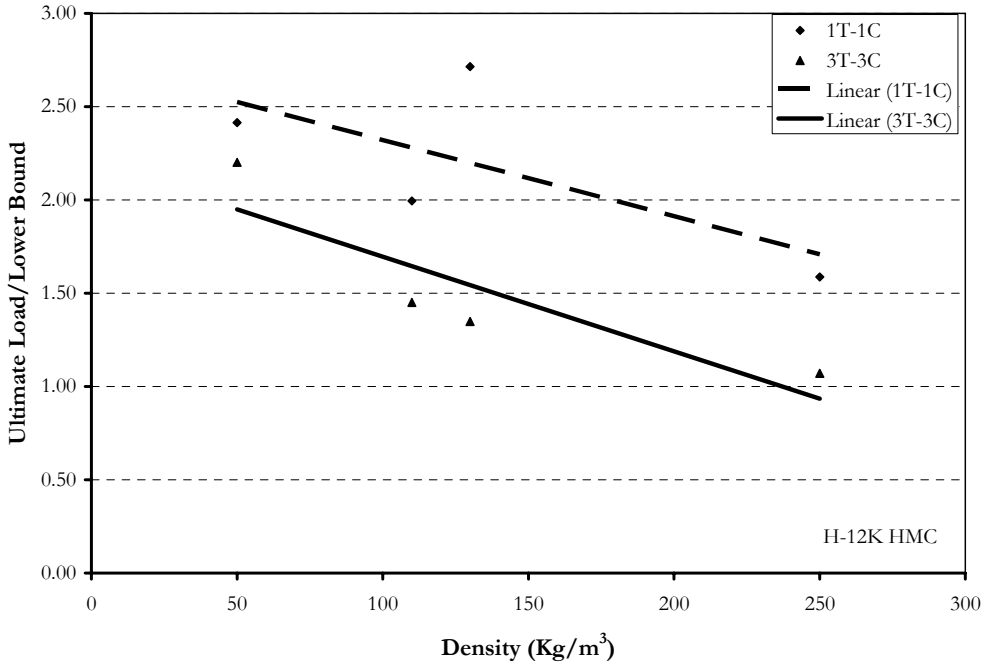

Figure 4.23 The relation between the ratio between the ultimate load and the lower bound solution for H-12K HMC and different core densities

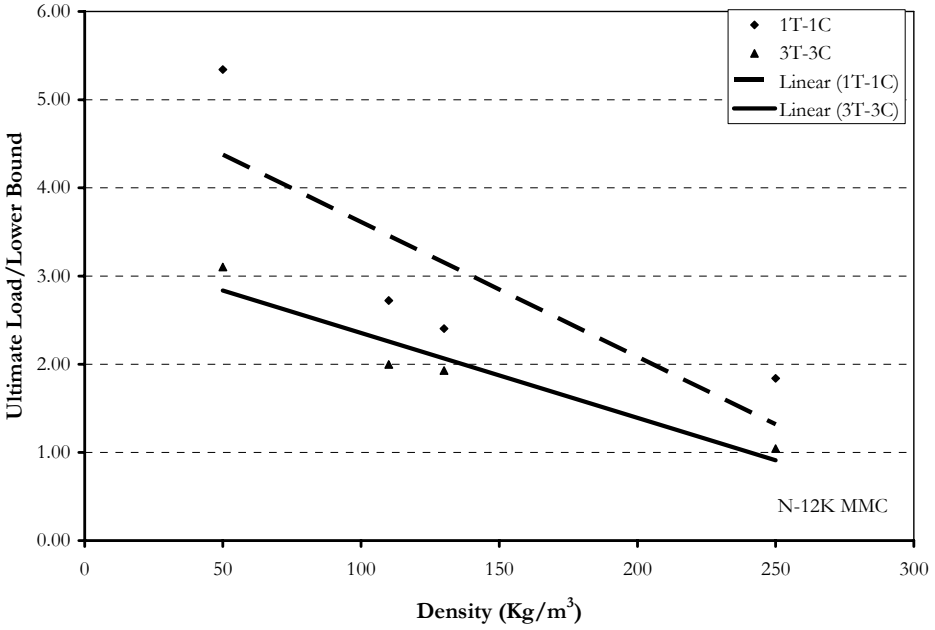

Figure 4.24 The relation between the ratio between the ultimate load and the lower bound solution for N-12K MMC and different core densities

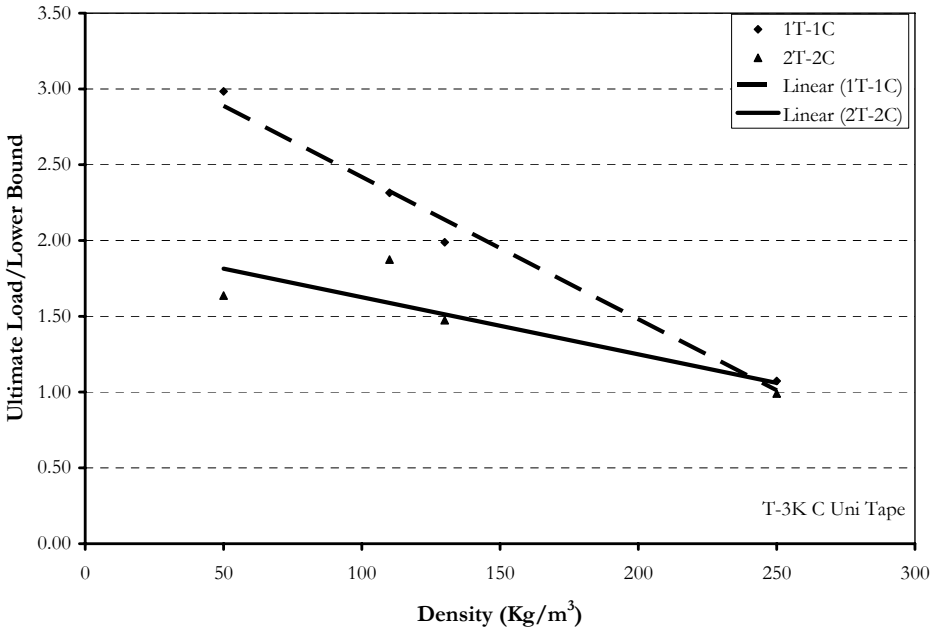

Figure 4.25 The relation between the ratio between the ultimate load and the lower bound solution for N-12K MMC and different core densities

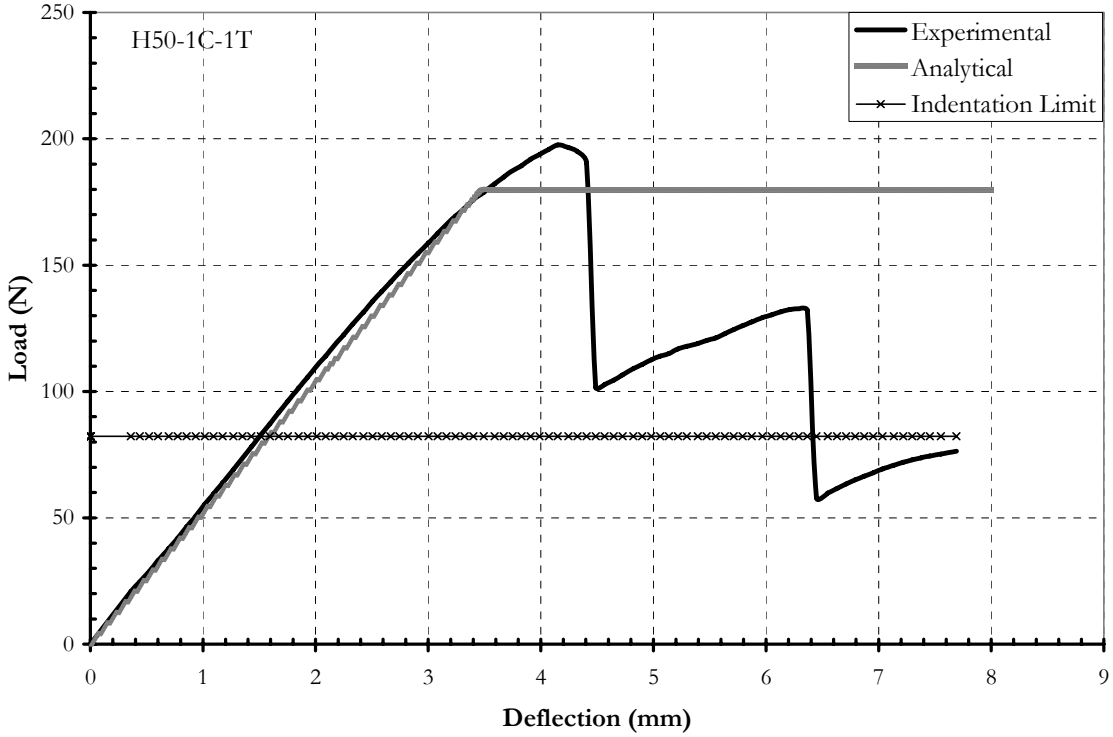

Figure 4.26 Experimental vs. analytical for H50 1C-1T

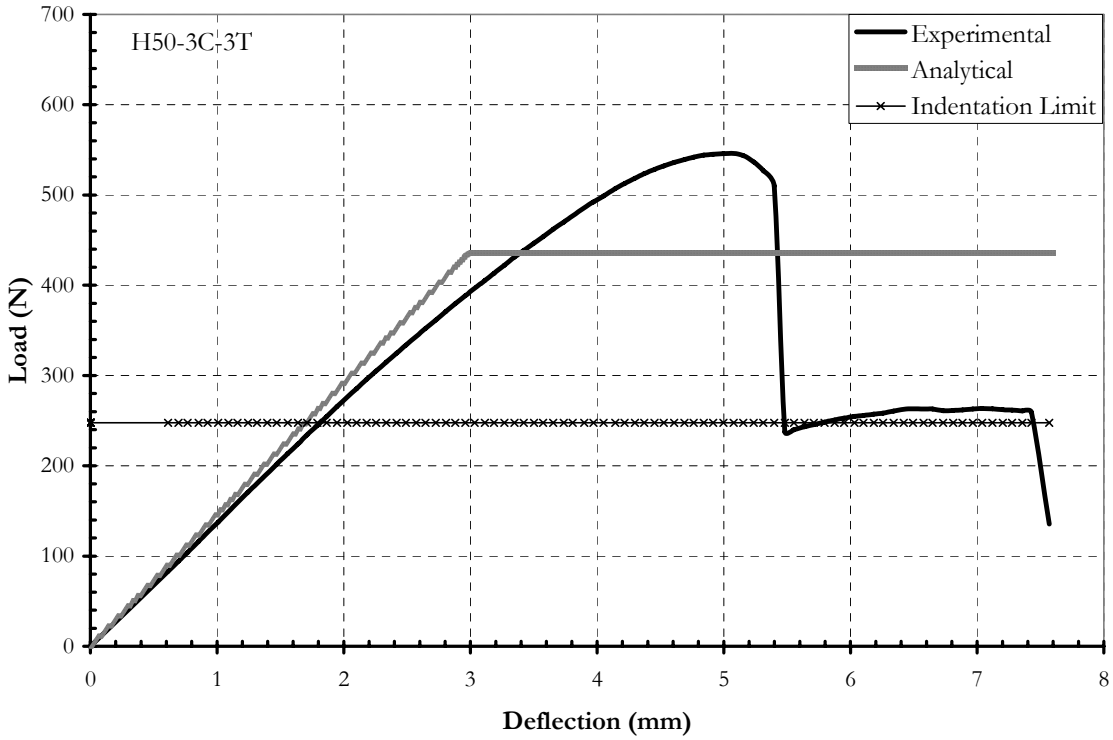

Figure 4.27 Experimental vs. analytical for H50 3C-3T

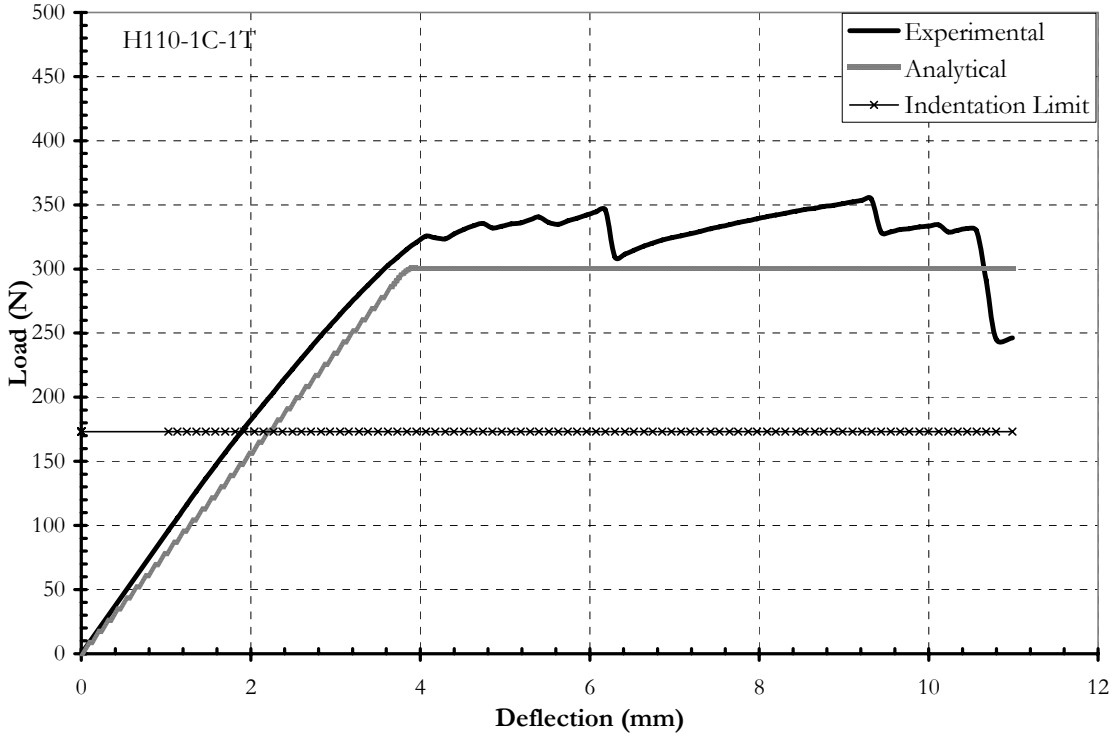

Figure 4.28 Experimental vs. analytical for H110 1C-1T

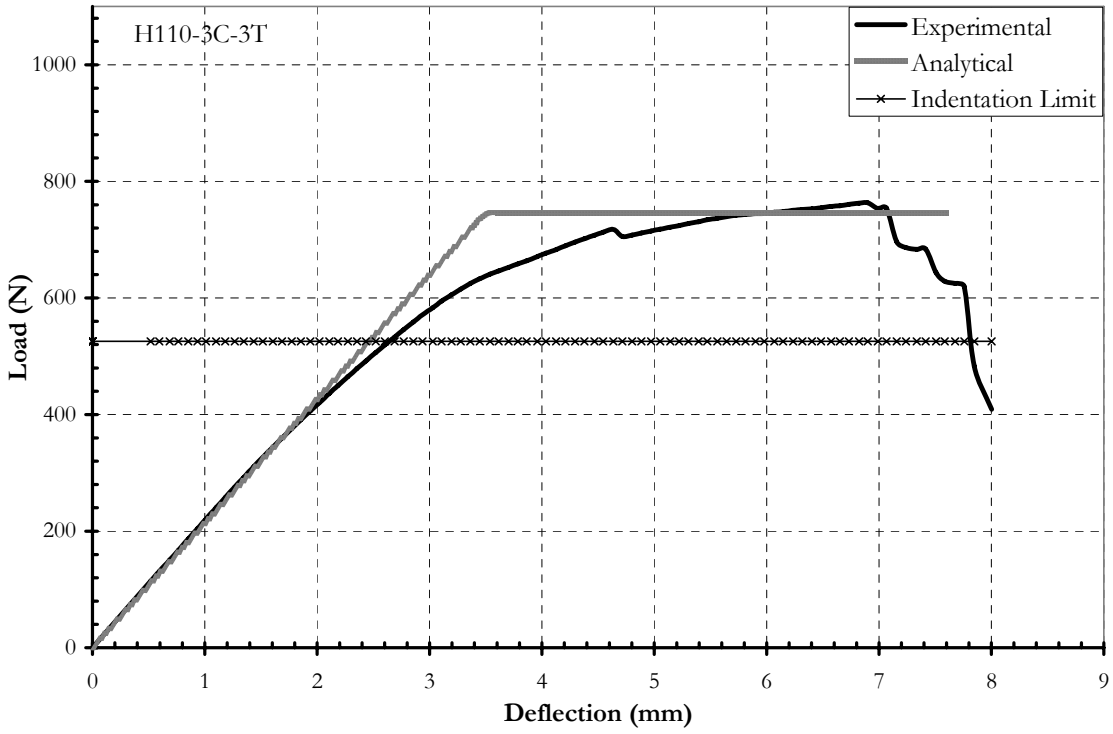

Figure 4.29 Experimental vs. analytical for H110 3C-3T

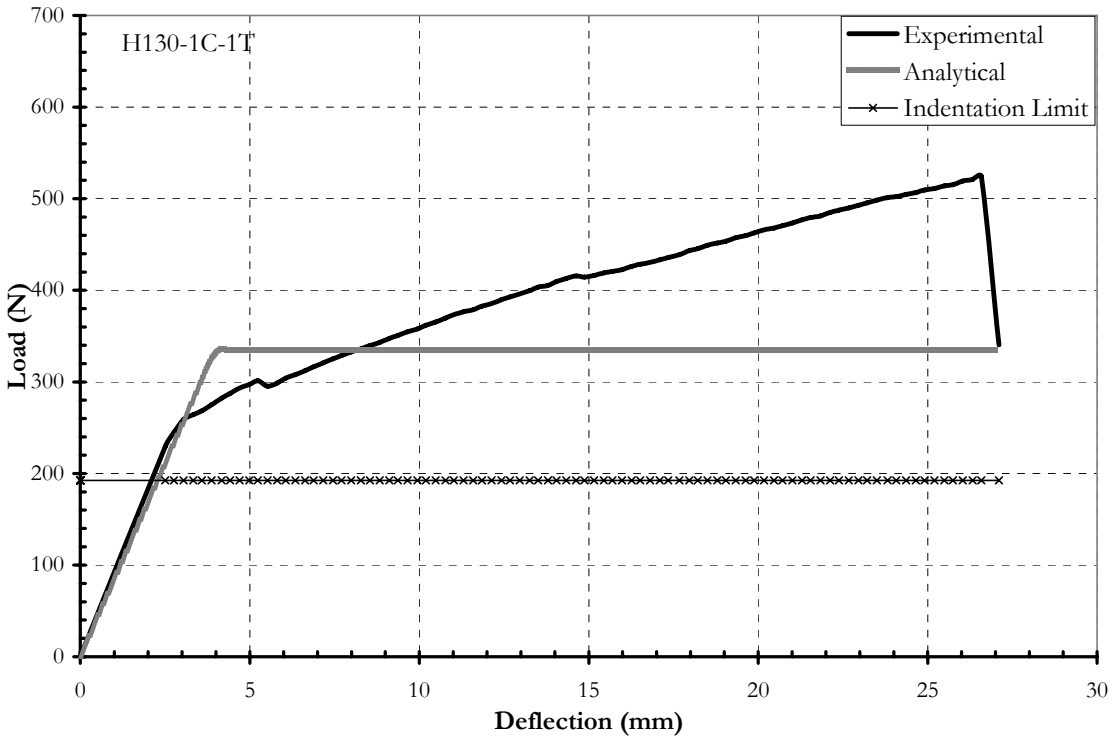

Figure 4.30 Experimental vs. analytical for H130 1C-1T

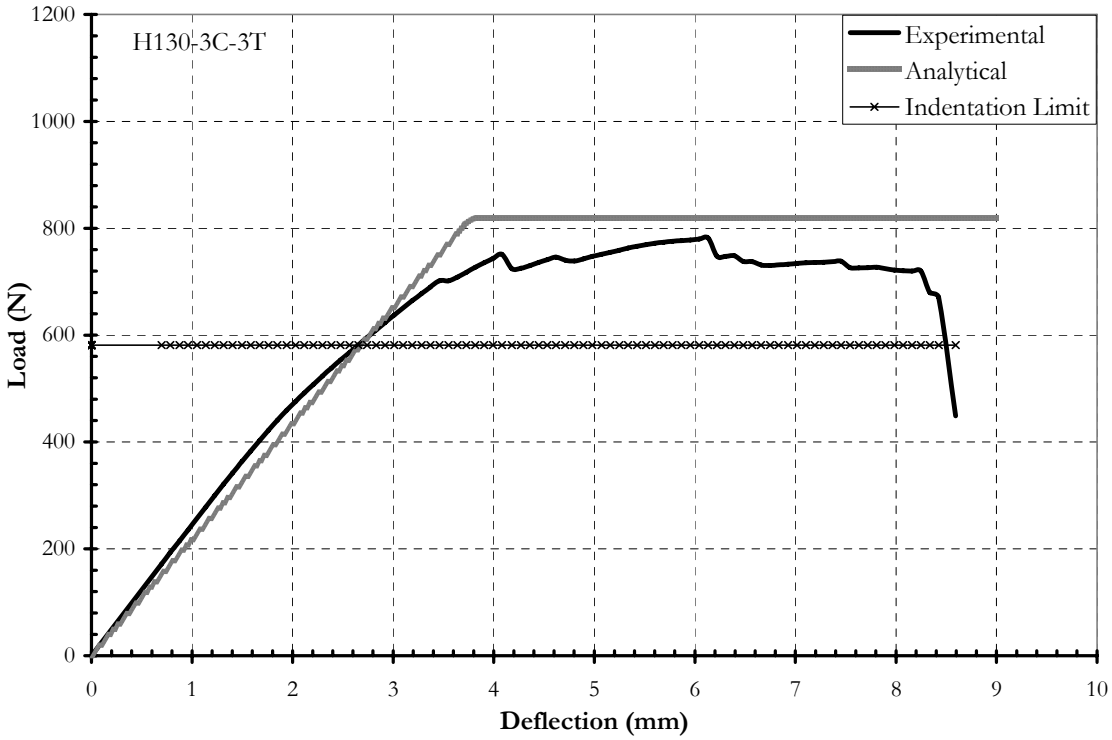

Figure 4.31 Experimental vs. analytical for H130 3C-3T

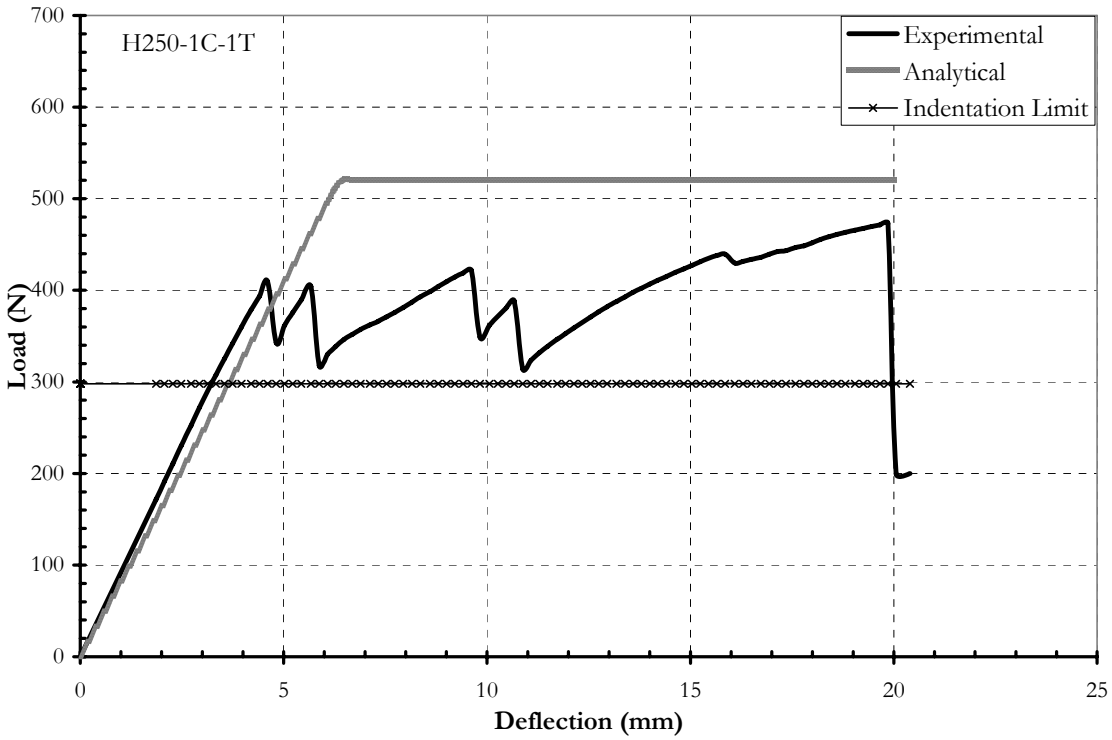

Figure 4.32 Experimental vs. analytical for H250 1C-1T

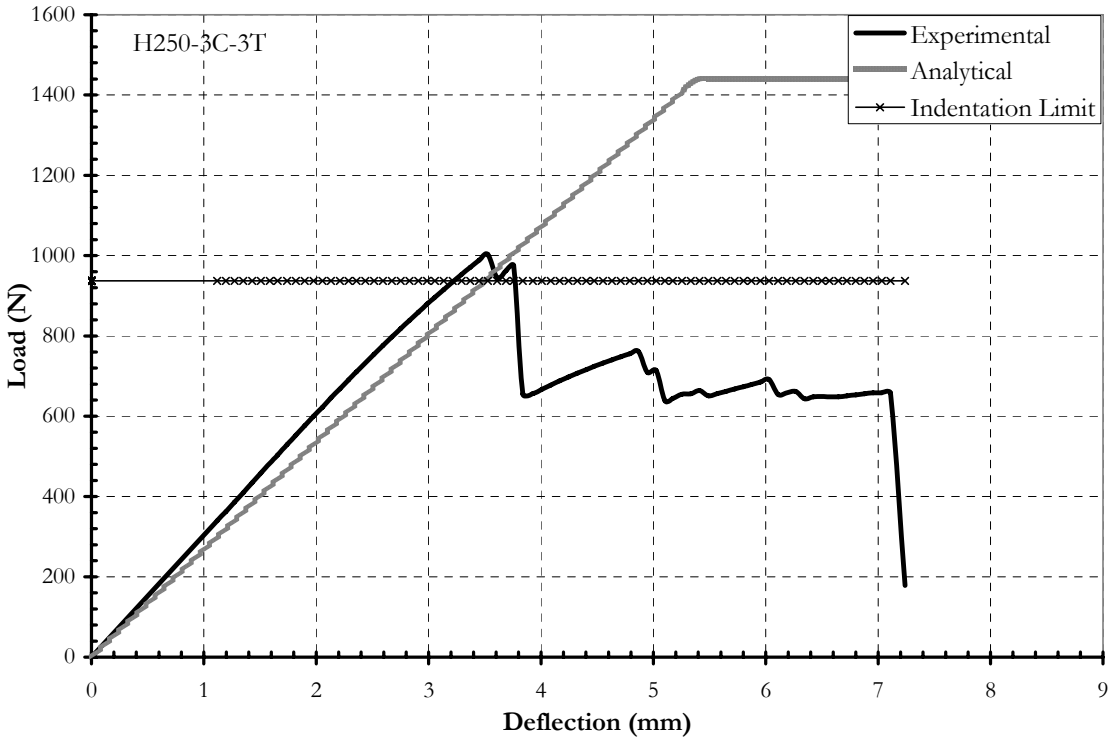

Figure 4.33 Experimental vs. analytical for H250 3C-3T

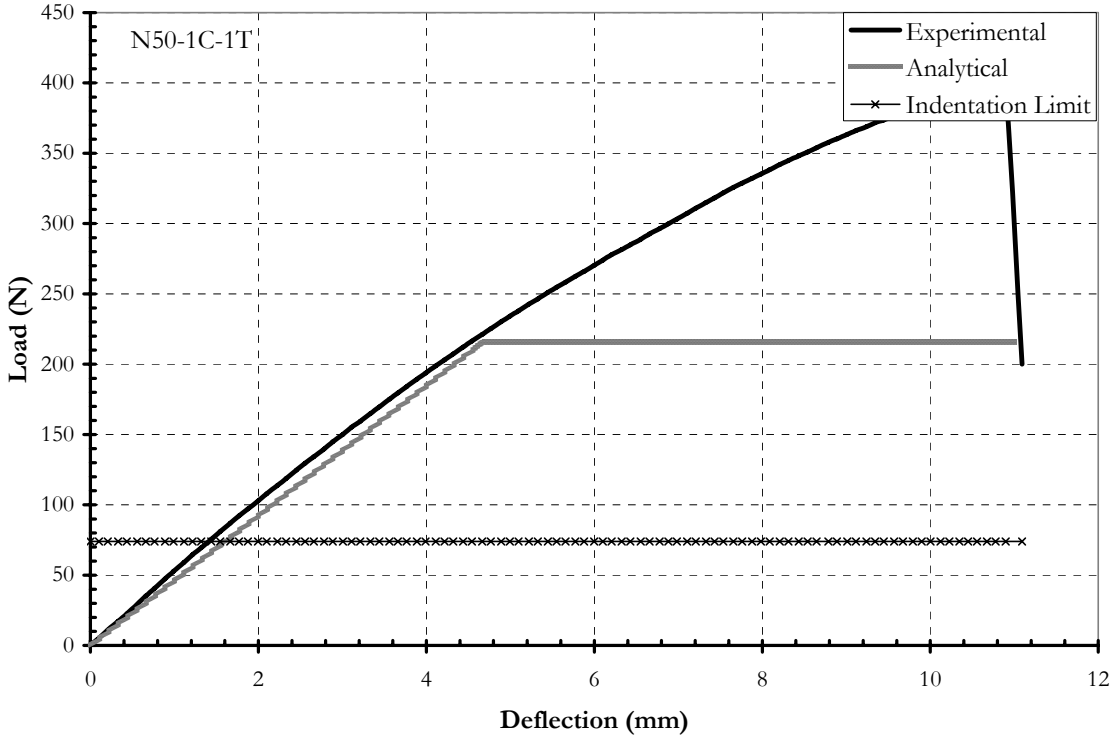

Figure 4.34 Experimental vs. analytical for N50 1C-1T

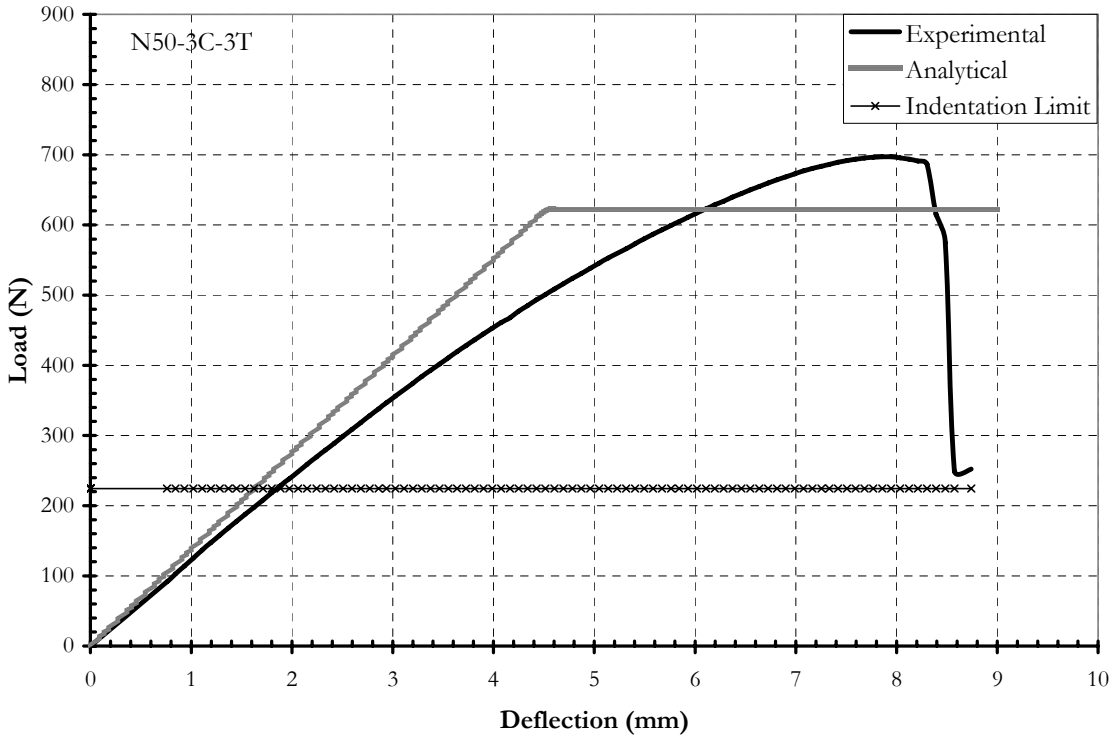

Figure 4.35 Experimental vs. analytical for N50 3C-3T

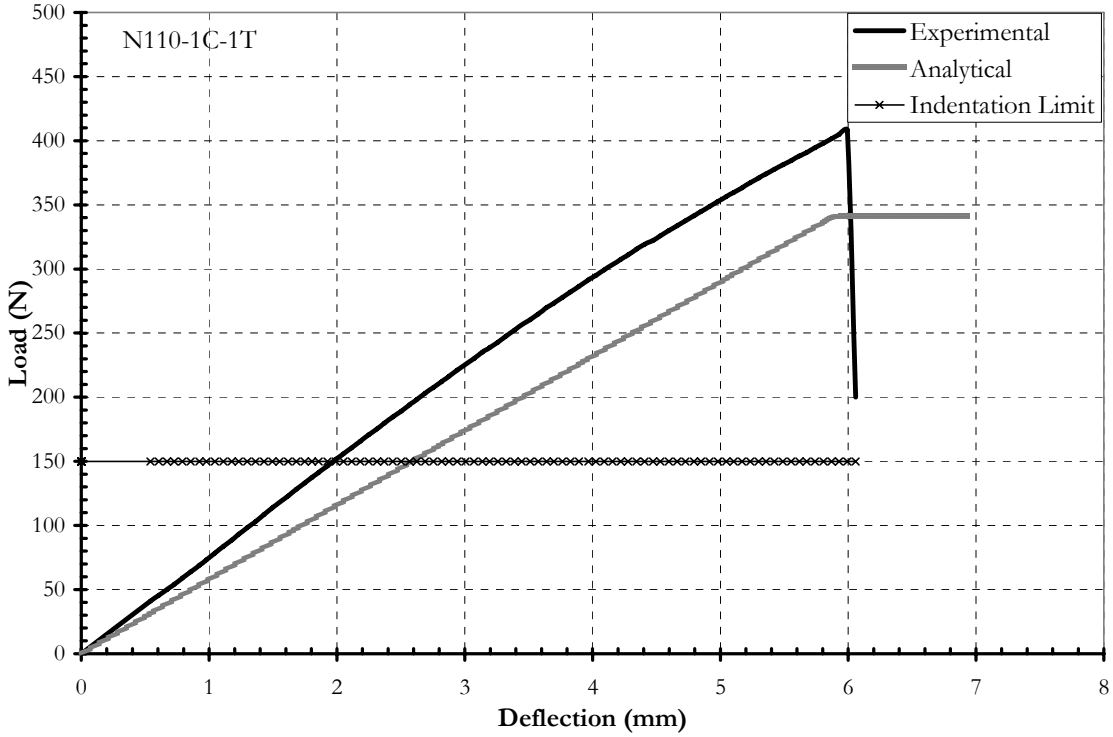

Figure 4.36 Experimental vs. analytical for N110 1C-1T

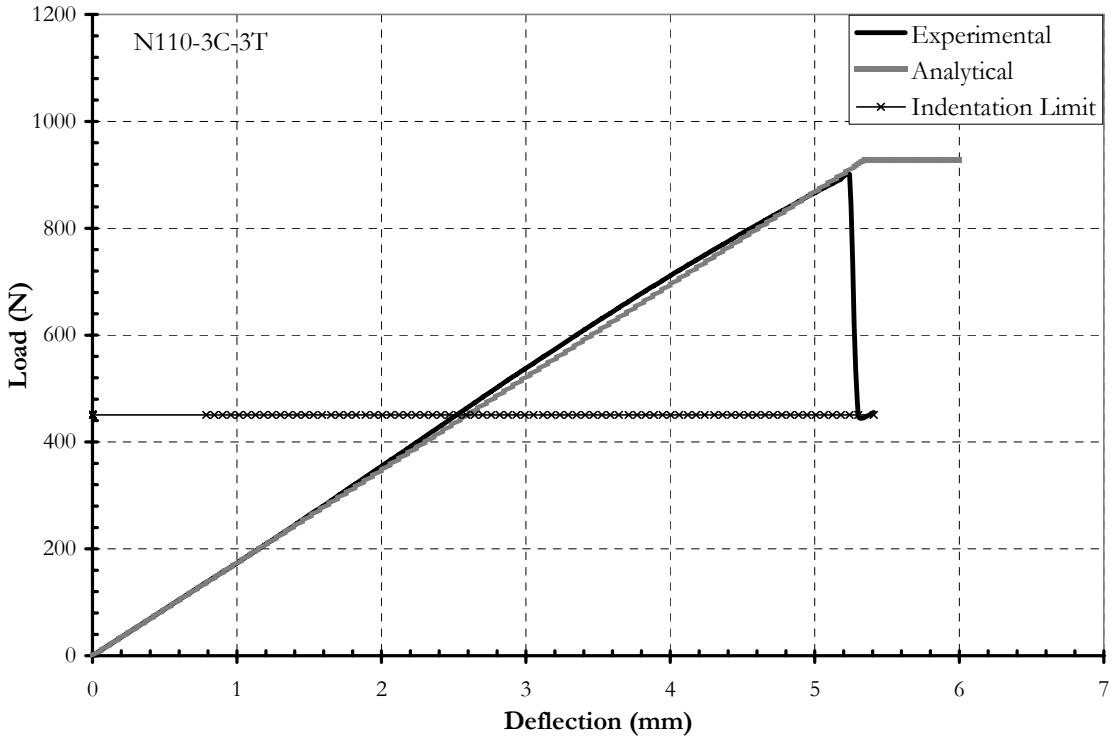

Figure 4.37 Experimental vs. analytical for N110 3C-3T

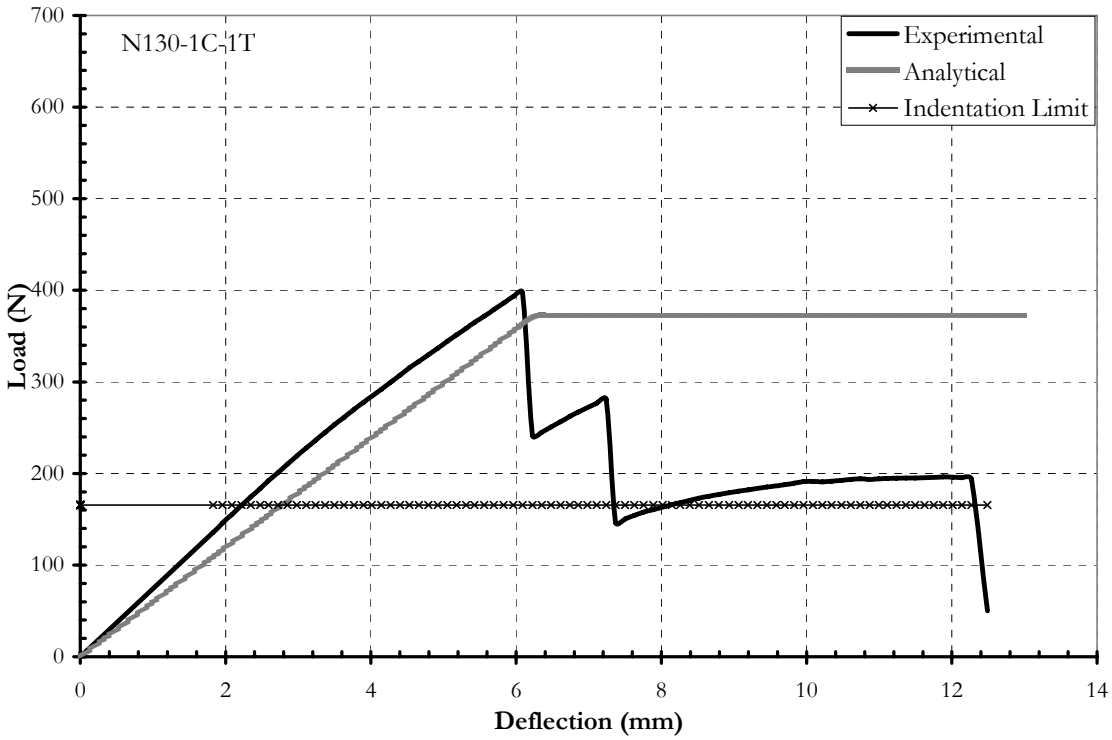

Figure 4.38 Experimental vs. analytical for N130 1C-1T

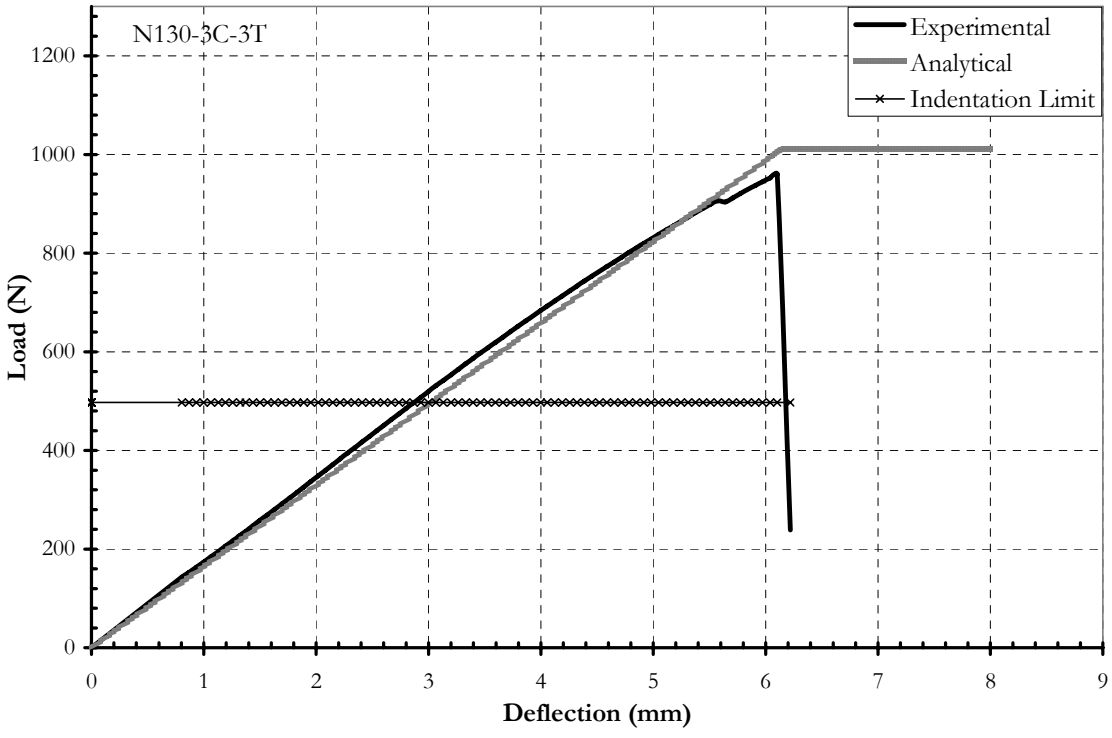

Figure 4.39 Experimental vs. analytical for N130 3C-3T

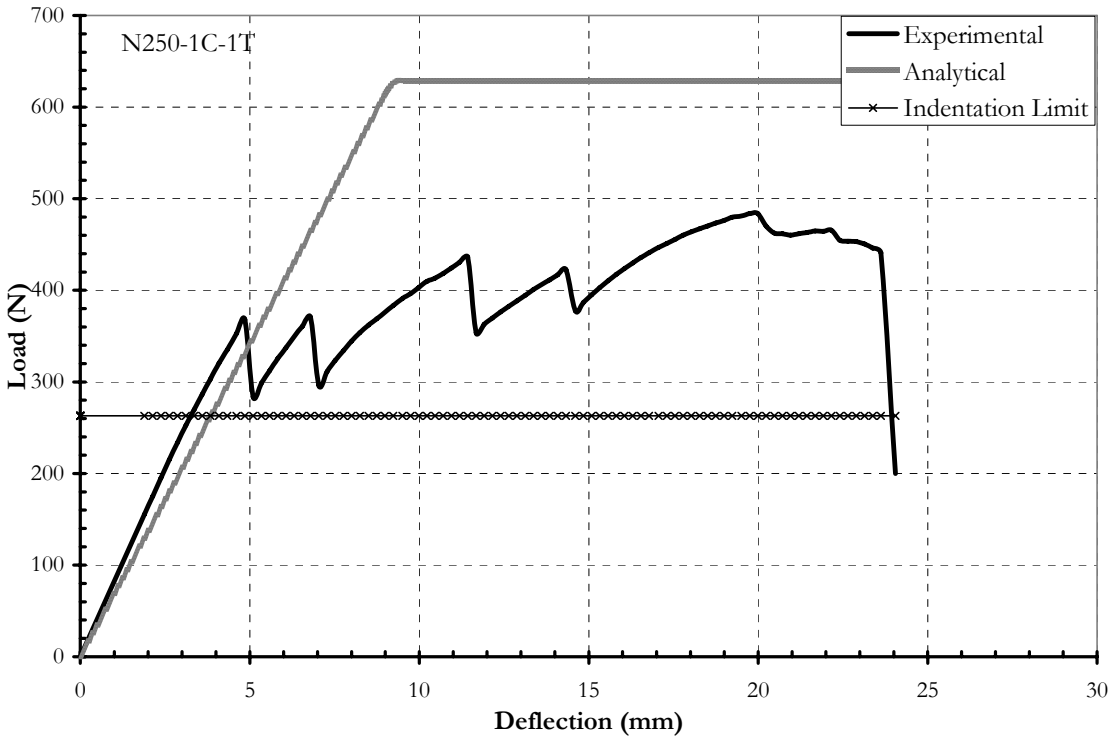

Figure 4.40 Experimental vs. analytical for N250 1C-1T

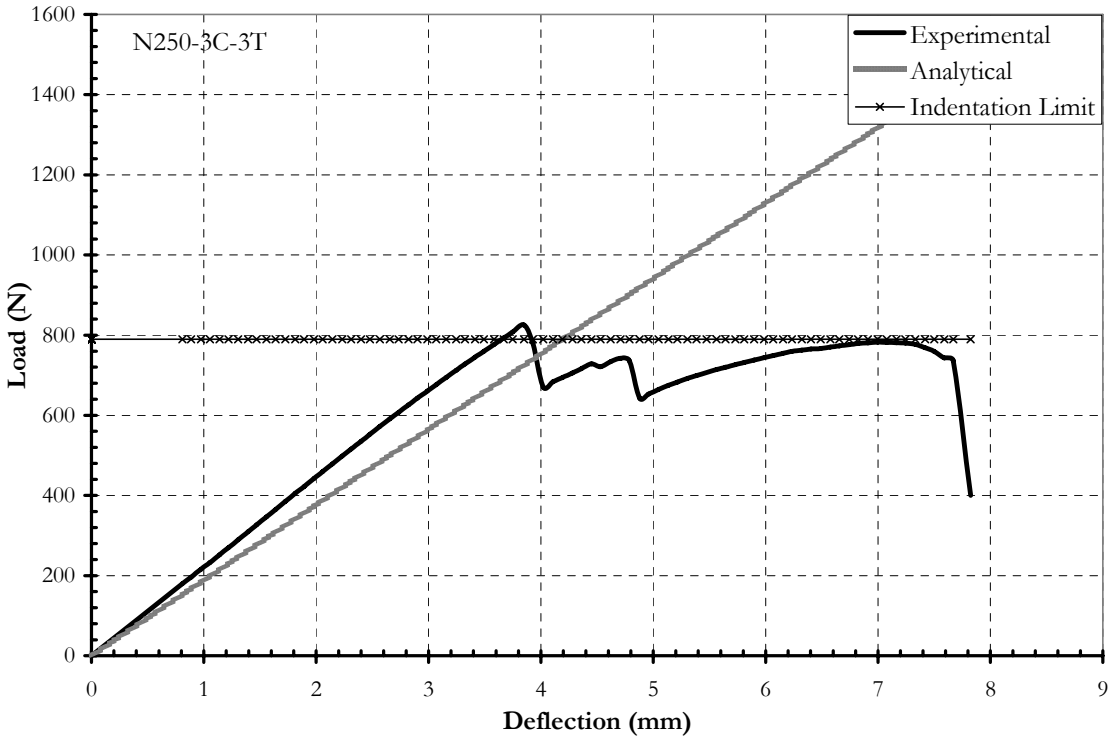

Figure 4.41 Experimental vs. analytical for N250 3C-3T

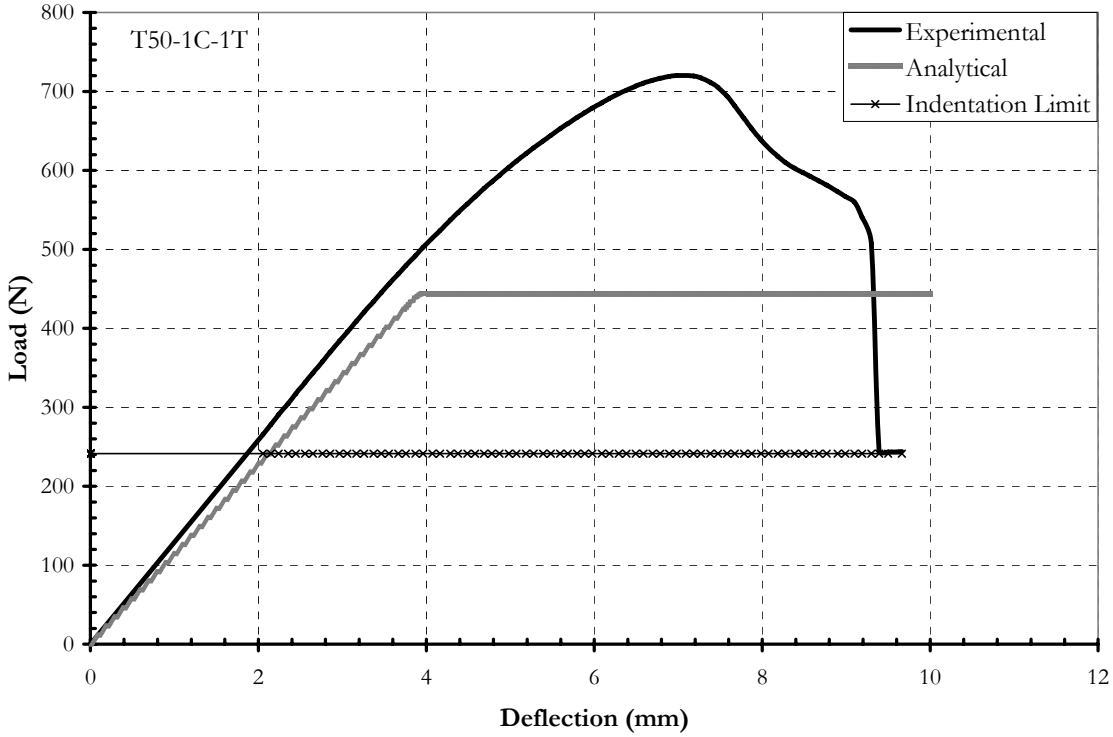

Figure 4.42 Experimental vs. analytical for T50 1C-1T

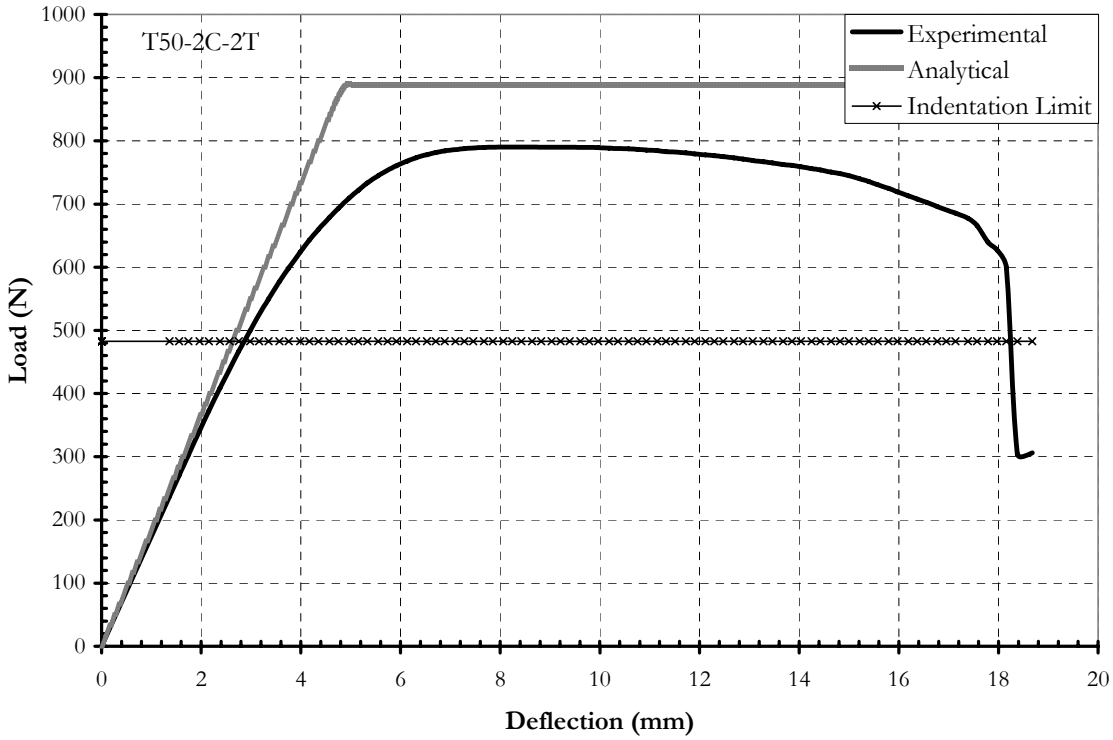

Figure 4.43 Experimental vs. analytical for T50 2C-2T

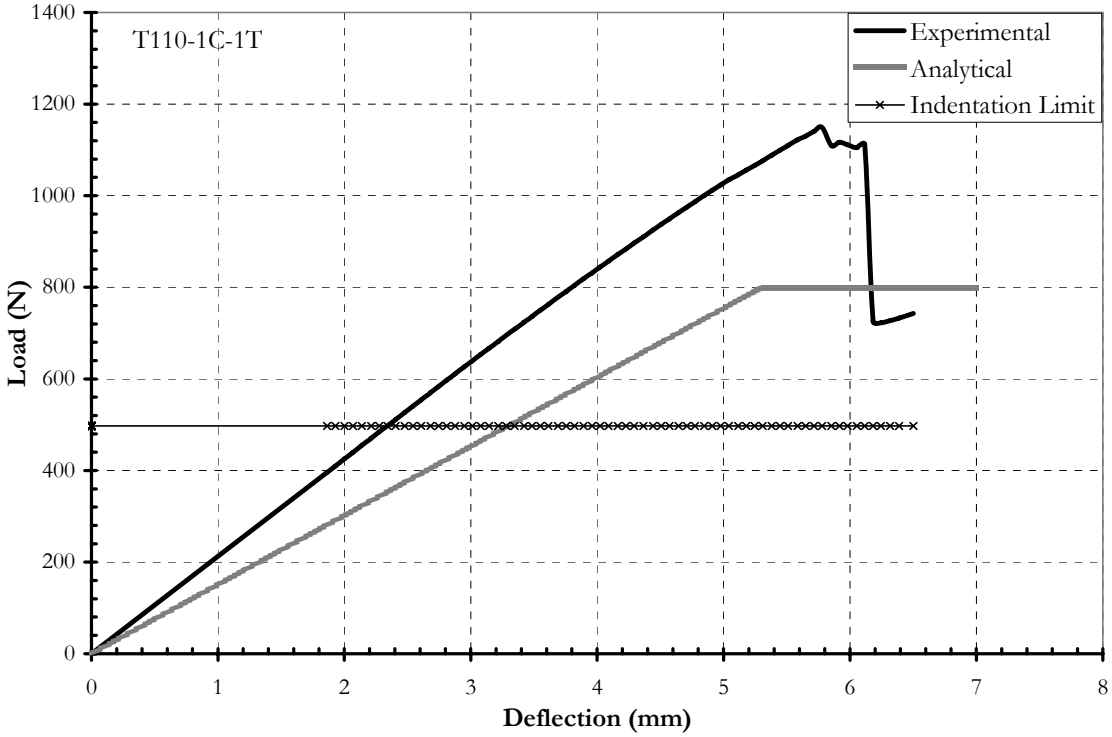

Figure 4.44 Experimental vs. analytical for T110 1C-1T

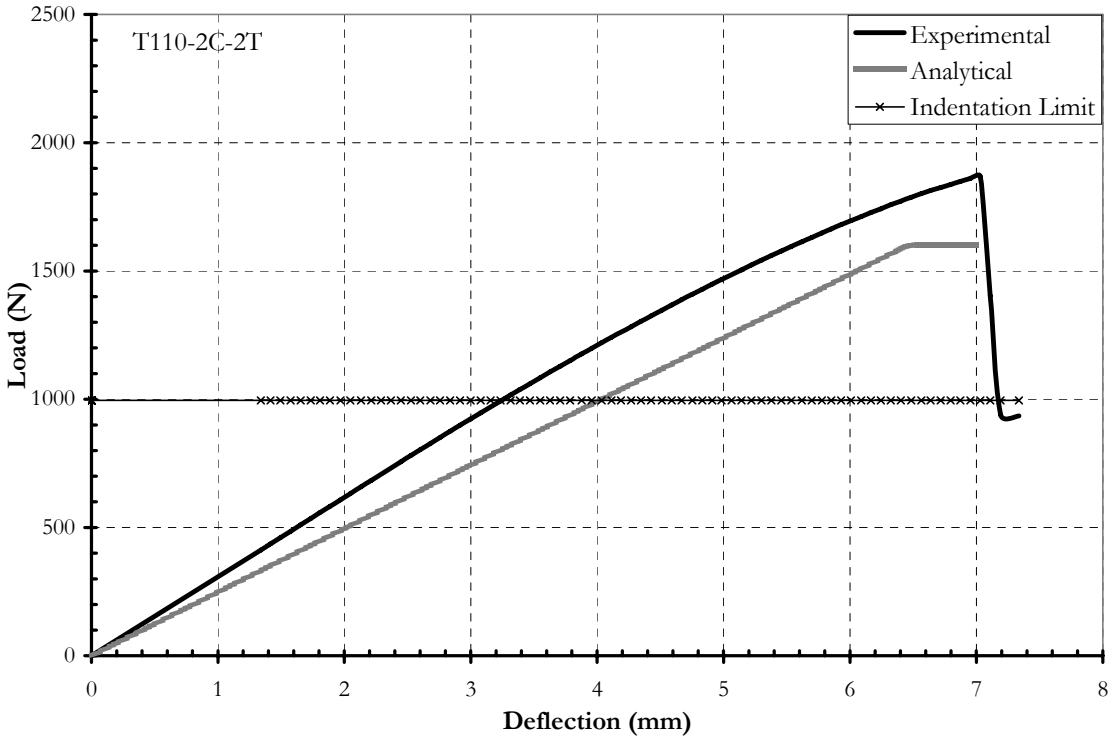

Figure 4.45 Experimental vs. analytical for T110 2C-2T

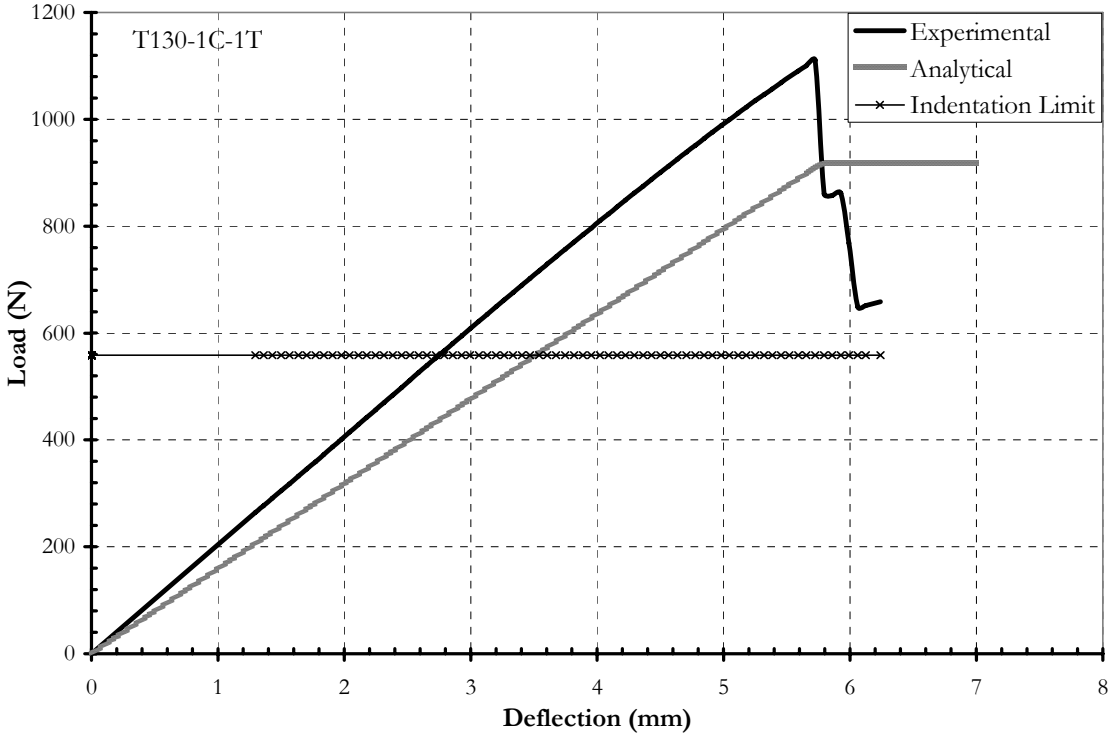

Figure 4.46 Experimental vs. analytical for T130 1C-1T

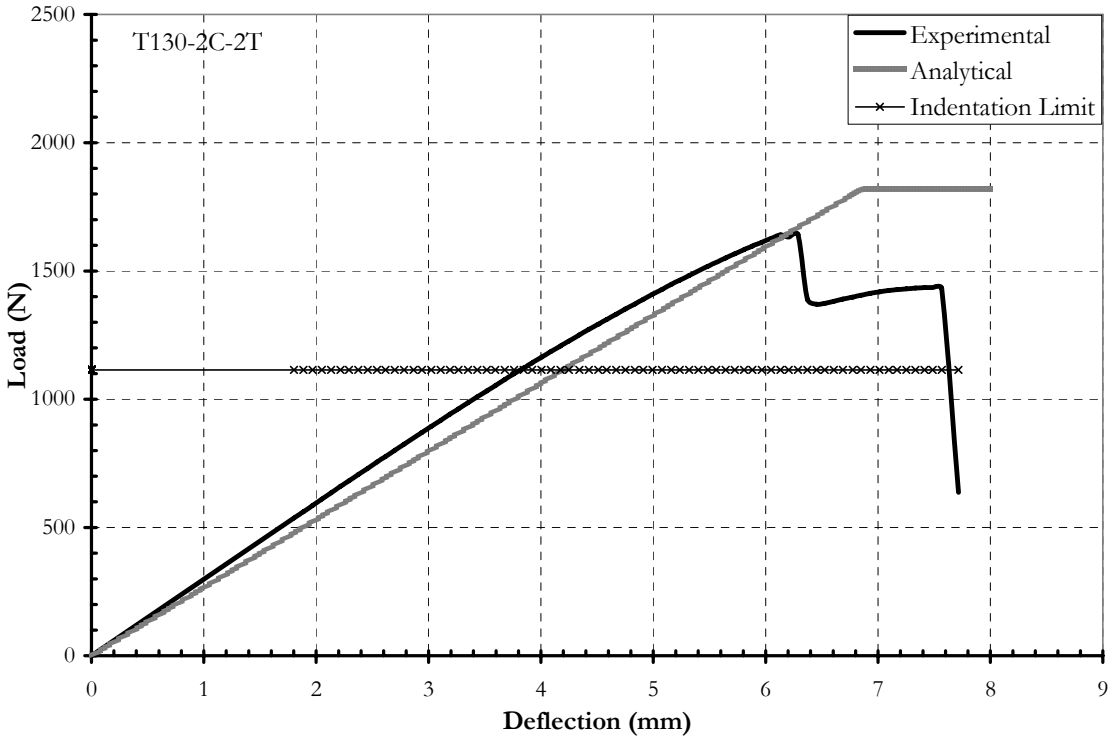

Figure 4.47 Experimental vs. analytical for T130 2C-2T

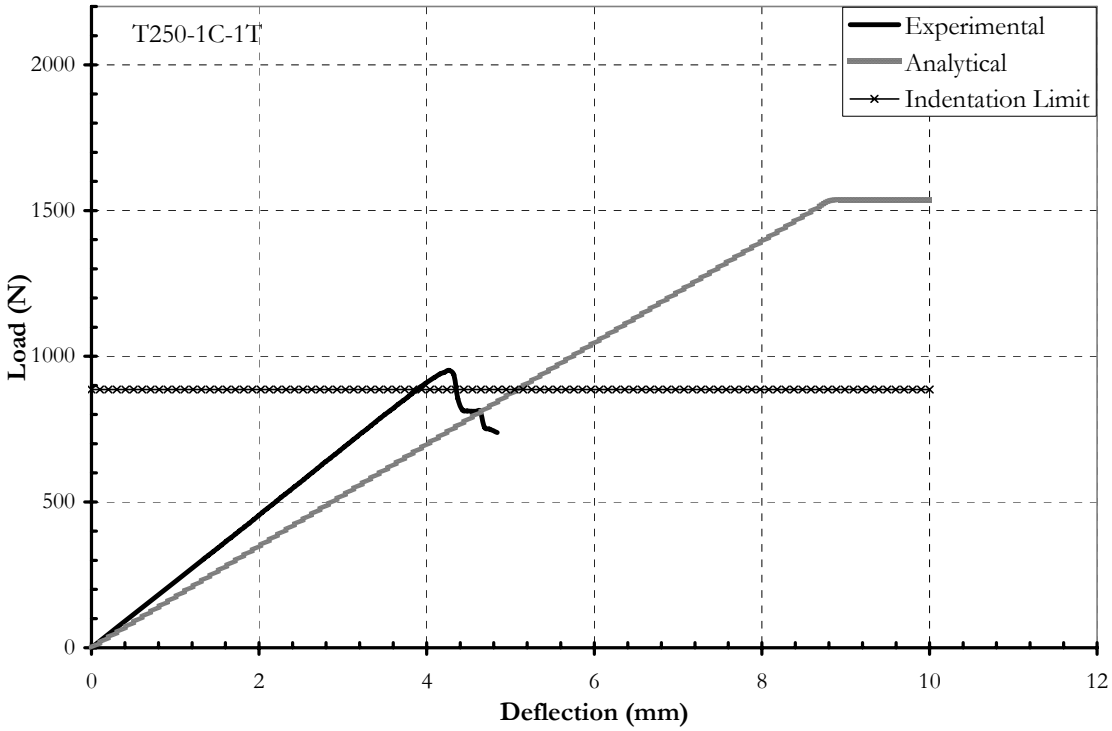

Figure 4.48 Experimental vs. analytical for T250 1C-1T

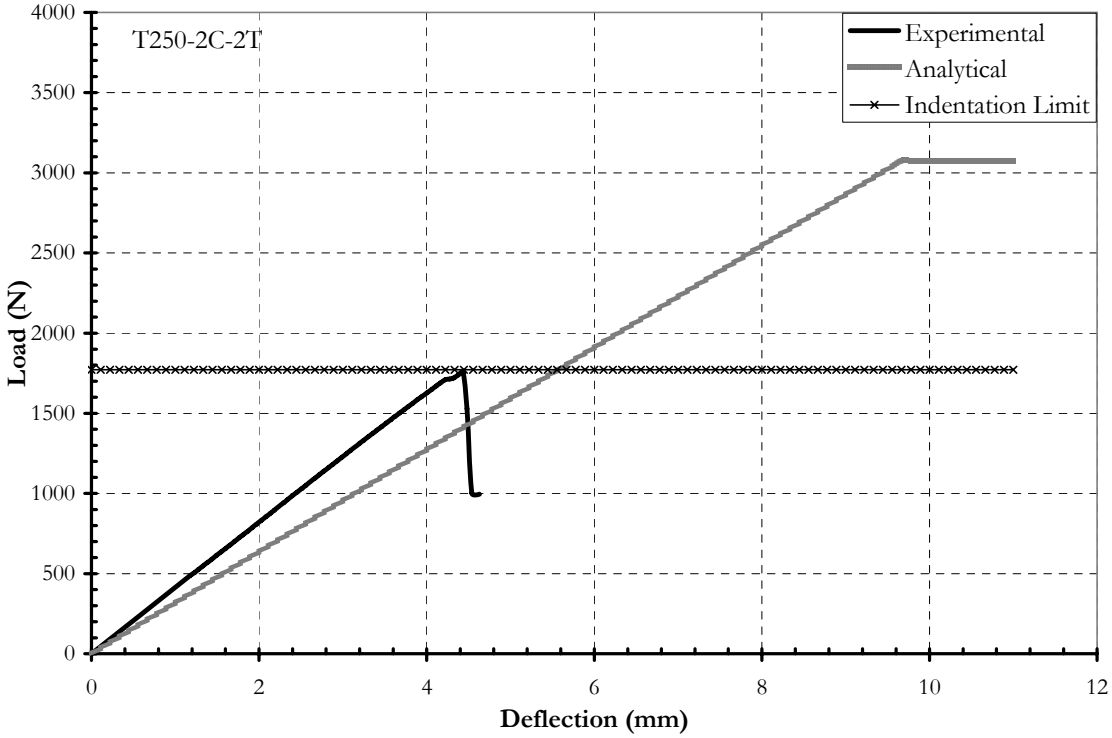

Figure 4.49 Experimental vs. analytical for T250 2C-2T

Chapter 5

Methodology for Design Guidelines for Weight Optimization of Sandwich Beams

5.1 Introduction

The applications of sandwich structures vary from common construction application to complex aerospace application. In aerospace and naval applications self weight of the structure is a critical parameter. In the construction industry, higher weights lead to higher cost. In the aerospace and marine application, higher weights lead to higher cost and less transportation capacity of the airplanes and vessels.

Therefore, there is a need for optimization methods in sandwich beams to minimize the weight for a given stiffness or strength or combination of stiffness and strength. Studies to find the minimum weight design of sandwich beams composed of rigid polyurethane foam and aluminum skin for a given strength are available in the literature (Triantafillou et al., 1987; Lingard, 1993). These methods are based on three modes of failure namely: face yielding, face wrinkling, and core shearing. For a given beam cross section, failure load maps were plotted between the density of the foamed core to the density of the unfoamed solid material on the vertical axes and the ratio between the skin thickness to the span length. Assuming failure by face yielding and core shearing or face wrinkling and core shearing simultaneously, the optimum dimensions could be found then they were analyzed to verify that it corresponded to the assumed failure mode (Triantafillou et al., 1987). A method of maximizing stiffness per unit weight in sandwich beams having rigid core made of polyurethane foam and ductile aluminum skins was introduced by Gibson (Gibson, 1984).

Using second order functions to describe the core moduli in terms of the density, the weight of a sandwich beam with known span, width and loading conditions, was minimized to find the optimum core density, core thickness and skin thickness. The weight of the beam was calculated in terms of the skin and core thickness then partial derivatives were taken with respect to the skin and core thickness. Using the determinant of the Hessian matrix, the global optimum values were found. Relationship between minimum weight and bending stiffness was developed for a given span and beam width. The sandwich beams were made of polyurethane core and aluminum skins (Gibson, 1984). GRP laminate/PVC foam sandwich beams were tested in three and four points bending by Lingard. Optimization of weight for a given strength was estimated by considering a wrinkling and core shear failure to occur simultaneously, giving core and skin thickness for known material properties and loading conditions. On the other hand, optimization of beams for a given stiffness was attempted by calculating the beam total weight and eliminating the skin thickness from the equation then taking the partial derivative with respect to the core thickness (Lingard, 1993).

5.2 Scope of present study

The method presented in this chapter is based on the approach of Lingard [1993]. The primary aim is to minimize the weight for a given stiffness. The core used in this study is flexible as compared to the rigid polyurethane core used by Triantafillou, 1987 and by Gibson, 1984. The studies conducted by Triantafillou and Gibson sought an optimum value for the core density while for PVC the density is limited to the availability of products in the market. The previous studies only considered laminate skins and introduced methods to estimate the skin thickness while the skin used in this study consisted of high modulus carbon tows and carbon tapes. Therefore, the total area of the skin and its effective width

were used for the computations. All the possible failure modes: tension fracture in the carbon skin, core shearing, wrinkling failure and the indentation limit for beams with concentrated loads, were considered to obtain the maximum moment capacity.

The aim of the present work is to develop an analytical method for optimization of PVC/inorganic composites. A methodology for guidelines is provided for choosing from different alternatives and combinations of different core densities and different carbon systems.

5.3 Optimization for stiffness

For sandwich beams, the flexural rigidity can be expressed in terms of

$$D = 2E_f A_f \left(\frac{d}{2}\right)^2 + E_c \frac{b_c c^3}{12} \tag{5.1}$$

After neglecting the second term as its contribution is minimal

$$D = E_f A_f \frac{d^2}{2} \tag{5.2}$$

The Shear rigidity for thin facings $t << c$ and $d \cong c$

$$N = G_c bc \tag{5.3}$$

The total weight of the sandwich beams

$$W = W_f + W_c = \left[2\rho_f A_f + \rho_c b_c c\right] L \tag{5.4}$$

The total deflection is the sum of deflection due to shear Δ_s and deflection due to bending moment Δ_b

$$\Delta = \Delta_b + \Delta_s = \frac{APL^3}{D} + \frac{BPL}{N} \tag{5.5}$$

Where *A* and *B* are constants that depend on the loading and the support conditions. A and B are 11/768 and 1/8, respectively for quarter span four point bending.

Then the stiffness could be expressed as

$$k = \frac{P}{\Delta} = \frac{E_f A_f \left(d^2/2\right) G_c bc}{AG_c bcL^3 + BE_f A_f \left(d^2/2\right) L} \tag{5.6}$$

For carbon tows $t/d << 1$ then it is fair to assume that $d = c$ and solve for A_f

$$A_f = \frac{1}{E_f}\left(\frac{2AG_c bL^3 k}{G_c c^2 b - BcLk}\right) \tag{5.7}$$

By substituting back in equation(5.4), the weight can be expressed as

$$W = \frac{\rho_f}{E_f}\frac{4AG_c bL^4 k}{G_c c^2 b - BckL} + \rho_c b_c cL \tag{5.8}$$

5.3.1 Optimization for core thickness

For optimizing the weight with respect to the thickness, the thickness has to satisfy the equation

$$\frac{\delta W}{\delta c} = 0 \tag{5.9}$$

By setting,

$$\phi = 4\rho_f AG_c bL^4 k$$

$$\zeta = BkLE_f$$

$$\psi = G_c bE_f$$

$$\theta = \rho_c b_c L$$

Equation (5.8) can be written as

$$W = \frac{\phi}{\psi c^2 - \zeta c} + \theta c \tag{5.10}$$

By combining equation (5.9) and(5.10), the thickness can be found by solving the following equation

$$\left(\theta\psi^2\right)c^4 - \left(2\theta\psi\zeta\right)c^3 + \left(\theta\zeta^2\right)c^2 - \left(2\psi\phi\right)c + \phi\zeta = 0 \tag{5.11}$$

If all the parameters are known, a simple computer program can give a graph between the stiffness and the core thickness. The flowchart to construct these graphs is shown in figure 5.1.

The solution of the previous equation gives four roots. Two roots are imaginary and two are real. The two real roots were tested by substituting the stiffness value and the corresponding core thickness into equation(5.7). It was found that one gives a negative area of fibers, which is not physically acceptable, and the other one was accepted as a solution for the equation.

The relation between area of fibers with the core thickness for different core densities and practical ranges of tow widths was plotted. It is shown that as the core becomes thicker, the effect of increasing the area of fibers diminishes.

Several graphs were developed for the minimum required thickness and the stiffness. Because the core density is not a continuous function, different graphs were required for each core density.

5.4 Design graphs

Design charts similar to figures 5.2 to 5.25 can be plotted using the flowchart shown in figure 5.1. The design charts role is to facilitate the design procedure and to help the designer to accomplish the design in an efficient way. It should be noted that these graphs were developed for a span length of 305 mm and quarter span four-point loading. Similar

graphs can be constructed using the methodology presented in chapter 4 and the flowchart shown in figure 5.1.

Two graphs can be plotted for each core and reinforcement combination. The first graph is between the stiffness and the core thickness and it is developed using equation (5.11). This graph is similar to the evenly numbered figures 5.2 to 5.24. The second graph is between the core thickness and the area of fibers. This graph is developed by substituting the stiffness and the optimum thickness in equation (5.7) to obtain the corresponding optimum area of fibers. This graph is similar to the oddly numbered figures 5.3 to 5.25.

5.5 Design procedure

The constraints in the design are strength, serviceability, and geometric constraint. The structure has to provide a required level of strength to resist the applying loads and to transfer them safely. It must have a certain level of stiffness to prevent excessive deformation, which may cause some level of discomfort and/or damage of supported elements. Geometric constraints could be a factor, as limitations in terms of the maximum thickness can be an issue.

The design procedures presented here are intended to give minimum weight design for a given stiffness. The system used in this study is a discrete system based on the availability of foam densities. The density of the PVC is represented by four discrete points. The area of fibers depends on the area of a single tow or a single tape.

For a given stiffness and span, the design procedures are simple to follow using the design aids introduced in this chapter, and by following the flowchart shown in figure 5.26. First of all, the designer has to determine the materials to be used based on availability and economics. The design procedure is summarized in the following steps:

1. Based on the stiffness, the stiffness and core thickness for minimum weight design graphs or equation (5.11) can be used to calculate the optimum thickness (c).
2. Knowing the core thickness and the stiffness, the area of fibers and core thickness for minimum weight design graphs can be plotted or equation (5.7) can be directly used to calculate the optimum required area of fibers (A_f).
3. Knowing the area of one tow or tape (A_{1f} = 1.14 mm^2 and 4.77 mm^2 for carbon tows and tape, respectively), the number of tows or tapes (n) can be determined
4. With the thickness to span ratio, the maximum fiber stresses due to indentation effect graphs from chapter 4, figures 4.4 to 4.16, or equation (4.30) can be used to determine the stress level (σ_f) that can be used. If the loading contact is not a criteria equation (4.11) can be used to determine the wrinkling and with the fibers tensile strength is the upper stress limit.
5. The moment capacity of the cross section for the given configuration can be calculated as $M = c \times \sigma_f \times n \times A_{1f}$ and the shear capacity can be evaluated $V = \tau_{\max} \times b \times d$

5.6 Example of design alternatives for concentrated loads

The method represented here gives the optimum weight design for a given stiffness. Many alternatives are available, and it is the designer's role to decide on the different alternatives based on the availability of materials, economics, strength, and/or any geometrical constraints. For any given stiffness, there is twelve different design alternatives that can be found based on the systems introduced in this study.

As an example, if a beam with span of 305 mm is loaded in four-point flexural setup, the required stiffness is to be 600 N/mm. The different design alternatives are discussed below.

5.6.1 Alternative 1: PVC core with a density of 50 Kg/m^3 and H-12K HMC carbon tows

First assume the width of the tow as b=15mm. Then from figure 5.2, the thickness of the core can be found as c=85 mm.

Using the thickness from figure 5.3, the required area of fibers for the skin can be found $A_f = 2.5$ mm^2. By dividing the required area by the area for one tow, 3 tows should be used.

From equation 4.30, the maximum stress in fibers can be found as 59 MPa. The maximum moment capacity of the beam can be calculated, Maximum moment= 59 x 3 x 1.14 x 85/1000=17.15 N.m.

5.6.2 Alternative 2: PVC core with a density of 110 Kg/m^3 and H-12K HMC carbon tows

Again, let b=15mm, from figure 5.4, c=45mm

From figure 5.4, the required area of fibers $A_f = 5.2$ mm^2, 6 tows should be used.

From equation 4.30, maximum stress=183 MPa

Maximum moment= 183 x 6 x 1.14 x 45/1000=56.32 N.m

5.6.3 Alternative 3: PVC core with a density of 130 Kg/m^3 and H-12K HMC carbon tows

Assume b=15mm, from figure 5.6, c=35mm

From figure 5.4, the required area of fibers $A_f = 6.2$ mm^2, use 6 tows

From equation 4.30, maximum stress=243 MPa

Maximum moment= 243 x 6 x 1.14 x 35/1000=58.17 N.m

5.6.4 Alternative 4: PVC core with a density of 250 Kg/m^3 and H-12K HMC carbon tows

Let b=15mm, from figure 5.8, c=19mm

From figure 5.9, the required area of fibers A_f = 11.2 mm^2, use 10 tows

From equation 4.30, maximum stress=516 MPa

Maximum moment= 516 x 10 x 1.14 x 19/1000=111.77 N.m

5.6.5 Alternative 5: PVC core with a density of 50 Kg/m^3 and N-12K MMC carbon tows

Assume b=15mm, from figure 5.10, c=90mm

From figure 5.11, the required area of fibers A_f = 2.9 mm^2, use 3 tows

From equation 4.30, maximum stress= 49 MPa

Maximum moment= 49 x 3 x 1.14 x 90/1000=15.08 N.m

5.6.6 Alternative 6: PVC core with a density of 110 Kg/m^3 and N-12K MMC carbon tows

Assume b=15mm, from figure 5.12, c=44mm

From figure 5.13, the required area of fibers A_f = 5.8 mm^2, use 6 tows

From equation 4.30, maximum stress= 164 MPa

Maximum moment= 164 x 6 x 1.14 x 44/1000= 49.36 N.m

5.6.7 Alternative 7: PVC core with a density of 130 Kg/m^3 and N-12K MMC carbon tows

Assume b=15mm, from figure 5.14, c=35mm

From figure 5.15, the required area of fibers A_f = 7.0 mm^2, use 7 tows

From equation 4.30, maximum stress= 215 MPa

Maximum moment= 215 x 7 x 1.14 x 35/1000= 60.05 N.m

5.6.8 Alternative 8: PVC core with a density of 250 Kg/m^3 and N-12K MMC carbon tows

Assume b=15mm, from figure 5.16, c=20mm

From figure 5.17, the required area of fibers A_f = 12.4 mm^2, use 11 tows

From equation 4.30, maximum stress=441 MPa

Maximum moment= 441 x 11 x 1.14 x 20/1000= 110.6 N.m

5.6.9 Alternative 9: PVC core with a density of 50 Kg/m^3 and T-3K Uni C Tape

From figure 5.18, c=35mm

From figure 5.19, the required area of fibers A_f = 5.8 mm^2, use 2 tapes

From equation 4.30, maximum stress=74 MPa

Maximum moment= 74 x 2 x 4.77 x 35/1000= 24.71 N.m

5.6.10 Alternative 10: PVC core with a density of 110 Kg/m^3 and T-3K Uni C Tape

From figure 5.20, c=22mm

From figure 5.21, the required area of fibers A_f = 10.4 mm^2, use 3 tapes

From equation 4.30, maximum stress=211 MPa

Maximum moment= 211 x 3 x 4.77 x 22/1000= 66.43 N.m

5.6.11 Alternative 11: PVC core with a density of 130 Kg/m^3 and T-3K Uni C Tape

From figure 5.22, c=18mm

From figure 5.23, the required area of fibers A_f = 11.6 mm^2, use 3 tapes

From equation 4.30, maximum stress= 270.4 MPa

Maximum moment= 270.4 x 3 x 4.77 x 18/1000=69.65 N.m

5.6.12 Alternative 11: PVC core with a density of 250 Kg/m^3 and T-3K Uni C Tape

From figure 5.24, c=13mm

From figure 5.25, the required area of fibers $A_f = 18$ mm^2, use 4 tapes

From equation 4.30, maximum stress= 475 MPa

Maximum moment= 475 x 4 x 4.77 x 12/1000= 108.76 N.m

5.7 Example of design alternatives for non-contacting loads

Another example is discussed for a beam with span of 305 mm has no contact loading i.e. the indentation failure is not a design criteria, and the same stiffness of 600 N/mm is required. The different design alternatives are shown below.

5.7.1 Alternative 1: PVC core with a density of 50 Kg/m^3 and H-12K HMC carbon tows

First assume the width of the tow as b=15mm. Then from figure 5.2, the thickness of the core can be found as c=85 mm.

Using the thickness from figure 5.3, the required area of fibers for the skin can be found $A_f = 2.5$ mm^2. By dividing the required area by the area for one tow, 3 tows should be used.

From equation 4.11, the maximum stress in fibers can be found as 540 MPa. The maximum moment capacity of the beam can be calculated, Maximum moment= 540 x 3 x 1.14 x 85/1000=157 N.m.

5.7.2 Alternative 2: PVC core with a density of 110 Kg/m^3 and H-12K HMC carbon tows

Again, let b=15mm, from figure 5.4, c=45mm

From figure 5.4, the required area of fibers $A_f = 5.2$ mm^2, 6 tows should be used.

From equation 4.11, maximum stress=920 MPa

Maximum moment= 920 x 6 x 1.14 x 45/1000=285 N.m

5.7.3 Alternative 3: PVC core with a density of 130 Kg/m^3 and H-12K HMC carbon tows

Assume b=15mm, from figure 5.6, c=35mm

From figure 5.4, the required area of fibers A_f = 6.2 mm^2, use 6 tows

From equation 4.11, maximum stress=1000 MPa

Maximum moment= 243 x 6 x 1.14 x 35/1000=239 N.m

5.7.4 Alternative 4: PVC core with a density of 250 Kg/m^3 and H-12K HMC carbon tows

Let b=15mm, from figure 5.8, c=19mm

From figure 5.9, the required area of fibers A_f = 11.2 mm^2, use 10 tows

From equation 4.11, maximum stress=1680 MPa

Maximum moment= 1680 x 10 x 1.14 x 19/1000=363.9 N.m

5.7.5 Alternative 5: PVC core with a density of 50 Kg/m^3 and N-12K MMC carbon tows

Assume b=15mm, from figure 5.10, c=90mm

From figure 5.11, the required area of fibers A_f = 2.9 mm^2, use 3 tows

From equation 4.11, maximum stress= 580 MPa

Maximum moment= 580 x 3 x 1.14 x 90/1000=178.5 N.m

5.7.6 Alternative 6: PVC core with a density of 110 Kg/m^3 and N-12K MMC carbon tows

Assume b=15mm, from figure 5.12, c=44mm

From figure 5.13, the required area of fibers A_f = 5.8 mm^2, use 6 tows

From equation 4.11, maximum stress= 920 MPa

Maximum moment= 920 x 6 x 1.14 x 44/1000= 277 N.m

5.7.7 Alternative 7: PVC core with a density of 130 Kg/m^3 and N-12K MMC carbon tows

Assume b=15mm, from figure 5.14, c=35mm

From figure 5.15, the required area of fibers A_f = 7.0 mm^2, use 7 tows

From equation 4.11, maximum stress= 1080 MPa

Maximum moment= 1080 x 7 x 1.14 x 35/1000= 301.6 N.m

5.7.8 Alternative 8: PVC core with a density of 250 Kg/m^3 and N-12K MMC carbon tows

Assume b=15mm, from figure 5.16, c=20mm

From figure 5.17, the required area of fibers A_f = 12.4 mm^2, use 11 tows

From equation 4.11, maximum stress=1800 MPa

Maximum moment= 1800 x 11 x 1.14 x 20/1000= 451.4 N.m

5.7.9 Alternative 9: PVC core with a density of 50 Kg/m^3 and T-3K Uni C Tape

From figure 5.18, c=35mm

From figure 5.19, the required area of fibers A_f = 5.8 mm^2, use 2 tapes

From equation 4.11, maximum stress=340 MPa

Maximum moment= 340 x 2 x 4.77 x 35/1000= 113.5 N.m

5.7.10 Alternative 10: PVC core with a density of 110 Kg/m^3 and T-3K Uni C Tape

From figure 5.20, c=22mm

From figure 5.21, the required area of fibers A_f = 10.4 mm^2, use 3 tapes

From equation 4.11, maximum stress=550 MPa

Maximum moment= 550 x 3 x 4.77 x 22/1000= 173.16 N.m

5.7.11 Alternative 11: PVC core with a density of 130 Kg/m^3 and T-3K Uni C Tape

From figure 5.22, c=18mm

From figure 5.23, the required area of fibers A_f = 11.6 mm^2, use 3 tapes

From equation 4.11, maximum stress= 625 MPa

Maximum moment= 625 x 3 x 4.77 x 18/1000=161 N.m

5.7.12 Alternative 11: PVC core with a density of 250 Kg/m^3 and T-3K Uni C Tape

From figure 5.24, c=13mm

From figure 5.25, the required area of fibers A_f = 18 mm^2, use 4 tapes

From equation 4.11, maximum stress= 1140 MPa

Maximum moment= 1140 x 4 x 4.77 x 12/1000= 261 N.m

5.8 Discussion

The first example shows the different design alternatives with accounting for the indentation stresses. The second example does not consider the indentation as a failure mode. The capacities are 2.4 to 11.8 folds the capacities when the indentation is considered. This effect is more significant with cores having low density. Economically, it is more recommended to provide the additional reinforcement in the area subjected to the local crushing due to the indentation i.e. under the concentrated load and its vicinity. The additional reinforcement area can be estimated as the lesser of the ratio between the fibers tensile strength to the maximum attainable stress ($\sigma_{f\max}/\sigma_f$) and the ratio of the wrinkling stress to the maximum attainable stress (σ_w/σ_f). It is the designer's choice to provide additional reinforcement or to account for the drop in the stresses due to the concentrated load effect. Factors like the

span, whether the load is static or moving, loading arrangement and fabrication cost can control the designer's choice.

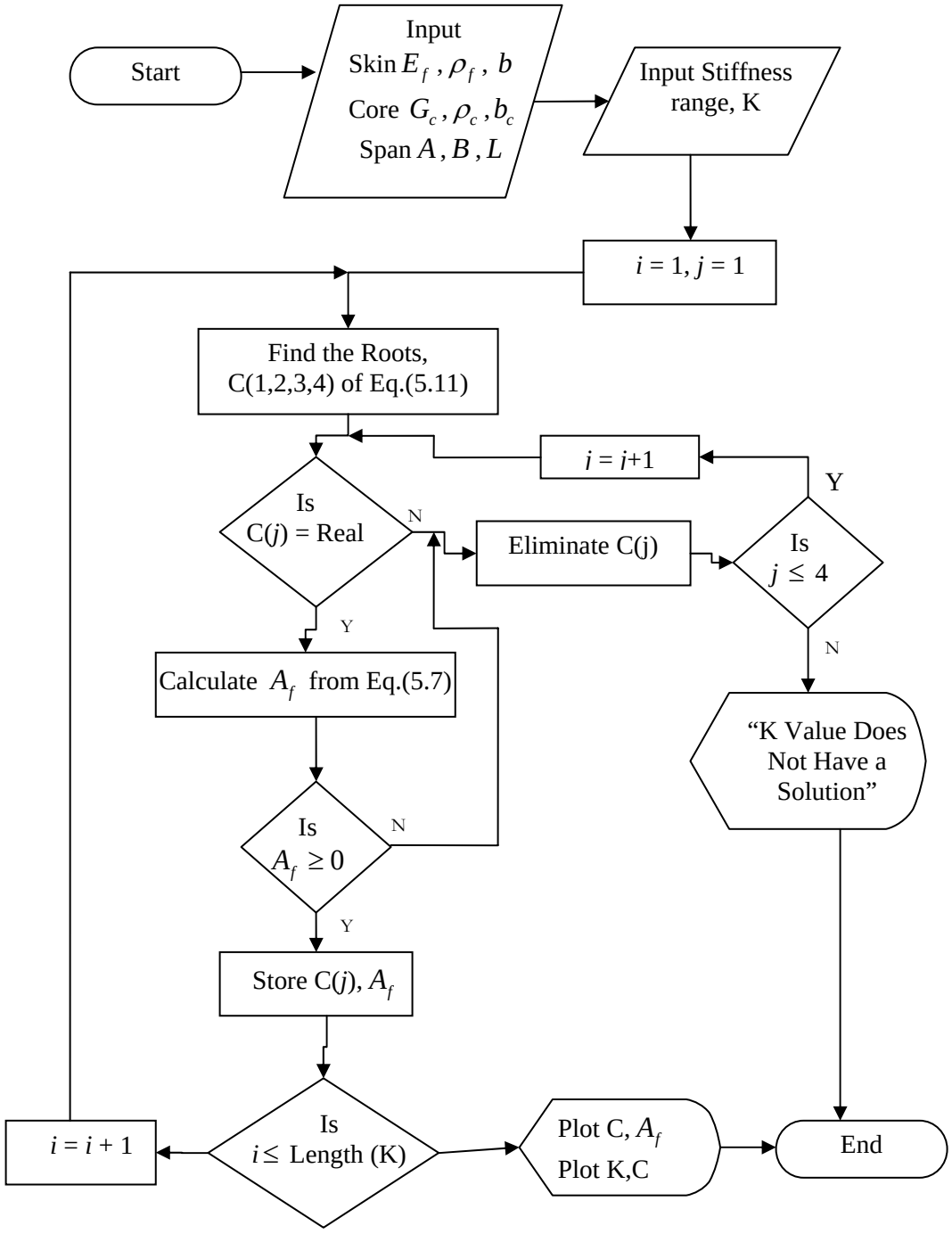

Figure 5.1 Flowchart to plot the design charts

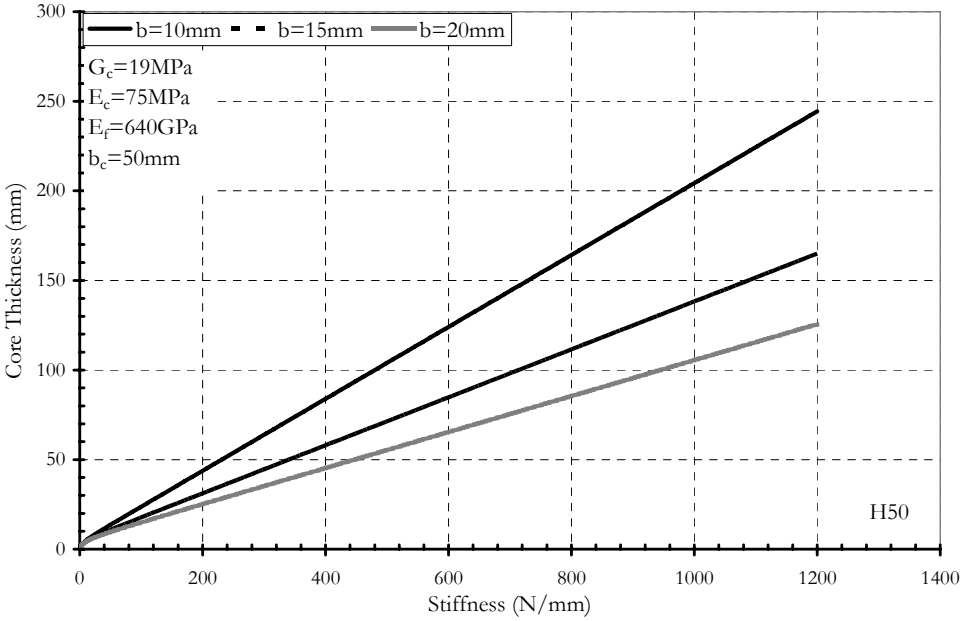

Figure 5.2 Stiffness and Core Thickness for minimum weight design for PVC 50 Kg/m^3 Core reinforced with H-12K HMC

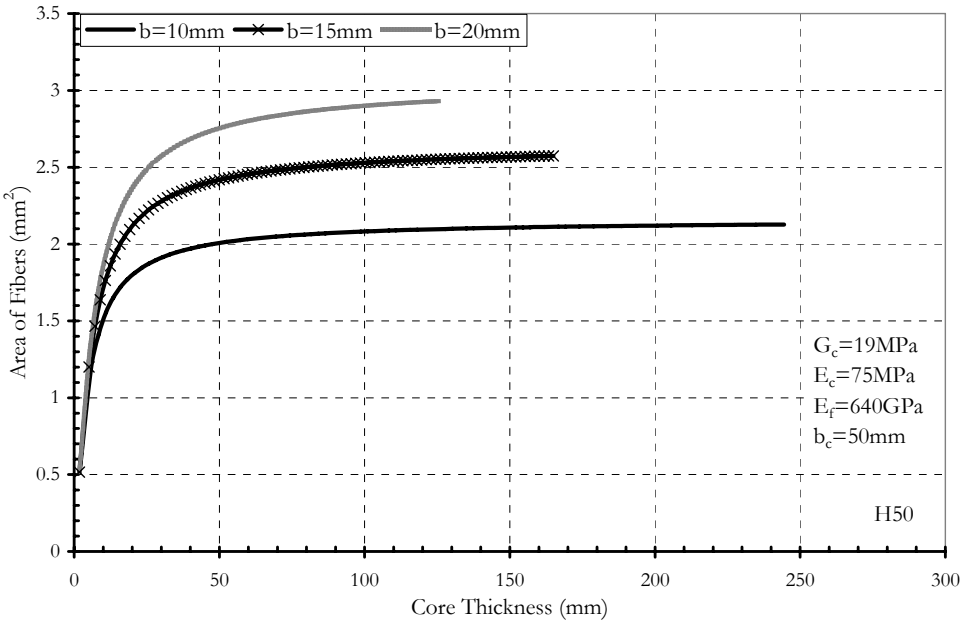

Figure 5.3 Area of fibers and Core Thickness for minimum weight design for PVC 50 Kg/m^3 Core reinforced with H-12K HMC

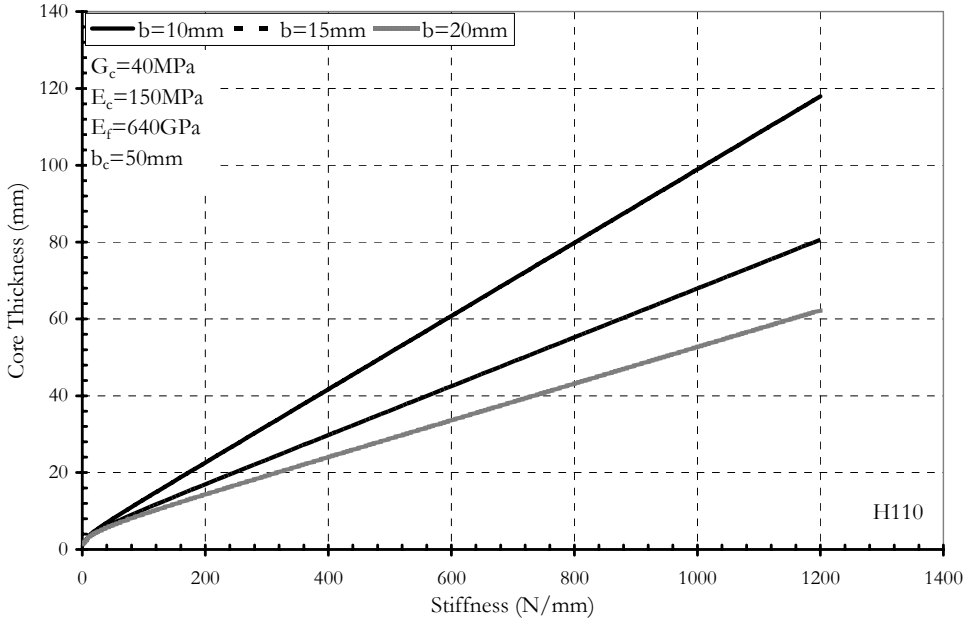

Figure 5.4 Stiffness and Core Thickness for minimum weight design for PVC 110 Kg/m^3 Core reinforced with H-12K HMC

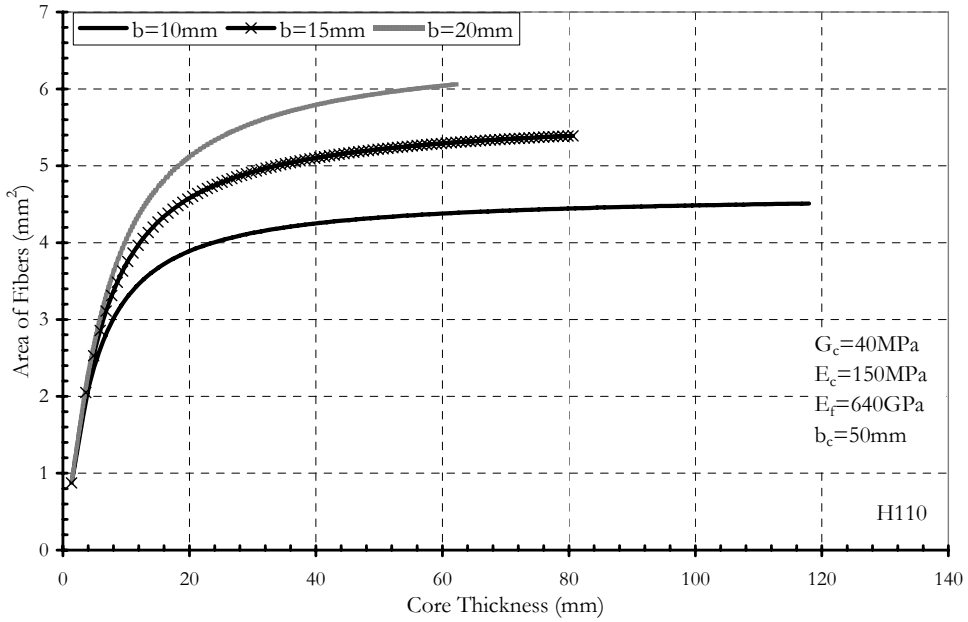

Figure 5.5 Area of fibers and Core Thickness for minimum weight design for PVC 110 Kg/m^3 Core reinforced with H-12K HMC

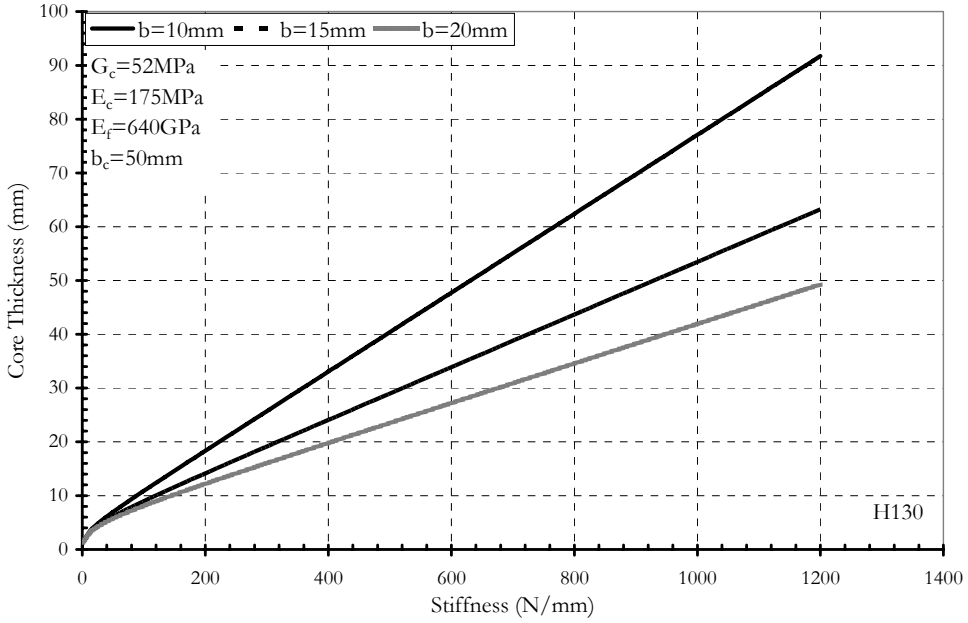

Figure 5.6 Stiffness and Core Thickness for minimum weight design for PVC 130 Kg/m^3 Core reinforced with H-12K HMC

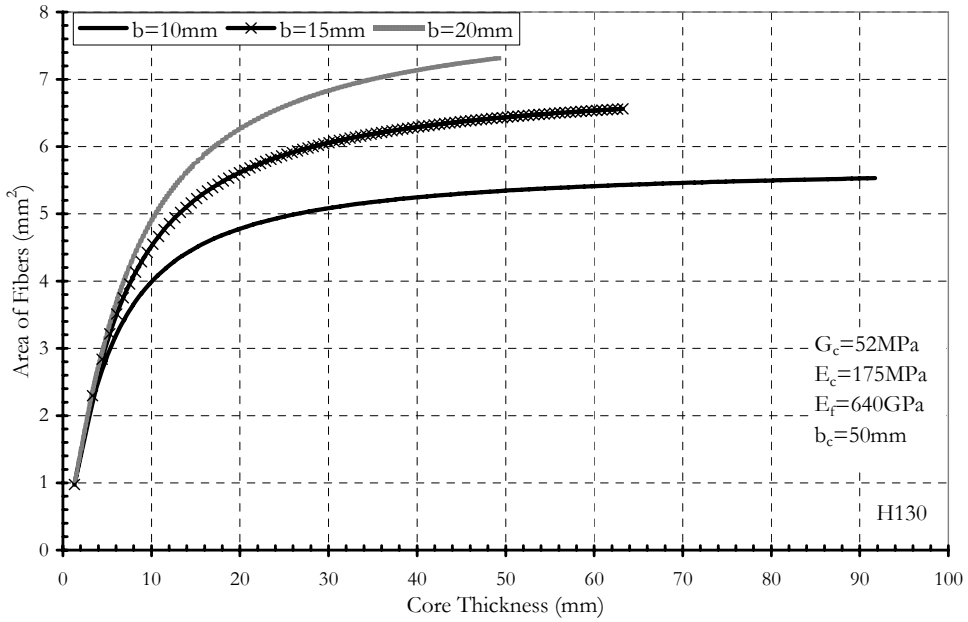

Figure 5.7 Area of fibers and Core Thickness for minimum weight design for PVC 130 Kg/m^3 Core reinforced with H-12K HMC

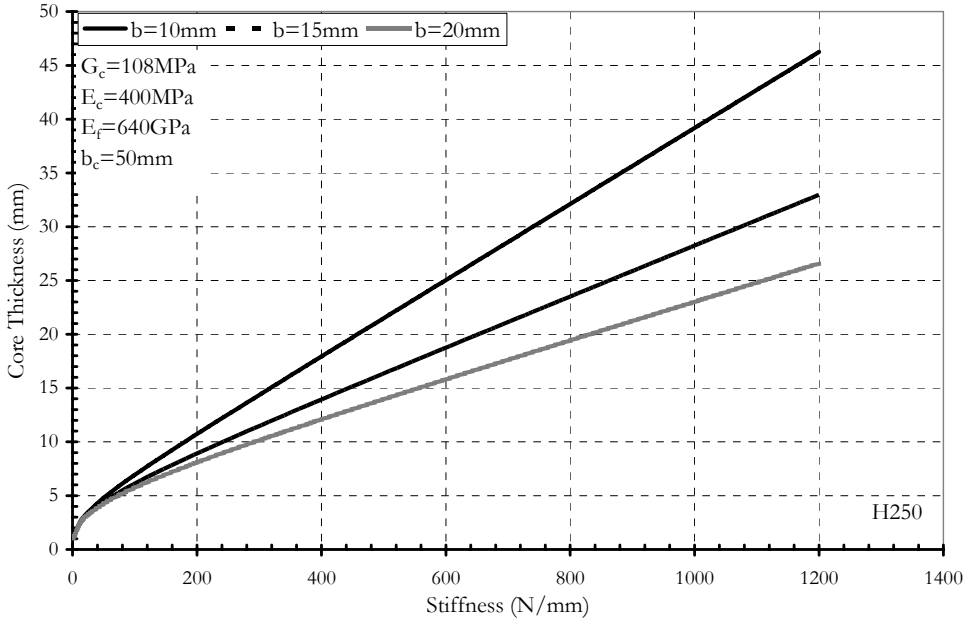

Figure 5.8 Stiffness and Core Thickness for minimum weight design for PVC 250 Kg/m^3 Core reinforced with H-12K HMC

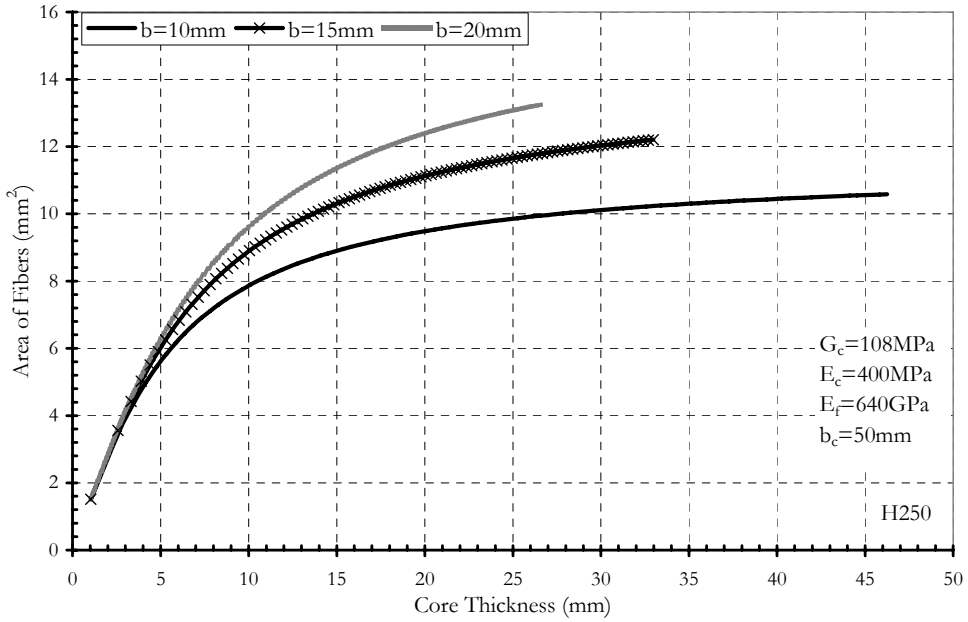

Figure 5.9 Area of fibers and Core Thickness for minimum weight design for PVC 250 Kg/m^3 Core reinforced with H-12K HMC

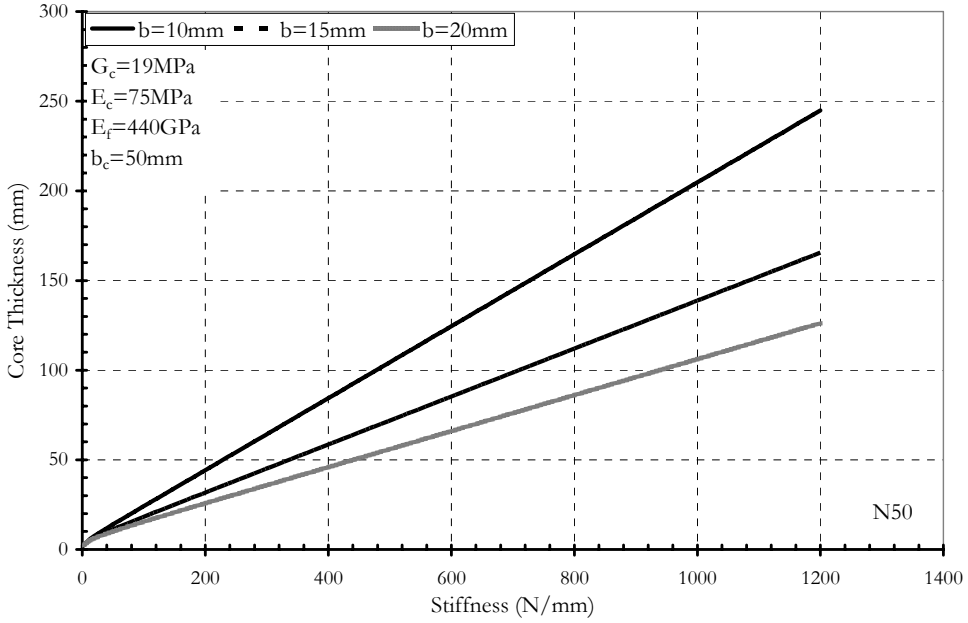

Figure 5.10 Stiffness and Core Thickness for minimum weight design for PVC 50 Kg/m^3 Core reinforced with N-12K MMC

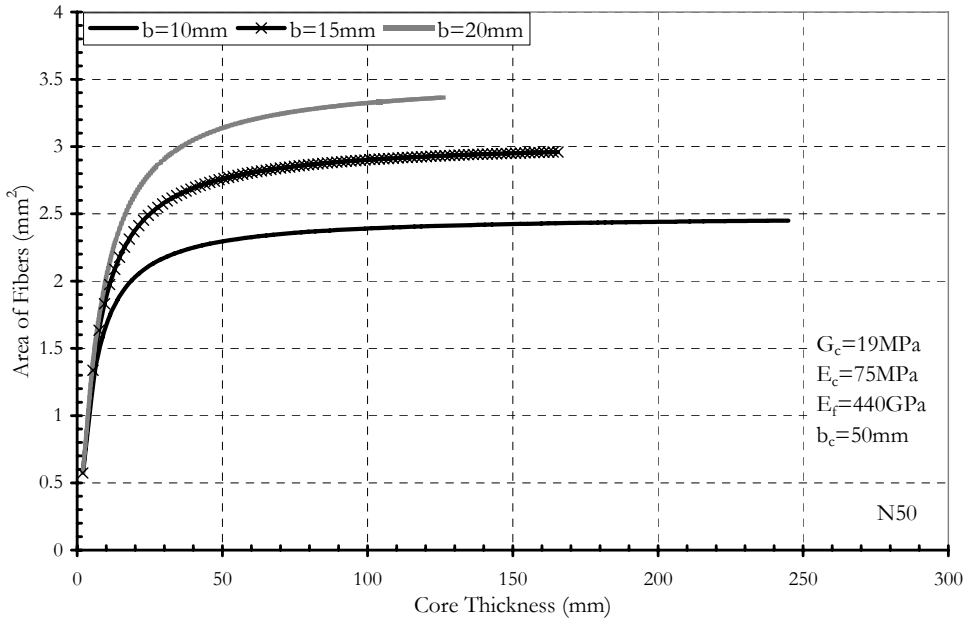

Figure 5.11 Area of fibers and Core Thickness for minimum weight design for PVC 50 Kg/m^3 Core reinforced with N-12K MMC

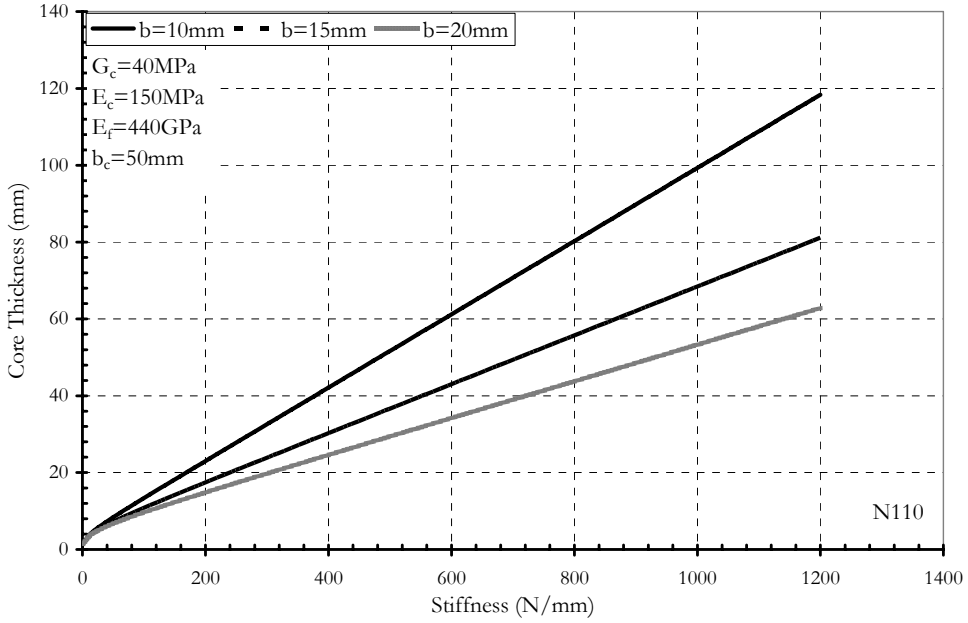

Figure 5.12 Stiffness and Core Thickness for minimum weight design for PVC 110 Kg/m^3 Core reinforced with N-12K MMC

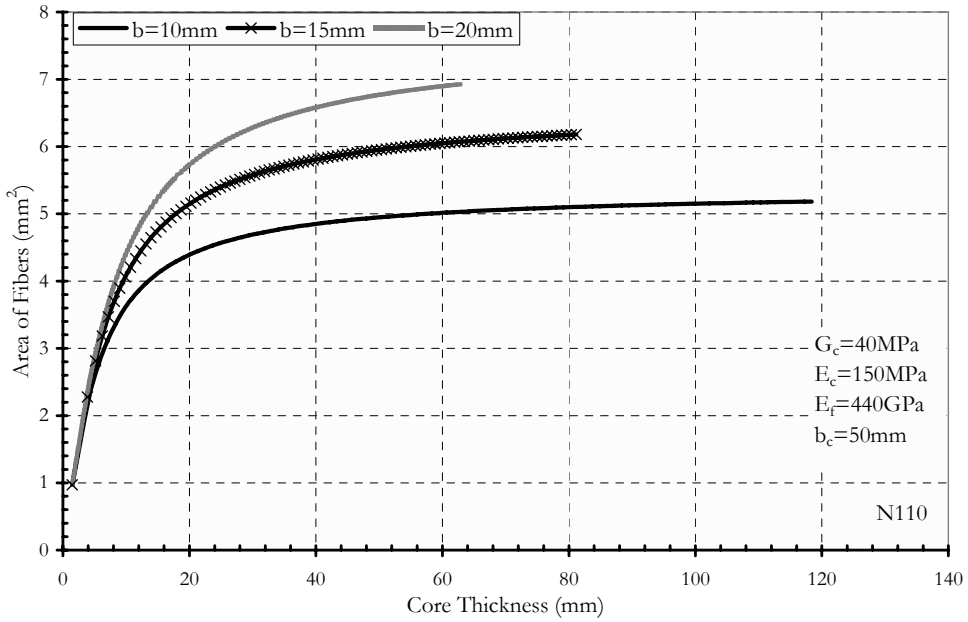

Figure 5.13 Area of fibers and Core Thickness for minimum weight design for PVC 110 Kg/m^3 Core reinforced with N-12K MMC

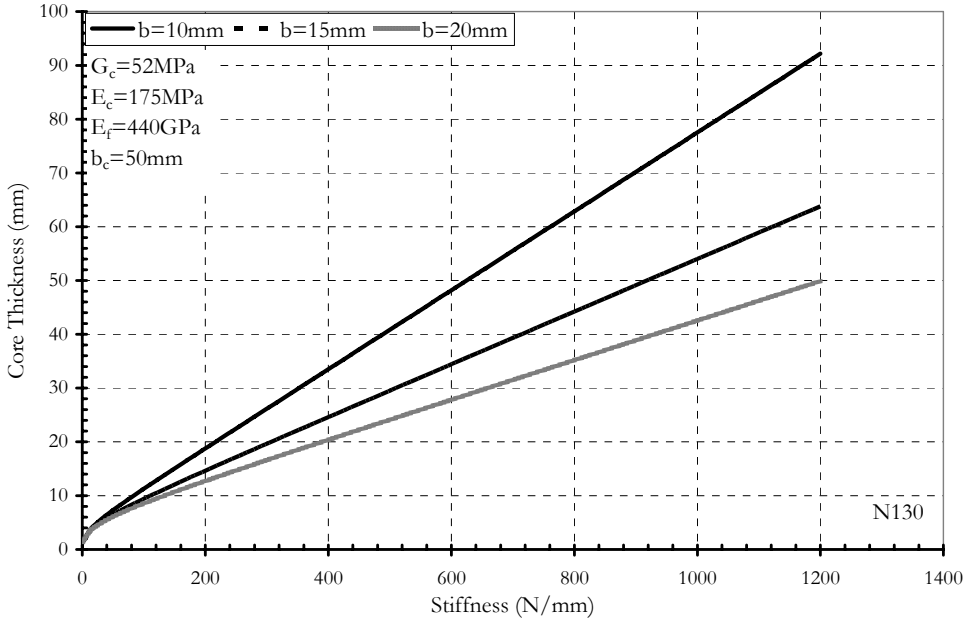

Figure 5.14 Stiffness and Core Thickness for minimum weight design for PVC 130 Kg/m^3 Core reinforced with N-12K MMC

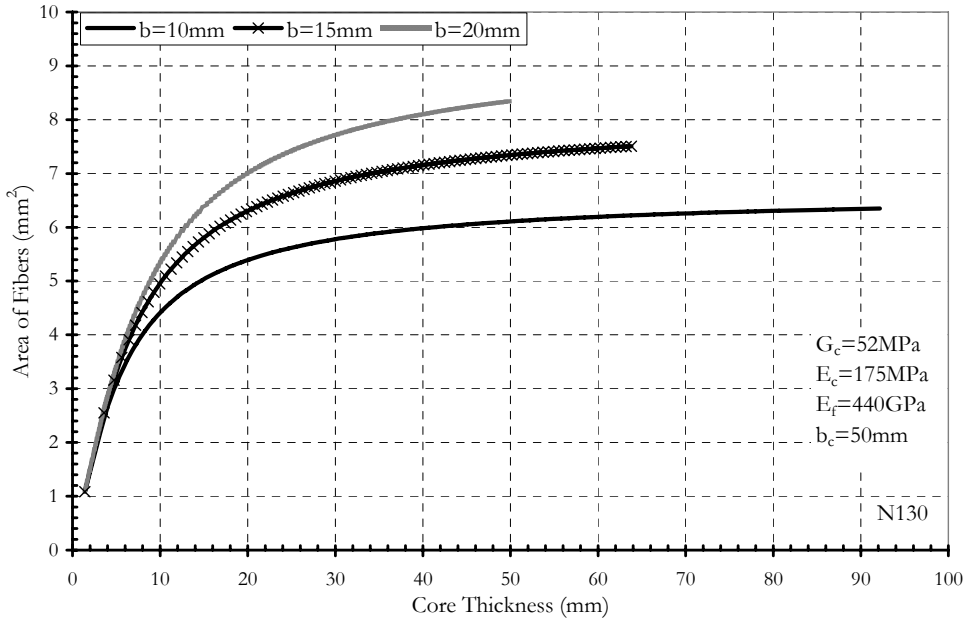

Figure 5.15 Area of fibers and Core Thickness for minimum weight design for PVC 130 Kg/m^3 Core reinforced with N-12K MMC

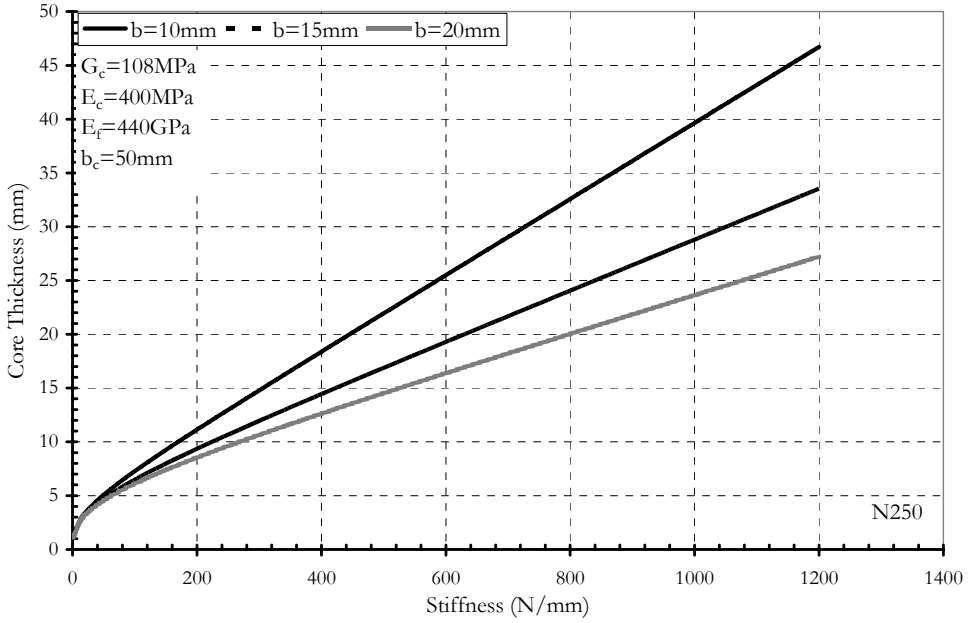

Figure 5.16 Stiffness and Core Thickness for minimum weight design for PVC 250 Kg/m^3 Core reinforced with N-12K MMC

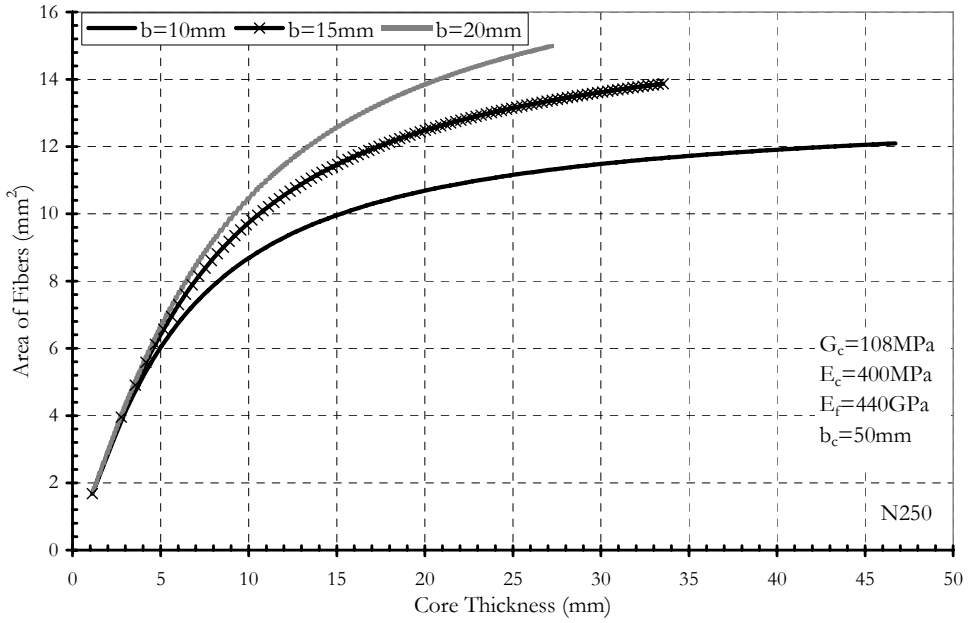

Figure 5.17 Area of fibers and Core Thickness for minimum weight design for PVC 250 Kg/m^3 Core reinforced with N-12K MMC

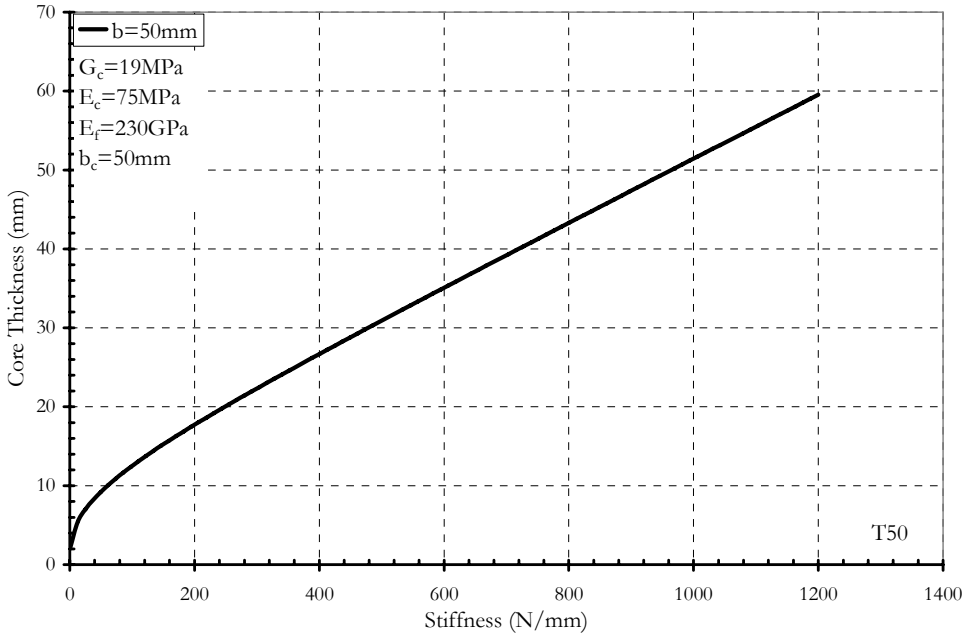

Figure 5.18 Stiffness and Core Thickness for minimum weight design for PVC 50 Kg/m^3 Core reinforced with T-3K Uni C Tape

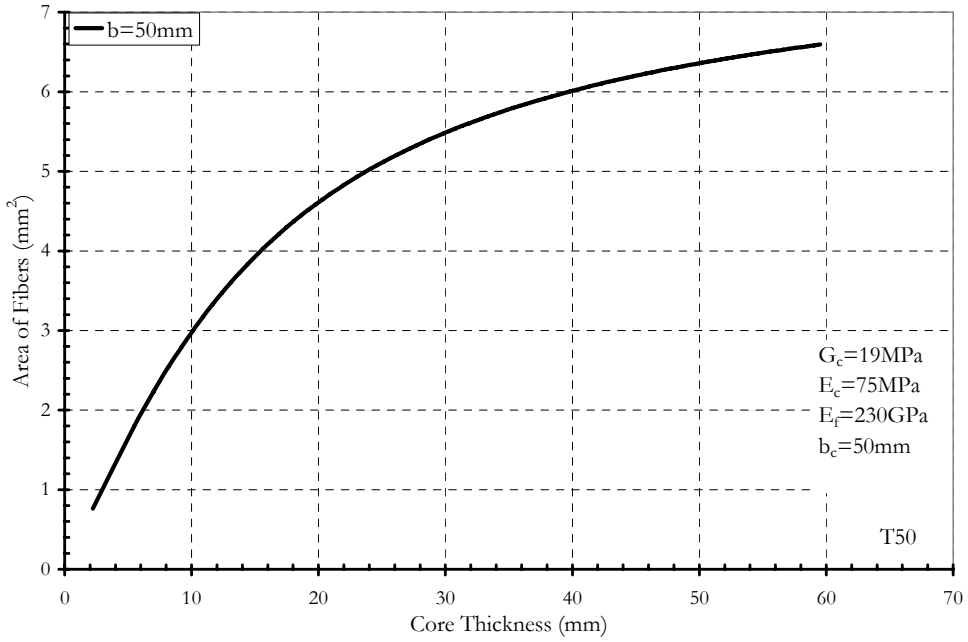

Figure 5.19 Area of fibers and Core Thickness for minimum weight design for PVC 50 Kg/m^3 Core reinforced with T-3K Uni C Tape

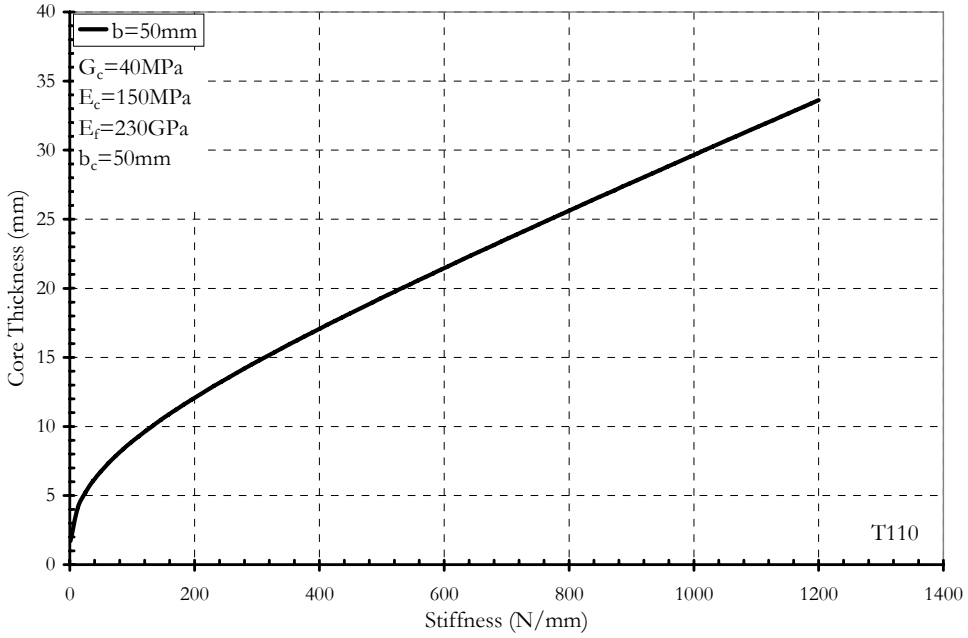

Figure 5.20 Stiffness and Core Thickness for minimum weight design for PVC 110 Kg/m^3 Core reinforced with T-3K Uni C Tape

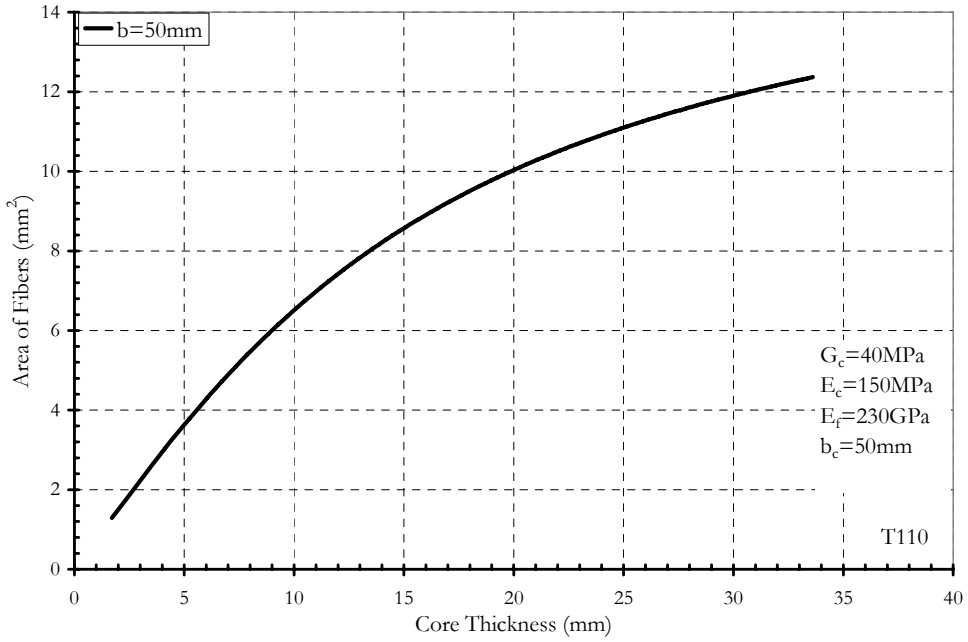

Figure 5.21 Area of fibers and Core Thickness for minimum weight design for PVC 110 Kg/m^3 Core reinforced with T-3K Uni C Tape

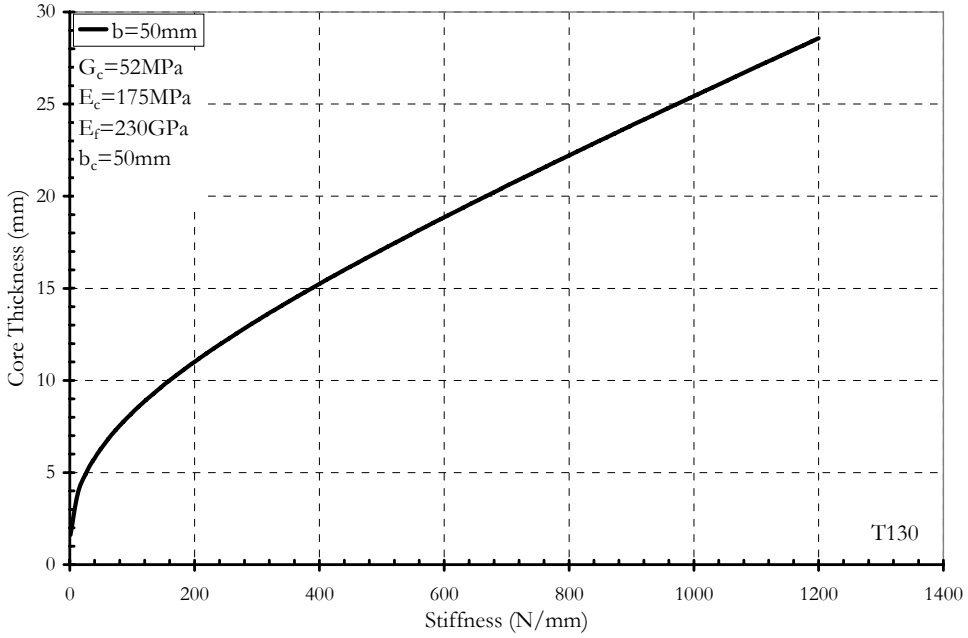

Figure 5.22 Stiffness and Core Thickness for minimum weight design for PVC 130 Kg/m^3 Core reinforced with T-3K Uni C Tape

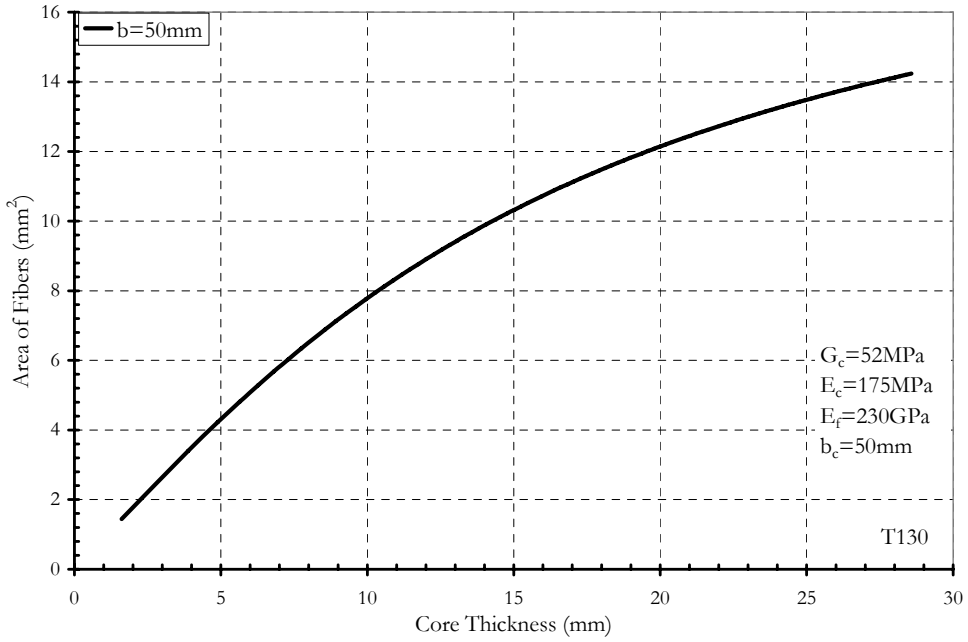

Figure 5.23 Area of fibers and Core Thickness for minimum weight design for PVC 130 Kg/m^3 Core reinforced with T-3K Uni C Tape

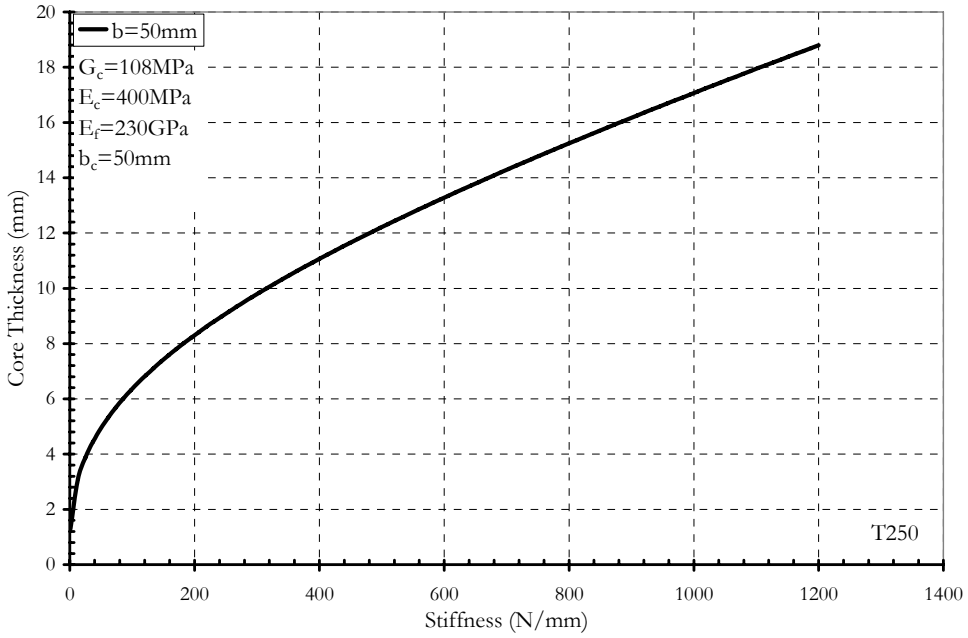

Figure 5.24 Stiffness and Core Thickness for minimum weight design for PVC 250 Kg/m^3 Core reinforced with T-3K Uni C Tape

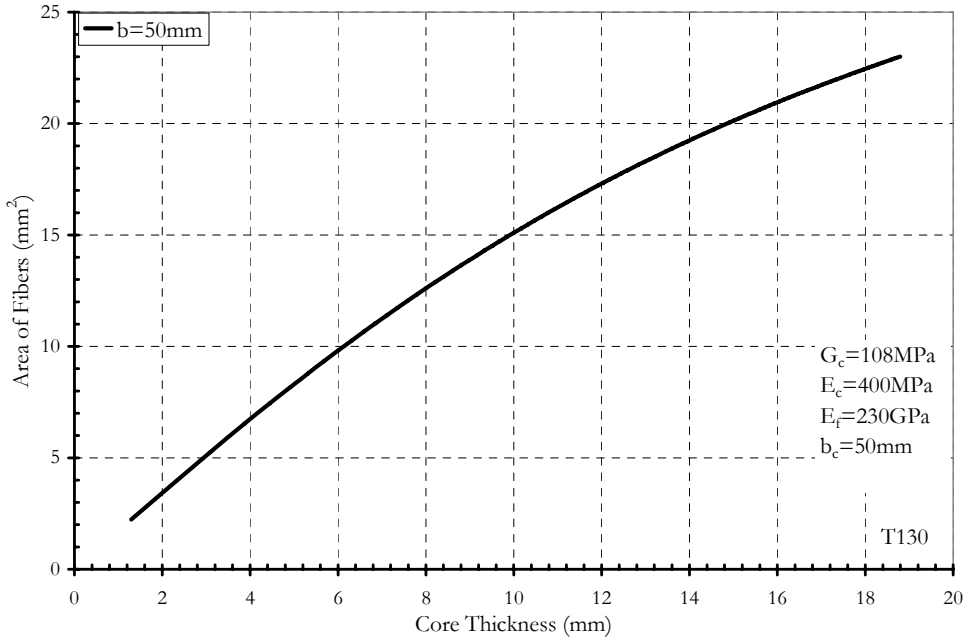

Figure 5.25 Area of fibers and Core Thickness for minimum weight design for PVC 250 Kg/m^3 Core reinforced with T-3K Uni C Tape

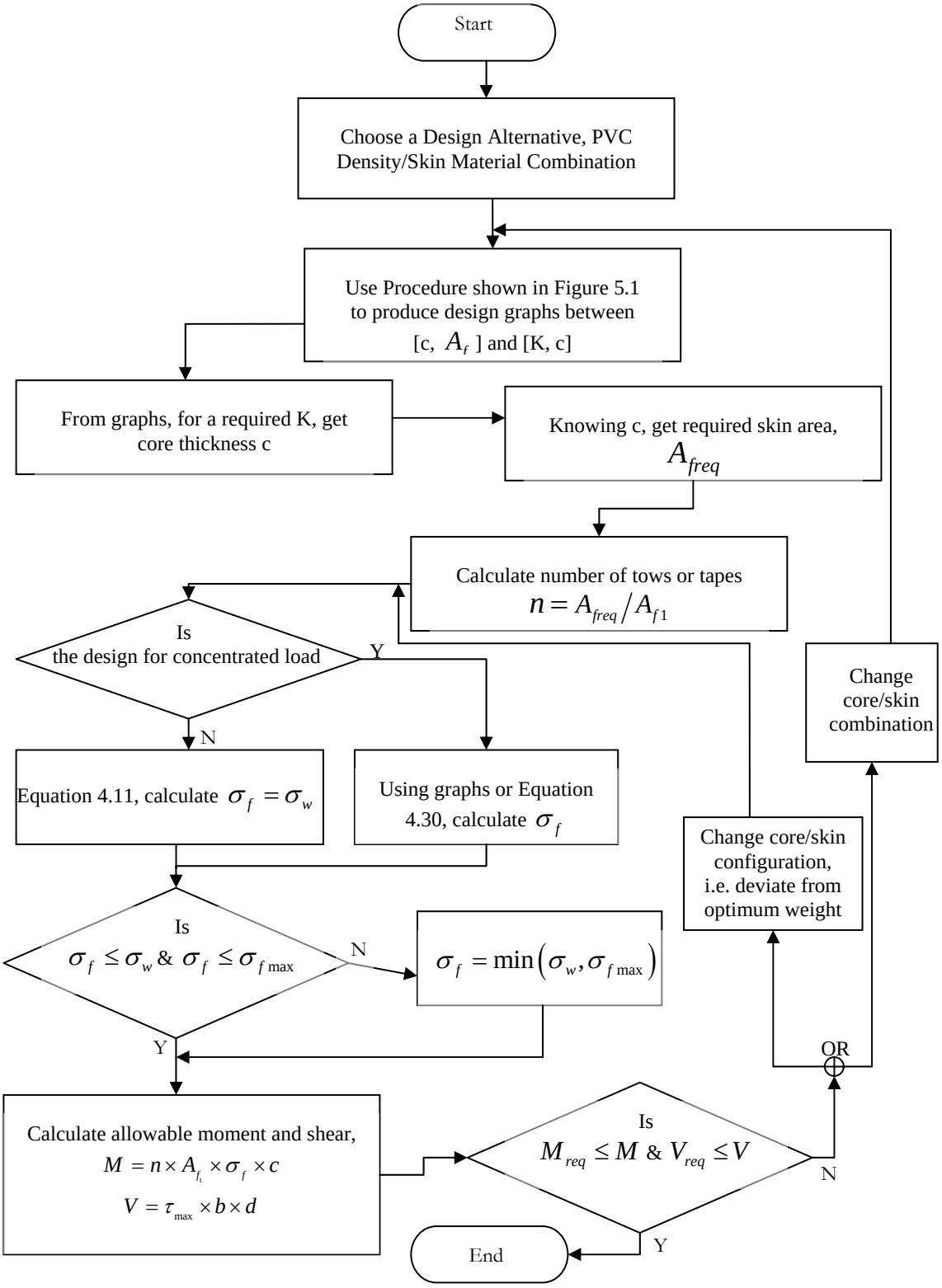

Figure 5.26 Design procedure flowchart

Chapter 6

Fire Safety Evaluation of PVC Sandwich Panels

6.1 Introduction

The fire safety in aircrafts involves both in-flight and post-crash fire consideration. Fire test criteria for aircraft cabin materials, required by the FAA, are based mainly on post-crash fire conditions (Sarkos, 1995). Between 1959 and 1993, twenty percent of the fatalities occurred due to burns, smoke inhalation, asphyxiation, or heat (Murray, 1995).

In addition to aircraft, marine vessels also share the same interest to find composites that are more fire resistant. This can be summarized by the statement given by Grenier et al.:

"*The Code of Federal Regulations (CFR), Title 46, contains the Coast Guard regulations for vessels under US jurisdiction. Current regulations for commercial vessels in the US generally do not allow the use of composite materials for ships' primary structure because they do not meet the requirements to be non-combustible. There are some exceptions for small passenger vessels of certain size and capacity. The international Maritime Organization (IMO) has adopted the High Speed Craft (HSC) Code as part of the 'International Convention for the Safety of Life at Sea' (SOLAS). The HSC Code contains a definition of new class of construction materials (Which may include composites) called 'fire-restricting materials.' The IMO's Maritime Safety Committee has adopted a resolution specifying the ISO 9705 Room Fire Test as the procedure to be used to qualify fire-restricting materials used for bulkheads and compartment linings."*(Grenier et al., 1998)

Therefore, to assure prescribed levels of fire safety in civil aircraft, the Federal Aviation Administration (FAA) requires a variety of fire tests, each test corresponding to certain conditions that will be found in case of fire. The purpose of these tests is to prove that

aircraft materials, especially cabin materials, meet the performance criteria set by the FAA, when exposed to heat or flame.

In this chapter the fire properties of the PVC core materials used in the research reported in this dissertation are investigated. Plain PVC foam core densities of 50 Kg/m^3 and 250 Kg/m^3, and PVC foam with inorganic matrix coating were subjected to the "Ohio State University (OSU) heat release" and the "NBS Smoke Burner" tests, which are the main FAA fire cabin safety tests.

The Ohio State University (OSU) heat release test is intended for use in determining heat release rates to show compliance with the requirements of FAR 25.853. Heat release rate is measured for the duration of the test from the moment the specimen is injected into a controlled exposure chamber and encompasses the period of ignition and progressive flame involvement of the surface (FAA, 2000).

The Smoke Test for Cabin Materials is used to determine the smoke generating characteristics of airplane passenger cabin interior materials to demonstrate compliance with the requirements of FAR 25.853 (FAA, 2000).

6.2 OSU Heat release test

6.2.1 Definitions

Heat Release is a measure of the amount of heat energy evolved by a material when burned. It is expressed in terms of energy by unit area ($KW\ min/m^2$).

Heat Release Rate (HRR) is a measure of the rate at which heat energy is evolved by a material when burned. It is expressed in terms of power per unit area (KW/m^2).

Heat flux is the intensity of the thermal environment to which a sample is exposed when burned. The heat flux density used in OSU is 3.5 W/cm^2.

6.2.2 Test apparatus

The test apparatus is shown in figures 6.1, 6.2 and 6.3. All the exterior surfaces, except the holding chamber, are insulated. The insulation is 1-inch thick of low density, high-temperature fiberglass board. A thermopile is used to monitor the temperature difference between the air entering and leaving the chamber.

Silicon Carbide elements are used as the radiant heat source, which can generate flux up to 10 W/cm^2. The elements are mounted in a stainless steel panel box. A truncated stainless steel diamond shaped mask is added to provide uniform heat flux density over the area of the vertical specimen. The heat flux is set at 3.5 W/cm^2, is uniform within 5 percent, and is monitored by heat flux sensor measurements at the center and the four corners of the specimen surface.

6.2.3 Test requirements

The passing criteria for this test are that the maximum heat release rate (HRR). During the 5-minute of tests HRR should not exceed 65 KW/m^2 and the average total heat released during the first five minutes should not exceed 65 $KW.min/m^2$ (65/65 criteria).

6.2.4 Test specimens

Two types of foams with density of 50 Kg/m^3 and 250 Kg/m^3 were chosen for evaluation. Control samples and sandwich panels were tested to obtain a comparative evaluation. Three samples were prepared from each type. After applying the carbon fabric, the samples were left to harden overnight. An insulating layer of inorganic matrix with 20 percent sol gel, which is Perlite based fine powder was applied over the carbon fabric. In order to apply the coating, the panels were placed into molds and the coating was poured on top of the panels,

as shown in figure 6.5. The specimens were left in the mold for 48 hours, taken out of the mold and left to cure in room temperature for three weeks. The weight and thickness of samples were taken after each phase. The size of the specimens was 150 by 150 mm in plan dimensions; a typical coated specimen is shown in figure 6.6. The thickness for the control samples was 13 mm, the unidirectional carbon fibers added 0.7 mm, and the coating was in the order of 1 mm. Sample details are shown in table 6.1. All specimens were conditioned at 21°C and 50% relative humidity for at least 24 hours prior to the test.

During the test, only one surface of the specimen was exposed to the flame (The coated side for the reinforced panels). This was done after placing the specimen into the holder shown in figure 6.4.

6.2.5 Test procedures and results

The results are presented in figures 6.7, 6.9 and 6.11 for the low density (50 Kg/m^3) samples, and figures 6.13, 6.15 and 6.17 show the results for the 250 Kg/m^3 samples. A summary of the results is presented in table 6.2.

The heat release rate, HRR, was calculated at any point in time, *t*, from thermopile output voltage reading, *V*, using the formula,

$$HRR = K_h \left(V - V_0 \right) \tag{7.1}$$

Where K_h and V_0 are the calibration factor and the thermopile millivolt baseline, respectively. They are shown in the figures for each test. The maximum heat release rate during the test was noted down with its occurrence time, t_{PHRR}. The total heat release was computed for 2 minutes and 5 minutes by integrating the HRR curve.

From figures 6.8 and 6.14, it can be seen that the control samples were totally destroyed during the test and failed both passing criteria. The performance of 50 Kg/m^3 is better as the

peak HRR and the heat release are closer to the limits specified by the FAA but it should be noticed that the mass of material for the 250 Kg/m^3 is much higher (5 times if they have the same volume). This can be seen by comparing the two graphs, the 50 Kg/m^3 core reaches the peak fast (50 sec), then it decays as the material either has charred completely or evaporated. The 250 Kg/m^3 core approaches the peak in about 40 sec, but it does not decay until 193 sec.

By adding the thin protective layer of inorganic polymer skin, all the PVC samples not only passed the FAA passing criteria, but sustained an average of heat release below 65 KW.min/m^2 after 5 minutes against FAA requirement of 2 minutes. The trend of the heat release rate of coated samples represented by small red circles on the graphs, totally reversed when compared to the control samples. The heat release rate increases gradually, and the peak is reached after a long wait, which is very crucial for a plane crash survivor so as to escape the plane before the interior burns out. The peak heat release rate dropped from 68 and 85 KW/m^2 to an average of 21 and 29 KW/m^2; the time to reach the peak value increased from 50 and 193 sec to 260 and 296 sec; and the heat release after 2 minutes decreased from 84 and 127 KW.min/m^2 to an average of 5 and -4.7 KW.min/m^2 for 50 Kg/m^3 and 250 Kg/m^3 cores, respectively.

6.2.6 Comparison with organic systems

For comparison with organic system, the results reported by Grenier et al. are presented in this section. Sandwich panels were fabricated using 25 mm-thick PVC foam of 80 Kg/m^3 and 2.4 mm-thick GRP laminates 2100 Kg/m^3. These panels were tested in the Cone Calorimeter, in accordance with ASTM E 1354 (Grenier et al., 1998).

By investigating the curves shown in figure 6.19, it can be seen that the curves have multiple peaks. The initial peak in HRR may be caused to surface pyrolysis[1] followed by a decrease caused by surface char formation. The second peak may be caused by an increase in gasification rate of the unburned substrate, caused by an increase in the bulk temperature of the composite (Brown et al., 1988). The PVC foam specimen reinforced with inorganic composites provided different trend, with gradual increase till it reached the peak by the end of the test.

The inorganic composite with the coating has a bulk density 1100 Kg/m^3 and its thickness is in the order of 1.7 mm and the maximum HRR 32.2 KW/m^2. The GRP organic composite had a density of 2100 Kg/m^3 and the thickness is about 2.4 mm. The maximum HRR for the GRP with no core was 132 KW/m^2 in 105 sec; the sandwich panel had a peak HRR 130 KW/m^2 at 135 sec. Therefore, it can be concluded that the performance of the inorganic matrix coating is significantly superior to the organic system.

6.3 FAA Smoke test for cabin materials (NBS)

6.3.1 Definitions

The main measurement from this test is the Specific optical density (D_s). Optical Density is a dimensionless measure of the amount of smoke produced per unit area by a material when it is burned. In this test, the maximum value of D_s that occurs during the first 4 minutes of a test, ^4D_m, is reported.

---

[1] Pyrolysis is the chemical decomposition of organic materials by heating in the absence of oxygen or any other reagents, except possibly steam.

6.3.2 Test apparatus

The test chamber and setup are shown in figure 6.20. The test chamber used for this experiment was a square-cornered box with inside dimensions of 914 mm wide, 610 mm deep, and 914 mm high and is shown in figure 6.21. The interior surfaces are porcelain-enameled metal or equivalent coating that is resistant to chemical attack and corrosion. It is shown also from figure 6.20 that the door has a viewing window to observe the sample and pilot flamelets behavior during the test. The chamber has a manometer or pressure transducer to monitor the pressure or any leakage. The burner used is a pilot burner, which is a multiple flamelet type with six stainless steel tubes. A close-up picture of the heat flux density gauge, specimen holders, and multidirectional pilot burner is shown in figure 6.22. The pilot burner will be centered in front of and parallel to the specimen holder. From this picture one can see that the outer flamelets oriented perpendicular to the specimen surface, while the inner flamelets oriented 45 degrees to the specimen surface. The specimen holder consists of stainless steel frame, a backing made of insulation millboard, a spring, a retaining rod to secure the specimen in place, and aluminum foil for wrapping the specimen. The specimen holder details are shown in figure 6.23. A typical support frame to support the radiant heat furnace and specimen holder is shown in figure 6.24.

6.3.3 Test specimens

The procedures similar to the OSU samples were followed to prepare the samples for this test, figure 6.25. The same inorganic matrix coating, mixed with Sol gel fine powder, was used as a coating on top of the carbon unidirectional fabric. The fabric had a thickness of 0.7 mm and the coating had a thickness of 1.4 mm. The specimen plan dimension was 73 mm x 73 mm. Samples details are shown in Table 6.3. All specimens were conditioned at 21^{o}C and

50% relative humidity for at least 24 hours prior to the test. All the surfaces of the specimen, except the surface to be exposed for the test were wrapped with aluminum foil prior to placing them in the specimen holder. After the specimen was placed in the holder, any aluminum foil on the exposed surface was removed. The specimen was placed in the holder, followed by an alumina-silica backing board, the spring plate, and the retaining rod; this can be shown in figure 6.23.

6.3.4 Test requirements

A maximum of 200 for the average of ${}^4D_m$ during the 4-minute test is the passing criterion for this test, as stated through FAR 25.853 (c-1) Amendment 25-72.

6.3.5 Test procedures and results

The NBS test results along with the tested samples are shown in figures 6.26 to 6.37. A summary of the results and the outcome according to the FAA criteria is shown in table 6.4. As mentioned earlier, the most important parameter obtained from the NBS smoke burner test is the maximum specific optical density occurring during the first 4 minutes. This value can be determined using the following formula,

$$ {}^4D_m = \left(\frac{V}{LA}\right)\log_{10}\left(\frac{100}{{}^4T_m}\right) = 132 \times \log_{10}\left(\frac{100}{{}^4T_m}\right) \tag{7.2} $$

Where: V = chamber volume = 0.510 m^3

L = light path length= 0.914 m

A = exposed specimen area= 0.00424 m^2

${}^4T_m$ = minimum percent light transmission during 4 minutes

$\log_{10}\left(\frac{100}{{}^4T_m}\right)$ = maximum optical density during 4 minutes

The following are the major observations:

- Both, the 50 Kg/m^3 and the 250 Kg/m^3 control samples failed the FAA passing criterion as they have a specific optical density after 4 minutes of 293 and 354, respectively, which exceeded the FAA limit of 200.
- The rate of smoke emission highly increases in the beginning of the test, and then it becomes almost constant. This can be seen in figures 6.26 and 6.32 for the control samples.
- After adding the inorganic matrix coating, the level of smoke decreased to 1.5% and 2.8% of the level originally exhibited for the control samples for the 50 Kg/m^3 and the 250 Kg/m^3 cores, respectively.
- The coated samples emitted very little or no smoke for the first three minutes.
- The rate of increase of smoke emission decreased dramatically, it became very minimal over the first three minutes, and then it started increasing.
- This behavior is very important in the post-crash scenarios.
- The specific optical smoke density for the 50 Kg/m^3 is less than the reciprocal ones for the 250 Kg/m^3 in all cases (coated and not coated). When investigating the tested samples, the 50 Kg/m^3 cores were completely destroyed for the control samples (see figure 6.27), and partially destroyed with the coating. The 250 Kg/m^3 cores without coating were less destroyed than the reciprocal ones from the 50 Kg/m^3, and by looking to the sides of the coated samples (figure 6.38), it can be seen that the core was not destroyed, but a char layer was formed.

6.4 Observations

By examining the previously discussed test results, it was shown that adding a thin layer of inorganic matrix skin improves the fire characteristic of the PVC core. These are the salient points:

- For the OSU test, the peak heat release rate dropped from 68 and 85 KW/m^2 to an average of 21 and 29 KW/m^2 for 50 Kg/m^3 and 250 Kg/m^3 cores, respectively.
- The time to reach the peak increased from 50 and 193 sec to 260 and 296 sec for 50 Kg/m^3 and 250 Kg/m^3 cores, respectively.
- The heat release after 2 minutes decreased from 84 and 127 KW.min/m^2 to an average of 5 and -4.7 KW.min/m^2 for 50 Kg/m^3 and 250 Kg/m^3 cores, respectively.
- The behavior of the HRR changed from abrupt increase to a rather gradual increase until it reached the peak by the end of the test.
- By comparing to organic system, the inorganic matrix composites are better than organics regarding the fire characteristics.
- All the samples with inorganic coating passed the FAA criteria and none of the organic ones did.
- For the NBS test, the level of smoke decreased to 1.5% and 2.8% of the level originally exhibited for the control samples for the 50 Kg/m^3 and the 250 Kg/m^3 cores, respectively
- The inorganic coated samples more or less did not emit any smoke for the 180 sec.
- The behavior of the smoke emission changed to a much desired behavior for the post-crash scenarios.

- All the samples with inorganic coating passed the NBS passing criteria with a level of emission that did not exceed 5% of the FAA upper limit.

Table 6.1 OSU samples details

Specimen ID		Weight	Original dimensions			After fabrics		After Coting	
		W	Length	Width	Thickness	Weight	Thickness	Weight	Thickness
		gm	mm	mm	mm	gm	mm	gm	mm
OSU	50-C1	15.30	148.83	148.14	13.20	-	-	-	-
OSU	50-T1	14.90	149.14	147.13	13.11	45.62	13.81	402.50	15.44
OSU	50-T2	14.90	147.46	148.32	13.03	45.52	13.73	418.10	15.43
OSU	250-C1	65.60	146.21	149.90	13.02	-	-	-	-
OSU	250-T1	66.00	147.99	147.79	12.92	79.12	13.62	402.50	15.10
OSU	250-T2	65.30	147.85	148.51	12.95	78.47	13.65	418.10	15.20

Table 6.2 OSU test results

Specimen ID		Peak *HRR*	t_{PHRR}	Heat Release		FAA Test Result (65-65)
				2 min	5 min	
		KW/m^2	sec	$KW.min/m^2$		Pass/Fail
OSU	50-C1	68.1	50	83.9	177.2	Fail
OSU	50-T1	25.4	281	9.3	62.1	Pass
OSU	50-T2	17.5	238	0.8	26.2	Pass
OSU	250-C1	85.2	193	127.2	330.4	Fail
OSU	250-T1	32.2	297	3.82	53.1	Pass
OSU	250-T2	24.8	294	-5.5	27.8	Pass

Table 6.3 NBS samples details

Specimen ID		Weight	Original dimensions			After fabrics		After Coting	
		W	Length	Width	Thickness	Weight	Thickness	Weight	Thickness
		gm	mm	mm	mm	gm	mm	gm	mm
NBS	50-C2	3.40	70.97	71.96	13.20	-	-	-	-
NBS	50-T1	3.20	67.55	71.27	13.17	10.10	13.65	239.80	15.75
NBS	50-T2	3.30	70.04	68.95	13.06	10.40	13.59	228.20	15.74
NBS	250-C3	14.10	69.60	68.17	12.88	-	-	-	-
NBS	250-T2	15.50	70.02	70.86	12.97	19.50	13.47	234.90	15.58
NBS	250-T3	14.20	69.49	68.55	12.89	17.70	13.27	232.50	15.40

Table 6.4 NBS test results

Specimen ID		^4D_m	FAA Test Result $^4D_m<200$
			Pass/Fail
NBS	50-C2	293.37	Fail
NBS	50-T1	4.25	Pass
NBS	50-T2	2.77	Pass
NBS	250-C3	354.17	Fail
NBS	250-T2	5.02	Pass
NBS	250-T3	9.87	Pass

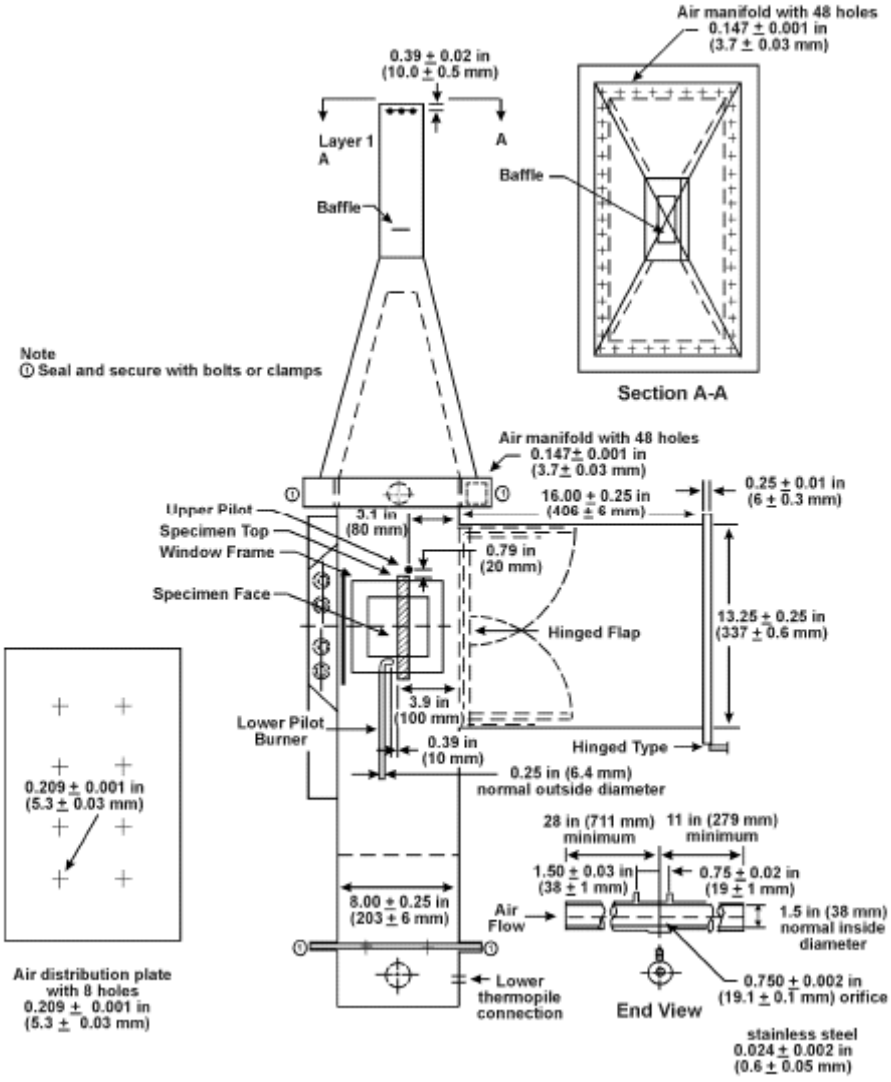

Figure 6.1 OSU apparatus details (FAA, 2000)

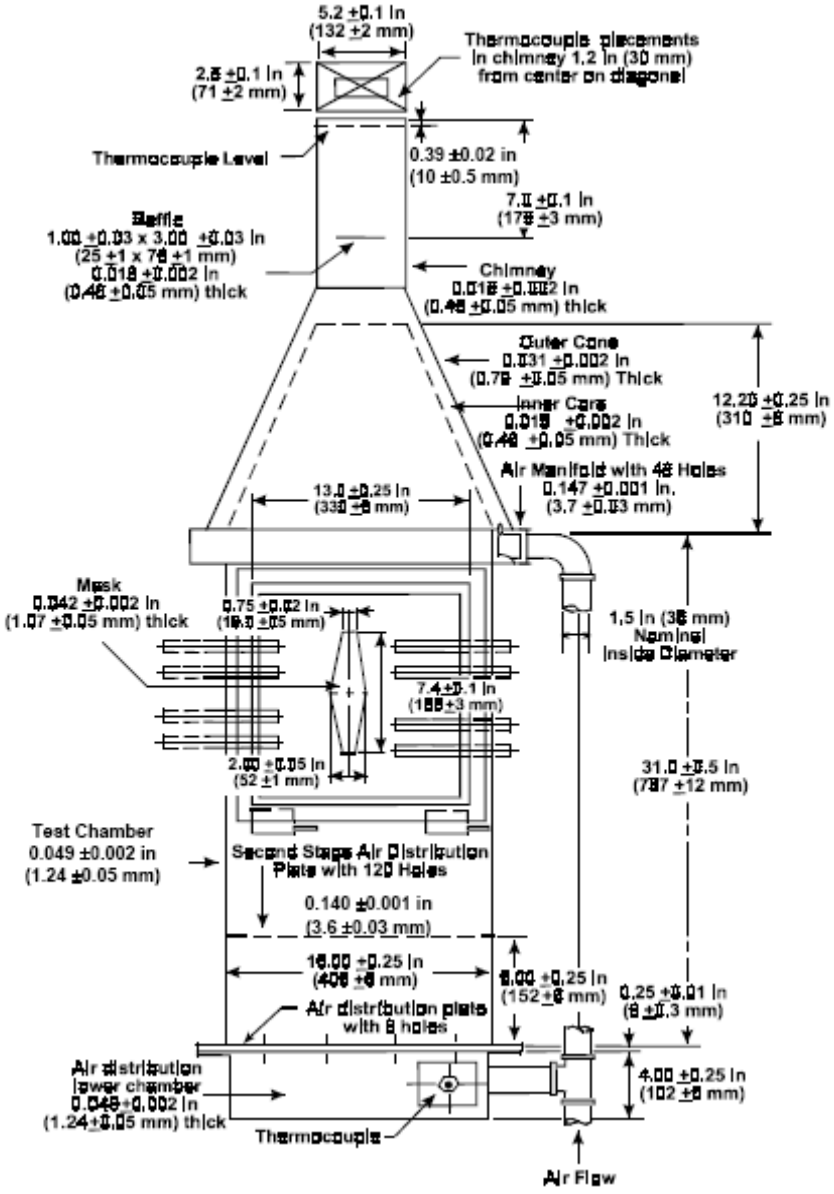

Figure 6.2 OSU apparatus details (FAA, 2000)

Figure 6.3 OSU heat release testing setup (Papakonstantinou, 2003)

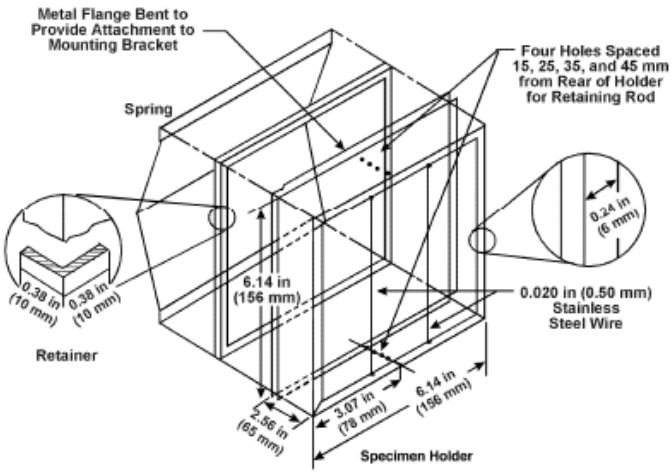

Figure 6.4 OSU specimen holder (FAA, 2000)

Figure 6.5 Samples preparation steps, (a) PVC foam core, (b) Core with unidirectional carbon in the mold, (c) Applying the coating (d) After coating application

Figure 6.6 Coated sample before testing

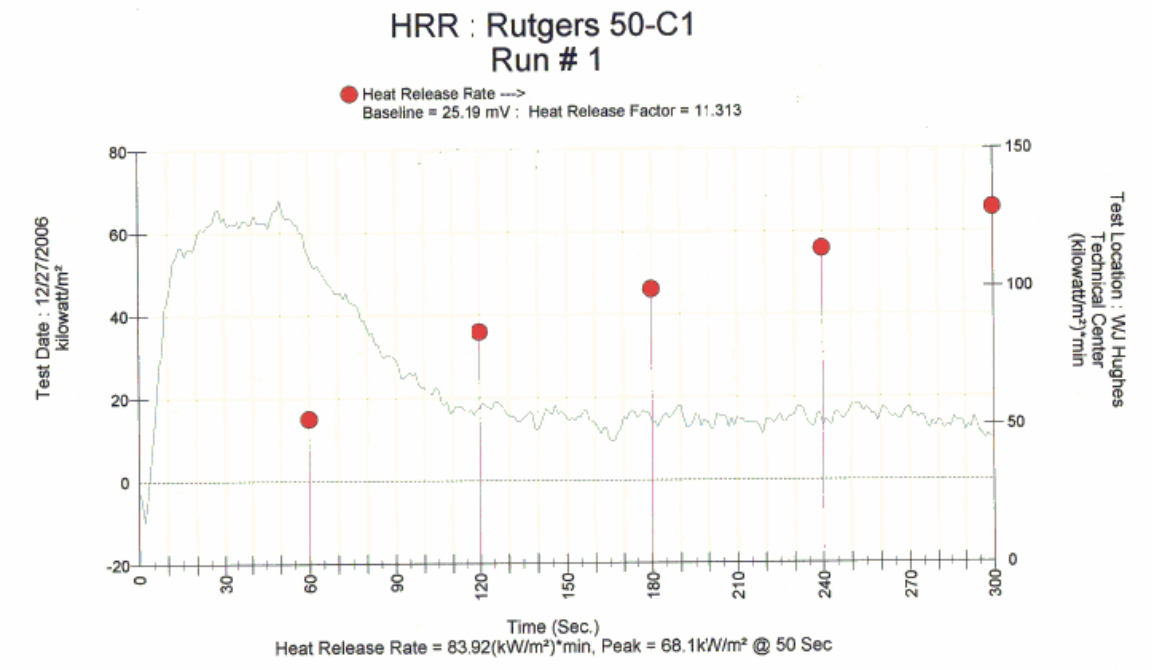

Figure 6.7 OSU test results for OSU-50-C1 (Control)

Figure 6.8 OSU-50-C1 tested sample

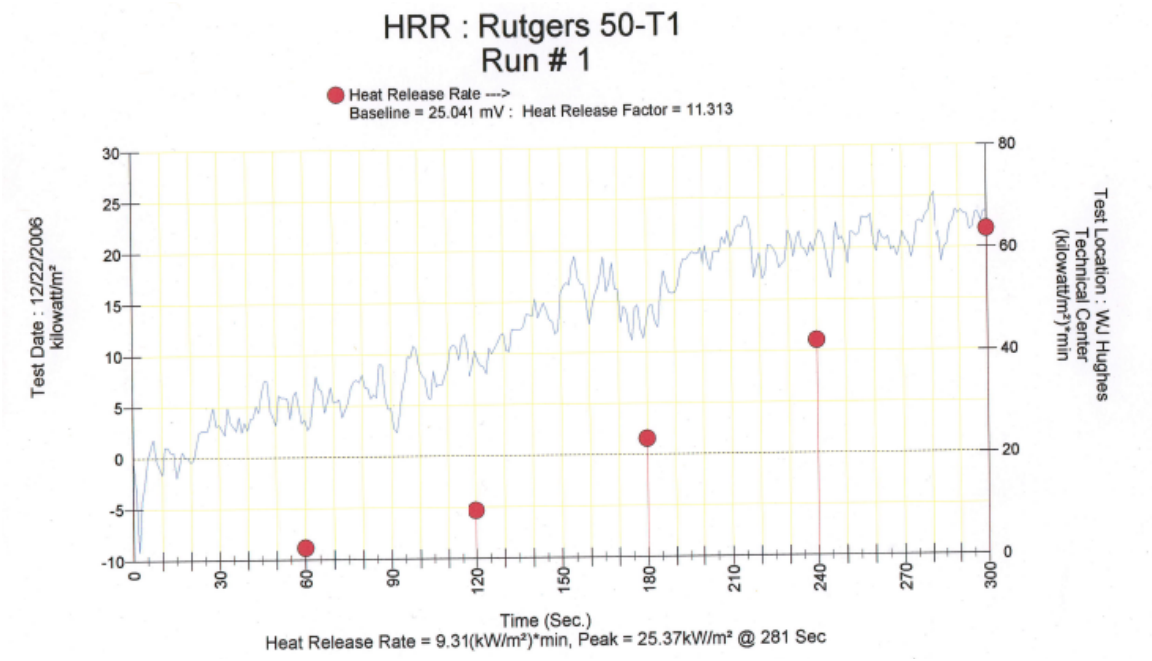

Figure 6.9 OSU test results for OSU-50-T1

Figure 6.10 OSU-50-T1 tested sample

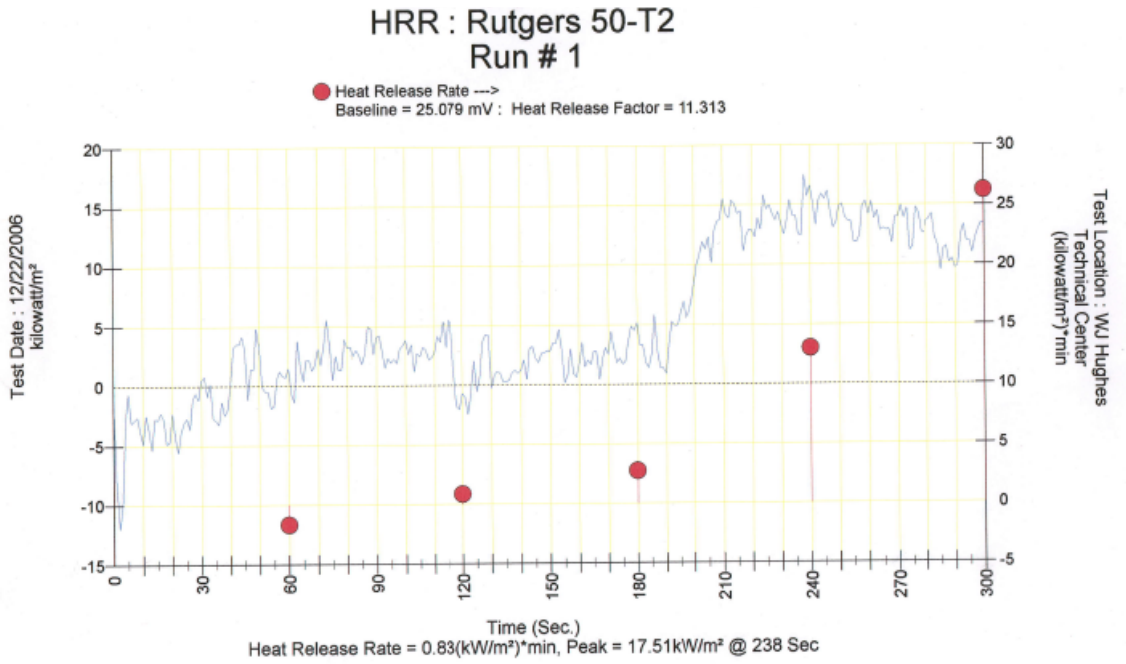

Figure 6.11 OSU test results for OSU-50-T2

Figure 6.12 OSU-50-T2 tested sample

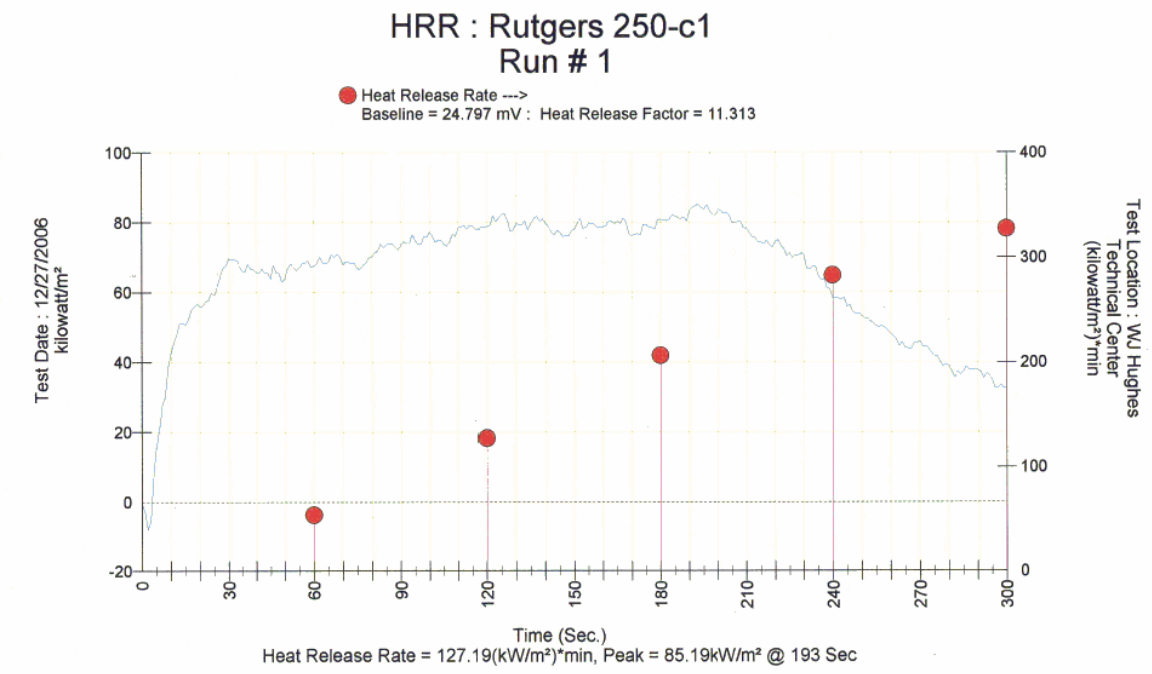

Figure 6.13 OSU test results for OSU-250-C1 (Control)

Figure 6.14 OSU-250-C1 tested sample

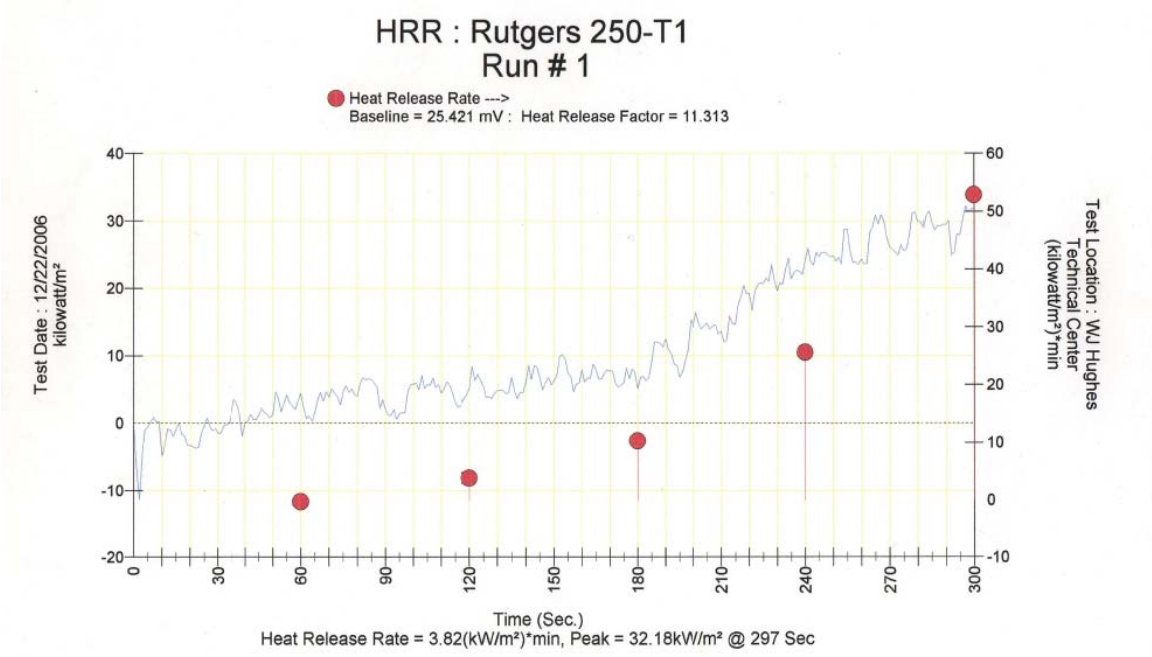

Figure 6.15 OSU test results for OSU-250-T1

Figure 6.16 OSU-250-T1 tested sample

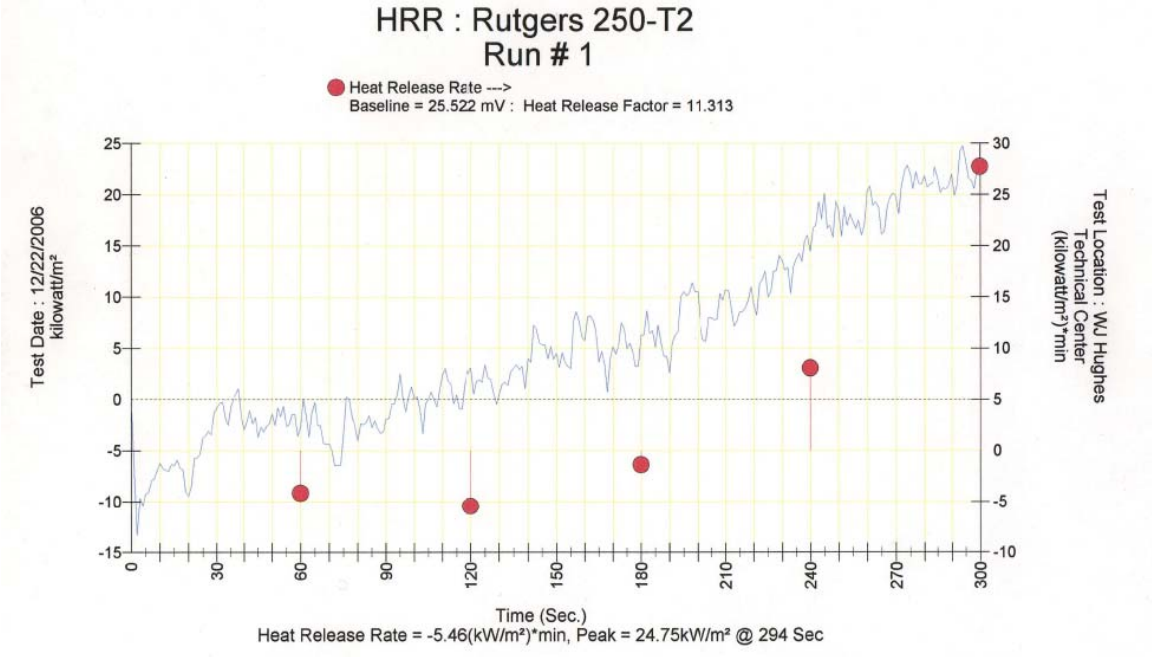

Figure 6.17 OSU test results for OSU-250-T2

Figure 6.18 OSU-250-T2 tested sample

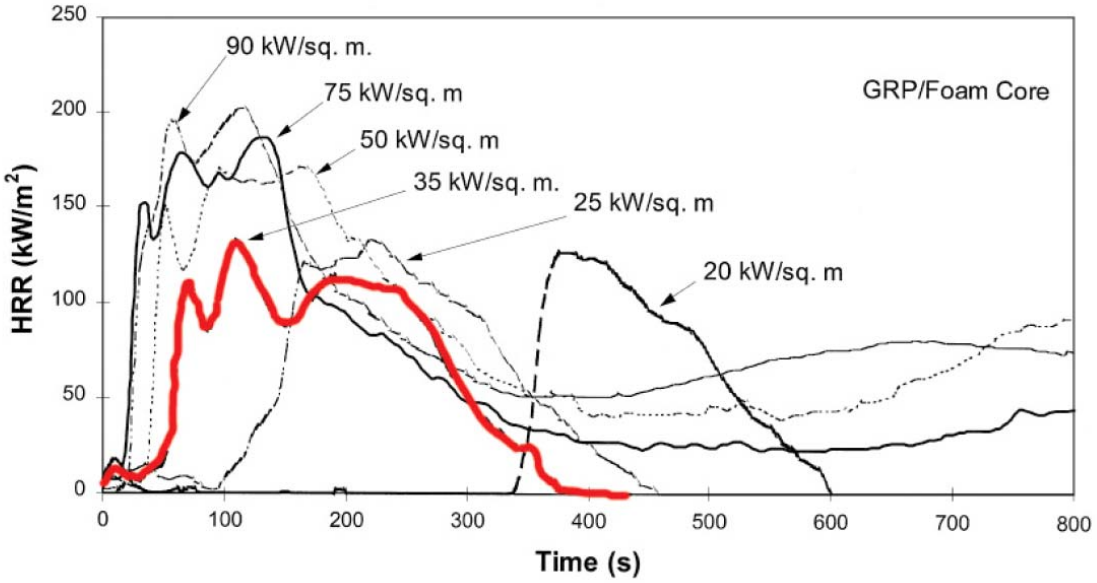

Figure 6.19 HRR curves for GRP/foam-core (Grenier, 1998)

Figure 6.20 NBS testing setup (Papakonstantinou, 2003)

Figure 6.21 NBS testing chamber (Papakonstantinou, 2003)

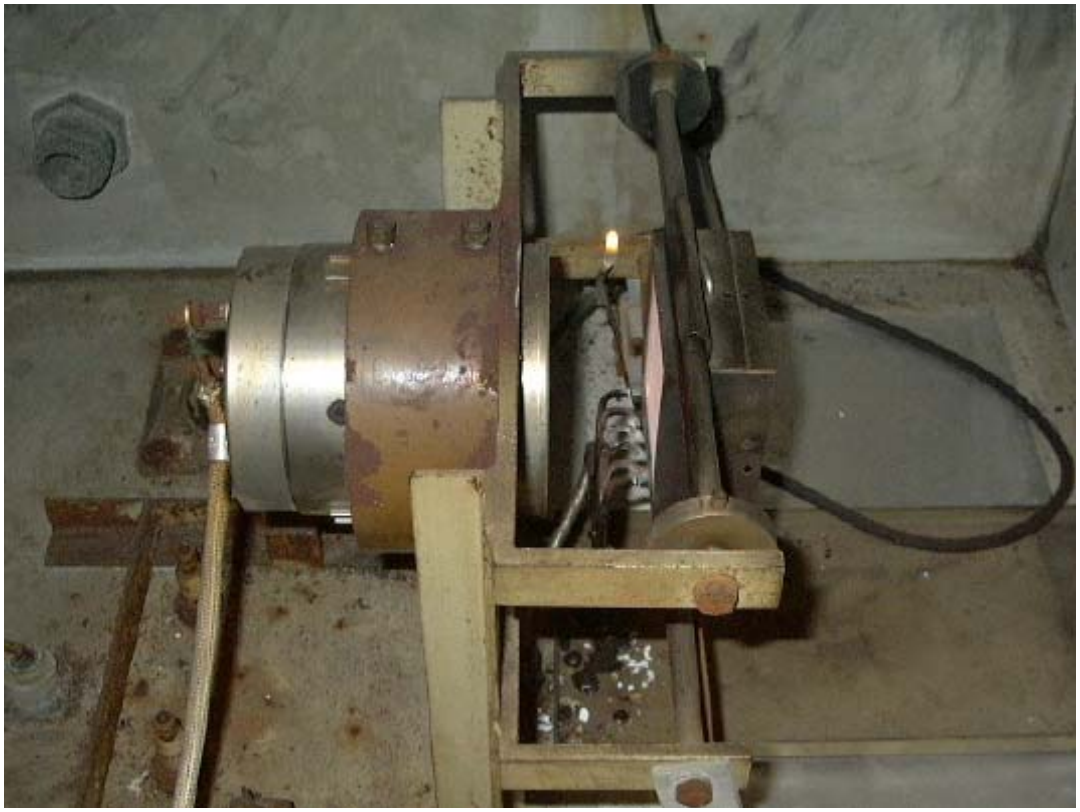

Figure 6.22 NBS testing holder and burner (Papakonstantinou, 2003)

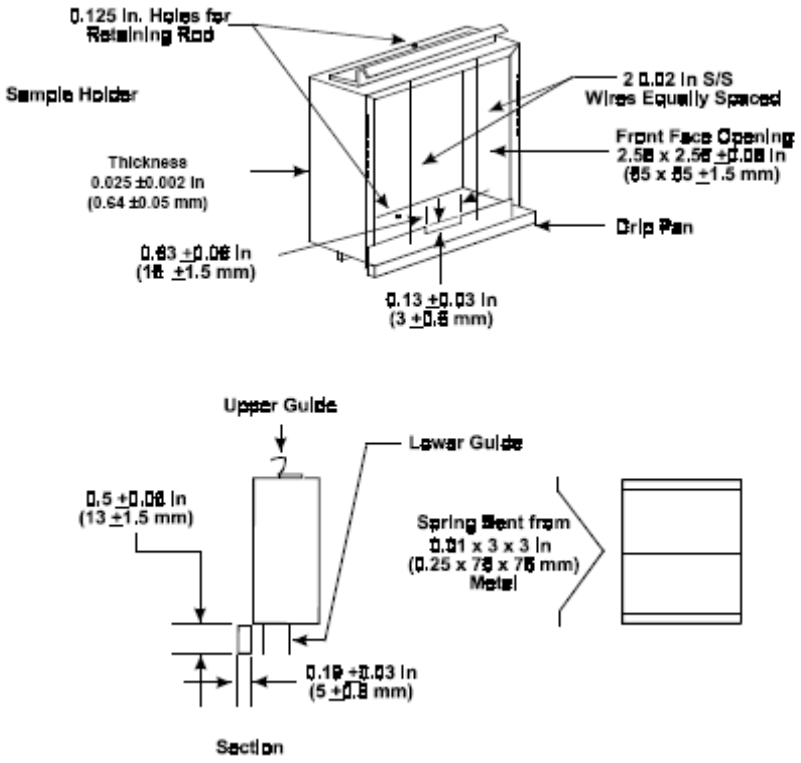

Figure 6.23 NBS specimen holder details (FAA, 2000)

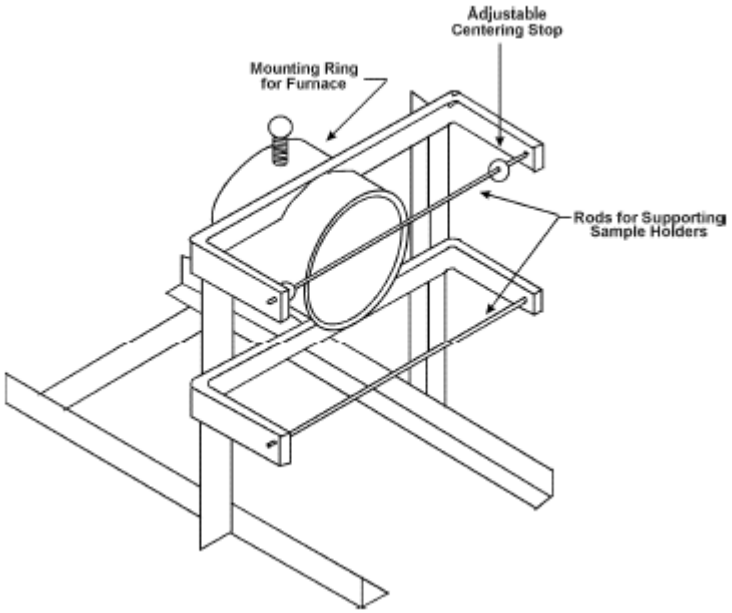

Figure 6.24 NBS typical furnace support (FAA, 2000)

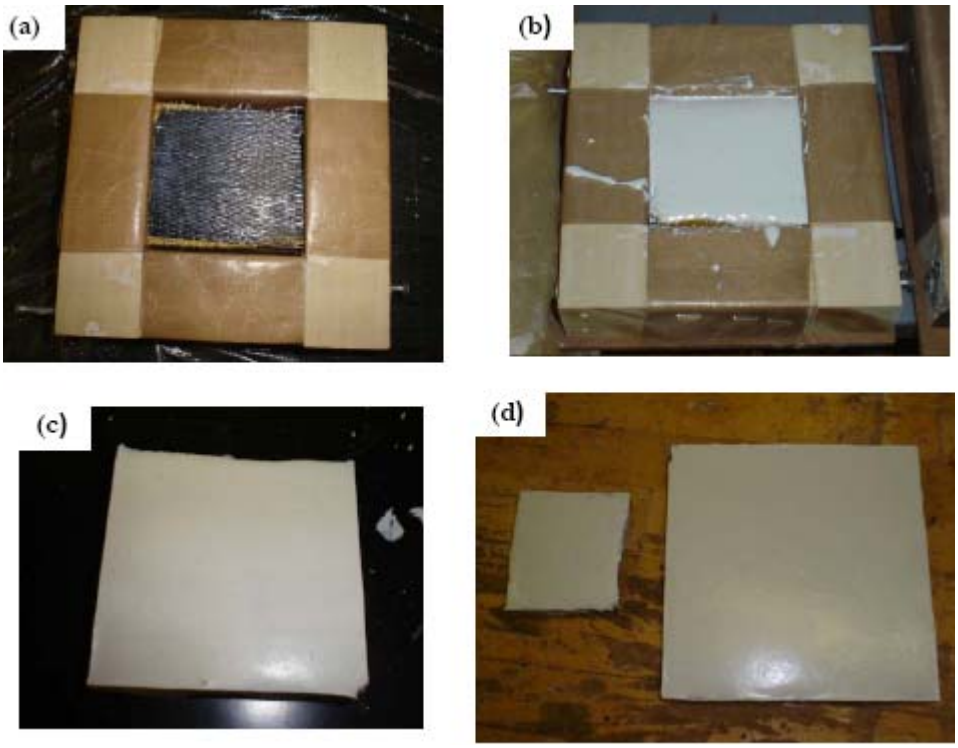

Figure 6.25 NBS sample preparation, (a) sample with unidirectional carbon, (b) After coating application, (c) sample before testing, (d) NBS and OSU samples before testing

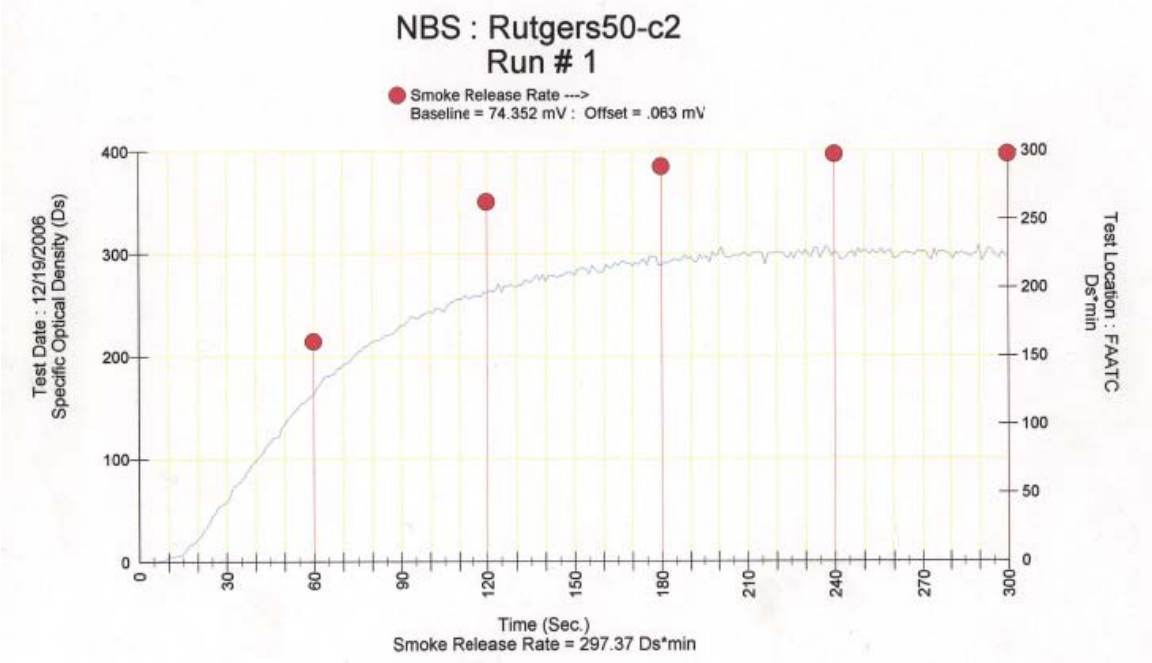

Figure 6.26 NBS test results for NBS-50-C2 (Control)

Figure 6.27 NBS-50-C2 tested sample

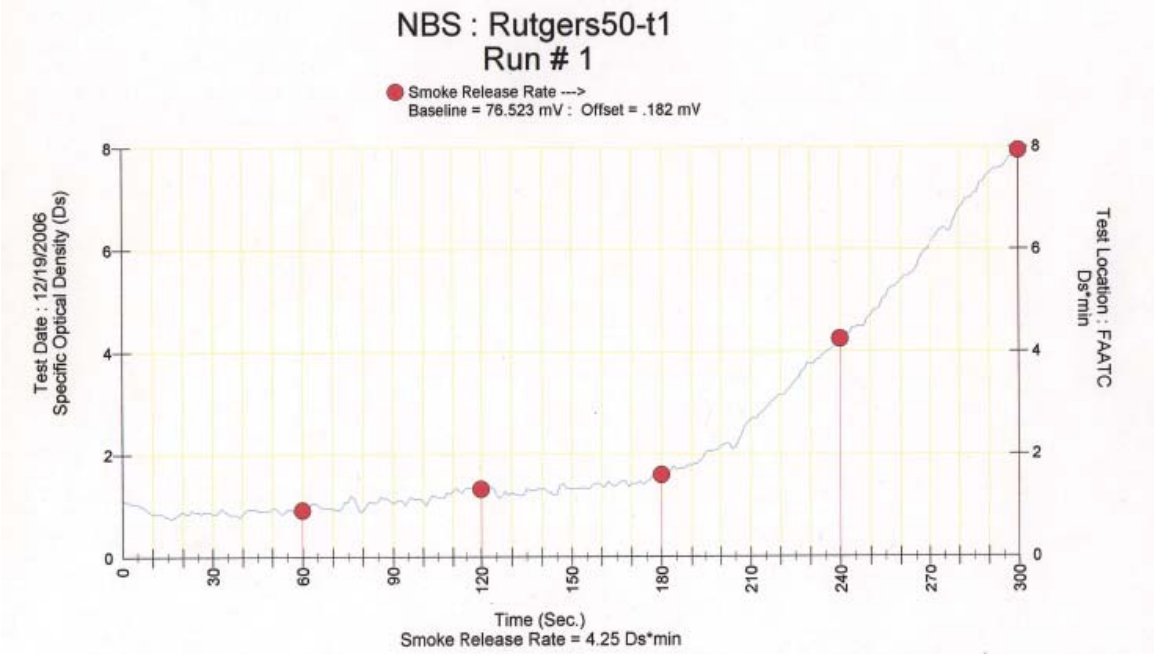

Figure 6.28 NBS test results for NBS-50-T1

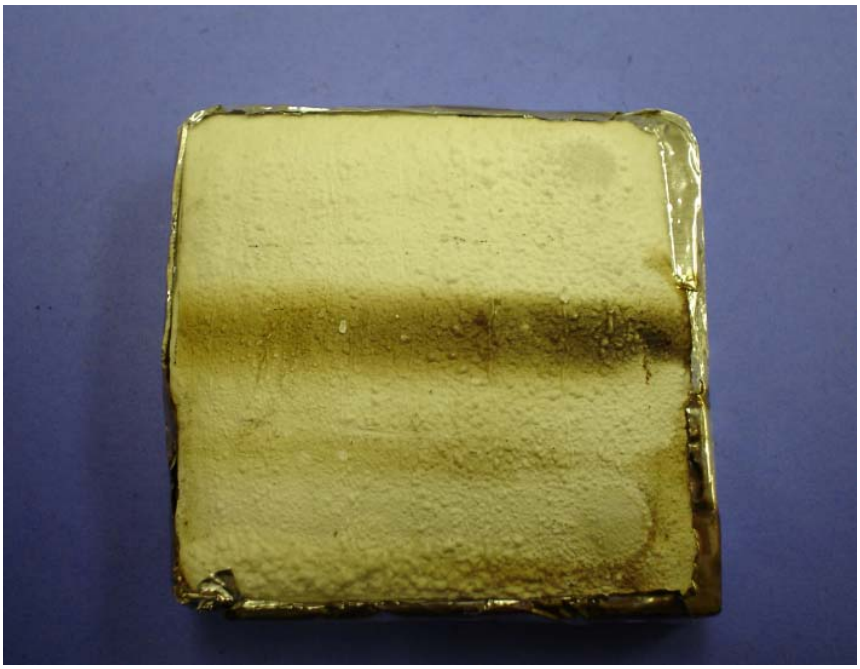

Figure 6.29 NBS-50-T1 tested sample

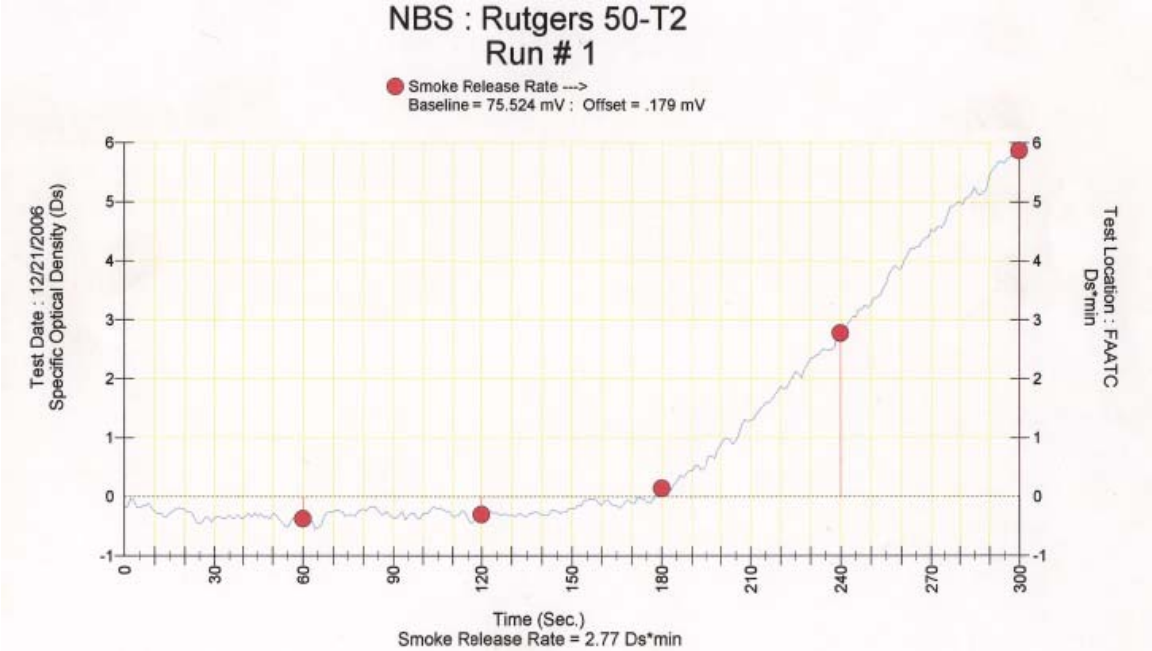

Figure 6.30 NBS test results for NBS-50-T2

Figure 6.31 NBS-50-T2 tested sample

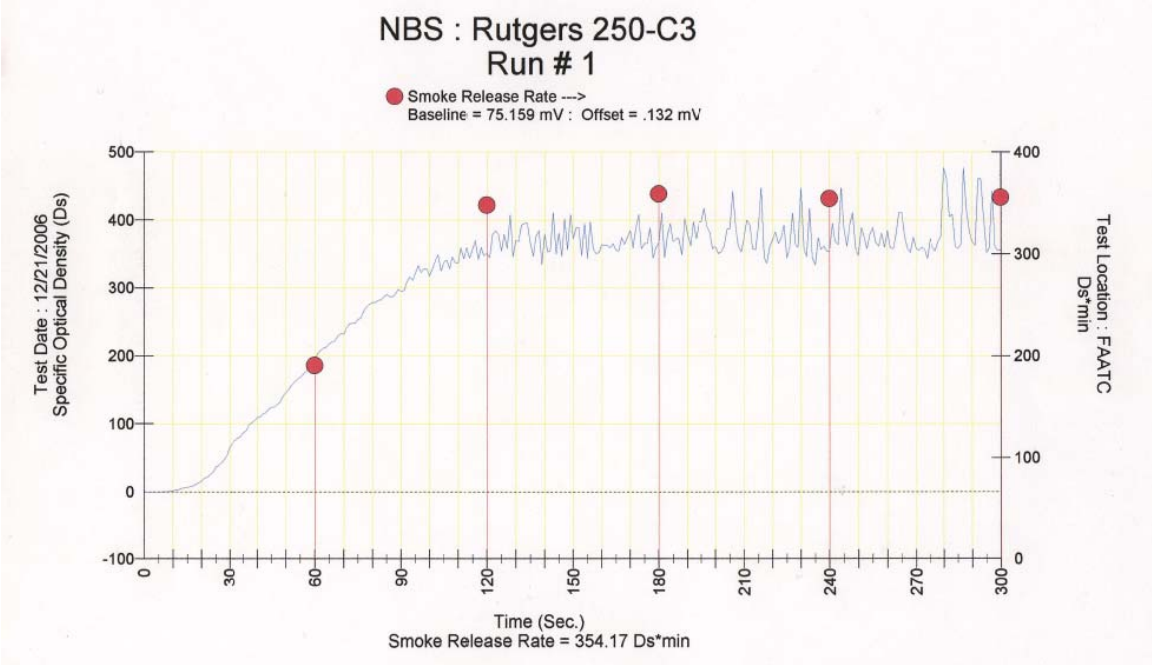

Figure 6.32 NBS test results for NBS-250-C3 (Control)

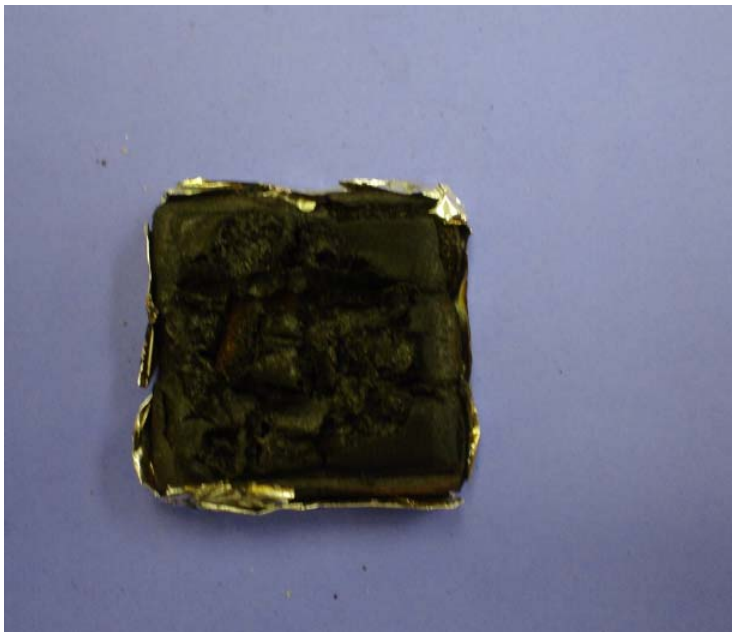

Figure 6.33 NBS-250-C3 tested sample

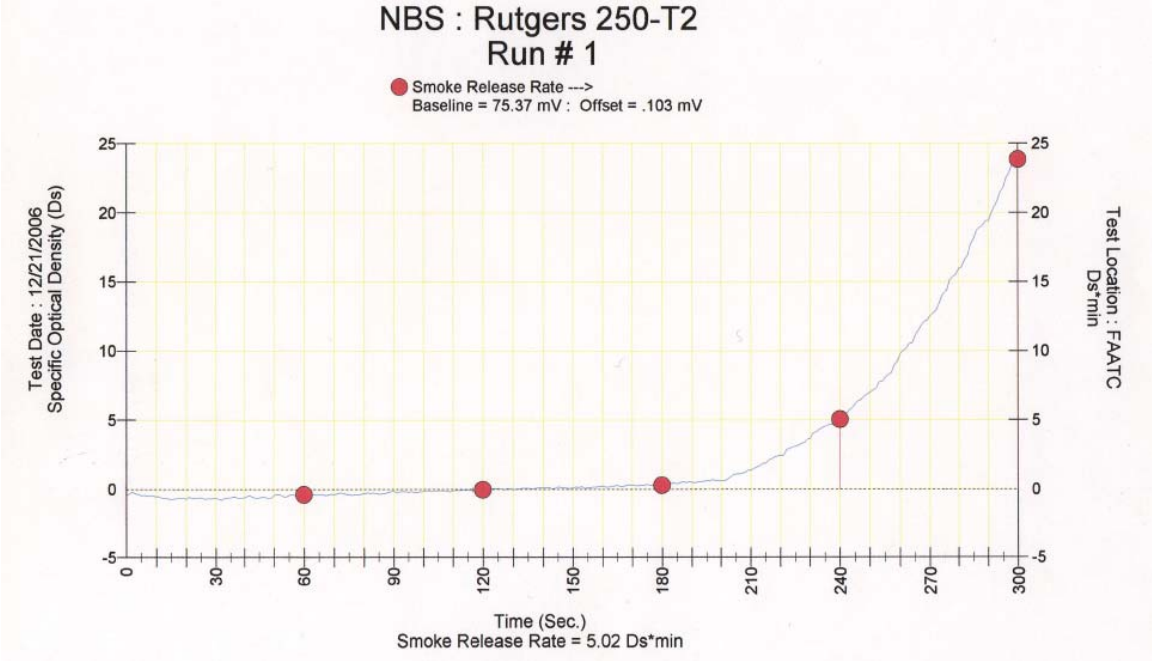

Figure 6.34 NBS test results for NBS-250-T2

Figure 6.35 NBS-250-T2 tested sample

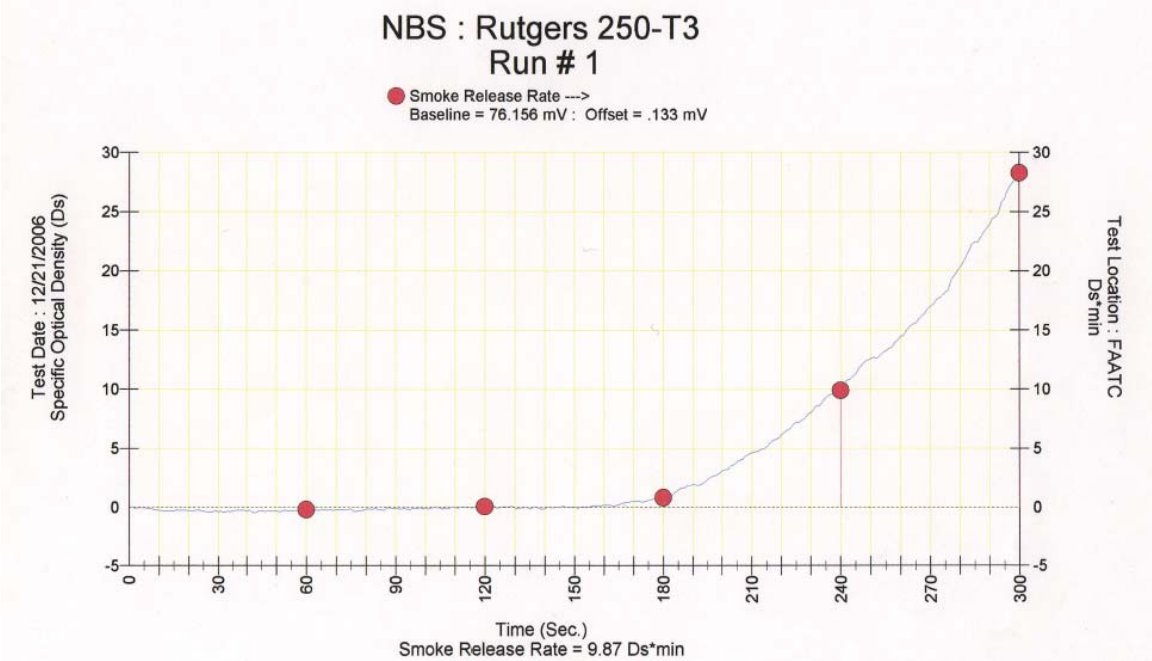

Figure 6.36 NBS test results for NBS-250-T3

Figure 6.37 NBS-250-T3 tested sample

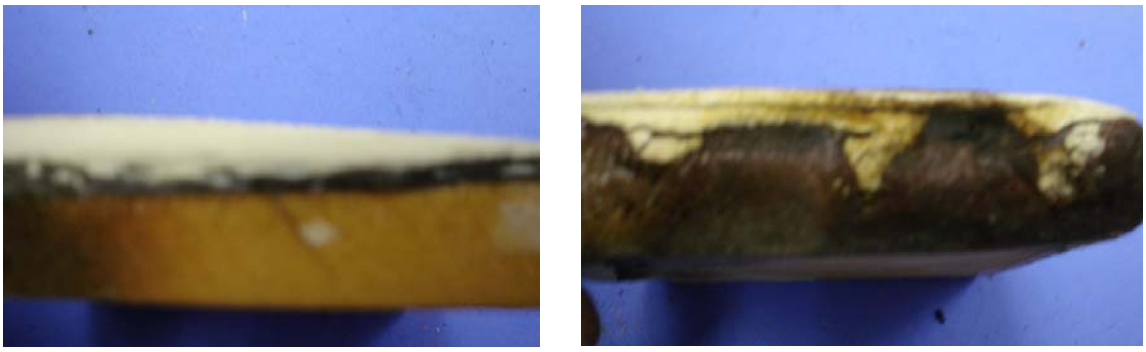

Figure 6.38 side photographs of (a) NBS-250-T2, (b) NBS-250-T3

Chapter 7

Flexural Strength of Sandwich Beams at High Temperature

7.1 Introduction

Sandwich panel construction is being extensively used for various structural applications from the building construction industry to the aerospace industry. Major world-wide consumption of composites is mostly in the marine and ship building industry. With their main advantages of relatively low cost, light-weight, durability in sea water, and good mechanical properties, the common organic structural sandwich panels have one major weakness in the area high-temperature resistance. They easily ignite generating large amount of smoke and in some cases toxic fumes. High temperature exposures also lead to structural failures. The mechanical properties of common sandwich construction, especially the ones having the PVC as a core, degrade dramatically with the increase of temperature. It was reported that composites of a thickness about 5 mm can lose more than 75% of their flexural strength after being exposed for 20 min to a heat flux of 25 KW/m^2. This value is equivalent to the heat emitted from low-to-medium fire (Sorathia et al., 1992).

A simple degradation function, shown in figure 7.1, illustrates the degredation of various mechanical properties with increase in temperature. The discrete data points correspond to the measured decrease in different mechanical properties like tensile, flexural, modulus, and strength for a 24 oz woven roving E-glass/vinylester composite. In figure 7.1, χ represents the different properties. It should be noted that the degradation represented in the figure is the reduction rather than the residual properties (Dao et al., 1999).

The flexural and compressive properties of glass reinforced polyester (GRP) plates were evaluated after fire exposure for 10 min. The tests were performed by placing the plates above a kerosene fuel fire. The average radiative intensity of the fire was about 30.3 KW/m^2. It was found that the remaining flexural strength was about 20 MPa after 10 minutes exposure for a sample that originally had 150 MPa when not exposed to a fire. Hence, the residual strength is 13% (Gardiner et al., 2004).

The results presented in this chapter deals with the effect of elevated temperature on the mechanical properties of sandwich beams reinforced with inorganic laminates. Chapter 6 provides basic information on the basic behavior of inorganic matrix at high temperature. This chapter focuses on flexural behavior of prisms at high temperature.

7.2 Research Program

Commercially available Divinycell™ closed-cell PVC foam was used for the entire program. The beam designations and details are presented in Table 7.1. For each designation, three identical beams were prepared and tested, resulting in a total of 36 beams.

The primary variables were: Core density, amount of reinforcement, and the level of exposure temperature.

7.2.1 Core density

Two densities were chosen for this study. PVC 50 Kg/m^3 and 250 Kg/m^3, which are the lightest and heaviest cores used in this study.

7.2.2 Reinforcement Thickness

A 3K unidirectional carbon tape was chosen for the skin This carbon tape was impregnated with inorganic matrix resin and placed on the core. One and two layers were used to study the effect of the reinforcement thickness on the high temperature behavior.

7.2.3 Exposure temperature

A heating element was used along with a current regulator. The heating element can produce heat up to 800^{o}C. Tests were conducted at room-temperature, 350^{o}C, and 700^{o}C.

7.3 Test Setup

After preparation, the sandwich beams were weighed to obtain the density and were tested under four points flexural test over a simply supported span. The test setup for the four-point flexure test is shown in Figure 7.3. Beams were tested using a 305 mm span. Aluminum flashings, as recommended by the ASTM, were used under the load points to avoid the mix between the deflection and the bearing failure readings. An MTS Sintech 10/GL was used to test the beams under deflection controlled procedures at deflection rate of 0.05 mm/min. A heating element was placed in the midspan as shown in figure 7.2. The heating element had a current regulator which allows the control of the heating element temperature. Using the dial regulator, the heating element was turned on and left for 10 minutes to guarantee that it reached the desired temperature. Then, the heating element was placed on the beam tension side and the test was set to start. A load that represents a fraction of the beam elastic limit (30 to 40%) was applied manually by a fine load tuner. This load was 120 N for sandwich beams made with PVC 50 Kg/m^{3}, and 320 N for beams made with 250 Kg/m^{3}. The deflection reading was reset to zero and the beams were exposed to high temperature. The test duration was 30 min for each beam. Each beam type was tested

under each of the aforementioned temperature to investigate the mechanical behavior of the sandwich beams. The load variation with time was recorded. A surface thermometer was used to measure the temperature on the far side (the compression side). Any smoke, fumes or smell detected were also recorded. Readings of load and deflection under the loading rollers were taken and the failure mode was recorded using photographs.

7.4 Test results

Table 7.1 shows that the additional weight for the PVC 50 Kg/m^3 due to the reinforcement is greater than the correspondent 250 Kg/m^3 ones. As it is shown in figures 7.8 and 7.12, the flexural strength of the beams when it is exposed to 350^{o}C was not affected for the PVC 50 Kg/m^3 reinforced with either one or two tapes.

When the temperature was increased to 700^{o}C, beams with 50 Kg/m^3 PVC and two carbon tapes did not loose any strength. It had the same behavior as the one tested in room-temperature and the one exposed to 350^{o}C, figure 7.9. The 50 Kg/m^3 core with one carbon tape did not behave similar to the not heated sample. The sample started deviating after about 4 minutes. The sample could resist additional load for another 11 minute, where its resistance becomes almost constant for another 10 minutes, then it starts loosing strength. Some smoke emission was detected during testing this beam.

For the 250 Kg/m^3 core, heated beams did not exhibit a behavior similar to the ones not exposed to heat. Beams reinforced with one tape and heated to 350^{o}C performed very close to the unheated one for about 17 minutes when a wrinkling failure, like the one shown in figure 7.7, was detected and the beam started to loose strength gradually for another 4 minutes before a sudden loss of strength occurred. On the other hand, the one heated to

700°C could only carry a load for 5 minutes when wrinkling occurred on the compression side and the beam failed, this can be seen in figure 7.10.

For the 250 Kg/m^3 core reinforced with two tapes, the beam exposed to 350°C exhibited a behavior very close to the unheated one. The beam heated to 700°C, performed in the same manner as both the unheated and the heated to 350°C beams for 10 minutes. Then, it started deviating gradually until it failed after 25 minutes due to wrinkling on the compression side, as shown in figure 7.11.

As shown in the bar charts in figures 7.12 to 7.15, beams with core of PVC 50 Kg/m^3 could maintain almost 100% of its capacity up to 700°C for beams reinforced with two tapes and up to 350°C for beams reinforced with one tape. Beams reinforced with one tape and heated to 700°C maintained 78% and 38% of its strength after 15 and 30 minutes, respectively. Beams made out of 250 Kg/m^3 core reinforced with one tape maintained 92% and 31% for 15 and 30 minutes, respectively, when it was exposed to 350°C. Similar beam exposed to 700°C maintained 40% and 30% of their strength after 15 and 30 minutes, respectively. When reinforced with two tapes, beams maintained more than 95% up to 30 minutes for an exposure of 350°C. For 700°C, the beam upheld 90% for its strength after 15 minutes, and 20% after 30 minutes.

7.5 Summary and observations

Based on the results discussed previously, it could be seen that:

- After 5 minutes of exposure to temperature up to 700°C, all the samples sustained more than 90% of their strength. This should be sufficient for the fire fighter crew to extinguish a small fire on a ship or for passengers to escape from an airplane in a post-crash scenario.

- Although, the effect of the heating element used in this study could be considered a localized effect, small fire on a ship with a hull made of this inorganic composite system is also localized.
- The performance of cores made with PVC 50 Kg/m^3 was better. The reason is this core absorbed more Geopolymer resin, which improved the mechanical behavior by providing some confinement for the cell walls. This prevented them from buckling and deforming, which barred the wrinkling from occurring. It improved the fire characteristics as well, by providing an extra layer of fire proof material. This can be easily verified by comparing the weight gained from the reinforcement for both core types.
- For up to 30 minutes, the system showed an acceptable level of integrity by sustaining 20% of its strength after being exposed to 700ºC.
- The top surface temperature decreased with the increase of the core density and the thickness of reinforcement.
- It should be mentioned that when this test is performed with an epoxy/carbon system, the heating element just cut through the materials with no noteworthy resistance.

Table 7.1 Sample details

Sample	Core Density	Reinforcement	Original		Before Test		Additional Weight	Reinforcement Thickness
			Weight	Thickness	Weight	Thickness		
	Kg/m^3		gm	mm	gm	mm	gm	mm
T50-1C-1T-RT	50	One Layer	12.50	13.06	54.9	14.01	42.40	0.47
T50-1C-1T-350	50	One Layer	12.70	13.19	58.8	14.02	46.10	0.42
T50-1C-1T-700	50	One Layer	12.60	13.00	59.9	14.01	47.30	0.51
T50-2C-2T-RT	50	Two Layers	13.20	12.94	75.2	14.46	62.00	0.76
T50-2C-2T-350	50	Two Layers	13.00	12.94	68.3	14.39	55.30	0.73
T50-2C-2T-700	50	Two Layers	13.00	12.96	78.1	14.48	65.10	0.76
T250-1C-1T-RT	250	One Layer	57.70	12.90	83.8	13.68	26.10	0.39
T250-1C-1T-350	250	One Layer	57.90	12.88	86.8	13.7	28.90	0.41
T250-1C-1T-700	250	One Layer	57.60	12.89	85.2	13.67	27.60	0.39
T250-2C-2T-RT	250	Two Layers	57.40	12.92	101.5	14.19	44.10	0.64
T250-2C-2T-350	250	Two Layers	57.50	12.82	99.3	14.1	41.80	0.64
T250-2C-2T-700	250	Two Layers	57.10	12.83	100.9	14.04	43.80	0.61

Table 7.2 Test observations

Sample	Final Weight	Weight Lost	Top Surface Temp	Observations
	gm	gm	^oC	
T50-1C-1T-RT	54.9	0	25	
T50-1C-1T-350	58.5	0.3	65	
T50-1C-1T-700	59.4	0.5	100	some smoke
T50-2C-2T-RT	75.2	0	25	
T50-2C-2T-350	68	0.3	50	
T50-2C-2T-700	77.6	0.5	75	No smoke, just smell
T250-1C-1T-RT	83.8	0	25	
T250-1C-1T-350	86.3	0.5	60	Smoke and smell. Wrinkling
T250-1C-1T-700	84.3	0.9	80	Smoke and smell. Wrinkling
T250-2C-2T-RT	101.5	0	25	
T250-2C-2T-350	99.1	0.2	50	
T250-2C-2T-700	100.3	0.6	60	Smoke and smell. Wrinkling

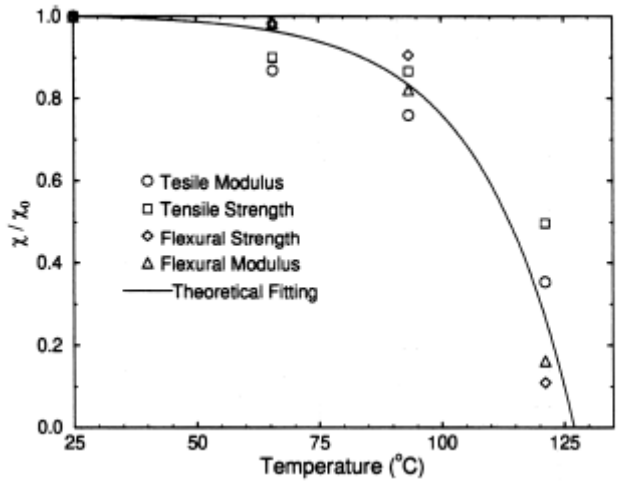

Figure 7.1 Property degradation curve for 24 oz woven roving E-glass/vinylester composite (Dao et al., 1999)

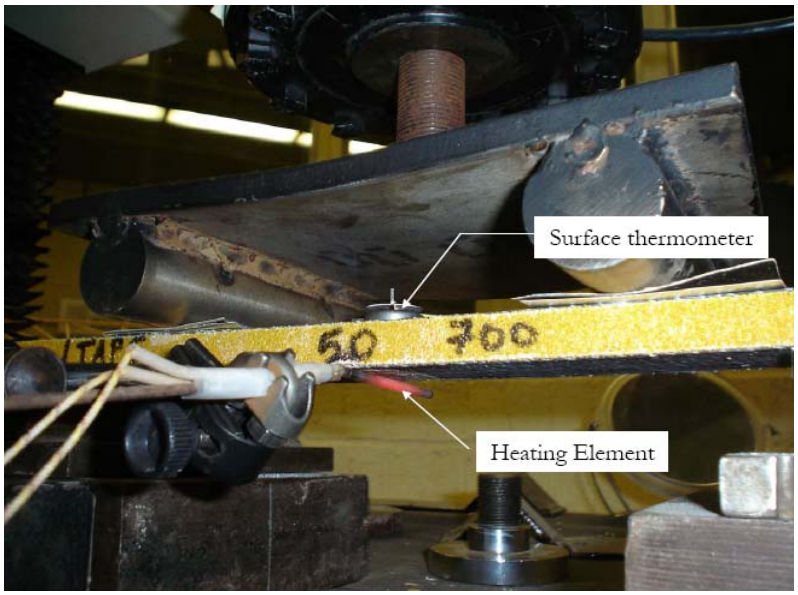

Figure 7.2 Heating element setup

Figure 7.3 Flexural test setup

Figure 7.4 Current regulator

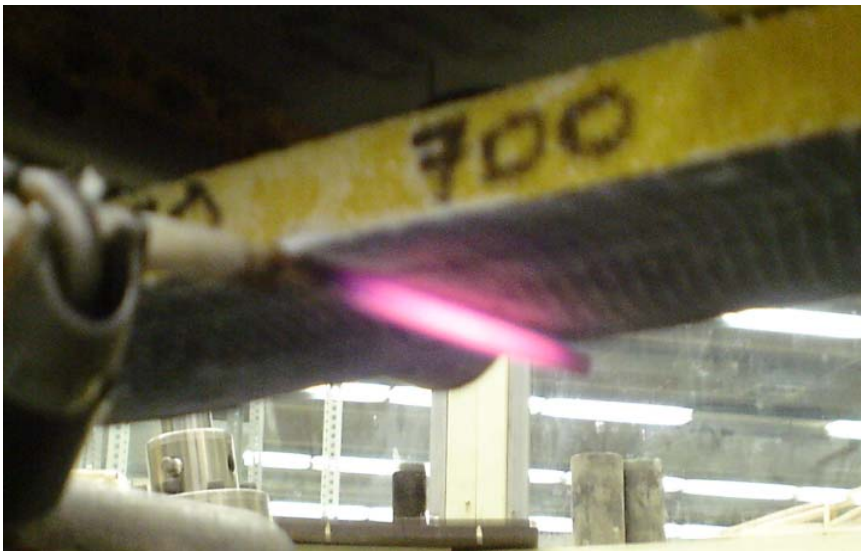

Figure 7.5 Heating element at 700ºC

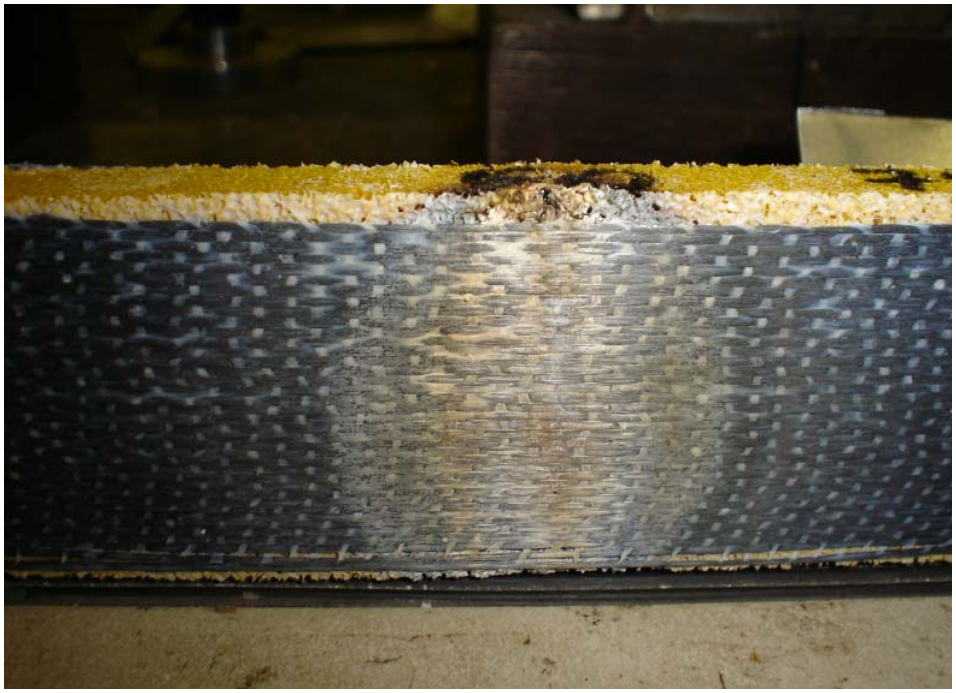

Figure 7.6 Beam tension side after testing

Figure 7.7 Beam compression side after testing

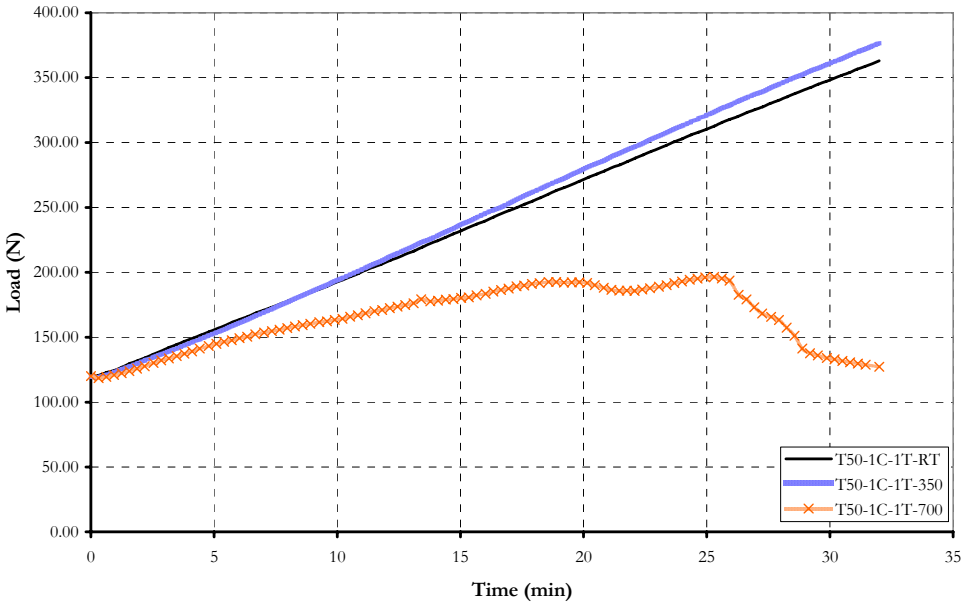

Figure 7.8 Test results for 50 Kg/m^3 PVC core with one tape

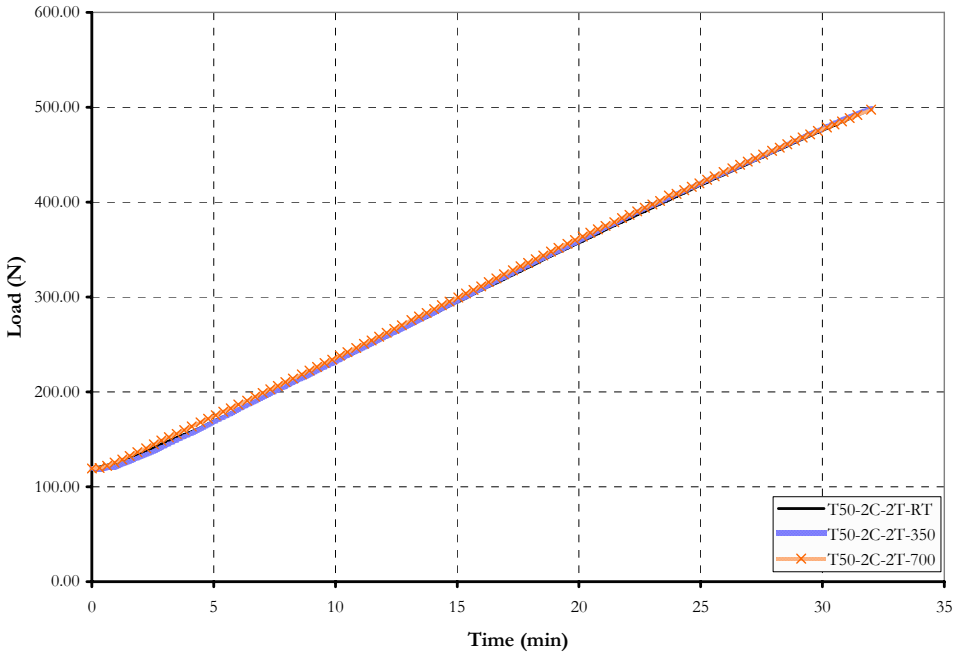

Figure 7.9 Test results for 50 Kg/m^3 PVC core with two tapes

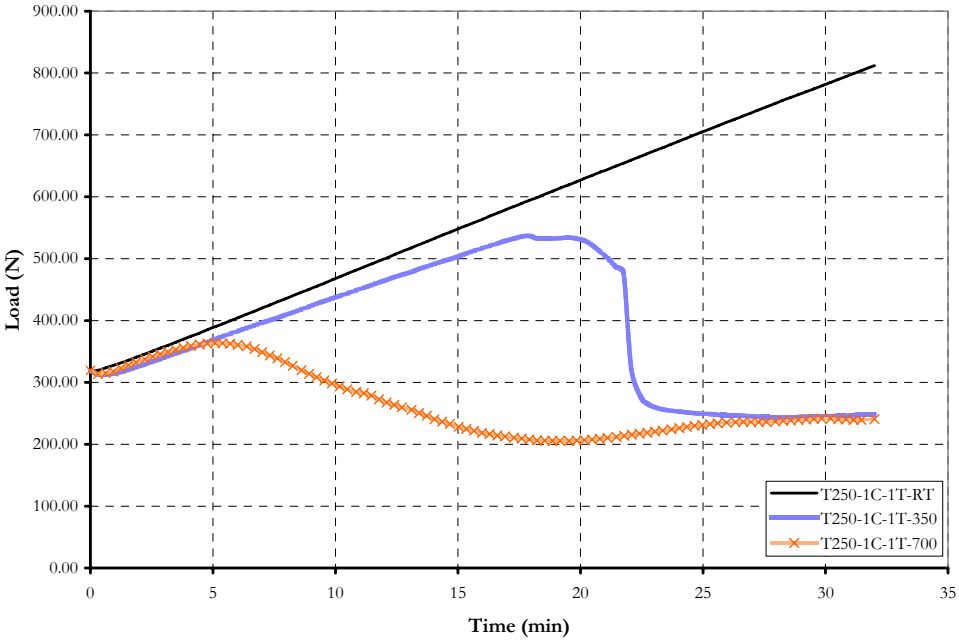

Figure 7.10 Test results for 250 Kg/m^3 PVC core with one tape

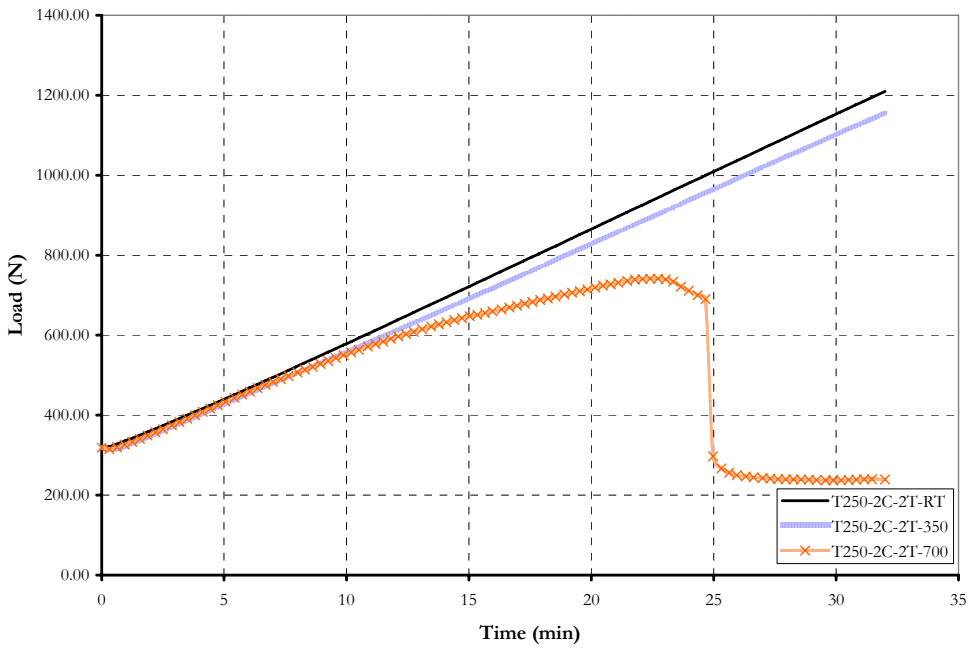

Figure 7.11 Test results for 250 Kg/m^3 PVC core with two tapes

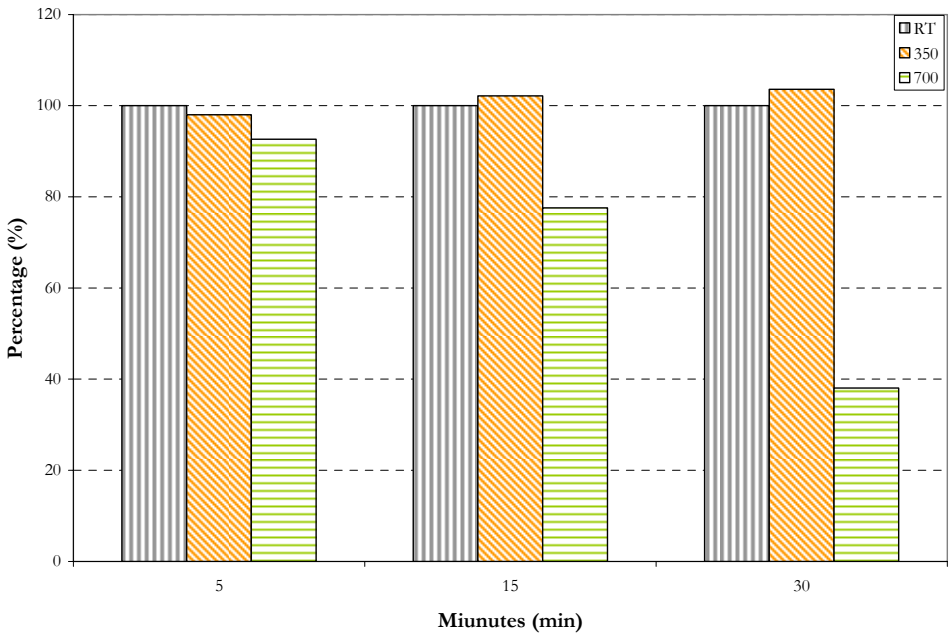

Figure 7.12 Remaining strength for 50 Kg/m^3 PVC core with one tape

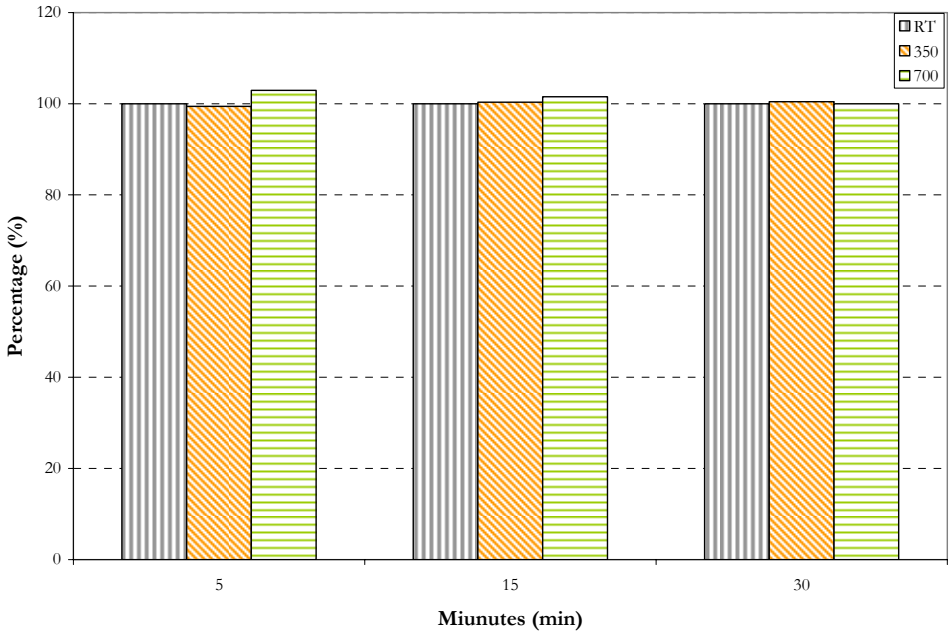

Figure 7.13 Remaining strength for 50 Kg/m^3 PVC core with two tapes

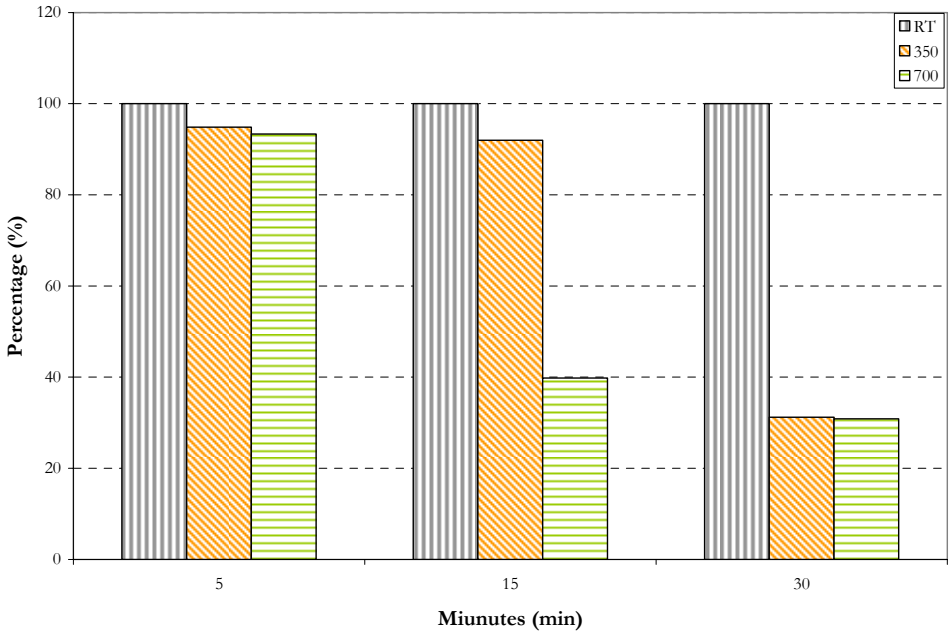

Figure 7.14 Remaining strength for 250 Kg/m^3 PVC core with one tape

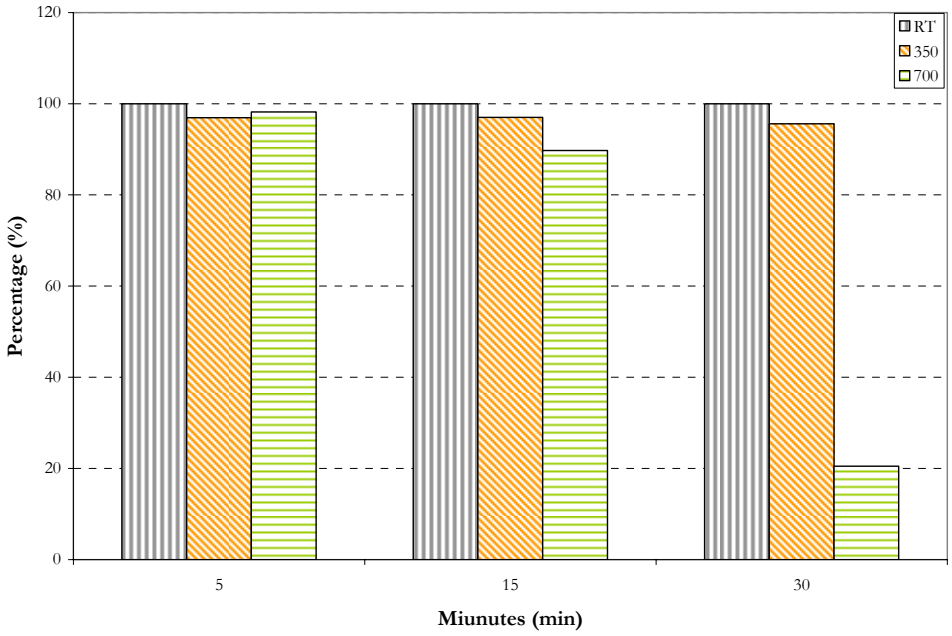

Figure 7.15 Remaining strength for 250 Kg/m^3 PVC core with two tapes

Chapter 8

Preliminary Study of High Temperature Inorganic Core Sandwich Beams

8.1 Introduction and background

Syntactic foams consist of a binder, which is a polymer matrix and gas-filled spheres (filler). The filler is in the form of hollow spherical particles, called microspheres, microcapsules or microballons, dispersed within the matrix. Syntactic foams are considered foamed plastics because they are similar in structure to cellular gas-expanded plastics in that they are heterophase, gas-solid systems. However, they differ from other foamed plastics in that the filler and the binder are not made from the same material. Syntactic foams are tertiary, and the conventional foams are binary (Shutov, 1982).

The cells in syntactic foams are closed, so they have better strength-to-weight ratio and very small water absorption properties compared to the conventional ones. The syntactic foams have heavier apparent densities than the conventional foams (Karthikeyan et al., 2004).

In their study, syntactic foams were prepared by mixing epoxy resin with glass hollow microspheres and chopped E-glass fibers, and then tested in compression and flexure. The incorporation of chopped fibers into the system improved the elastic properties and the strength of foam without increasing the density. The flexural strength ranged between 37 and 49 MPa for densities of 0.67 to 0.72 g/cc (Karthikeyan et al., 2004 and 2005).

In another study, inorganic microspheres were used with phenolic resin to produce phenolic foams that led to the improvement of mechanical and fire retardant properties. The foam had a density of 0.8 g/cc and flexural strength between 9.3 and 27.5 MPa depending on the

microspheres type. It also exhibited temperature resistance up to 300°C (Okuno et al., 1974). Phenolic based foam, Alba-Core®, a combination of hollow glass microspheres and phenolic matrix, was studied. Alba-Core® with a density of 0.2 g/cc was reinforced with fiberglass/phenolic system. The flexural strength was 3.2 MPa for the core and 14 MPa for sandwich composite. The system exhibited a temperature resistance up to 205°C (Tessier, 2001).

Research was also carried out to study the effect of change in the internal radius in cenospheres on the compression strength. The syntactic foams were made from epoxy resin and five different types of Scotchlite cenospheres. The compressive strength increased from 30 to 72 MPa with the decrease of the inner to outer radius ratio from 0.922 to 0.863. The volume fraction was kept at 0.35 (Gupta et al., 2004). The flexural strength did not change with the radius ratio (Gupta et al., 2005).

Ceramic foams were also made by incorporating cenospheres into a silicon carbide matrix. A pyrolysis procedure was carried out in a box furnace, and a continuous flow of ultra high-purity nitrogen was used to prevent material oxidation. Pyrolysis cycles up to 900°C were used for curing. Reinfiltration cycles were used to achieve optimal densification and to reduce material porosity. The usage of 0 to 8 cycles of reinfiltration increased the density from 0.48 to 1.6 g/cc. The flexural strength increased from 6 to 30 MPa with the density increase. The flexural modulus and compressive strength followed the same behavior with the increase in density (Ozcivici, 2005).

In another study, syntactic foam was prepared by mixing ceramic spheres (Macrolite™) with a Geopolymer matrix. Different mixing ratios and sphere sizes were used, and their effect on the density was recorded. The syntactic foam was tested in tension and compression, and

had the values of 3.7 and 39 MPa, respectively. The samples retained their compressive strength after exposure to 800°C for 15 minutes (Papakonstantinou et al., 2005).

8.2 Scope of the current investigation

The Primary objective of the research presented in this chapter is to develop a lightweight structural element that can withstand 1050°C. The results presented in the previous chapters deal with the sandwich panels incorporating organic foams. Organic foam is conducive for producing flexible lightweight components but has limitation on fire resistance. The preliminary investigation reported in this chapter attempt to fabricate a structural element with least weight but can withstand high temperatures with no weak links. Two avenues were pursued to obtain high temperature composites. One strategy was to create a sandwich structure with inorganic foam and the other strategy was to formulate a homogeneous fiber composite. The results for homogenous fiber composite were evaluated by DeFazio can be found in the reference (DeFazio, 2007).

This chapter deals with sandwich structures. The concept is similar to the one followed by Papakonstantinou but ceramic fibers were used for the skin instead of carbon and silicon carbide fibers. Cenospheres were used to create the syntactic foam instead of Macrolite (Papakonstantinou, 2003).

8.3 Research program

The primary variables for the evaluation were the core density and the amount of reinforcement for skins. Three densities and three reinforcement ratios were evaluated. The density of the core varied by changing the content of cenospheres. Three different weight ratio contents are used. The flexural properties of sandwich beams having the syntactic foam as core and ceramic fibers as skin were evaluated in room temperature, and after having been

exposed to 1050°C for 30 minutes. The cenospheres and the ceramic fibers properties are presented in tables 2.3 and 2.6, respectively. It should be noted that cenospheres have 1200°C as melting temperature and the ceramic fibers loose 65% of their strength when exposed to high temperature (3M, 2004).

8.4 Samples preparation

The sample preparation process starts by preparing a Geopolymer matrix by mixing part A (liquid) and part B (powder) using a high shear mixer. Cenospheres were added to the mix on three stages to ensure a homogenous mixing. The weight ratios for the fillers were 30, 40, and 50 percent. After mixing, the slurry was poured into molds and left to dry out for a week. Then, the foam was taken out of the mold and cut in smaller beams using a dry-saw. A slow heating process was used to cure the samples by heating them for four hours at 150°C then for an additional two hours at 200°C.

Ceramic tows were used to fabricate the sandwich beams. One side was reinforced then left to dry out overnight before reinforcing the other sides. Then, the samples were left in the oven for two hours at 150°C to cure the facings resin.

8.5 Test results

After curing, the samples were grouped based on the fillers content (30%, 40%, and 50%) and the skin reinforcements (no reinforcement i.e. control samples, 1 tow each side, and 2 tows each side), resulting in nine different groups with six beams each. Then, three beams were taken from each group and put in an oven at 1050°C for 30 minutes. Finally, the flexural properties of all the samples were evaluated using a three-points bending test. The apparent stress was calculated using.

$$\sigma = \frac{6PL}{4bh^2} \tag{8.1}$$

P is the applied load, L is the span, b is the beam width, and h is the beam thickness.

Samples tested without being exposed to 1050°C, are designated starting with "R", and the exposed ones started with "H". The letter is followed by a number indicating the filler weight ratio, then a description of the reinforcement. The apparent stresses versus the deflection of the different samples are presented in figures 8.1 to 8.9.

The density of different mixes was measured according to ASTM D1622 (ASTM, 2002). It was found that for 30% mix the density was 0.91 gm/cc, and for the 40 and 50% the density was 0.89 gm/cc. After heating the samples, the weight and sample dimensions did not significantly change and the density stayed constant.

8.5.1 Strength results before heating

For the control samples, the flexural strength was: 2, 4 and 3 MPa for 30%, 40% and 50%, respectively. By adding one tow of ceramic fibers, the apparent flexural strength increased to 8 MPa for the 30% mix and 9 MPa for the 40 and 50% mixes. The area of cross section of the core was 77 mm^2 and the area of one tow was 0.24 mm^2 and therefore for one tow the reinforcement ratio was 0.31%. For samples reinforced with two tows, the apparent flexural strength was: 12, 11 and 18 MPa for 30%, 40% and 50%, respectively. Except for the 50% mix, doubling the reinforcement area did not double the strength. A summary of the strength results are presented in figure 8.10.

8.5.2 Strength results after heating

Generally, the control samples gained strength due to heating; this can be seen in figure 8.11. The 50% mix was the most affected due to the heat exposure, while the 30% mix was the

least affected. The retention ratio decreased with the increase of number of tows, which gave way to the conclusion that the decrease was driven by the skin more than the core.

8.5.3 Modulus results before heating

The modulus was calculated using the equation

$$E = \frac{\Delta P}{\Delta \delta} \frac{L^3}{48I} \tag{8.2}$$

$\Delta P/\Delta\delta$ is the slope of the load-deflection curve and I is the moment of inertia of the cross section.

For the control samples, the modulus was about 3.5 GPa. The modulus increased with the filler content and the increase of reinforcement as anticipated. This increase was not linearly proportional with the fibers area. A summary of the modulus of elasticity is shown in figure 8.12.

8.5.4 Modulus results after heating

After heating, the modulus exhibited higher values for the control samples. By investigating figure 8.13, all the samples maintained at least 90% of their modulus before heating, except for the 40% mix reinforced with one tow. This sample originally showed an odd modulus value.

8.6 Comparison with previously developed inorganic systems

In order to evaluate the comparative performance of the inorganic sandwich core presented in this chapter, the results are compared with other inorganic high temperature systems. Homogenous fiber composites were evaluated by DeFazio (DeFazio, 2007). The composites were composed of inorganic alumina/silica mix reinforced with various types of discrete

fibers. Sample fabrications and details can be found in his master thesis (DeFazio, 2007). Inorganic cores were prepared using Macrolite™ spheres and reinforced with carbon tows and silicon carbide fibers by Papakonstantinou (Papakonstantinou, 2003). Only the beams with silicon carbide skin will be considered in the comparison because beams reinforced with carbon skin loose more than 80% of its strength after being exposed to 600°C because of the oxidization of carbon fibers, which is a relatively low temperature compared to 1050°C.

Two performance indices were used to compare different systems. These indices do not have a physical significant but they account for the critical performance criteria in high temperature resistant materials: the maximum temperature exposure, the density, the strength retention and the specific strength (Strength by unit weight).

$$I_1 = \frac{SRP \times T}{1000 \times \rho} \tag{8.3}$$

I_1 is the first performance index, SRP is the strength retention percentage, T is the maximum temperature exposure and ρ is the density.

$$I_2 = \frac{SS \times T}{1000} \tag{8.4}$$

I_2 is the second performance index and SS is the specific strength.

The results presented in Table 8.1 for the comparison lead to the following observations:

- The inorganic core sandwich structures have lower densities (0.7 and 0.89 gm/cc) than the homogenous fiber composites (1.7, 2.5, 2.6, and 2.7 gm/cc).
- The cenospheres core/ceramic fiber skin beams have high strength retention (80%), which is as high as the homogenous fiber composites (82%).
- Combining the effect of strength retention, maximum temperature, and density, the first performance index is the highest for the cenospheres core/ceramic fiber skin

(94.4) and the second highest is the homogenous fiber composite bulk alumina (32.3).

- The second performance index is highest for homogenous fiber composite chopped ceramic fibers (30.2).
- Comparing the two sandwich structures, the cenospheres core/ceramic fiber skin beams have higher strength retention (80% versus 25%), specific strength (9.0 versus 3.9 MPa.cc/gm), first performance index (94.4 versus 28.6), and second performance index (9.5 versus 3.1).
- The specific strength of the homogenous fiber composite is higher than the sandwich structures. But, the sandwich structure is very efficient when the total weight is a design concern

8.7 Observations

The following additional observations pertain to the evaluation of cenosphere composites:

- It is feasible to produce inorganic syntactic foams by mixing cenospheres and Geopolymer matrix. The mixes exhibit shrinkage and sometimes lead to cracking during curing. The author believes that these cracks could be controlled by introducing chopped fibers into the mix.
- Flexural properties of the core (strength and stiffness) improve after the exposure to 1050^{o}C.
- The reinforced samples lost strength, which is confirmed by the literature available about the ceramic fibers having tendency to loose 65% of strength at 1050^{o}C (3M, 2004).
- The workability of the slurry decreased with the increase of the filler content.

Table 8.1 Comparison between various high temperature inorganic composites

Composite		Max. Temperature Exposure	Density	Strength Retention	Specific Strength	Performance Index 1	Performance Index 2
		°C	gm/cc	%	MPa/(gm/cc)	I_1	I_2
Homogenous Fiber Composite	Alumina Ply[1]	1050	1.7	48	7.0	29.6	7.4
	Carbon[1]	1050	2.7	82	16.7	31.9	17.5
	Bulk Alumina[1]	1050	2.5	77	20.0	32.3	21.0
	Chopped ceramic fibers[1]	1050	2.6	58	28.8	23.4	30.2
Sandwich Structure	Macrolite Core/Silicon carbide skin[2]	800	0.7	25	3.9	28.6	3.1
	Cenospheres Core/Ceramic fiber skin	1050	0.89	80	9.0	94.4	9.5

[1] Defazio, 2007 [2] Papakonstantinou, 2003

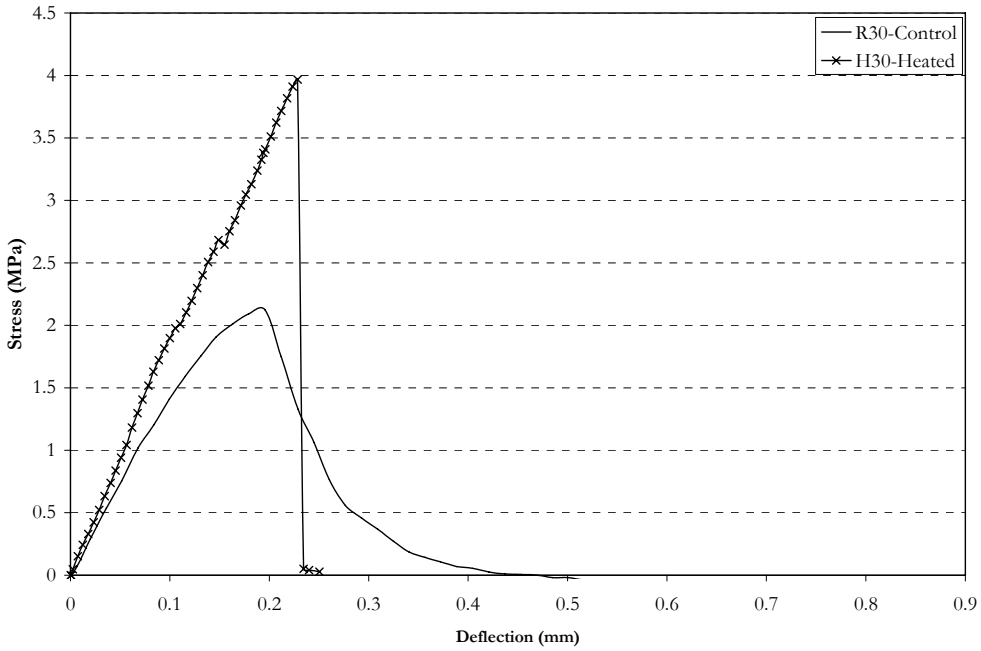

Figure 8.1 Test results for 30% mix-control samples

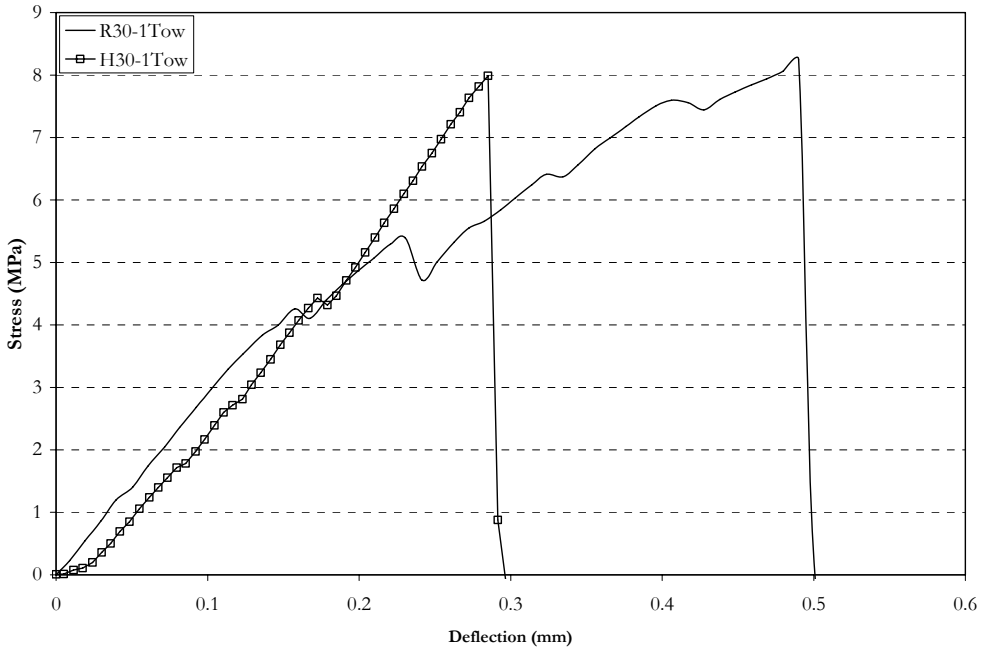

Figure 8.2 Test results for 30% mix-Samples reinforced with 1 tow

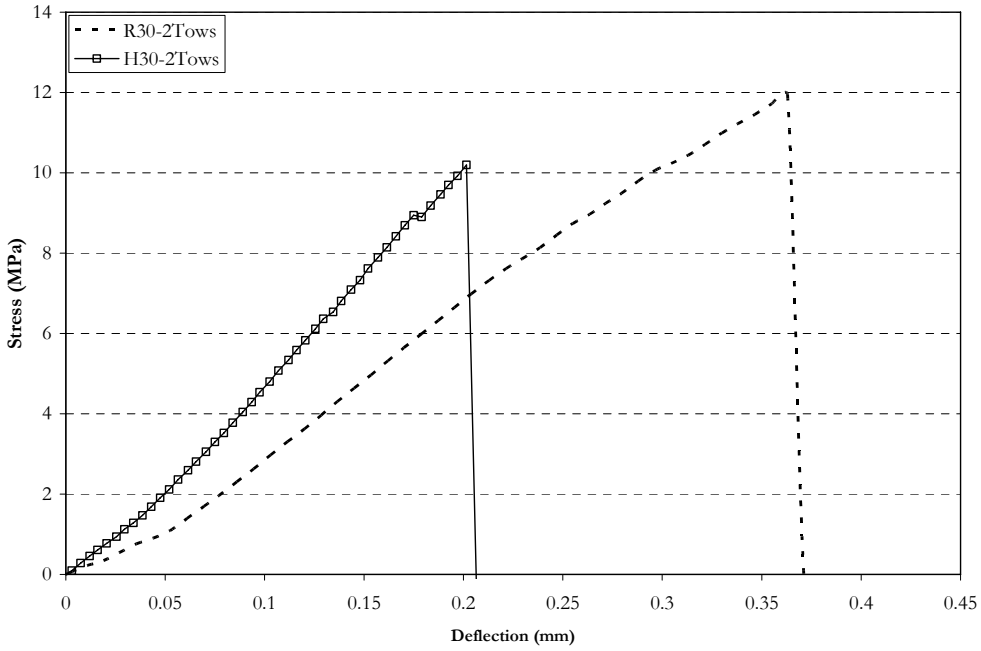

Figure 8.3 Test results for 30% mix-Samples reinforced with 2 tows

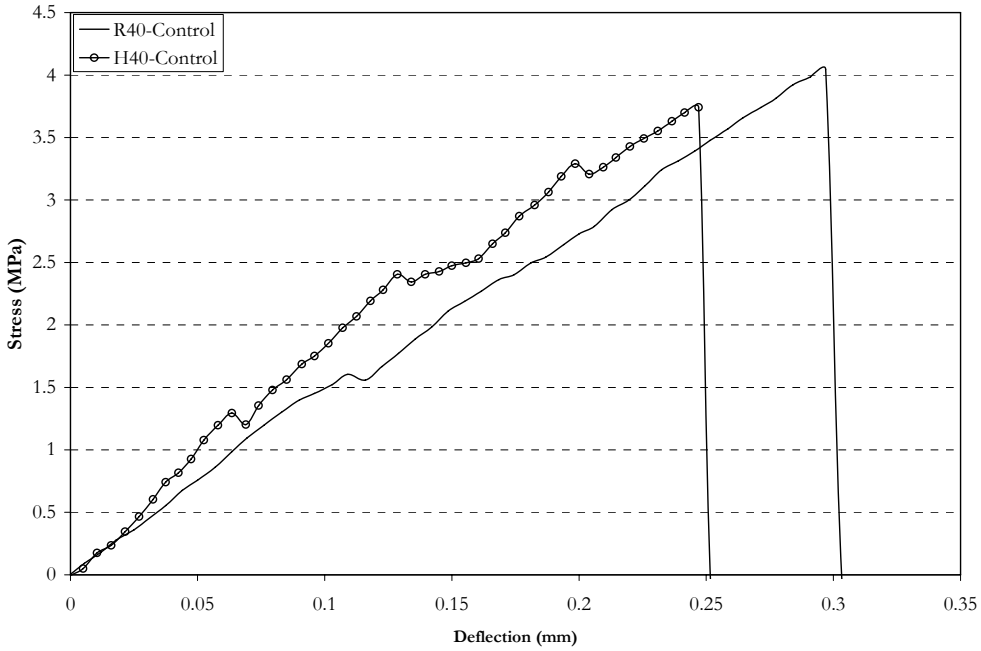

Figure 8. 4 Test results for 40% mix-control samples

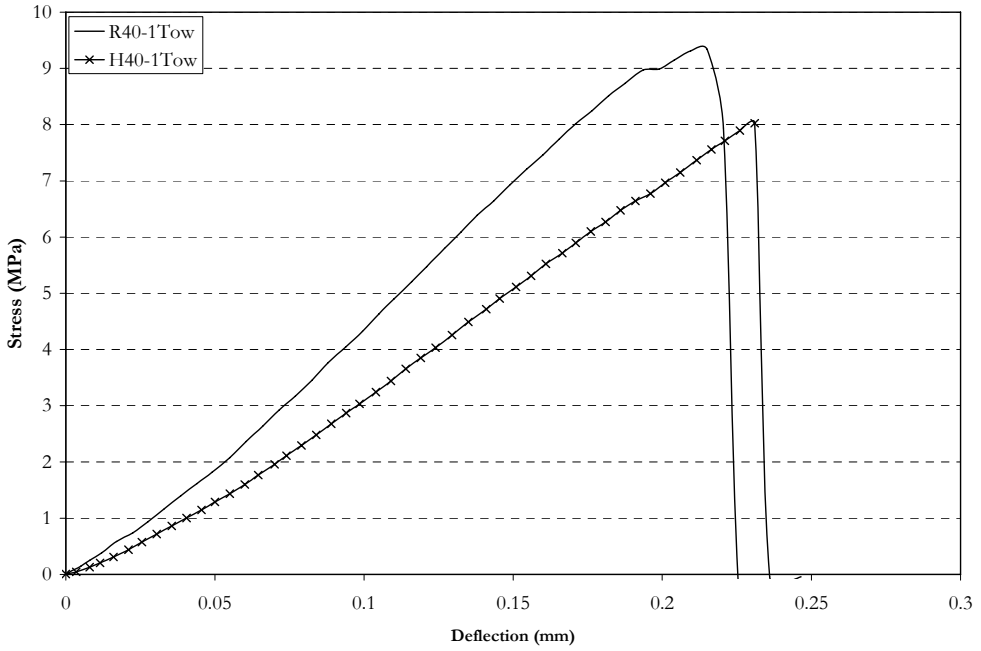

Figure 8.5 Test results for 40% mix-Samples reinforced with 1 tow

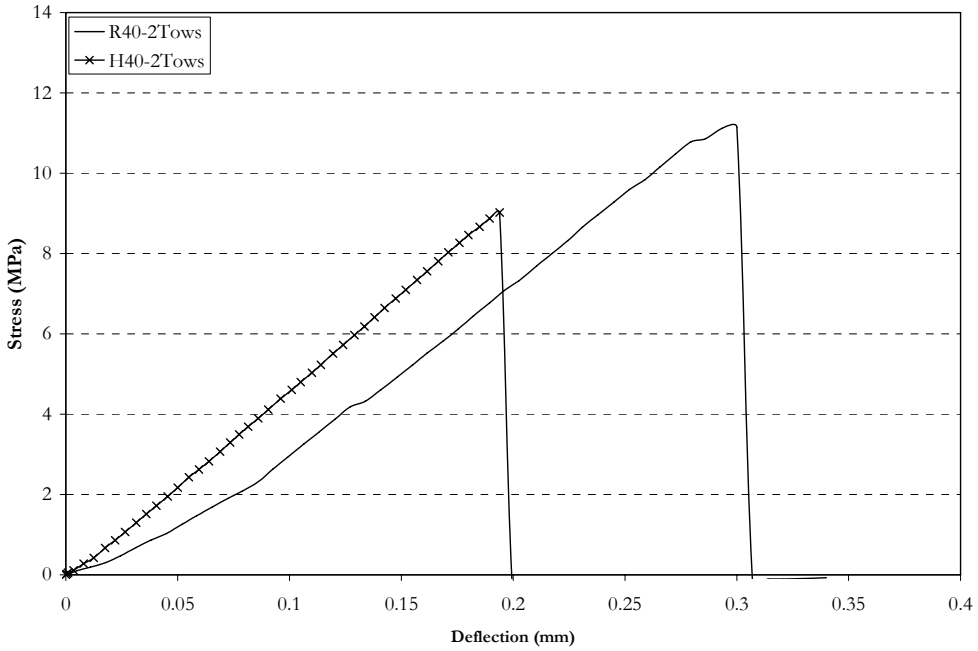

Figure 8.6 Test results for 40% mix-Samples reinforced with 2 tows

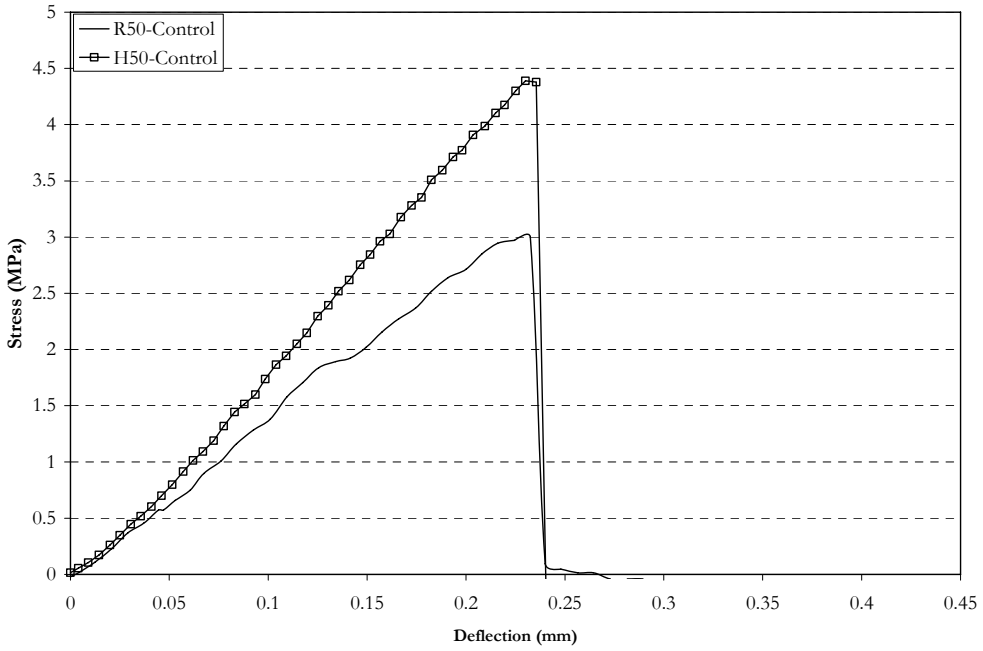

Figure 8.7 Test results for 50% mix-control samples

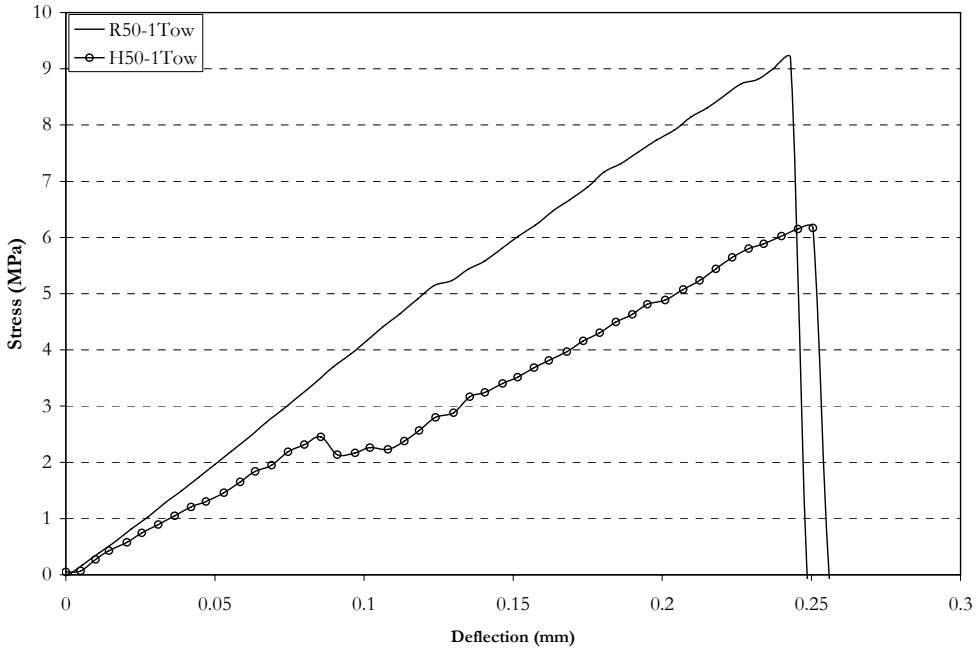

Figure 8.8 Test results for 50% mix-Samples reinforced with 1 tow

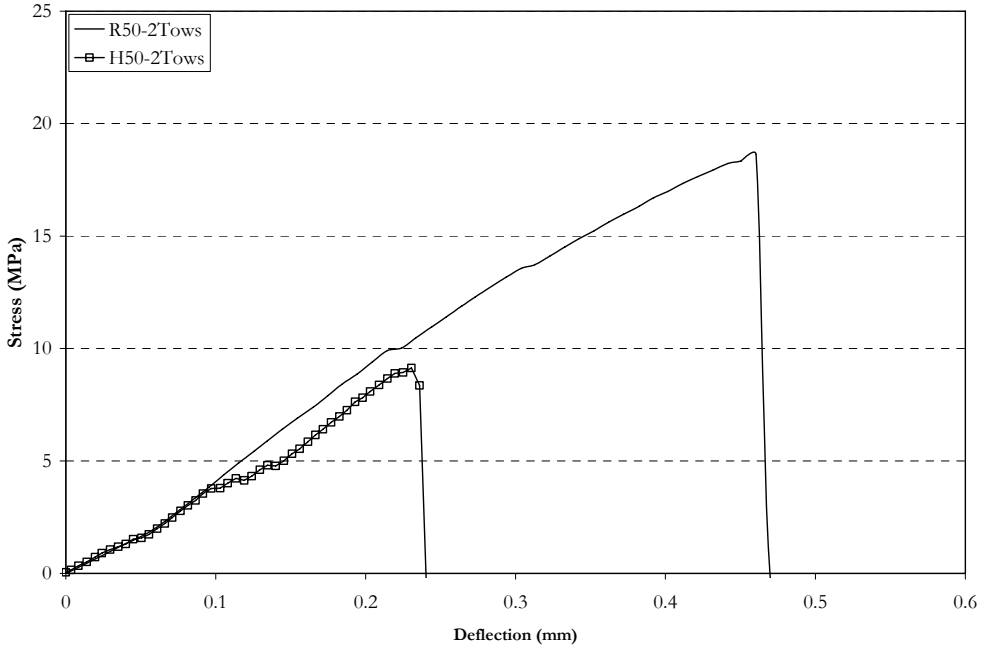

Figure 8.9 Test results for 50% mix-Samples reinforced with 2 tows

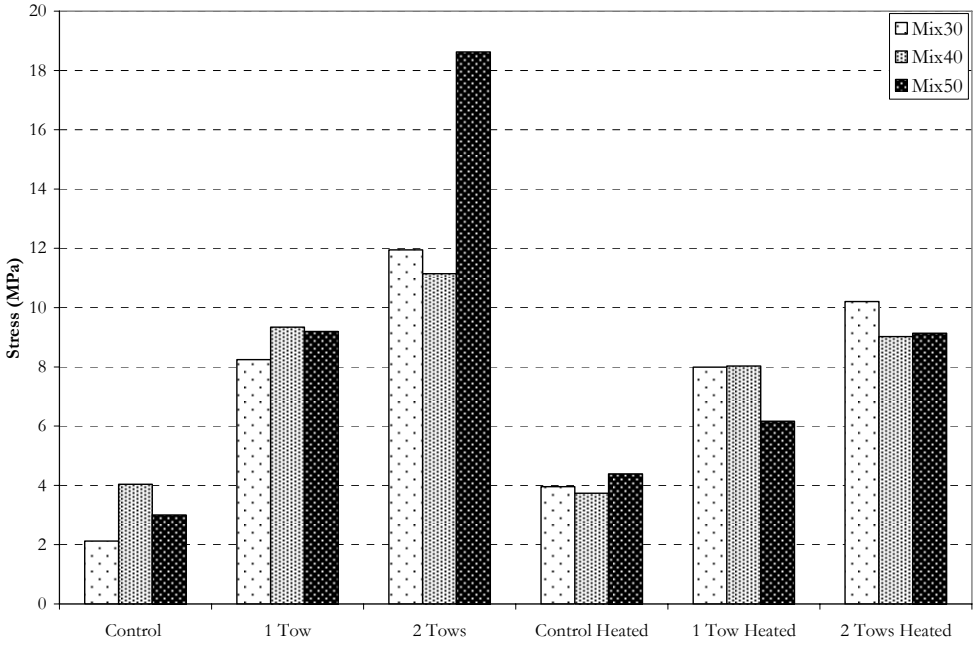

Figure 8.10 Apparent strength- all samples

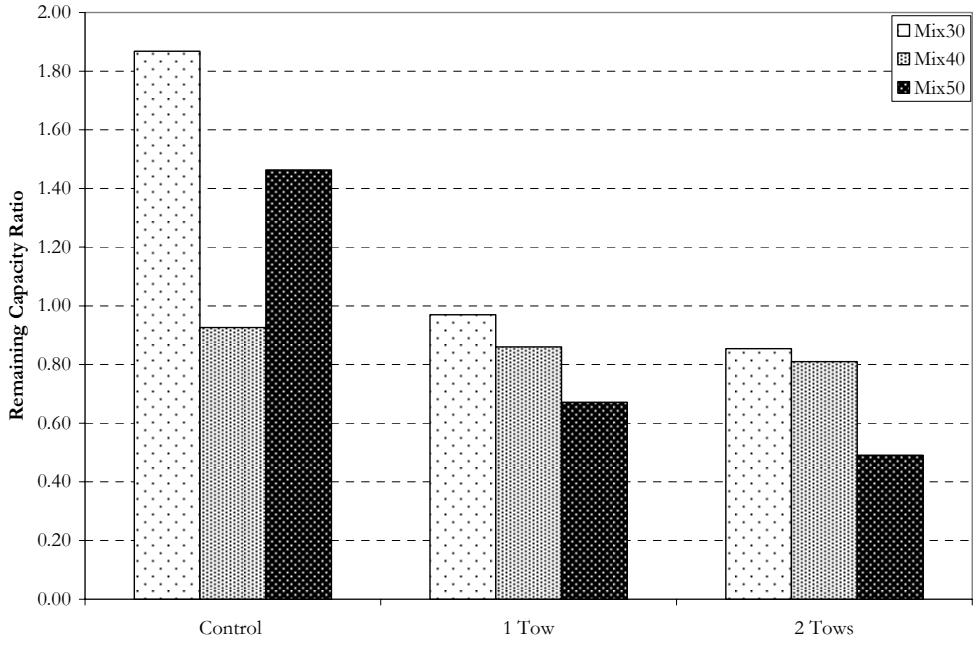

Figure 8.11 Strength retention ratio after heating

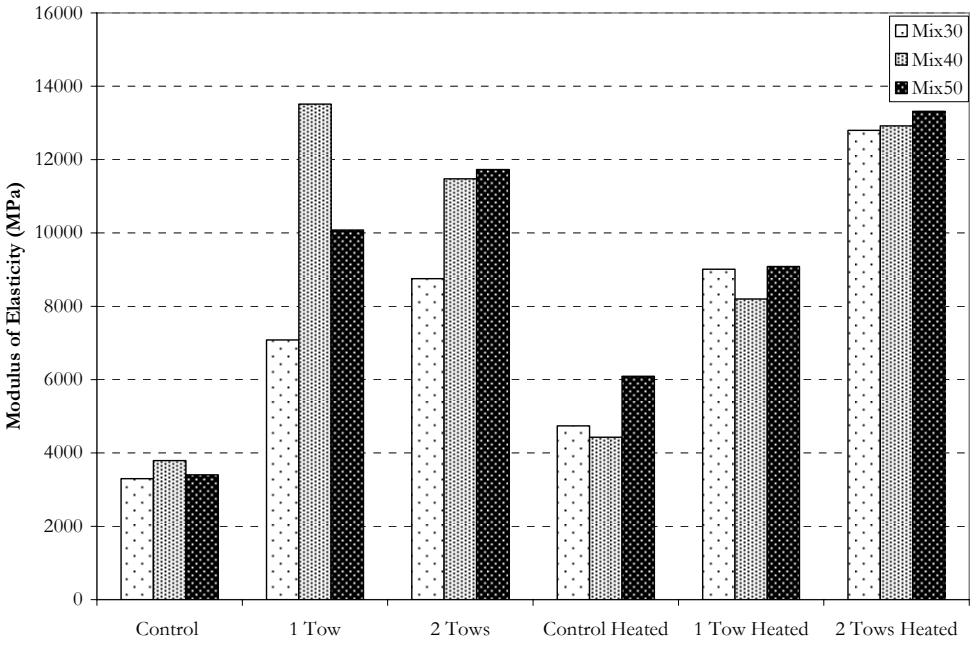

Figure 8.12 Stiffness-all samples

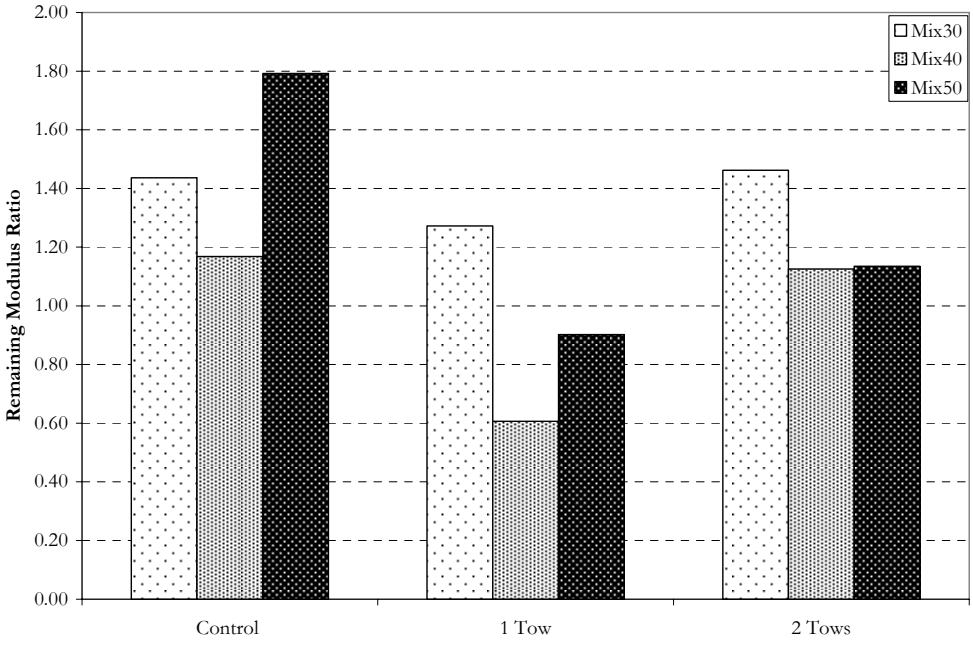

Figure 8.13 Stiffness retention ratio after heating

Chapter 9

Conclusions and Future Research

9.1 Conclusions

The results presented in this dissertation focus on the evaluation of sandwich beams made using polyvinyl chloride (PVC) foam and inorganic facings as reinforcement. The literature review, presented in chapter 2, provides information on the various materials used for cores, facings and resins, sandwich panel commonly available configurations, a brief description of the analytical models available, and a detailed description of the evolution of Geopolymer research at Rutgers, the State University of New Jersey.

The results of the state-of-the art indicate that while considerable progress is made on the development of lightweight sandwich structural elements with excellent mechanical properties, there is a critical need for the development of fire resistant sandwich structures. Development of fire resistant panels is a prerequisite for increasing their use in aerospace and naval structures. Fire resistance will also promote the use of the system in general building construction and automobile structures.

Chapter 3 presents the results of the experimental study on the mechanical properties of sandwich beams having PVC core and carbon/Geopolymer facings. Based on observations made during fabrication and tests, test results presented in chapter 3 and their analysis lead to the following conclusions.

- It is feasible to fabricate sandwich panels using PVC core and carbon/Geopolymer composites. Excellent bond could be achieved between the inorganic resin and the PVC core, the bond is strong enough to eliminate skin delamination.
- The lighter cores tend to absorb more resin than the more dense ones, which provides better adhesion but this may affect its specific strength, and could be critical in applications where the total weight is a design parameter. The weight increase for the lighter foams is in the range of 234% to 473% where as the corresponding percentages for denser foams are 36% to 54%.
- Since the specimens were fabricated using hand-laying process, increase in fiber content seems to result in increase of fiber damage. Therefore, three fold increase in reinforcement provides only two fold increase in moment capacity.
- Increase in core density provides consistent increase in moment capacity.
- Increase in flexural stiffness with the increase of carbon fiber area is consistent with improvements in moment capacity.
- The denser the core is the higher stiffness that could be attained. The increase in density from 50 Kg/m^3 to 250 Kg/m^3 provides an average increase in the stiffness of 180%.
- Compression failure is more prevalent for low density cores.
- N-12K MMC (440 GPa modulus) fibers provide higher moment capacity than H-12K HMC (640 GPa modulus fibers) even though it has lower modulus.
- Most failures are initiated by crimping of compression reinforcement. But increasing compression reinforcement does not increase moment capacity or stiffness significantly.

- The toughness increases as the reinforcement area increases. Beams reinforced with N-12K MMC fibers provide higher toughness than the ones reinforced with H-12K HMC. On the whole, beams reinforced with carbon tape exhibited the largest toughness.
- Beams reinforced with organic polymer composites are 10% lighter and the additional weight per tow is 40% less than the corresponding beams reinforced with inorganic resin.
- The organic polymer composites provide only 3% higher moment capacity than those reinforced with inorganic polymer composites.
- The stiffness for inorganic polymer composites is 14% higher than the organic polymer composites.
- Organic composites provide higher ductility than beams with inorganic polymers.
- The failure in the skin occurs at a fraction of the ultimate strength of the fibers (53%), in other words, the skin is not fully stressed at failure. The maximum moments are controlled by bearing stresses or compression buckling of the skin.
- Without skin and 36% more dense, the balsa control beams have 2000% more moment capacity and 2750% more stiffness than PVC control beams.
- For reinforced beams, the balsa beams have an average of 170% more moment capacity and 230% more stiffness. The difference decreases with the increase of the reinforcement ratio.
- The long grain balsa sandwich beams have higher mechanical properties but their use is only limited to one dimensional elements (beams). However, the Polyvinyl (PVC)

sandwich beams can be used in fabricating two dimensional elements (plates and shells).

The analytical model presented in chapter 4, which takes into account the vertical stress field imposed from the indentation stresses, leads to the following conclusions.

- Most of the failures are triggered by compression in the core.
- Indentation stresses can not be neglected in applications involving concentrated or contact loads.
- The effect of indentation stresses increases with the increase of the depth to span ratio.
- As expected, the effect of indentation stresses has more influence in cores with lighter density.
- Based on the failure hypothesis and its verification, the load deflection deviates from linearity when the core yields, and the ultimate load corresponds to the ultimate capacity of the PVC core.
- In typical cases, the ultimate stress of fibers can not be attained, if the concentrated are present. The failure will occur due to indentation. Special details may be used to increase the fiber stresses at failure.
- The ultimate load approaches the lower bound solution with the increase of density and the increase of reinforcement ratio.

The proposed optimum design method presented in chapter 5, leads to the following conclusions:

- The PVC/carbon sandwich beams can be optimized for weight for a required stiffness.
- Design aids and charts can be constructed for different PVC core densities and carbon fibers arrangement
- For a given stiffness, the required core thickness decreases as the tow width increases.
- The same solution methodology can be used for other loading configurations.

The fire tests results discussed in chapter 6, lead to the following conclusions:

- For the OSU test, the peak heat release rate can be lowered from 68 and 85 KW/m^2 to an average of 21 and 29 KW/m^2 for 50 Kg/m^3 and 250 Kg/m^3 cores, respectively. The improvement can be attained by applying 1 mm inorganic polymer coating.
- The time to reach the peak heat release rate can be increased from 50 and 193 sec to 260 and 296 sec for 50 Kg/m^3 and 250 Kg/m^3 cores, respectively.
- The heat release after 2 minutes decreased from 84 and 127 KW.min/m^2 to an average of 5 and -4.7 KW.min/m^2 for 50 Kg/m^3 and 250 Kg/m^3 cores, respectively.
- The behavior of the HRR changed from abrupt increase to a rather gradual increase till it reached the peak by the end of the test.
- All the samples with inorganic coating passed the Federal Aviation Administration (FAA) criteria and none of the organic ones did.

- For the NBS test, the level of smoke decreased to 1.5% and 2.8% of the level originally exhibited for the control samples for the 50 Kg/m^3 and the 250 Kg/m^3 cores, respectively
- The inorganic polymer coated samples almost did not emit any smoke for the 180 sec.
- The behavior of the smoke emission changed to much desired behavior for the post-crash scenarios.
- All the samples with inorganic polymer coating passed the NBS passing criteria with a level of emission that did not exceed 5% of the Federal Aviation Administration (FAA) upper limit.

Based on the results presented in chapter 7, the following conclusions can be drawn. Note that the maximum bending moment region was heated using a heating element.

- After 5 minutes of exposure to temperature up to 700°C, all the samples sustained more than 90% of its strength. This time limit is important for passengers to escape from an airplane in a post-crash scenario.
- The performance of cores made with PVC 50 Kg/m^3 was better. The reason is this core absorbed more Geopolymer resin, which improved the mechanical behavior by providing some confinement for the cell walls preventing them from buckling and deforming, which prevented the wrinkling from occurring. It improved the fire characteristics as well, by providing extra layer of fire proof material. This can be easily verified by comparing the weight gained from the reinforcement for both core types. The weight gain was 330% for the lightest core and the corresponding number for the heaviest core was 45%.

- After 30 minutes, the 50 Kg/m^3 core reinforced with one and two tapes sustained its full strength after being exposed to 350°C. The 50 Kg/m^3 core reinforced with one tape and two tapes sustained 30% and 95% of their strength after exposure to 350°C.
- For exposure temperature of 700°C, the 50 Kg/m^3 core reinforced with one sustained 40% of its strength and two tapes reinforcement provide the full strength after 30 minutes of exposure. On the other hand, the 250 Kg/m^3 core sustained about 20% of its strength after 30 minutes.
- Because of its high flammability, this test could not be performed on organic composites.

Evaluation of sandwich beams with inorganic syntactic foam and inorganic polymer skin presented in chapter 8 lead to the following conclusions.

- It can be feasible to produce inorganic syntactic foams by mixing cenospheres and Geopolymer matrix. The primary problem is shrinkage during curing. This aspect needs further investigation.
- Flexural properties of the core (strength and stiffness) improved after the exposure to 1050°C. The author believes that further curing or polymerization occurs when the samples are heated to 1050°C.
- The reinforced samples lost strength when exposed to higher temperature. This is consistent with the behavior of the ceramic fibers used for reinforcement, that loose 65% of strength at 1050°C.
- The workability of the slurry decreased with the increase of the filler content.

- The mixes exhibited some shrinkage cracks during curing; it could be detected the most in the 50% mix. The author believes that these cracks could be controlled by introducing chopped fibers into the mix.

9.2 Suggestions for future research

Since this investigation was the initial trial to evaluate the mechanical properties of sandwich panels made with polyvinyl chloride core (PVC) and inorganic polymer resin there is still a need for additional research. The author believes that the most important parameters that need further investigation include:

- Different span to depth ratios should be tested for the PVC sandwich beams.
- Different loading and boundary conditions should be tested (Fixed-Fixed, cantilever beams).
- Testing the sandwich beams in cantilever configuration should be adopted by the American Society of Testing and Materials (ASTM) standards, which will provide more accurate evaluation for the composites by avoiding the indentation effect; especially, if concentrated loads are not a design parameter.
- Sandwich beams with inorganic skin should be tested for impact loading.
- Vacuum bagging techniques in preparing the beams should be investigated.
- Syntactic foams using cenospheres and chopped ceramic fibers to improve the mechanical properties of the core should be evaluated.
- Engineering economics study on the different alternatives is needed
- Full scale fire and mechanical tests should be conducted.
- Methods to control the shrinkage of Geopolymer matrix are needed.

References

3M Inc, (2004), "Nextel™ Ceramic Textiles Technical Notebook," [On-line], Available: www.3M.com

3M Inc, (2007). [On-line], Available: www.3M.com

Abot J., (2000) "Fabrication, testing and Analysis of Composite Sandwich Beams", Doctorate Dissertation, Northwestern University, Illinois

Allen G.H., (1969), Analysis and Design of Structural Sandwich Panels, Pergamon Press

American Society for Testing and Materials, (1992), "Standard test method for heat and visible smoke release rates for materials and products using oxygen consumption calorimeter," ASTM Test Method E-1354

American Society for Testing and Materials, (1999), "Standard Test Method for Flexural Properties of Sandwich Constructions," ASTM Test Method C393-94, Annual Book of ASTM Standards, Vol. 15.03, pp. 22-25.

American Society for Testing and Materials (2002), "Standard Test Method for Apparent Density of Rigid Cellular Plastics," ASTM Test Method D1622, Annual Book of ASTM Standards, Vol. 8.01, pp. 362-365.

Argatov I.I., (2005) "An approximate solution of the axisymmetric contact problem for an elastic sphere," Journal of Applied Mathematics and Mechanics, Vol. 69, pp. 275-286

Argatov I.I., (2006) "The solution of hertz axisymmetric contact problem," Journal of Applied Mathematics and Mechanics, Vol. 70, pp. 621-635

Borsellino C., Calabrese L., Valenza A., (2004) "Experimental and numerical evaluation of sandwich composite structures," Composites Science and Technology, Vol.64, pp.1709-1715

Brown J.E., Braun E., Twilley W.H., (1988), "Cone calorimeter evaluation of the flammability of composite materials," Technical Report NBGIR 88-3733, National Bureau of Standards, Center for Fire Research

Dai J., Hahn H.T., (2003), "Flexural behavior of sandwich beams fabricated by vacuum-assisted resin transfer molding," Composite Structures, Vol.61, pp.247-253

Daniel I.M., Gdoutos E.E., Wang K.-A., Abot J.L., (2002) "Failure modes of composite Sandwich beams", International journal of damage mechanics, Vol.11, pp.309-334

Daniel I.M, Gdoutos E.E., Abot J.L., Wang K.-A.., (2003), "Deformation and failure of composite Sandwich Structures", Journal of thermoplastic composite materials, Vol.16, pp.345-364

Dao M., Asaro R.J., (1999), "A study on failure prediction and design criteria for fiber composites under fire degradation," Composites: Part A, Vol. 30, pp.123-131

Davidovits J., (1989), "Geopolymers and geopolymeric materials," Journal of thermal analysis and calorimetry, Vol. 35, pp.429-441

Davidovits J., (2002), "30 years of successes and failures in Geopolymer applications. Market trends and potential breakthroughs," Geopolymer 2002 Conference, Melbourne, Australia

DeFazio C., (2007) "High temperature/high strength discrete fiber reinforced composites," Master Thesis, Rutgers University, New Jersey

Demsetz L.A., Gibson L.J., (1986), "Minimum weight design for stiffness in sandwich plates with rigid foam cores," Materials Science and Engineering, Vol.85, pp. 33-42

DIAB Group, Inc. (2007). [On-line], Available: www.diabgroup.com

Foden A.J., (1999) "Mechanical properties and characterization of polysialate structural composites," Doctorate Dissertation, Rutgers University, New Jersey

Gardiner C.P., Mathys Z., Mouritz A.P., (2004), "Post-fire structural properties of burnt GRP plates," Marine Structures, Vol.17, pp.53-73

Garon R.J., (2000), "Effectiveness of high strength composites as structural and protective coatings for structural elements," Doctorate Dissertation, Rutgers University, New Jersey

Gdoutos E.E., Daniel I.M., Wang K.-A., (2003) "Compression facing wrinkling of composite sandwich structures," Mechanics of Materials, Vol.35, pp. 511-522

Giancaspro J.W., (2004), "Influence of reinforcement type on the mechanical behavior and fire response of hybrid composites and sandwich structures," Doctorate Dissertation, Rutgers University, New Jersey

Gibson L.J., (1984) "Optimization of stiffness in sandwich beams with rigid foam cores," Materials Science and Engineering, Vol.67, pp. 125-135

Gibson R.,(1994), Principles of composite material mechanics, McGraw-Hill, Inc

Grenier A.T., Dembsey N.A., Barnett J.R., (1998), "Fire characteristic of cored composite materials for marine use," Fire Safety Journal, Vol. 30, pp.137-159

Gupta N., Woldesenbet E., Mensah P., (2004), "Compression properties of syntactic foams: effect of cenosphere radius ratio and specimen aspect ratio," Composites: Part A, Vol. 35, pp. 103-111

Gupta, N., and Woldesenbet, E., (2005), "Characterization of flexural properties of syntactic foam core sandwich composites and effect of density variation," Journal of Composite Materials, Vol.39, pp 2197-2212

Hammell, J.A., (2000), " The influence of matrix composition and reinforcement type on the properties of polysialate composites," Doctorate Dissertation, Rutgers University, New Jersey

Hoff, N.J., and Mautner, S.E., (1945) "The Buckling of Sandwich-Type Panels", Journal of aerospace sciences 12, 1945, 285-297

Judd N.C.W., (1971) "The Chemical Resistance of Carbon Fibers and a Carbon Fiber/Polyester Composite," Proceedings of the First Int. Conf. on Carbon Fibers, Plastics Institute, pp. 258

Karthikeyan C.S., Sankaran S., Kishore, (2004), "Elastic behaviour of plain and fibre-reinforced syntactic foams under compression," Materials Letters, Vol. 58, pp. 995-999

Karthikeyan C.S., Sankaran S., Kishore, (2005), "Flexural behaviour of fibre-reinforced syntactic foams," Macromolecular Materials and Engineering, Vol. 290, pp. 60-65

Kim J., Swanson S.R., (2001) "Design of sandwich structures for concentrated loading," Composite Structures, Vol. 52, pp. 365-373

Kindinger J., (2003) "Lightweight Structural Cores," Composites, ASM Handbook, Vol21, ASM international

Kinetico Incorporated, (2007). [On-line], Available: www.Kinetico.com

Konsta-Gdoutos, M.S., and Gdoutos, E.E., (2005) "The effect of load and geometry on the failure modes of sandwich beams," Applied Composite Materials, Vol. 12, pp. 165-176

Ley R.P., Lin W., and Mbanefo U., (1999). "Facesheet Wrinkling in Sandwich Structures," National Aeronautics and Space Administration, NASA/CR-1999-208994

Lingard, J.R., (1993) "Development of a Theory for Optimising Sandwich Composites", Advanced composites'93, International Conference on Advanced Composite Materials, 259-265

Lyon R.E., Balaguru P.N., Foden A.J., Sorathia U., Davidovits J., Davidovics M., (1997), "Fire-Resistant Aluminosilicate Composites," Fire and Materials, Vol.21, pp 67-73

M.C. Gill Corporation. (1997). "Sandwich panel Review," The M.C. Gill Doorway, 34, (1).

Mallick P.K., (1993). Fiber-Reinforced Composites: Materials, Manufacturing, and Design. Marcel Dekker, Inc., New York, pp. 566.

Mazumdar S.K., (2002), Composites Manufacturing: Materials, Product and Process Engineering, CRC Press

McKee D.W., and Memeault V.J., (1981), "Surface Properties of Carbon Fibers," *Chemistry and Physics of Carbon*, Vol. 17, Marcel Dekker, pp. 1

Miller R.B., (1999). "Chapter 1 – Characteristics and Availability of Commercially Important Woods," Wood Handbook – Wood as an Engineering Material, Forest Products Laboratory Gen. Tech. Rep. FPL-GTR-113, Madison, WI: U.S. Department of Agriculture, Forest Service, Forest Products Laboratory, 463 p.

Murray T.M., (1995), "Airplane accidents and fires," Improved Fire- and Smoke- Resistant Materials for Commercial Aircraft Interiors proceedings, Publication NMAB-477-2, National Academy Press, Washington D.C., pp. 25-36

Nazier M., (2004) "Evaluation of high strength composites and new construction techniques for their effective use," Doctorate Dissertation, Rutgers University, New Jersey

Okuno K., Woodhams R.T., (1974), "Mechanical properties and characterization of phenolic resin syntactic foam," Journal of Cellular Plastics, Vol.10, pp. 237-244

Ozcivici E., Singh R.P., (2005), "Fabrication and characterization of ceramic foams based on silicon carbide matrix and hollow alumino-silicate spheres," Journal of the American ceramic society, Vol.88, pp. 3338-3345

Papakonstantinou C.G., (2003), "High temperature structural sandwich panels" Doctorate Dissertation, Rutgers University, New Jersey

Papakonstantinou C.G., Balaguru P.N., (2005), "Effect of microsphere size on the properties of a Geopolymer syntactic foam," Proceedings of 50th International SAMPE Symposium, Long Beach, CA, pp.2925-2937

Perlite.net & Redco II, (2003). [On-line], Available: www.perlite.net

Reddy N.J., (2004) Mechanics of laminated composite plates and shells: Theory and Analysis, Second Edition, CRC Press LLC

Sarkos C.P., (1995), "Heat exposure and burning behavior of cabin materials during aircraft post-crash fuel fire," Improved Fire- and Smoke- Resistant Materials for Commercial Aircraft Interiors proceedings, Publication NMAB-477-2, National Academy Press, Washington D.C., pp. 25-36

SP Systems: Guide to Composites. (2001). [CD-ROM]. Structural Polymer Systems Limited, Isle of Wight, United Kingdom.

Specialized Balsa Wood, LLC. (2007). Balsa Wood Road Map. [On-line], Available: www.zimsweb.com/balsa/information/info.htm

Steeves C.A., Fleck N.A., (2004-a),"Collapse mechanisms of sandwich beams with composite faces and a foam core, loaded in three-point bending. Part I: Analytical models and minimum weight design," International Journal of Mechanical Sciences, Vol. 46, pp. 561-583

Steeves C.A., Fleck N.A., (2004-b),"Collapse mechanisms of sandwich beams with composite faces and a foam core, loaded in three-point bending. Part II: Experimental

investigation and numerical modelling," International Journal of Mechanical Sciences, Vol. 46, pp. 585-608

Shutov F.A., (1983) "Foamed polymers. Cellular structure and properties", Advances in Polymer Science, Vol.51, pp 155-218

Shutov F.A., (1986) "Syntactic polymer foams", Advances in Polymer Science, Vol.73, pp 65-121

Sorathia U., Rollhauser C.M., Hughes A.W., (1992), "Improved fire safety of composites for naval applications," Fire and Material, Vol.16, pp. 119-125

Swanson S.R., Kim J., (2003), "Failure modes and optimization of sandwich structures for load resistance," Journal of Composite Materials, Vol.37, pp. 649-667

Tagarielli V.L., Fleck N.A., Deshpande V.S., (2004), Composites: Part B, Vol.35, pp.523-534

Tessier N.J., (2001), "Fire performance and mechanical property characterization of a phenolic matrix syntactic foam core composite sandwich structures," Proceedings of 46th International SAMPE Symposium, Long Beach, CA, pp.2593-2599

The Federal Aviation Administration (FAA), (2000), Aircraft Materials Fire Test Handbook, Report DOT/FAA/AR-00/42

Trelleborg Fillite Ltd., (2007), [On-line] Available: www.fillite.com

Triantafillou T.C., Gibson L.J., (1987) "Failure mode maps for foam core sandwich beams," Materials Science and Engineering, Vol.95, pp. 37-53

Triantafillou T.C., Gibson L.J., (1987) "Minimum Weight Design of Foam Core Sandwich Panels for a Given Strength," Materials Science and Engineering, Vol.95, pp 55-62

Walsh P.J., (2003) "Carbon fibers," Composites, ASM Handbook, Vol21, ASM international

Wilson D.M., DiCarlo J.A. Yun H.M., (2003) "Ceramic fibers", Composites, ASM Handbook, Vol21, ASM international

Wilson D.M, Visser L.R., (2000) "High performance oxide fiber for metal and ceramic composites," Proceedings of the processing of fibers and composites conference, Barga, Italy

Zenkert D., Shipsha A., Persson K., (2004). "Static indentation and unloading response of sandwich beams", Composites: Part B, Vol. 35, 511–522

VITA

Mohamed DA I. Arafa

Education

Ph.D., Structural Engineering, October 2007
Rutgers, The State University of New Jersey; New Brunswick, NJ
Dissertation Title: "High strength-High Temperature Laminated Sandwich Beams"

M.Phil., Civil & Environmental Engineering, May 2006
Rutgers, The State University of New Jersey; New Brunswick, NJ
Report Title: "High strength-High Temperature Laminated Sandwich Beams"

M.S., Engineering Mechanics, February 2004
Cairo University, Giza, Egypt
Thesis Title: "Vibration and Buckling of Rectangular Tall Buildings Modeled as Flexural-Shear Plates"

B.S., Civil & Environmental Engineering, May 2000
Cairo University, Giza, Egypt

Experience

May 2000- September 2000	Egyptian Engineer Consultants, Cairo, Egypt Structural Engineer
September 2000 – December 2003	Cairo University, Department of Engineering Mechanics and Physics Teaching Assistant and Lecturer
January 2004 – June 2006	Rutgers, The State University of New Jersey, Civil & Environmental Engineering Graduate Assistant
June 2006 – April 2007	UrbanTech Consultants & Thornton Tomasetti, NY Structural Engineer
April 2006 – Continuing	Severud Associates, NY Structural Engineer

Publications

Arafa Mohamed, Balaguru P. N., "Evaluation of Geopolymer Coatings," Final Report, Submitted to NJDOT, September 2004.

Arafa Mohamed, Balaguru P. N., "Geopolymer Coating Demonstration Project for I-295 Scenic," Final Report, Submitted to NJDOT, August 2005.

Arafa Mohamed, DeFazio Christian, Balaguru Balamuralee, "Nano-Composite Coatings for Transportation Infrastructures: Demonstration Projects," Proceedings of second International symposium on Nanotechnology in construction, Bilbao, Spain, November 2005.

Arafa Mohamed, Balaguru P.N., "Flexural Behavior of High Strength-High Temperature Laminate Sandwich beams," Proceedings of 8th International symposium on Ferrocement and thin reinforced cement composites, Bangkok, Thailand, February, 2006.

Arafa Mohamed, Balaguru P.N., Lyon Richard, " Flexural Evaluation of Lightweight Sandwich beam," Proceedings of SAMPE 2006 conference, long beach, CA, April, 2006.

DeFazio Christian, Arafa Mohamed, Balaguru P.N., "Discrete fiber reinforced high temperature composites," Proceedings of SAMPE 2006 conference, long beach, CA, April, 2006.

DeFazio Christian, Arafa Mohamed, Balaguru P.N. "Geopolymer Column Wrapping" Final Report, Submitted to DOT RITA and University of Maryland, June 2006.

DeFazio Christian, Arafa Mohamed, Balaguru P.N. "Functional Geopolymer Composites for Structural Ceramic Applications" Final Report, Submitted to Ceramatec Inc., June 2006.